Cellular and molecular mechanisms of neural tube formation and axial elongation

Evangelos Vasileios Papastergios

Thesis submitted to University College London

for the degree of Doctor of Philosophy

August 2022

Developmental Biology of Birth Defects

Developmental Biology & Cancer Programme

UCL Great Ormond Street Institute of Child Health

Declaration

I, Evangelos Vasileios Papastergios confirm that the work presented in this thesis is my own. Where information has been derived from other sources, I confirm that this has been indicated in the thesis.

Abstract

During primary neurulation, the flat neural plate folds into a hollow tube which later forms the brain and spinal cord. Primary neurulation begins with elongation and bending of the neural plate, bringing its lateral folds into contact. It is then completed through a process of "zippering", whereby the neural folds progressively fuse along the antero-posterior axis of the embryo.

Previous research from our lab highlighted the importance of the extracellular matrix receptor integrin β1 for successful neural fold fusion and suggested an interaction with fibronectin. The current project investigated the role of fibronectin in neural tube formation. As fibronectin production and trafficking dynamics were unclear, three conditional knock-out strategies were employed to target fibronectin in a variety of tissues. Assessment of mutant embryos in terms of morphology, fibronectin localisation and associated cellular processes revealed two distinct roles of fibronectin in spinal development. First, fibronectin produced by the surface ectoderm at the posterior neuropore fusion site was found to be important in the formation of cellular semi-rosettes that facilitate zippering. Second, fibronectin produced primarily by the paraxial mesoderm was shown to be necessary for mechanical coupling and symmetric elongation of neural and mesodermal tissues.

Elongation of the caudal trunk and tail of the embryo is underpinned by the continuous incorporation of neuromesodermal progenitors (NMPs) in the tailbud region. While NMPs are often defined based on the co-expression of the neural marker Sox2 and the mesodermal marker T/Brachyury, lineage tracing experiments from our lab indicated that Sox2-expressing cell derivatives colonise only the neural tube after E8.5. This project consolidated these findings by employing RNAscope to validate the previously used $Sox^{CreERT2}$ line and to evaluate Sox2 expression in NMP-harbouring regions. Furthermore, Sox2 was deleted in NMPs, and mutant embryos were examined in terms of developmental progression, and NMP colonisation, fate choice and genetic compensation.

Impact statement

The genetic causes of NTDs and congenital spine disorders remain largely unknown. Studying the embryonic mechanisms that give rise to the spine and spinal cord, and developing models of these conditions in mice can pinpoint relevant pathogenic pathways in humans and hence potential targets for preventative interventions. The current project contributes towards this goal in two important respects:

Firstly, the evidence presented here reveals two novel roles of the extracellular matrix protein fibronectin in early spinal development. Fibronectin was shown to facilitate neural tube closure by allowing propagation of neural fold zippering, and to ensure symmetric axial elongation by maintaining inter-tissue adhesion between the neural tube and paraxial mesoderm. Genetic ablation experiments revealed that failure of the former function gives rise to open spina bifida, while failure of the latter results in axial abnormalities bearing resemblance to the human conditions of scoliosis and short stature. While a lot of additional research is required, preliminary evidence from population studies suggests that these previously unappreciated roles of the extracellular matrix in spinal development might be conserved in humans.

Secondly, the current work represents a significant advancement in our understanding of neuromesodermal progenitors (NMPs); the cells that generate neural and mesodermal tissues along most of the antero-posterior axis of the body. Previous research on NMPs has been dominated by the assumption that these cells co-express the neural marker Sox2 and the mesodermal market T. As a result, in vivo studies of NMPs have focused on T/Sox2 double-positive cell populations, while in vitro studies attempting to derive NMPs from pluripotent stem cells have used T/Sox2 co-expression as their endpoint. The current project, in combination with previous work from our lab, demonstrates that Sox2 is not in fact expressed in NMPs, but only downstream of neural commitment. Furthermore, contrary to previous assumptions, Sox2 is shown to be redundant for NMP fate choice and early neural development. These findings necessitate substantial revisions in the interpretation of previous studies, and the experimental design of future ones. An improved understanding of NMPs will in turn facilitate the successful in vitro derivation of these

cells for research and therapeutic purposes, as well as the study of the developmental mechanisms that form the lower body, and related human conditions, such as spina bifida and sacral agenesis.

Acknowledgements

I would first like to thank the Anatomical Society and Hjelt Foundations for funding my research. I am extremely grateful to my primary supervisor, Professor Andy Copp, for giving me the opportunity to work with him on this amazing project, allowing me the freedom to pursue my ideas, and always being available to talk and guide me when I needed it. Every interaction with Andy has been a valuable lesson and I hope I can continue to learn from him for years to come. I would also like to thank my secondary supervisor, Professor Nick Greene, for his many insightful contributions to both the conceptual and experimental aspects of my work. In addition, I am deeply indebted to Dr Gabe Galea for always being there for me with the solution to every question and lab-related emergency.

I would like to thank Eirini, Makis, Zoe, Rosie and Elliot for being such wonderful friends and colleagues, and never letting me down. Special thanks also to Chloe, Sandra, Kit-Yi, Raasib, Maryam, Jake and all other past and present members of our group whose constant support and friendly attitude made it impossible to have a bad day at work.

I will always be deeply grateful to the brilliant doctors and nurses at the Macmillan Cancer Centre and the NHNN, without whom this studentship would have ended far too soon.

I want to thank Natashia from the bottom of my heart for being with me every step of the way, no matter how difficult it got. There is no way I could have done it without you, and despite the obstacles, you made the last few years the best time of my life.

Finally, a huge “Ευχαριστώ!” to my parents for being a never-ending source of love and encouragement, my biggest role models and scientific enablers. It seems that the children’s microscope and biology books you bought me 20 years ago had a bigger impact than you expected!

Table of Contents

List of Figures

List of Tables

Abbreviations

ANP	anterior neuropore
AP	antero-posterior
BM	basement membrane
BMP	bone morphogenetic proteins
bp	base pairs
BSA	bovine serum albumin
CCasp3	cleaved caspase 3
cDNA	complementary DNA
cKO	conditional knock-out
CLE	caudal lateral epiblast
CNH	chordo-neural hinge
DAPI	4',6-diamidino-2-phenylindole
DLHP	dorsolateral hinge point
DMEM	Dulbecco's modified Eagle media
DNA	deoxyribonucleic acid
dNTP	deoxynucleotide triphosphate
DV	dorsoventral
E	embryonic day
ECM	extracellular matrix
EGFP	enhanced yellow fluorescent protein
EMT	epithelial-to-mesenchymal transition
EYFP	enhanced yellow fluorescent protein
FA	focal adhesion
FAK	focal adhesion kinase
FBS	foetal bovine serum
FGF	fibroblast growth factor

fl	floxed
FN	fibronectin
GAG	glycosaminoglycan
GFP	green fluorescent protein
Grhl	grainyhead-like
HNP	hindbrain neuropore
HSPG	heparan sulfate proteoglycan
ILK	integrin linked kinase
KD	knock-down
KO	knock-out
lgd	likely gene disrupting
MES	paraxial mesoderm
mG	membrane-targeted EGFP
MHC	myosin heavy chain
MHP	median hinge point
ML	medio-lateral
MP	mesodermal progenitor
mRNA	messenger RNA
mT	membrane-targeted tdTomato
n	sample size
NC	notochord
NE	neuroepithelium
NMP	neuromesodermal progenitor
NP	neural progenitor
NSB	node-streak border
NT	neural tube
NTDs	neural tube defects
PBS	phosphate-buffered saline

PBT	0.1% Triton X-100 in PBS
PCP	planar cell polarity
PCR	polymerase chain reaction
PFA	paraformaldehyde
pHH3	phospho-histone H3
PNP	posterior neuropore
PNP	posterior neuropore
PSM	presomitic mesoderm
qRT-PCR	quantitative real-time PCR
RA	retinoic acid
RGD	Arginine-Glycine-Aspartic acid
RNA	ribonucleic acid
S	somite
SD	standard deviation
SE	surface ectoderm
Shh	sonic hedgehog
WT	wild type

1. General Introduction

1.1 Germ layer patterning across the anterior-posterior axis

1.1.1 Gastrulation

Early in the development of most vertebrates, the highly dynamic process of gastrulation transforms the embryo from a pluripotent monolayer, called the epiblast, into a three-layered structure (Tam et al., 1993). In the mouse, gastrulation begins on embryonic day (E) 6.25 with the formation of the primitive streak at the dorsal midline of the posterior epiblast (Williams et al., 2012). At this stage, a proportion of epiblast cells undergo epithelial-to-mesenchymal transition (EMT), ingress through the primitive streak and migrate into the space between the epiblast and underlying visceral endoderm. Adoption of a mesenchymal character involves a transcriptional switch from E- to N-cadherin adhesion molecules and is tightly coordinated through a combination of signals from Wnt, BMP and FGF pathways (Bardot & Hadjantonakis, 2020). Cells that migrate through the primitive streak give rise to the mesoderm and endoderm, whereas the remainder of the epiblast forms the ectoderm. Fate choice is determined by the balance of opposing, cross-inhibitory gradients of Nodal in the anterior - required for ectoderm and endoderm - and BMP in the posterior - specifying the mesoderm (Conlon et al., 1994; Vincent et al., 2003; Winnier et al., 1995). As a result, lineage choice of epiblast cells is highly dependent upon their position along the antero-posterior (AP) axis of the embryo: the anterior epiblast forms the ectoderm, while anterior and posterior areas of the primitive streak form the endoderm and mesoderm, respectively (Lawson et al., 1991; Tam & Beddington, 1987). The resulting three germ layers ultimately generate distinct specialised tissues: ectoderm gives rise to the nervous system and skin, mesoderm forms the musculoskeletal system, and endoderm produces various organs, such as the liver and gastrointestinal tract. The cell lineages of the three germ layers were originally thought to diverge during gastrulation and remain separate thereafter.

1.1.2 Axial elongation

Head, trunk and tail develop in a consecutive fashion in amniote organisms. The initial formation of the head and upper trunk is a relatively brief morphogenetic event which is known to conform to the traditional germ layer model (described above). The lower body, on the other hand, follows a protracted process of anterior-to-posterior growth through progressive deposition of tailbud progenitors, whose mechanism of germ layer patterning has been largely undefined. This process sets up the posterior body plan including the neural tube (the spinal cord precursor) and underlying notochord (a mesoderm-derived transient rod-like structure) in the midline (axially), laterally flanked by two columns of paraxial mesoderm. These tissues are framed by two epithelia: the surface ectoderm dorsally and endoderm ventrally. Axial growth then consists of the regular appearance of paraxial blocks of undifferentiated mesoderm, called somites, and the gradual elongation of the notochord and neural tube (Kimelman, 2016).

The first clues on the underlying tissue-patterning mechanisms came in 1884 when the anatomist Albert von Kölliker proposed that the posterior neural tube arises from mesenchymal progenitors with neuromesodermal potential, based on morphological examination (Kölliker, 1884). Kölliker's observation was confirmed more than a century later, partly through prospective fate-mapping studies that homotopically grafted various caudal regions of GFP-expressing mouse embryos into wild type (WT) embryos (Cambray & Wilson, 2002, 2007). Culturing these embryos from E8.5 and monitoring the grafted cells' colonisation patterns later in development revealed two regions capable of producing both neural and mesodermal tissues throughout the elongating body axis: the node-streak border (NSB) and the caudal lateral epiblast (CLE) adjacent to the primitive streak. These findings were further delineated by subsequent experiments that fate mapped small groups of cells in these regions by utilising fluorescent dye injections (Mugele, 2018; Mugele et al., 2018). In particular, the NSB was found to contribute to the ventral parts of the neural tube and somites, while the CLE gave rise to the more dorsal parts of these tissues. Furthermore, at E9 these progenitors were shown to be internalised and retained in the chordo-neural hinge (CNH) – a region directly posterior to the notochord – where they maintain

their potency until the end of axial elongation at E12.5 (Cambray & Wilson, 2002). These studies decisively clarified the spatial dynamics of the axial progenitors forming the spinal neural tube and somites. However, as they lacked single-cell resolution, they were unable to discern whether these progenitors represented a single population of bipotent cells or a mixed pool of separately committed precursors.

1.1.3 Neuromesodermal progenitors and the question of *T/Sox2* co-expression

This question was resolved through the retrospective clonal lineage analysis performed in mouse embryos by Tzouanacou and colleagues (Tzouanacou et al., 2009). Their method utilised the rare spontaneous recombination of a mutant laacZ transgene into the functional LacZ form; expression of which labels the recombinant cell and its descendants (Bonnerot & Nicolas, 1993). In this way, they were able to identify clones that spanned both neural tube and paraxial mesoderm caudal to the 6th somite, while also being retained in the CNH. The study, therefore, confirmed for the first time the existence of neuromesodermal progenitors (NMPs), as opposed to two separate, spatially overlapping populations of neural and mesodermal progenitors. Endoderm, surface ectoderm and all anterior tissues, on the other hand, were shown to originate from independently committed progenitors. These findings were recently also replicated and extended in the chick embryo where single cells in the anterior CLE, traced through a barcoded retroviral library and a Brainbow method, were shown to contribute to both neural tube and paraxial mesoderm (Guillot et al., 2021).

The discovery of these bipotent progenitors, which persist after the end of gastrulation, stood in contrast to the traditional germ layer model and indicated that neural and mesodermal tissues can be induced through different mechanisms across the AP axis. As a result, NMPs have received widespread interest. However, their study is obscured by the current lack of unique molecular markers. In this regard, some studies identified cells within the NSB and CLE that co-express the early

mesodermal marker T (also known as Brachyury) and the neural progenitor marker Sox2 (Wymeersch et al., 2016). As this co-expression pattern correlates with the position and dual potency of NMPs, T/Sox2 double-positivity has since then often been used as an NMP marker (Henrique et al., 2015). Notably, lineage tracing studies using T^{Cre} lines have shown that the descendants of T-expressing cells widely colonise both posterior neural tube and paraxial mesoderm, thus, supporting the expression of T in NMPs (Anderson et al., 2013; Mugele, 2018; Mugele et al., 2018; Perantoni et al., 2005). However, unlike T, Sox2 expression in NMPs is assumed but has not been conclusively demonstrated. Indeed, T/Sox2 double-positive cells and NMPs both represent subgroups of the NSB/CLE/CNH cell populations which need not overlap (Koch et al., 2017; Wymeersch et al., 2016).

To decisively assess for potential Sox2 expression in NMPs, our lab recently performed a number of genetic lineage tracing experiments in mouse embryos (Mugele, 2018; Mugele et al., 2018). If NMPs expressed Sox2, then the descendants of Sox2-expressing cells would be expected to colonise both neural tube and somites when traced after the end of gastrulation. To test this prediction, a tamoxifen-inducible *Sox2*$^{CreERT2/+}$ line was crossed with the *Rosa26*$^{mTmG/mTmG}$ reporter, and the recombinase was activated at E8.5. Strikingly, when the embryos were analysed at E9.5, the GFP-labelled lineage of Sox2-expressing cells was found exclusively within the neural population. This finding demonstrated that Sox2 is only upregulated in progenitors which have committed to a neural fate. Furthermore, deleting Sox2 in the T lineage caused no detectable defects in the early stages of neural tube and mesoderm formation (Mugele, 2018; Mugele et al., 2018). These results appear to contradict previous research on NMPs, which might be explained by conceptual or methodological differences, or inefficiencies in the genetic tools employed. As T/Sox2 double-positive cells are the focus of intensive research, however, accurate interpretation of previous data and appropriate design of future NMP studies necessitate a definitive description of the potential role of Sox2 in NMPs (Gouti et al., 2014; Javali et al., 2017; Wymeersch et al., 2016).

1.1.4 Divergent mechanisms of neural specification

The discovery of NMPs showed the process of germ layer formation to be much more complex and spatiotemporally protracted than first thought. It also highlighted the diverse mechanisms underpinning neural specification along the AP axis. The first phase of neural induction takes place at the end of gastrulation when BMP antagonists emanating from the node promote an apicobasal thickening of the rostralmost region of the ectoderm layer (Harland, 2000; Sander & Faessler, 2003; Stern, 2005). At that stage, the transcription factor Otx2 becomes restricted to the anterior epiblast where it promotes Sox2 expression and adoption of the neural fate (Iwafuchi-Doi et al., 2012; Kimura et al., 2000; Rhinn et al., 1998). These events establish the anterior neural plate and will eventually form the brain and some of the anterior spinal cord.

Specification of NMPs, on the other hand, is primarily controlled through the right balance of extrinsic cross-inhibitory signals from the Wnt and retinoic acid (RA) signalling pathways and is highly position-dependent (Figure 1.1) (Wymeersch et al., 2021). Exposure to moderate levels of Wnt ligands, produced from the tailbud, is thought to be important for the maintenance of NMP bipotency and pool size (Wymeersch et al., 2016). However, higher levels of Wnt signalling (e.g., upon exit from the NMP niche) trigger T upregulation and differentiation into paraxial mesoderm (Garriock et al., 2015; Hofmann et al., 2004). In turn, RA produced by the somites, directs NMPs toward the neural fate through upregulation of Sox2 and concomitant downregulation of T (Gouti et al., 2017; Molotkova et al., 2005). In accordance, loss of Wnt3a or T in mouse embryos leads axial elongation defects, loss of paraxial mesoderm and excess formation of ectopic neural tissues. Interestingly, RA-deficiency in Raldh2 mutant embryos also leads to neural defects and axial truncation, yet no excess mesoderm formation, thus revealing certain asymmetries in the fate choice plasticity of NMPs (Niederreither et al., 1999).

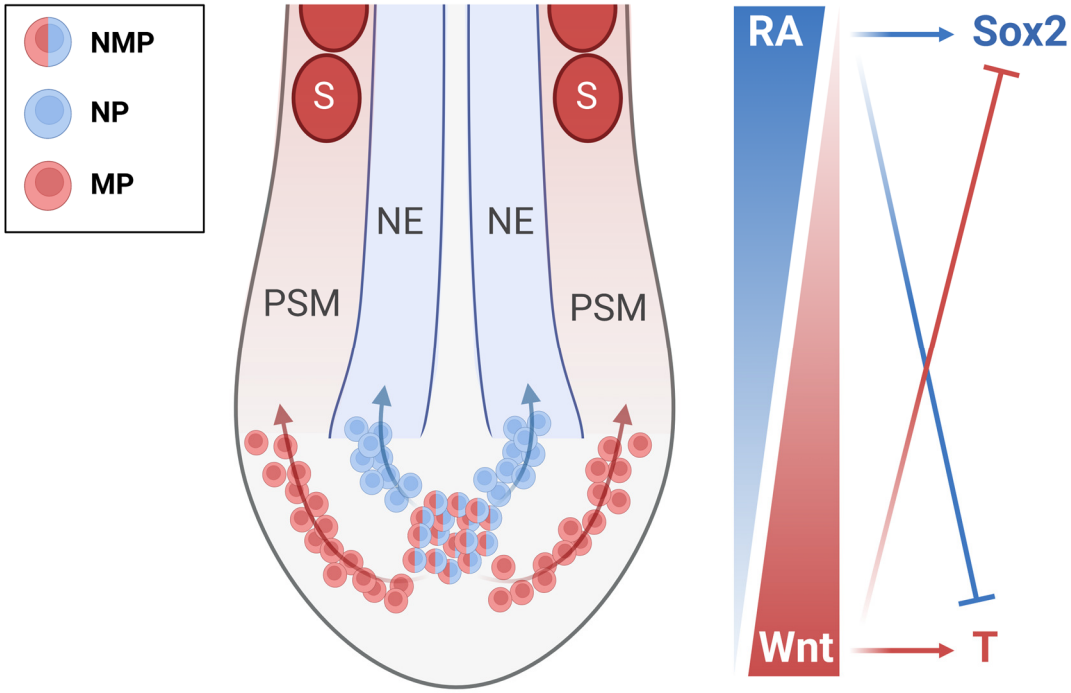

Figure 1.1 NMP fate choice and axial incorporation. Schematic of mouse embryo tailbud region (left) illustrating how specification of NMPs depends on their position along opposing AP gradients (right) of RA (blue) and Wnt (red). The moderate levels of Wnt ligands present at the NMP niche (CLE or CNH depending on embryonic stage) maintain NMPs in a bipotent state. Exposure to higher levels of Wnt caudally directs NMPs into mesodermal progenitors (MPs; red) through *T* upregulation and *Sox2* repression, while RA produced anteriorly by the somites (S) has antagonistic regulatory effects, thus promoting the specification of NMPs into neural progenitors (NPs; blue). Additional abbreviations: NE, neuroepithelium; PSM, presomitic mesoderm.

1.1.5 Relative contribution of NMPs to the body axis

Evidently, these sensitive feedback mechanisms are critical for the balanced production of neural and mesodermal derivatives throughout the process of axial elongation. However, the relative contribution of NMPs, versus anteriorly originating distinct neural and mesodermal progenitors, to the growing body axis remains poorly understood. Tzouanacou and colleagues found clones spanning both neural tube and

paraxial mesoderm only posterior to the 6th somite (Tzouanacou et al., 2009). In agreement, the lineage of T-expressing cells (of which NMPs are thought be a subset) colonise the neural tube exclusively below the 6th somite (Perantoni et al., 2005). Furthermore, lineage tracing studies have shown that at those cervical spine levels NMPs selectively form the ventral part of the neural tube; whereas the dorsal part presumably derives from anterior neural plate progenitors (Anderson et al., 2013). As axial elongation advances further caudally, the contribution of NMPs becomes uniform across the dorso-ventral (DV) axis of the neural tube (Chalamalasetty et al., 2014; Perantoni et al., 2005). Even in those posterior segments, however, NMPs have been reported to account for only 60% of the neural tube, with the remainder being of uncertain origin (Chalamalasetty et al., 2014).

1.2 Formation of axial and paraxial tissues

1.2.1 Neural tube

1.2.1.1 Primary and secondary neurulation

Anteroposterior differences also extend to the morphogenetic processes that shape the neural tube. The portion of the neural tube that will ultimately produce the brain and greater part of the spinal cord is formed through the process of primary neurulation. During primary neurulation, the recently specified flat neural plate folds and fuses dorsally to construct a hollow tube. This process is independently initiated at multiple sites along the AP axis (Figure 1.2). The neural folds first make contact at the hindbrain-cervical boundary (closure 1) at E8.5, followed by the forebrain midbrain-boundary (closure 2) and rostral extremity of the forebrain (closure 3) at E9.0 (Copp & Greene, 2010). A ‘zippering’ process of neural fold fusion then proceeds bidirectionally from the closure sites to gradually seal the open regions of the neural tube, known as neuropores. The anterior neuropore (closure 2 to 3) and the hindbrain neuropore (closure 1 to 2) become fully sealed at the 16-somite stage, thus

completing cranial neural tube closure first. Primary neurulation then concludes with closure of the posterior neuropore (PNP) in the lower spinal region (30th somite level) by E10.5 (Copp et al., 2003). Conversely, the lowest sacral and coccygeal segments of the neural tube (caudal to somite 30) are formed through a different mechanism, termed secondary neurulation, which takes place after PNP closure (Copp et al., 2015). Secondary neurulation involves an initial condensation of NMP-derived neural progenitors into a long cord-like structure which then undergoes canalisation to generate neuroepithelium surrounding a lumen (Schoenwolf, 1984).

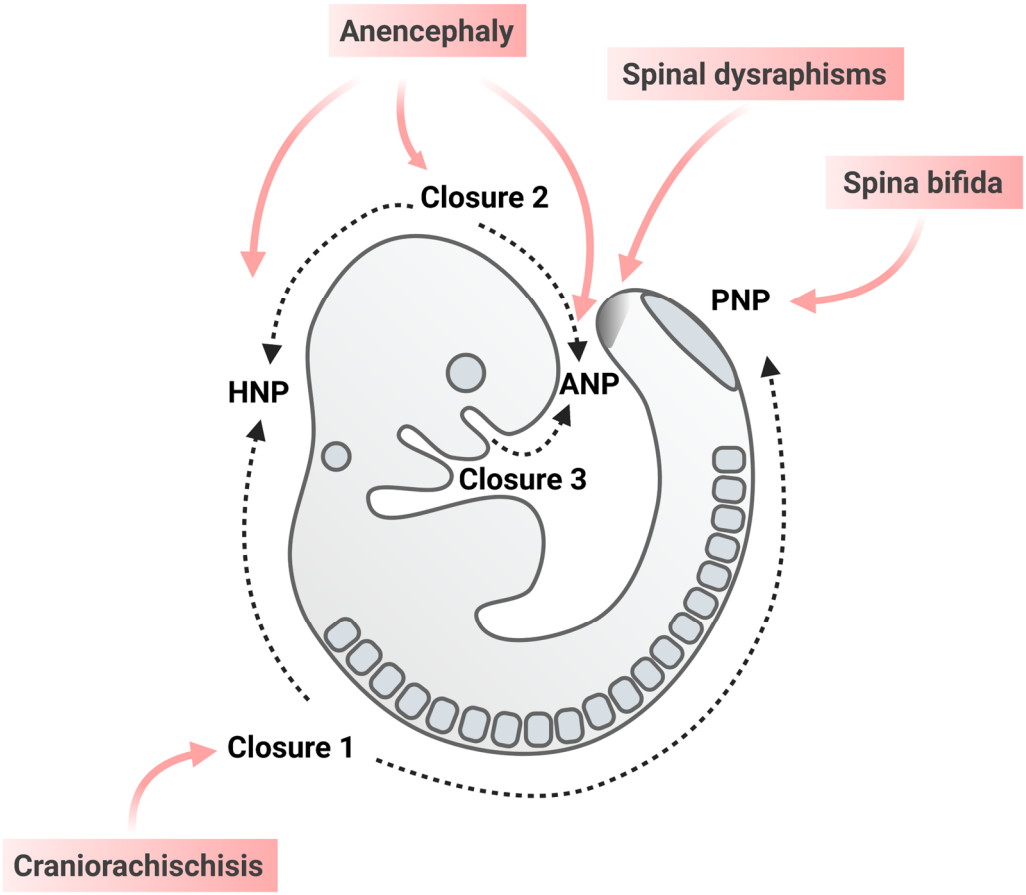

Figure 1.2. Neurulation and associated defects. Schematic of an E9.5 mouse embryo indicating the sequence of neurulation events (shown in black) and the origins of various neural tube defects (shown in red). Neural tube closure is sequentially initiated at the hindbrain-cervical boundary (closure 1), forebrain midbrain-boundary (closure 2) and rostral extremity of the forebrain (closure 3). Waves of closure

(indicated by dashed arrows) then spread from these points to seal the anterior neuropore (ANP; between closure 2 to 3), hindbrain neuropore (HNP; between 1 to 2) and posterior neuropore (PNP; between closure 1 and the 30th somite pair). The region of neural tube caudal to the PNP is formed by secondary neurulation (indicated by shaded tailbud area) through a process of canalisation. Failure to initiate closure 1 gives rise to craniorachischisis. Failure of closure 2 or 3, or zippering between them, leads to anencephaly. Failure of closure 1 to complete zippering along the spinal region, to entirely seal the PNP, produces spina bifida. Defects in secondary neurulation are likely at the root of spinal dysraphisms.

1.2.1.2 Neural tube defects

The complex morphogenetic mechanisms of neurulation have been shown to depend on over 300 genes in mice and 82 genes in humans, based on genetic knock-out and candidate association studies, respectively (Greene et al., 2009; Pangilinan et al., 2012; Wilde et al., 2014). Primary neurulation in humans takes place between the 18th and 28th day post-fertilisation and its failure results in serious congenital malformations, termed neural tube defects (NTDs) (Copp et al., 2013). The frequency of NTDs ranges between 0.5 and 2 per 1000 pregnancies globally, and their severity is highly dependent upon the position of the lesion along the AP axis (Figure 1.2) (Copp et al., 2015). Accordingly, failure to initiate closure results in the most severe form of NTD – craniorachischisis – consisting of an open neural tube along the entire AP axis of the embryo. Incomplete cranial closure leads to exencephaly, which progresses to anencephaly. Alternatively, a failed PNP closure can give rise to open spina bifida. Pathogenesis in these conditions involves failure of skeletal structures (e.g., skull, vertebrae) to form over the open neural tube and progressive degeneration of the neural tissue due to exposure to the amniotic environment. Consequently, craniorachischisis and anencephaly are pre- or perinatally lethal, while spina bifida is compatible with survival but associated with a range of neurological abnormalities. Lastly, there is a broad range of closed (skin-covered) spinal dysraphisms where the lowest segments of the spinal cord are tethered to adjacent

tissues. Based on their axial position and skin-covered nature, these conditions are thought to be caused by defects in secondary neurulation. Notably, these lesions are characterised by poor specification and spatial separation of neural and mesodermal tissues which indicates a possible NMP dysfunction (Copp et al., 2015).

1.2.1.3 Mechanisms of neural tube closure

1.2.1.3.1 Shaping the neural plate

Neural tube closure represents a paradigm of morphogenesis in the developing embryo since it is underpinned by a plethora of molecular, cellular and biomechanical processes happening in parallel (Nikolopoulou et al., 2017). Neural tube closure is initiated through the process of convergent extension, whereby the neural plate undergoes medio-lateral (ML) convergence and AP extension (Wallingford et al., 2002; Ybot-Gonzalez, Savery, et al., 2007). Convergent extension is mediated by the ML intercalation of cells across the midline which in turn depends on the function of the non-canonical Wnt/Planar cell polarity (PCP) pathway. Accordingly, mouse embryos carrying mutations in the PCP gene Vangl2 fail to initiate closure 1 and develop craniorachischisis, as the neural folds are too widely spaced to meet at the dorsal midline (Greene et al., 1998). Furthermore, live imaging studies have revealed that PCP signalling orchestrates cell intercalation through an intermediate step of multicellular rosette formation underpinned by the selective AP-oriented myosin IIB enrichment basally and contraction of cell junctions apically (Williams et al., 2014).

1.2.1.3.2 Bending of the neuroepithelium

Concurrently, the initially flat neural plate begins to form a midline V-shaped groove, called the median hinge point (MHP), causing its lateral sides (i.e. neural folds) to elevate (Moury & Schoenwolf, 1995). As neural tube closure moves caudally, two additional focal bending sites appear at the lateral regions where the

neuroepithelium first contacts the surface ectoderm; these are termed dorsolateral hinge points (DLHPs). In anterior spinal regions, neural plate bending is primarily mediated through the MHP, while at progressively posterior regions the relative contribution gradually shifts towards the DLHPs (Shum & Copp, 1996).

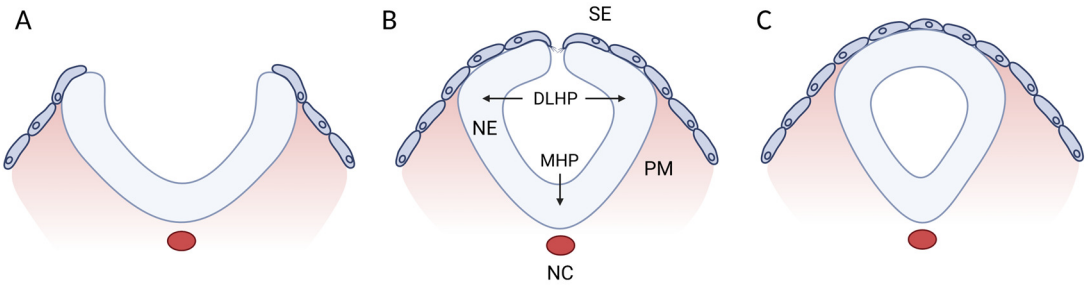

Figure 1.3. Morphogenetic events in spinal neural tube closure at E9.5. Schematic demonstrates cross-sectional view of the main steps in PNP closure. Primary neurulation at intermediate AP spinal levels includes (A) an initial elevation of the neural folds through the action of the median hinge point (MHP), (B) further bending at the dorsolateral hinge points (DLHP), and (C) eventual fusion of the contralateral layers of neuroepithelium (NE) and surface ectoderm (SE) dorsally. Additional abbreviations: PM, paraxial mesoderm; NC, notochord.

This AP divergence is well reflected in the spatial dynamics of the signalling pathways responsible for hinge point induction. For example, MHP formation has been shown to depend on Sonic hedgehog (Shh) signalling from the notochord, which is strongest anteriorly and gradually wanes posteriorly (Ybot-Gonzalez et al., 2002). Conversely, DLHPs are inhibited by BMP signalling from the SE, and require the action of the BMP-antagonist noggin secreted by the dorsal neural plate. In anterior spinal regions, strong Shh signalling represses noggin, thus preventing DLHP formation. Posteriorly, on the other hand, weakening of Shh permits noggin expression, thus leading to BMP repression and DLHP induction (Ybot-Gonzalez, Gaston-Massuet, et al., 2007). In accordance, notochordless embryos lack MHPs but are able to achieve spinal neural

tube closure through compensation by increased bending at the DLHPs (Davidson et al., 1999; Ybot-Gonzalez et al., 2002).

At the cellular level, neuroepithelial bending is often conceptualised as a widespread reduction in apical surface area. However, a growing body of evidence highlights the diversity of mechanisms underpinning such cell shape changes in different regions of the neural tube. In addition to the important role of apical constriction, cell shape in the pseudostratified neuroepithelium can be influenced by the localisation of the nucleus, which moves basally during the S-phase of the cell cycle and apically during mitosis (a process known as interkinetic nuclear migration). Unlike the rest of the neural plate (including the DLHPs) that demonstrates a random assortment of nuclear positions, MHP cells display a prolonged and synchronised S-phase which causes them to simultaneously adopt a wedge shape, thus elevating the neural folds (McShane et al., 2015).

In contrast, bending of the neural plate at lower spinal levels has been associated with actomyosin dynamics, rather than cell cycle regulation. For instance, disruption of actin turnover through mutations in cofilin 1 or pharmacological inhibition (jasplakinolide) results in stiffening of the neural tube and inability of neural folds to meet dorsally (Escuin et al., 2015). In addition, pharmacological inhibition of Rho kinase (Y27632) leads to PNP widening by preventing myosin-II recruitment and contraction apically (Butler et al., 2019). Surprisingly, mosaically deleting Vangl2 in as few as 16% of neuroepithelial cells was shown to be sufficient at preventing neural fold elevation in the final stages of PNP closure. Detailed assessment of these mutant embryos demonstrated that neuroepithelial cells normally facilitate bending through apical ML-oriented actomyosin localisation and ultimately polarised constriction in non-cell-autonomous PCP-dependent manner (Galea et al., 2018, 2021).

The importance of long-range biomechanical processes in neural tube closure was also highlighted through the discovery of a supracellular F-actin cable encircling the PNP at the surface ectoderm-neuroepithelium boundary of the neural fold tips (Galea et al., 2017). Laser ablations of the cable at the zippering point combined with tissue strain mapping then demonstrated that the cable biomechanically couples the

zippering point to the constricting caudoventral neuroepithelium; hence supplying the necessary force for the dorsal apposition of the neural folds.

1.2.1.3.3 Neural fold fusion

Following neuroepithelial extension and bending, the final and perhaps least understood step of neural tube closure consists of fusion of the dorsally apposed neural folds to establish epithelial continuity (Pai et al., 2012). During this process, tissue remodelling disrupts the originally continuous ectodermal layer of each neural fold to generate two separate epithelia: the closed neural tube covered by a layer of surface ectoderm. As in previously discussed morphogenetic processes, the mechanistic details of neural fold fusion also seem to differ along the AP axis. For example, fusion is initiated by neural cells in the forebrain, but surface ectoderm cells in the midbrain, hindbrain and spinal areas (Geelen & Langman, 1977, 1979). Furthermore, fusion sites are characterised by actin-rich cellular protrusions in the form of spike-like filopodia during early neural tube closure, and sheet-like lamellipodia at later stages. By virtue of their position, these protrusions appear to make the first contralateral contact between the neural folds. Notably, separate genetic ablations of Rac1 in the surface ectoderm and neuroepithelium revealed that protrusions originate specifically from the surface ectoderm and are in fact necessary for successful closure of the spinal neural tube (Rolo et al., 2016).

In a more recent study, high-resolution live imaging of PNP closure demonstrated that surface ectoderm cells at the zippering point selectively contract their caudal junctions giving rise to a semi-rosette configuration and bringing contralaterally positioned cells into close proximity, as a result (Molè et al., 2020). Interestingly, semi-rosette formation at the zippering point and successful spinal neural tube closure were shown to primarily depend on expression of the extracellular matrix (ECM) receptor subunit integrin β1 in the surface ectoderm (compared to the neuroepithelium). While the critical ligand for this cell-ECM interaction was not identified, transcriptomic and immunohistochemical analyses of ECM components

and integrin subunits expressed in the PNP suggested fibronectin as the most likely candidate. This study therefore revealed a vital previously unrecognised role for the ECM in neural fold fusion: potentially as a temporary substrate for cell anchorage and junction remodelling prior to the establishment of stable cell-cell adhesions. The final steps of cell-cell recognition and remodelling, on the other hand, have been shown to involve ephrinA-EphA interactions, but the underlying processes remain largely unknown (Abdul-Aziz et al., 2009; Holmberg et al., 2000).

1.2.2 Surface ectoderm

It has therefore gradually become apparent that despite being just a thin monolayer, the surface ectoderm is hugely important for successful neural tube closure. Surface ectoderm ultimately gives rise to the epidermis and associated glands, and it is first induced through a BMP signalling gradient during gastrulation. High levels of BMP signalling guide the ventral and lateral ectoderm towards the epidermal fate, while BMP antagonists secreted dorsally specify the neural ectoderm (Pla & Monsoro-Burq, 2018). The surface ectoderm then assists neural tube closure through a variety of signalling as well as biomechanical functions. These, for example, include the previously described regulation of DLHP formation through BMP signalling, where even a small fragment of surface ectoderm has been found to be sufficient (Ybot-Gonzalez et al., 2002). Concurrently, the surface ectoderm cell dynamics facilitate neural fold fusion by mediating the initial contact through cellular protrusions and propagating zippering through the formation of integrin-dependent semi-rosettes (Molè et al., 2020; Rolo et al., 2016).

Therefore, it is perhaps not surprising that numerous recent studies have found neural tube closure to be highly dependent upon precise regulation of epithelial identity in the surface ectoderm. Epithelial specification throughout neurulation and other developmental contexts is closely associated with members of the grainyhead-like (Grhl) family of transcription factors, such as Grhl2 and Grhl3. Strikingly, both loss and excess of Grhl2 or Grhl3 expression have been shown to lead to highly penetrant

spina bifida (De Castro et al., 2018b; De Castro et al., 2018a; Nikolopoulou et al., 2019). These transcription factors are expressed in the surface ectoderm from the beginning of neural tube closure and at later stages (E10) also appear in the hindgut (Auden et al., 2006; Gustavsson et al., 2007). However, the early appearance of defects in PNP closure, as well as tissue-specific deletion experiments, have indicated that spina bifida is largely arising through abnormalities in the surface ectoderm.

In particular, Grhl2-deficient surface ectoderm displays a partial transition into a neural identity, a disrupted actomyosin network, and failure to successfully oppose the anti-closure forces acting on the neural folds (revealed by recoil after laser ablations), hence leading to an overly wide PNP (Nikolopoulou et al., 2019). Conversely, excess Grhl2 expression results in a super-epithelial surface ectoderm, characterised by increased cell-cell adhesion and myosin activation, and a narrow PNP with apposed neural folds that fail to fuse. In this case, excessive upregulation of cell-cell adhesion molecules could hinder neural tube fusion by preventing the dynamic junction remodelling and neighbour exchange that is necessary for zippering. Surface ectoderm-related abnormalities have been less extensively studied in *Grhl3* mutant embryos. However, PNP morphology in null and hypermorph *Grhl3* mutants as well as the significant overlap in transcription targets between Grhl2 and *Grhl3*, suggest a similar mechanism (De Castro et al., 2018b; De Castro et al., 2018a).

1.2.3 Paraxial Mesoderm

With the exception of the dorsal side that is covered by surface ectoderm, the neural tube is otherwise surrounded by mesodermal tissues. The first stage of mesoderm specification takes place during gastrulation whereby the position of epiblast cells, and consequently the timing of their ingression through the primitive streak, determine the choice among diverse mesodermal fates (Stower & Srinivas, 2018; Tam & Behringer, 1997). Furthermore, position along the AP axis of the primitive streak translates into mediolateral position in the post-gastrulation embryo. In this

manner, ingression from the posterior to the anterior of the primitive streak successively gives rise to lateral plate, intermediate, paraxial and midline mesoderm (i.e., notochord). Lateral plate mesoderm generates the extraembryonic, cardiac and cranial lineages; intermediate mesoderm forms the urogenital system; and paraxial and midline mesoderm produce the axial skeleton and musculature fates (Kinder et al., 1999; Tam & Behringer, 1997). A second, more protracted stage of mesodermal specification takes place throughout axial elongation. In this process, the gradual incorporation of axial progenitors from the tailbud forms the paraxial mesoderm and notochord starting at the thoracic region and extending all the way to the posterior end of the embryo (Tzouanacou et al., 2009; Wymeersch et al., 2019).

Formation of this caudal segment of paraxial mesoderm begins with the mesodermal commitment of NMPs and constant migration of mesodermal progenitors into the posterior end of the presomitic mesoderm (PSM), laterally to the neural tube. A process of segmentation at the anterior PSM then periodically produces bilaterally symmetrical blocks of tissue (called somites) in an anterior-to-posterior direction, thus giving vertebrate organisms their characteristic body plan (Maroto et al., 2012). The periodicity of somitogenesis is regulated by waves of expression of so-called 'clock' genes, such as Hes1 and Hes7 in the mouse, that sweep along the PSM in a posterior-to-anterior direction (Pourquié, 2011). The arrival of each wave at the anterior end of the PSM coincides with the demarcation of a somite pair and the appearance of a new wave at the posterior end of the PSM. Genes from the Notch, Wnt and FGF signalling pathways also show such periodic patterns of expression in the PSM and are thought to interact with the segmentation clock, but the exact mechanistic details remain elusive (Pourquié, 2022).

Concurrently, somite size is regulated by opposing gradients of RA emanating anteriorly to the newly forming somite pair and Fgf8 from the posterior. A midpoint between these gradients is thought to define a threshold for segmentation, called the determination front (Diez del Corral & Storey, 2004; Dubrulle et al., 2001). Cells anterior to the determination front activate the transcription factor Mesp2 and become part of the budding somite pair, while cells posterior to the front are kept

undifferentiated for that cycle due to higher FGF activity (Oginuma et al., 2008; Saga, 2007; Sasaki et al., 2011). Mesp2 is considered instrumental for the morphogenetic processes that then produce an epithelial somite with a mesenchymal core. For example, Mesp2 promotes effective cell sorting and somite boundary formation by activating Eph-ephrin signalling at the AP somite borders (Barrios et al., 2003; Nakajima et al., 2006; Watanabe et al., 2009). Eph/Ephrin signalling in turn recruits integrin α5 which assembles a fibronectin matrix considered important for boundary consolidation (Girós et al., 2011; Jülich et al., 2009; Koshida et al., 2005). Following epithelisation, Shh signalling from the notochord induces the ventral part of the somite to form the sclerotome which later gives rise to vertebrae and ribs, while Wnt signalling from the surface ectoderm and neural tube patterns the dorsal part of the somite into the dermomyotome which eventually produces the back and body wall muscles and dermis of the back (Maroto et al., 2012).

The role of the paraxial mesoderm in the process of neural tube closure is less clearly understood. In the mouse midbrain region, expansion of the cranial mesoderm (likely mediated by the secretion and hydration of a hyaluronate-rich matrix) is thought to be responsible for the elevation and initially biconvex shape of the overlying neural folds (Zohn & Sarkar, 2012). This hypothesis is supported by the mesodermal defects and concomitant exencephaly observed in mouse embryos mutant for Twist – a basic helix-loop-helix transcription factor which is selectively expressed in the cranial mesoderm (but not the neural plate or surface ectoderm) (Chen & Behringer, 1995; Füchtbauer, 1995; Stoetzel et al., 1995). In the spinal region, on the other hand, the neural folds do not exhibit a biconvex elevation phase and mesodermal volume is much lower (Nikolopoulou et al., 2017). Furthermore, neural fold bending and the overall rate of spinal closure have been shown to unaffected by the removal of paraxial mesoderm (Alvarez & Schoenwolf, 1992; Ybot-Gonzalez et al., 2002). Interestingly, a recent study in zebrafish found that genetic ablation of the fibronectin matrix between the neural tube and paraxial mesoderm, and the resulting uncoupling of the two tissues leads to improved medial convergence (the morphogenetic equivalent of closure) of the neuroepithelium (Guillon et al., 2020).

These findings therefore raise the possibility that the paraxial mesoderm could even oppose closure in the spinal region.

1.2.4 Notochord

The other major mesodermal structure present during neurulation and axial elongation is the notochord, a defining characteristic of all chordates. The notochord (also called axial mesoderm or chordamesoderm) has a rod-like shape and runs along the AP axis of the embryo ventrally to the neural tube. The most anterior part of the notochord originates from cells that ingress through the anterior primitive streak during gastrulation, while the rest of the notochord derives from the node (Balmer et al., 2016; Tam & Beddington, 1987; Yamanaka et al., 2007). Mouse notochordal precursors initially migrate to the ventral midline of the embryo where they form the notochordal plate; an epithelium contiguous with the prospective gut endoderm (Jurand, 1974). Shortly after, the notochordal plate progressively ingresses in an anterior-to-posterior direction to leave the ventral surface and form the rod-like notochord internally. Being centrally located along both the DV and ML planes, the notochord is then ideally positioned to carry out its structural function as a transient axial skeleton, as well as its signalling role by secreting ligands that pattern the neighbouring neural tube, somites and gut endoderm (Corallo et al., 2015). For example, Shh signalling from the notochord has been shown to regulate neural plate bending by inducing MHP formation, while inhibiting DLHP formation (Smith & Schoenwolf, 1989; Ybot-Gonzalez et al., 2002). Accordingly, mouse embryos lacking this signalling function, due to Shh KO or node ablation (preventing notochord formation), fail to form a MHP but exhibit enhanced DLHPs and are therefore still able to complete neural tube closure. At later stages of development, the notochord becomes ossified and forms the nucleus pulposus of the intervertebral discs (McCann et al., 2012).

1.2.5 Endoderm

Endoderm arises from a subset of the cells that ingress through the anterior end of the primitive streak during gastrulation, immediately lateral to the prospective notochord. Nodal signalling plays a critical role in endoderm specification. Adoption of the endodermal fate at that stage is highly dependent upon Nodal signalling, with high levels of Nodal promoting endoderm specification and low levels specifying mesoderm (Spence et al., 2011; Vincent et al., 2003). Moreover, the timing of ingression is linked to AP identity with the first cells forming the foregut and subsequent waves giving rise to the midgut and hindgut (Franklin et al., 2008; Tam & Loebel, 2007). These migrating definitive endoderm progenitors were originally believed to displace the underlying visceral endoderm layer which mainly generates extraembryonic structures. However, it was later demonstrated that the definitive endoderm in fact intercalates with the visceral endoderm. As a result, the visceral endoderm was shown to contribute to the embryonic gut with varying degrees along the AP axis: 10% of foregut, 15% of midgut and 35% of hindgut (Kwon et al., 2008).

Following gastrulation, an elaborate morphogenetic programme converts the endoderm from an epithelium on the ventral surface of the embryo into the closed gut tube. This process is initiated when the endoderm invaginates at the AP extremities, thus forming the anterior intestinal portal and the caudal intestinal portal. These two portals then extend towards the middle of the AP axis of the body where the midgut folds ventrally, eventually forming a sealed gut tube running across the length of the embryo by E9 (Spence et al., 2011). Analogously to the neural tube, the gut undergoes convergent extension in a PCP-dependent manner which is required for successful gut tube closure and for the considerable elongation occurring afterwards (Cervantes et al., 2009; Wen et al., 2010). Concurrently, a combination of FGF, Wnt, BMP and RA signalling orchestrates distinct differentiation programs along the AP axis of the endoderm to produce the various segments of the gastrointestinal tract and many other organs such as the lungs, liver and pancreas (Zorn & Wells, 2007, 2009).

Interestingly, correct morphogenesis of the hindgut has been shown to biomechanically support the completion of spinal neural tube closure. This relationship was first illustrated through the Grhl3 hypomorphic mutant curly tail which exhibits an enlarged PNP at E10.5, leading to partially penetrant spina bifida and tail flexion defects (Gustavsson et al., 2007; van Straaten & Copp, 2001). As mentioned previously, Grhl3 shows a dynamic pattern of expression which encompasses the hindgut from approximately E10. In this regard, curly tail mutant embryos showed a reduction in cell proliferation in the hindgut, while maintaining normal proliferation in the neuroepithelium (Copp et al., 1988). The resulting growth imbalance between the two tissues was found to cause increased ventral curvature in the caudal region which mechanically opposed neural tube closure (Brook et al., 1991). This important role of Grlh3 in the gut endoderm was also confirmed by a subsequent hindgut-specific conditional deletion of Grhl3 which similarly gave rise to increased ventral curvature and late-arising spina bifida in 60% of mutant embryos (De Castro et al., 2018a).

1.3 Mechanisms of axial elongation

1.3.1 Cell rearrangements

Evidently, formation of the AP body axis is a highly protracted process that requires coordinated elongation of the neural tube, paraxial mesoderm, notochord and gut from the beginning of gastrulation until the end of somitogenesis. Axial elongation is mediated by a variety of mechanisms that are largely shared between these different tissues, but differ depending on the developmental stage and position along the AP axis (Mongera et al., 2019). In amniotes, the AP axis of the embryo is established with the extension of the primitive streak (Bénazéraf, 2019; Bénazéraf & Pourquié, 2013). The earliest stages of elongation of the embryo are then underpinned by convergent extension. Convergent extension consists of cell intercalation in the ML plane, causing cell displacement and consequently tissue elongation in the AP plane

(Mongera et al., 2019). In mesenchymal tissues, such as the mesoderm, cell intercalation is thought to be mediated through the action of polarised protrusions that apply traction and elongate cells mediolaterally (Huebner & Wallingford, 2018; Keller et al., 1992). Conversely, in epithelial tissues, intercalation has been thought to mainly take place through actomyosin-driven contraction of cell junctions leading to neighbour exchange (Bertet et al., 2004; Huebner & Wallingford, 2018). Nevertheless, the two mechanisms were more recently shown to also work in concert, as in the mouse neural plate, where protrusion-driven cell crawling occurs basally and junctional modification apically (Williams et al., 2014). In this first stage of axial elongation, convergent extension utilizes small but widespread cell rearrangements and is thus able to rapidly alter the shape of the embryo, without however changing its volume.

1.3.2 Volumetric growth

Later stages of axial elongation, on the other hand, are characterised by substantial volumetric growth (e.g., through the gradual incorporation of progenitors from the tailbud). This involves slower mechanisms, such as cell proliferation, cell growth and ECM deposition, and therefore takes place over a much larger timescale (Mongera et al., 2019). Volume changes are particularly apparent in amniote embryos, most likely due to the increased availability of nutrients. This growth is partly mediated by much higher rates of cell proliferation observed in these embryos (Bénazéraf et al., 2017; Steventon et al., 2016). Surprisingly, cell proliferation rates are not preferentially increased in the tailbud region (where they are thought to underpin NMP self-renewal), but are rather uniformly high in the entire caudal region up to the level of anterior PSM (Bulusu et al., 2017; Sambasivan & Steventon, 2021). Therefore, progenitors seem to maintain their proliferative potential after exiting the NMP zone.

Nevertheless, cell proliferation alone is not sufficient to drive tissue growth, as demonstrated in early cleavage-stage embryos, but needs to be combined with

increases in cell mass through biomaterial synthesis (Olivier et al., 2010). A striking example of cell growth is the vacuole-mediated cell swelling observed in the middle cell layer of the zebrafish notochord. ECM, secreted by the notochord's outer layer, plays a critical role in this process by providing a radial barrier and limiting dilation to the AP plane. AP-oriented dilation of vacuoles then drives notochord elongation, while the mechanical coupling of the notochord to neighbouring tissues by the ECM ensures symmetric growth of the entire body axis (Dray et al., 2013; Ellis et al., 2013). In amniotes, however, the smaller relative size of the notochord and delay observed in swelling indicate a less prominent role for this mechanism (Mongera et al., 2019; Stemple, 2005). Instead, notochord elongation in amniotes is more likely to depend on convergent extension (Sutherland et al., 2020).

1.3.3 Cell migration and motility

As cell proliferation and cell growth increase the size of the elongating body axis, a variety of cell movements continuously refine its shape. One category of such movements includes the long-range migration of committed progenitors from the tailbud into their target tissue. Accordingly, live imaging and DiI tracing studies of the mouse PNP have demonstrated an anteriorly directed stream of neural progenitors from the NMP-containing CLE into the dorsal neural folds (Molè, 2017). Posteriorly directed streams of neural and mesodermal progenitors have also been observed. However, this latter apparent motion was shown to be mirrored by the adjacent ECM, revealing that it represents passive posterior displacement of the entire tailbud region rather than active progenitor migration (Bénazéraf et al., 2010; Czirók et al., 2004; Zamir et al., 2006, 2008).

Generation and incorporation of axial progenitors is vital for body elongation, as demonstrated by inhibition of cell proliferation or removal of the progenitor region (Bénazéraf et al. 2010). Surprisingly, however, such interventions fail to immediately halt axial elongation in the short-term. This residual growth is instead mediated by an anterior-to-posterior increasing gradient of random cell motility (Bénazéraf et al.,

2010; Mongera et al., 2019). Live imaging studies in the chick found the posterior PSM to be in a fluid-like state, characterised by low cell density and high cell motility and mixing. Conversely, a gradual reduction in cell motility and mixing produces an increasingly dense and solid-like anterior PSM. Furthermore, mathematical simulations showed that high motility in the posterior PSM results in high levels of pressure (Regev et al., 2017). When combined with the constraints of ECM-mediated tissue coupling laterally and the solid-like PSM anteriorly, this pressure then gives rise to a posteriorly directed force, ultimately driving tissue elongation and tailbud displacement (Xiong et al., 2020).

1.4 Basement membrane composition and assembly

Complex morphogenetic processes, such as neural tube closure and axial elongation, and the elaborate three-dimensional tissue and organ structures they give rise to, would be impossible without the mechanical support of the ECM. The ECM is composed of a wide variety of proteins and polysaccharides, locally produced and secreted by embryonic cells since the earliest stages of development (Rozario & DeSimone, 2010). ECM macromolecules assemble into intricate networks by binding each other as well as an assortment of cellular receptors, thus forming the physical microenvironment within which cells reside (Theocharis et al., 2016). Accordingly, the ECM has been shown to provide a substrate for cell adhesion, migration and polarity, while also determining the physical properties (e.g., stiffness, elasticity) of each tissue as a whole (Trapani et al., 2017). Furthermore, an increasing number of research findings in the last few decades have shown the ECM to be much more than a passive scaffold, by demonstrating extensive ECM remodelling in response to environmental stimuli, as well as its participation in a diversity of biochemical processes. For example, the ECM was shown to control pH and hydration levels, and morphogen diffusion, in addition to directly regulating gene expression by binding cell-surface receptors (Mouw et al., 2014; Walma & Yamada, 2020). It has therefore

emerged as a central coordinator of cell survival, proliferation, differentiation and function. The ECM's multifaceted importance in human development and physiology is also highlighted by the range of genetic disorders resulting from mutations in ECM proteins (Järveläinen et al., 2009; Lamandé & Bateman, 2020; Pozzi et al., 2017).

The ECM's diverse roles are underpinned by its huge complement of different matrix components. In mammals, this "core matrisome" spans almost 300 proteins, including about 36 proteoglycans, 40 collagens and over 200 glycoproteins (Hynes & Naba, 2012). Different combinations of these ECM components then produce an almost infinite heterogeneity of matrices, tailored to the chemical and biophysical needs of the various tissues and developmental stages in which they are assembled. A specialised type of ECM that is crucial for normal development is the basement membrane (BM). BMs are thin (40–120 nm), strong and flexible ECM sheets present in all metazoans from the earliest stages of embryogenesis (Alberts, 2015). They are localised at the basal side of all epithelia and around individual muscle, fat, and Schwann cells, separating them from surrounding mesenchymal tissues, while also providing a mechanical link to them (Yurchenco, 2011). Basement membranes are predominantly made of two inter-connected sheet-like networks of laminin and collagen IV, respectively (Halfter et al., 2015). Facilitated by its cell-binding properties, the laminin network appears early during BM assembly and provides a nascent scaffold for the recruitment of additional ECM components. Assembly of the type IV collagen network is then thought to provide mechanical stability to the BM structure. In addition, BMs often include heparan sulfate proteoglycans (HSPGs), such as perlecan, that crosslink the two networks, as well as a range of other glycoproteins, like fibronectin, that modulate the BM's mechanical properties and receptor binding capabilities.

1.4.1 Laminins

Laminins are one of the most abundant components and critical organizers of BM structure, already present from the pre-implantation stage in mouse embryos. They

are large heterotrimeric glycoproteins, composed of an α, β and γ polypeptide chain. In vertebrates, there are five α, four β and three γ subunits, each encoded by a different gene, that variably combine to give rise to 16 distinct laminin isoforms (Theocharis et al., 2016). The structure of each laminin isoform resembles a cross: the long arm is formed through the twisting together of the chains' tails (C-termini) into a triple-helical coiled-coil domain, while the heads (N-termini) of the chains remain separate, each forming one of the three short arms (Walker et al., 2018). Laminins can self-assemble into a honeycomb-like network through co-operative interactions at the LN domains on the short arms (LeBleu et al., 2007). Conversely, the LG (globular) domain on the long arm of the molecule mediates interactions with cell-surface receptors (i.e., integrins, dystroglycan) that further refine the organisation of the laminin network (Alberts, 2015). Laminin then facilitates the recruitment of further BM components, such as type IV collagen.

1.4.2 Type IV collagen

Type IV collagen forms the second fundamental network of mature BMs. It is a triple-helical molecule composed of 3 α chains. While there are 6 distinct α chain-encoding genes in mammals, only three heterotrimers have been identified (α1α1α2, α3α4α5, α5α5α6). Of those, α1α1α2 is found in most BMs, from the earliest stages of development, while the other two variants only have specialised functions in certain mature tissues (Yurchenco, 2011). Type IV collagen is secreted from cells as a long (400 nm) protomer, consisting of an N-terminal 7S domain, a triple-helical collagenous domain and a C-terminal non-collagenous globular (NC1) domain. It is differentiated from fibrillar collagens (found in connective tissues) mainly through the existence of multiple bends along its collagenous domain that provide flexibility to the collagen molecule, and tensile strength to the BM as a whole (LeBleu et al., 2007). Similarly to laminin, type IV collagen is capable of self-assembly into a branching network. This is mediated by both the 7S and NC1 domains (producing

protomer tetramers and dimers, respectively), allowing formation of a stable collagen scaffold for the BM (Walker et al., 2018).

1.4.3 Nidogens and HSPGs

While laminin and type IV collagen represent the foundational scaffolds of the BM, a number of additional non-polymerizing ECM molecules provide collateral linkages and facilitate BM maturation. These, for example, include the small glycoproteins nidogen-1 and nidogen-2 (also known as entactins). Nidogens are encoded by different genes with low sequence homology but display a similar triple-globular domain structure (G1-G3), as well as significant functional redundancy (LeBleu et al., 2007). Nidogens bind to laminin through their G3 domain and collagen through their G2 domain, effectively bridging the two networks. In turn, large secreted HSPGs, such as perlecan and agrin, consolidate the connection of the BM to the cell surface by binding integrin and dystroglycan receptors on the one side and nidogen on the other (Walker et al., 2018). Unlike laminin and collagen, however, nidogens, perlecan and agrin are expressed at later stages of development and are not required for assembly of the BM. Instead, their role relates to stabilisation of the BM at late foetal and postnatal periods when mechanical stresses are likely higher (Yurchenco, 2011).

1.4.4 Fibronectin

Fibronectin is a large glycoprotein, consisting of two subunits covalently linked with disulphide bonds at their C-termini (Figure 1.4A). In mammals, both subunits are encoded by the same gene (*Fn1*), but alternative RNA splicing produces a variety of isoforms ranging from 230 kDa to 270 kDa in size (Schwarzbauer & DeSimone, 2011). Fibronectin is composed of multiple repeated domains interspersed by flexible polypeptide chains. Each subunit consists of 12 Type I repeats, 2 Type II repeats, and 15–17 Type III repeats (Zollinger & Smith, 2017). While the Type I and Type II repeats

have stable conformations maintained by intramodular disulphide bonds, the Type III repeats are 7-stranded β-barrels lacking such bonds and can therefore undergo conformational changes in response to mechanical stimuli (Schwarzbauer & DeSimone, 2011). These varied modules also contain multiple binding motifs that mediate interactions with collagen and cell surface receptors, such as integrins and syndecans. For example, integrins primarily recognise the arginine-glycine-aspartic acid (RGD) motif in domain III10 of fibronectin. Conversely, syndecans, which are a group of transmembrane HSPGs, use their glycosaminoglycan (GAG) chains to bind the heparin II region found in the 12th to 14th FN type III repeats (FNIII12-14) of fibronectin and are thought to act as co-receptors with integrins in cell–fibronectin interactions (Morgan et al., 2007; Schwarzbauer & DeSimone, 2011). Fibronectin is found in two forms: soluble plasma fibronectin which is secreted by hepatocytes and circulates in the blood, and cellular fibronectin which is first secreted as a soluble dimer by a range of cell types and is then crosslinked into insoluble fibrils through additional disulphide bonds (Alberts, 2015).

Fibronectin must be in its fibrillar state in order to carry out its functions in vivo. However, unlike laminin and type IV collagen which are capable of self-polymerisation, assembly of fibronectin into fibrils is instead a cell-mediated process (Figure 1.4B). Following secretion, fibronectin dimers are characterised by a compact conformation (stabilised by long-range interactions of the type III modules), which prevents polymerisation and maintains their soluble state (Schwarzbauer & DeSimone, 2011). Fibronectin fibrillogenesis is initiated upon binding to the integrin receptor. Receptor activation is then thought to induce integrin clustering and an associated focal increase in fibronectin concentration on the cell surface. Moreover, activated integrins mechanically link fibronectin to the internal actin cytoskeleton and stimulate cellular contractility. This linkage transmits tension to the fibronectin molecule inducing a conformation change and thus revealing a cryptic binding site. This allows association with other fibronectin molecules, first leading to the formation of small fibrils and eventually of extensive insoluble networks spanning developing tissues or even the entire embryo (Theocharis et al., 2016). Interestingly, the tension-dependent nature of fibronectin fibrillogenesis means that fibronectin

networks are assembled where they are mechanically needed (Alberts, 2015). Consequently, during morphogenesis fibronectin often forms the provisional scaffold upon which further ECM components are later recruited (Zollinger & Smith, 2017).

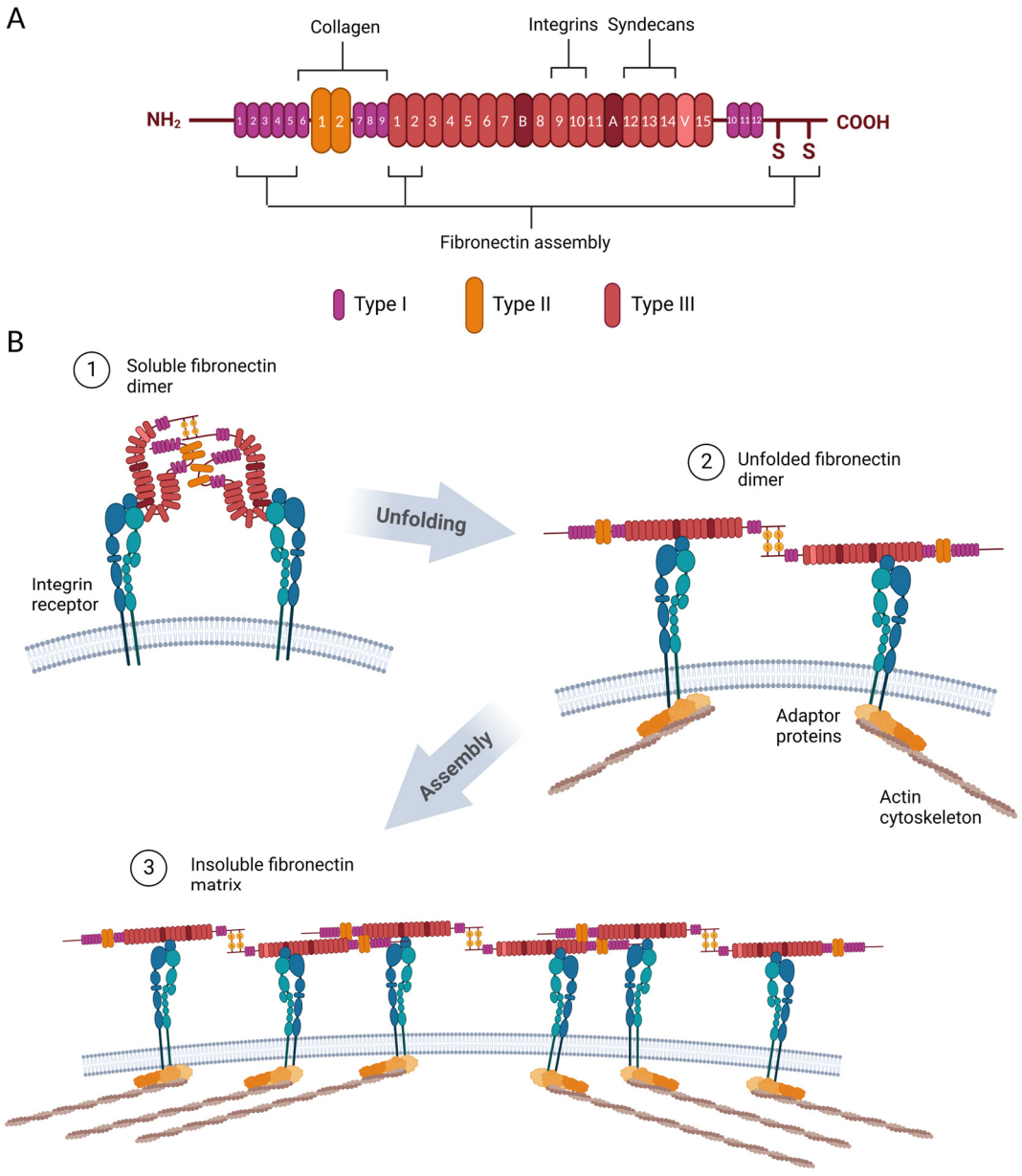

Figure 1.4. Fibronectin structure and fibrillogenesis.Fibronectin domain organisation. Each fibronectin subunits consists of 12 Type I repeats (purple), 2 Type II repeats (orange), and 15–17 Type III repeats (red). The latter include the EIIIA and EIIIB repeats (dark red) and V region (light red) that can be included or omitted in the

various fibronectin isoforms through alternative splicing. Domains mediating interactions with integrins, syndecans, collagen as well as other fibronectin monomers are indicated by brackets. (B) Main steps of fibronectin fibril assembly. The process begins when a compact soluble fibronectin dimer is bound by integrin receptors on the cell surface (step 1). Integrin activation then triggers the recruitment of intracellular adaptor proteins that connect integrins to the actin cytoskeleton, thus supplying the necessary tension for the unfolding of the fibronectin dimer and exposure of its fibronectin-fibronectin binding sites (step 2). Integrin activation also induces further clustering of integrins on the cell surface which brings multiple unfolded fibronectin dimers into proximity and facilitates the assembly of small fibrils and larger insoluble fibronectin networks (step 3).

1.5 Integrin receptors

1.5.1 Structure

Adhesion of cells to the ECM is primarily mediated through the integrin family of cell surface receptors. Functional integrin receptors are non-covalently linked heterodimers of an α and a β subunit (Humphries et al., 2006). Vertebrates express 18 α and 8 β subunits that variably combine to produce 24 different integrin receptors. Integrins can interact with a broad range of ECM proteins and the exact combination of (α and β) subunits determines the ligand-binding properties of the receptor. Hence, integrins can be grouped according to their ligand specificity. Each cell type displays a distinct signature of integrin receptors. However, the β1 subunit is ubiquitously expressed and can associate with 12 different α subunits, and is thus central to overall integrin function (Kechagia et al., 2019). Furthermore, unlike α subunits, the β1 subunit is translated in excess. Therefore, expression of α subunits represents the limiting step and dictates the type and amount of functional integrin receptors present on the cell surface.

Integrin subunits are type I transmembrane proteins consisting of a large extracellular domain, a single-pass transmembrane helix and a short cytoplasmic tail (Kechagia et al., 2019). Ligand specificity is in most cases jointly determined by the epitopes in the extracellular domains of both α and β subunits, while interactions with the cytoskeleton and a range of other intracellular proteins are primarily mediated by the cytoplasmic tail the β subunit. In fact, integrins were named after their important role as integrators between the external matrix and the internal cytoskeleton (Hynes, 2004). This linkage across the plasma membrane permits the bi-directional transmission of mechanical forces that regulate cytoskeletal organisation and matrix assembly (Harburger & Calderwood, 2009). In addition to their structural role, integrins have also been shown to operate as environmental sensors and transduce chemical signals (outside-in signalling) that regulate cell migration, polarity, differentiation and survival.

1.5.2 Activation

A key characteristic of integrin receptors is their ability to adopt a spectrum of physical conformations with different affinities for their target ligands. The mechanism of integrin activation was first characterised in the process of coagulation where integrin-mediated platelet aggregation must be strictly induced at the wound region but suppressed everywhere else in the circulation (Harburger & Calderwood, 2009). Nevertheless, precise spatial and temporal regulation of integrin affinities is now recognised as a common feature of many biological processes, including the coordination of cell migration and motility during morphogenesis.

Integrin activation (inside-out signalling) is initiated through the synergistic binding of the talin and kindlin adaptor proteins to the cytoplasmic tail of the β subunit (Kechagia et al., 2019). This binding event destabilises the close association between the cytosolic and transmembrane domains of the α and β subunits (Kim et al., 2012; Wegener et al., 2007). This conformation change eventually propagates to the extracellular domain of the receptor, converting it from a low-affinity bent state to a

high-affinity extended state by revealing a pocket for ECM ligand binding. Following ligand binding, talin associates directly with the actin cytoskeleton, as well as the actin-binding protein vinculin, thus allowing transmission of mechanical force between the ECM and cytoskeleton (Kadry & Calderwood, 2020). The tension then completes and stabilises integrin activation by further extending the receptor and minimising conformational fluctuations, consequently maximising binding affinity and bond lifetimes (Kechagia et al., 2019).

1.5.3 Mechanical functions

Following inside-out activation and ECM ligand binding, integrins cluster into nascent adhesions. This clustering and the force applied through the preliminary talin-mediated link to the cytoskeleton then trigger a gradual process of adhesion growth maturation, whereby numerous multi-protein complexes are recruited to the cytoplasmic tails of integrins (Goult et al., 2018; Kadry & Calderwood, 2020). The resulting mature focal adhesion (FA) assemblies include a network of 156 integrin-associated proteins, known as the integrin adhesome (Zaidel-Bar et al., 2007; Zaidel-Bar & Geiger, 2010). These proteins further consolidate ECM adhesion and cytoskeletal anchorage, while also initiating a variety of intracellular signalling cascades. For example, the initial tension applied on talin reveals a cryptic binding site for the actin-binding protein vinculin (Del Rio et al., 2009). Vinculin stabilises the integrin-actin linkage and permits distribution of mechanical forces through the cytoskeleton (Humphries et al., 2007). Kindlins, on the other hand, are thought to recruit the integrin-linked kinase (ILK) - now recognised as a pseudokinase – which forms the heterotrimeric IPP complex with PINCH and parvin (Fukuda et al., 2009; Lange et al., 2009; Vaynberg et al., 2018). The IPP complex is thought to have roles in actin bundling and mechanosensation. Another early event in adhesion maturation is the recruitment of paxillin, a scaffold protein that can interact with many different FA components (such as kindlin, vinculin, parvin and FAK) depending on its phosphorylation state (Rajah et al., 2019).

1.5.4 Signalling functions

In addition to its mechanical role, integrin-ECM binding can also activate a range of downstream signalling pathways that regulate cell polarity, migration, differentiation and survival (outside-in signalling). Central to this signalling function is the focal adhesion kinase (FAK). Shortly after integrin clustering, FAK is recruited at the site of the FA and partly activated through autophosphorylation, thus creating a binding site for the Src kinase. The FAK-Src complex then forms and becomes fully activated through cross-phosphorylation (Mitra et al., 2005). The FAK-Src complex is instrumental for the control of cytoskeletal dynamics, mainly through the regulation of Rho family small GTPases. In this way, the FAK-Src complex can stimulate actin polymerisation, actomyosin contractility and formation of stress fibres and cellular protrusions. These processes underpin dynamic cellular behaviours, such as cell shape changes and migration, but can also have more indirect outcomes relating to transcriptional regulation (Kechagia et al., 2019). Actin polymerization, for instance, can influence mechano-sensitive transcription factors, such as MRTFA and YAP/TAZ, while stress fibres can transmit tension to the nucleus thus causing chromatin remodelling and transcription factor entry (e.g., YAP/TAZ) through the nuclear pore (Chang et al., 2018; Elosegui-Artola et al., 2017; Kirby & Lammerding, 2018; Pawłowski et al., 2010; Tajik et al., 2016). It is therefore not surprising that integrin signalling has been implicated in the differentiation of various tissues, such as the mammary epithelium (Kadry & Calderwood, 2020). Concurrently, the FAK-Src complex also integrates integrin signalling with that of associated growth factor receptors and directly regulates cell cycle progression and survival through activation of the ERK and AKT pathways, respectively (Chiarugi & Giannoni, 2008; Yazlovitskaya et al., 2015).

1.6 The role of cell-matrix interactions in early development

1.6.1 Expression analyses

Evidently, cell-ECM interactions are intimately involved in almost all aspects of cellular function. As a result, the dynamic developmental processes of tissue growth, morphogenesis and differentiation all depend on the strict regulation of ECM composition, quantity and architecture. During embryonic development, the emergence of any epithelium is tightly associated with the assembly of a new BM. This phenomenon is already observed from the pre-implantation stage with the formation of a basement membrane between the epiblast and underlying primitive endoderm (Futaki et al., 2019). As the neural plate and surface ectoderm become specified from the ectodermal germ layer, two continuous BMs appear at the basal border of these epithelia with the paraxial mesoderm. Furthermore, after initiation of neurulation a third type of BM becomes deposited inside the elevating neural folds, where the dorsal neuroepithelium exchanges its contact from the mesoderm to the surface ectoderm (Martins-Green, 1988).

All the main BM components, including laminin, type IV collagen and fibronectin, were known to be expressed in mouse neurulation for decades (O'Shea, 1987; O'Shea & Liu, 1987; Sternberg & Kimber, 1986a, 1986b). However, our lab recently completed the first thorough characterisation of ECM ligands and integrin receptors present in spinal neural tube closure (Molè et al., 2020). This study included an RNA-seq analysis of the caudal region from E9.5 WT embryos for core matrisome genes. *Fn1* (coding for fibronectin) was found to be the most highly expressed matrisome gene, while the main collagen (Col4a1, Col4a2) and laminin (Lama5, Lamb1, Lamc1) subunits were also highly expressed. Moreover, immunostaining for these ECM proteins revealed that the various BMs surrounding the neural tube display significant heterogeneity in both physical architecture and molecular composition. The BMs underlying the surface ectoderm, for instance, are structurally mature from the beginning of spinal neural tube closure, while the BM at the neuroepithelium-mesoderm boundary is thin and discontinuous, and only matures towards the stage

of neural fold fusion. Furthermore, in terms of composition, the BMs separating the paraxial mesoderm from the surface ectoderm and neural tube were shown to contain laminins, collagen type IV and fibronectin. The dorsal BM separating the neural tube from the surface ectoderm, on the other hand, was rich in fibronectin but mostly devoid of laminin and collagen type IV.

This characterisation was then also extended to integrin subunits expressed in spinal neurulation, thus allowing deduction of the available dimeric integrin receptors and their respective ligand specificities (Molè et al., 2020). An analogous RNA-seq analysis of the caudal region of E9.5 WT embryos identified only 6 out of the 24 potential integrin receptors. The most prominent and highly expressed β1 subunit was predicted to combine with subunits α3 and α6 to form laminin receptors and subunits α5 and αv to form RGD (mainly fibronectin) receptors. The αvβ5 and α9β1 receptors were also detected, but the previous matrisome analysis had shown that their ligands vitronectin and tenascin-C are not actually expressed. Surprisingly, no collagen IV-binding integrins were expressed at this stage. Therefore, these findings jointly indicated that spinal neurulation is most likely facilitated by cell adhesion to laminin and/or fibronectin.

1.6.2 Genetic ablation studies

Studies utilising integrin and ECM gene deletions in mice have also been hugely informative in terms of the importance of cell-ECM adhesion in embryonic development. These studies have been complicated by the considerable functional redundancy and binding promiscuity of cell-ECM interactions (i.e., an integrin receptor can interact with various ECM ligands, and an ECM ligand can interact with various integrin receptors). Nevertheless, it has become apparent that different integrins and matrix ligands can have diverging roles in vivo based on their diverse transcriptional regulation, binding and polymerisation dynamics and activation of intracellular pathways (Kechagia et al., 2019). Gene knock-outs (KOs) can therefore

produce phenotypes ranging from early embryonic lethality to mild defects compatible with postnatal survival.

1.6.2.1 Integrin β1

Unsurprisingly, the most severe phenotype is produced by loss of the integrin β1 subunit which is found in half of all the integrin receptors and mediates binding to all the major ligand groups. Despite successfully initiating implantation into the endometrium, integrin β1-null mouse embryos already show collapsed blastocoeles at E4.5, and begin to degenerate leading to developmental arrest at E5.5 (Fässler & Meyer, 1995; Stephens et al., 1995). A recent study revealed that this defect results from loss of integrin β1's important role in epiblast maturation during the pre- to post-implantation transition. This includes inhibition of apoptotic pathways and suppression of actomyosin contractility in the basolateral domain of the epiblast, thus facilitating formation of a central lumen (Molè et al., 2021).

While demonstrating the fundamental role of integrin β1 in early embryonic development, such global KO approaches can mask potential defects arising at later stages of development. To circumvent the early embryonic lethality of the integrin β1 KO, our lab recently utilised a conditional integrin β1 deletion to assess the role of cell-ECM adhesion in the process of neural tube closure (Molè et al., 2020). These experiments utilised a *Grhl3*^{Cre} driver to specifically target the floxed *Itgβ1* gene (from approximately E8) in the surface ectoderm cells which mediate the initial contact between apposing neural folds in the spinal region (Rolo et al., 2016). The deletion led to arrest of PNP closure at the 20-somite stage, ultimately giving rise to spinal NTDs in 78% of mutant embryos (56% spina bifida, 22% tail flexion defect). These defects were shown to arise due to perturbation of the biomechanical and cell shape properties of the dorsal surface that are important for the propagation of neural fold zippering.

Another recent study, also utilising a conditional approach, highlighted a role for integrin β1 in axial elongation. This time a Foxa2mNE^{Cre} was used to delete *itgβ1* in the notochord and tailbud region from E8 (Guo et al., 2020). Shortly after the deletion, the notochord of mutant embryos showed impaired convergent extension, discontinuities across the AP axis and displacement (from the midline) in the ML and DV axes. Interestingly, the fibronectin sheath surrounding the notochord in WT embryos was lost in the mutants, while laminin was unaffected. Moreover, these early defects in notochord development eventually led to malformed vertebrae and truncated tails in affected embryos.

1.6.2.2 Laminin and related integrin subunits

Similar to integrin β1, global KO of the laminin β1 or γ1 subunit results in early embryonic lethality at E5.5 (Miner et al., 2004; Smyth et al., 1999). As α1β1γ1 and α5β1γ1 are the main laminin heterotrimers expressed during early development, loss of either (β1 or γ1) subunits completely prevents laminin assembly at this stage. As a result, mutant embryos show increased cell death and failure of cavitation, endoderm differentiation and Reichert's membrane formation. Conversely, a certain degree of functional compensation existing between the α1 and α5 laminin subunits means that removal of either one does not fully prevent laminin BM assembly and therefore results in comparatively milder phenotypes. For example, α1 mutant embryos are able to complete implantation but die by E7 due to lack of a Reichert's membrane (Miner et al., 2004). α5 mutant embryos, on the other hand, can survive even up to E17, at which stage they die due to dysmorphogenesis of the placental labyrinth (Miner et al., 1998). Interestingly, 60% of α5-null embryos also fail to complete cranial neurulation leading to exencephaly. In accordance, 43% of double mutants for the laminin-binding α3/α6 integrin subunits were shown to exhibit a variety of NTDs, ranging from exencephaly and craniorachischisis to a kinked tail (De Arcangelis et al., 1999). However, when the experiment was replicated in our lab, only a very small number of exencephaly cases were observed in double homozygotes (Carvalho and Copp, unpublished).

1.6.2.3 Type IV collagen and related integrin subunits

Despite its broad pattern of expression and central place among BM components, type IV collagen appears to be dispensable for early embryonic development. For instance, removal of the major collagen IV isoform α1(IV)2α2(IV) was found to be compatible with normal BM deposition and developmental progression up to E9.5 (Pöschl et al., 2004). However, Col4a1-null embryos die at E10.5-E11.5 due to failure of Reichert's membrane to maintain its structural integrity in response to the increased mechanical stress occurring at this stage. Furthermore, loss of individual collagen-binding integrin subunits, such as α10 and α11, is compatible with postnatal survival and only produces mild phenotypes relating to bone and tooth abnormalities (Bengtsson et al., 2005; Popova et al., 2007). These findings are in accordance with the lack of collagen-specific integrin receptors observed in neurulation stage embryos (Molè et al., 2020).

1.6.2.4 Fibronectin and related integrin subunits

Unlike laminin, fibronectin appears to be dispensable for the process of gastrulation. However, a growing body of evidence shows it has a crucial role in formation of the embryonic trunk during the neurulation stage. Loss of fibronectin results in arrest of AP axis formation, as well as heart and vasculature defects that lead to embryonic lethality at E8.5 (George et al., 1993). Furthermore, fibronectin-null embryos show a deformed anterior neural tube and lack notochord and somites. Interestingly, analyses of lineage markers showed that mesodermal precursors are successfully induced and migrate to the right regions of the embryo but are unable to condense into the notochord and somites (Georges-Labouesse et al., 1996). Therefore, it seems that fibronectin is particularly important for the correct morphogenesis of these structures, rather than their initial specification.

Gene ablation studies in mice have shown that fibronectin binding and assembly are primarily mediated by the α5β1 integrin, but αv-containing integrins can compensate

for some of these functions. Removal of either α5 or αv integrin, for example, does not prevent formation of the fibronectin network (Bader et al., 1998; Yang et al., 1993). Nevertheless, α5 and αv integrin receptors do exhibit differences in binding, mechanotransduction and signalling properties which ultimately give rise to divergent phenotypes in their respective mutants (Schiller et al., 2013; Strohmeyer et al., 2017; Wennerberg et al., 1996).

Accordingly, α5-null embryos display similar but milder defects to the fibronectin KO and survive up to E10-11 (Yang et al., 1993). Defects include reduced body length, a kinked neural tube, loss of posterior somites and vascular defects. Interestingly, head, brachial arches and anterior trunk form normally for the most part, including the notochord and the first 7-10 somite pairs that condense but fail to epithelialize (Yang et al., 1999). Thus, integrin α5β1 integrin function appears to be mostly redundant for the early formation of the anterior but not the posterior parts of the embryo. Conversely, ablation of the αv subunit produces an even milder phenotype without any mesodermal defects (Bader et al., 1998). Instead, 80% of mutant embryos die around E10.5 due to placental abnormalities, while the remaining 20% survive to birth but present a range of other defects, such as brain and intestinal haemorrhage and a cleft palate. Therefore, the role of αv integrin in formation of the AP axis during neurulation is fully compensated by α5 integrin.

Lastly, simultaneous removal of both α5 and αv integrins completely prevents assembly of a fibronectin network and consequently has a much bigger impact than either of the individual KOs (Yang et al., 1999). Surprisingly, however, the resulting phenotype is even more severe than that of the fibronectin KO, as the mesodermal germ layer is fully missing, and double-mutants die during gastrulation (at E7.5-8). Hence, α5 and αv integrins seem to jointly be fully responsible for assembly and adhesion to the fibronectin matrix, while also facilitating development through fibronectin-independent functions (likely relating to another ECM ligand or constitutive intracellular signalling).

In vitro studies have shown that α5β1 and αv-class integrins bind fibronectin and mediate its assembly through recognition of the RGD motif (Singh et al., 2010). In

order to further elucidate fibronectin binding and fibrillogenesis dynamics in vivo, mouse mutants were generated in which the aspartate residue of fibronectin's RGD motif was substituted with glutamate to generate an inactive RGE motif (Girós et al., 2011; Takahashi et al., 2007). Based on the previous in vitro research, these embryos (FN-RGE) were expected to recapitulate the severe Fn-null phenotype. Surprisingly, however, FN-RGE mutants were instead identical to the α5-null embryos, showing a largely normal fibronectin network and anterior trunk formation, but posterior truncation and vascular defects leading to lethality at E10. This unexpectedly mild phenotype was then taken as evidence that αv-class integrins can interact with fibronectin and mediate fibril assembly through a yet unrecognised (non-RGD) binding site (Takahashi et al., 2007).

To probe further into the contradiction between in vitro and in vivo findings and search for this new integrin binding site, a recent study used single-cell force spectroscopy to characterise integrin interactions with Fn-RGE, as well as a novel form of fibronectin (Fn-ΔRGD) completely lacking the RGD motif (Benito-Jardón et al., 2020). Their results demonstrated that while the RGE motif prevents α5β1 integrin binding, it does not affect αv-class integrin–mediated cell adhesion, thus explaining the mild phenotype of Fn-RGE mutant embryos. RGD-deficient fibronectin, on the other hand, completely lost its ability to bind both α5β1 and αv-class integrins. Furthermore, RGD-deficient mouse embryos (*Fn1*ΔRGD/ΔRGD) failed to assemble a normal fibronectin network (instead showing only abnormal syndecan-mediated fibrils) and closely resembled Fn-null embryos in terms of developmental defects. These experiments therefore demonstrated the essential role of fibronectin's RGD motif for integrin binding, fibrillogenesis and overall morphogenesis of the embryonic AP axis during neurulation. However, they also highlighted the need for conditional gene deletion approaches in order to effectively assess the significance of fibronectin-integrin interactions in specific processes, such as neural tube closure.

1.7 Thesis overview

The current thesis investigates two aspects of lower body development in the mouse embryo:

- The role of the ECM protein fibronectin in neural tube formation and axial elongation (Chapters 3 and 4)
- The role of the transcription factor Sox2 in NMPs and neural specification (Chapters 5)

Chapter 3 aimed to clarify the origin and functional significance of the various parts of the fibronectin network for posterior development by employing three separate conditional deletion strategies to remove fibronectin from different tissues. The recombination domains of the three Cre drivers were mapped using the mTmG reporter, and each set of mutant embryos was characterised in terms of morphology, fibronectin localisation, and related cellular processes. Grhl3^{Cre}-mediated ablation of fibronectin in the surface ectoderm was shown to give rise to spinal NTDs, while Cdx2^{Cre}-mediated ablation of fibronectin at the neuroepithelium-paraxial mesoderm boundary led to shortening and abnormal bending of the tail. Immunohistochemical analyses of the NTD-affected Grhl3^{Cre}; *Fn1*$^{fl/fl}$ embryos demonstrated that the importance of integrin-fibronectin adhesion in neural tube closure derives from its role in the dynamic remodelling of cell junctions at the fusion site that is required for neural fold zippering.

Chapter 4 sought to clarify how fibronectin in the neuroepithelium-paraxial mesoderm boundary ensures symmetric elongation of the tail by further characterising *Cdx2*^{Cre}; *Fn1*$^{fl/fl}$ mutant embryos. These analyses examined external embryo morphology, internal tissue structure and the cellular processes that underpin axial elongation. No deficits were found in cell proliferation and survival, or in mesodermal development, but the neural tube of mutant embryos exhibited abnormal undulation and detachment from the paraxial mesoderm. These findings

therefore indicated that fibronectin facilitates symmetric elongation by mechanically coupling the neural tube to the paraxial mesoderm.

Chapter 5 aimed to consolidate and extend previous research from our lab suggesting that, contrary to common assumptions, Sox2 is not expressed in NMPs or required for posterior development (Mugele, 2018; Mugele et al., 2018). Accordingly, the first part of this chapter utilised in situ hybridisation (RNAscope) studies to assess for Sox2 expression in NMP-harbouring regions and to validate the previously used *Sox2*^{CreERT2} line, while the second part included a genetic ablation of Sox2 in NMPs and subsequent examination of mutant embryos in terms of developmental progression, NMP function and genetic compensation. Overall, the results support a model whereby Sox2 is expressed only downstream of neural commitment but is not required for neural specification or axial elongation, as its function can be likely compensated for by the closely related transcription factor Sox3.

2. Materials and Methods

2.1 Mouse colonies

The following mouse lines were used:

- Inbred C57BL/6J wild type mice
- *Grhl3*$^{Cre/+}$ (Camerer et al., 2010)
- *T*$^{CreERT2/+}$ (Anderson et al., 2013)
- *Cdx2*$^{Cre/+}$ (Hinoi et al., 2007)
- *Sox2*$^{CreERT2/+}$ (Andoniadou et al., 2013)
- *Rosa26*$^{mTmG/mTmG}$ (Muzumdar et al., 2007)
- *Rosa26*$^{EYFP/EYFP}$ (Srinivas et al., 2001)
- *Sox2*$^{fl/fl}$ (Shaham et al., 2009)
- *Fn1*$^{fl/fl}$ (Sakai et al., 2001)

All lines were maintained on the C57BL/6 background. Mice were mated overnight and checked for a copulation plug the following morning which was designated as E0.5. All animal studies were performed according to the regulations of the UK Animals (Scientific Procedures) Act 1986 and the Medical Research Council's Responsibility in the Use of Animals for Medical Research (July 1993).

2.2 Tamoxifen administration

Tamoxifen (Sigma Aldrich, T-5648) was suspended in 100% ethanol at a concentration of 100 mg/ml. The solution was then diluted into corn oil (Acros

Organics, 10616051-500G) to a final concentration of 10 mg/ml. For all experiments where tamoxifen administration is indicated, pregnant females were injected intraperitoneally with 1 mg of tamoxifen per 20 g body weight (e.g., 100 µl of 10 mg/ml solution for a mouse weighing 20 g). The timing of tamoxifen administration for each experiment is described in the corresponding figure legend.

2.3 Embryo collection and storage

Pregnant females were sacrificed by cervical dislocation and the uterine horns were isolated between E8.5 and E12.5. The embryos were dissected out of the uterus on the stage of a Zeiss SV11 stereomicroscope. Embryos were dissected in Dulbecco's Modified Eagle's Medium (DMEM) containing 25 mM HEPES, supplemented with 10% heat-inactivated Foetal Bovine Serum (FBS) and pre-warmed to 37 °C. For each embryo, the somite number was recorded, and the yolk sac was isolated for genotyping. Subsequently:

1) Embryos intended for morphological analysis were imaged with a Leica MZ FLIII stereoscope with Leica DC500 camera.

2) Embryos intended for immunohistochemistry were rinsed in ice-cold phosphate-buffered saline (PBS) and fixed in 4% PFA (in PBS) (pH 7.4) from 2 h to overnight (depending on stage) at 4 °C. Embryos were then washed twice in PBS and stored in PBS with 0.1% sodium azide (to prevent fungal and bacterial growth) at 4 °C.

3) Embryos intended for RNAscope were rinsed in ice-cold RNase-free PBS and then fixed in 10% neutral buffered formalin overnight at room temperature. Embryos were then washed twice in PBS, dehydrated through a standard ethanol series and stored in 70% ethanol at 4 °C.

4) Embryos intended for quantitative real-time PCR (qRT-PCR) were rinsed in ice-cold RNase-free PBS. The tail was then isolated, snap frozen in dry ice and stored at -80 °C.

2.4 Genotyping

DNA was extracted from the yolk sac. Samples for DNA extraction were rinsed in PBS and stored at - 20°C. Each sample was incubated in 24 µl of DNA lysis buffer (Peqlab, 31-102-T) and 1 µl of proteinase K (10 mg/ml, Peqlab, 04-1071) at 55°C for 3 hours. Proteinase K was inactivated through incubation at 85°C for 45 minutes. 2 µl of the resulting solution was used for PCR genotyping (ThermoFisher, 18038018) according to the protocols listed below. Finally, PCR products were separated by electrophoresis in a 2% agarose gel.

Table 2.1. PCR reaction mix for genotyping.

Reagent	Stock concentration	Final concentration	Volume per sample
PCR buffer	10x	1x	5.0 µl
dNTP mix	2 mM	0.2 mM	5.0 µl
MgCl2	50 mM	1.5 mM	1.5 µl
Primer 1	40 µM	0.25 µM	0.3 µl
Primer 2	40 µM	0.25 µM	0.3 µl
Taq polymerase	5 U/µl	1 U	0.2 µl
DNA sample			2.0 µl
DNAse-free water			35.7 µl
Total			50.0 µl

2.4.1 Cre detection: Grhl3$^{Cre\ vs.\ +}$, T$^{CreERT2\ vs.\ +,}$ Cdx2 $^{Cre\ vs.\ +}$, Sox2$^{CreERT2\ vs.\ +}$

The reaction amplified a 500 base pair (bp) fragment of the Cre recombinase-coding sequence inserted into all four mouse strains. Genotyping was based on the presence or absence of this band product.

Primer 1 (forward): ACCCTGATCCTGGCAATTTCGGC

Primer 2 (reverse): GATGCAACGAGTGATGAGGTTCGC

Table 2.2. PCR cycles for Cre genotyping.

Step	Temperature	Duration	Number of cycles
Initial denaturation	94 °C	2 min	1
Denaturation	94 °C	30 s	30
Annealing	63 °C	30 s	
Extension	72 °C	45 s	
Final extension	72 °C	5 min	1
Final hold	4 °C	∞	1

2.4.2 Fn1$^{fl\ vs.\ +}$

Fn1^{fl} mice were created by flanking exon 1 of the *Fn1* gene with loxP sites inserted into the 5' untranslated region and intron 1 (Sakai et al., 2001). The reaction amplified both wild type (195 bp) and loxP-containing (240 bp) fragments of the gene.

Primer 1 (forward): CCGGACAACTTCTGGTCCT

Primer 2 (reverse): CCCAGGCACAGGACTGC

Table 2.3. PCR cycles for $Fn1^{fl\ vs.\ +}$ genotyping.

Step	Temperature	Duration	Number of cycles
Initial denaturation	94 °C	2 min	1
Denaturation	94 °C	30 s	10
Annealing	65 °C (-0.5 °C per cycle)	30 s	
Extension	68 °C	45 s	
Denaturation	94 °C	30 s	28
Annealing	60 °C	30 s	
Extension	72 °C	45 s	
Final extension	72 °C	5 min	1
Final hold	4 °C	∞	1

2.4.3 $Sox2^{fl\ vs.\ +}$

$Sox2^{fl}$ mice were created by inserting a loxP site upstream and downstream of the coding exon of the *Sox2* gene (Shaham et al., 2009). The reaction amplified both wild type (427 bp) and loxP-containing (546 bp) fragments at the 3' end of the gene.

Primer 1 (forward): TGGAATCAGGCTGCCGAGAATCC

Primer 2 (reverse, wild type): TCGTTCTGGCAACAAGTGCTAAAGC

Primer 3 (reverse, mutant): CTGCCATAGCCACTCGAGAAG

Table 2.4. PCR cycles for $Sox2^{fl\ vs.\ +}$ genotyping.

Step	Temperature	Duration	Number of cycles
Initial denaturation	94 °C	2 min	1
Denaturation	94 °C	30 s	29
Annealing	63 °C	30 s	
Extension	72 °C	45 s	
Final extension	72 °C	5 min	1
Final hold	4 °C	∞	1

2.5 RNA extraction

The caudal region (posterior to somite pair 14 at E9.5 and posterior to the hindlimb at E12.5) was isolated, washed in RNase-free PBS and snap frozen in dry ice. Samples were then stored at -80°C until processing. RNA was extracted using the RNeasy Mini Kit (Qiagen, 74104) and eluted in Sigma water. To remove any DNA contamination, samples were then DNase-treated using the Ambion RNA Kit (AM1906). RNA concentration was measured using a Nanodrop (ThermoFisher) and, based on the measurements, samples were processed for cDNA synthesis SuperScript™ VILO™ Kit (Thermo Fisher Scientific, 11756050). cDNA samples were stored at -20°C.

2.6 Quantitative real-time PCR

qRT-PCR was performed using the iTAQ Universal SYBR Green Supermix assay (Biorad, 1708884) on a CFX96 real-time PCR detection system (Biorad) and the data was analysed using the 2-ΔΔCT method. In total, four biological replicates were processed per genotype and three technical replicates per sample. Primers for Sox2, Sox3 and GAPDH were as previously reported (Adikusuma et al., 2017; Nikolopoulou

et al., 2019) and are listed below. The primers were validated on cDNA from wild-type mice, using a standard PCR, to ensure the resulting bands had the expected product size.

Table 2.5. Primer sequences for qRT-PCR.

Primer	Sequence (5' – 3')
Sox2 (Forward)	TTCGAGGAAAGGGTTCTTGCTG
Sox2 (Reverse)	CCTTCCTTGTTTGTAACGGTCCT
Sox3 (Forward)	AACCTAGGAATCCGGGAAGA
Sox3 (Reverse)	CGTAACTGTCGGGGTTTTGT
GAPDH (Forward)	ATGACATCAAGAAGGTGGTG
GAPDH (Reverse)	CATACCAGGAAATGAGCTTG

2.7 In situ hybridization by RNAscope

Embryos (fixed in 10% neutral buffered formalin and stored in 70% ethanol as described in section 2.3) were fully dehydrated by successive 30-minute incubations in 80% and 95% ethanol and two 45-minute incubations in 100% ethanol at room temperature. Embedding moulds were decontaminated with RNaseZap™ (ThermoFisher, AM9780). Embryos were then placed in embedding moulds and incubated in Histoclear for 30 minutes at room temperature, Histoclear for 30 minutes at 60°C and a Histoclear:Paraffin 50:50 mix for 30 minutes at 60°C. Next, embryos were incubated 3 times for 1 h in paraffin at 60°C. Finally, after a 4th change of paraffin, embryos were appropriately oriented for sectioning using forceps and the paraffin was allowed to solidify overnight at room temperature. Solidified blocks were stored in airtight plastic bags at 4°C until processing.

Subsequently, the embedded tissue was cut into 5 µm serial sections using a microtome and slices were mounted on Superfrost Plus slides (VWR). Slides were then air dried overnight and stored at room temperature. Sections were visually inspected using a Leica MZ FLIII stereoscope and slides containing the desired anatomical regions were selected for staining. In preparation for staining, the chosen slides were baked in a dry oven for 1 h at 60°C and then deparaffinised by incubating twice for 5 minutes in xylene and twice for 2 minutes in 100% ethanol at room temperature with agitation. Once dry, the sections were stained with the RNAScope® Multiplex Fluorescent V2 Assay (Cat.No. 323100) according to the manufacturer's (Advanced Cell Diagnostics) protocol. This assay employs 20 different custom-designed probe pairs against each target RNA molecule (Wang et al., 2012). The two probes in each pair hybridise in tandem to a target RNA region and jointly form a binding site for a preamplifier molecule. Each pre-amplifier has 20 binding sites for amplifier molecules, and each amplifier has 20 binding sites for fluorescently labelled probes. This strategy therefore achieves up to 8,000-fold amplification of signal, while the paired probe design minimises background staining (since it is very unlikely that non-specific hybridisation events will bring matching probes into juxtaposition). The following probes were used:

- RNAscope® Probe- Mm-T-O1 (Cat No. 538111)
- RNAscope® Probe- Mm-Sox2-C2 (Cat No. 401041-C2)
- RNAscope® Probe- Cre-C3 (Cat No. 312281-C3)

And fluorophores:

- Opal™ 520 Reagent Pack (PN: FP1487001KT)
- Opal™ 570 Reagent Pack (PN: FP1488001KT)
- Opal™ 690 Reagent Pack (PN: FP1497001KT)

Finally, fluorescent images were obtained with a Zeiss Observer microscope with a Hamamatsu Flash 4v3 camera using 20x/0.8 and 40x/1.3 dry objectives.

2.8 Whole-mount immunofluorescence

Following dissection, embryos were rinsed in PBS and fixed as specified in section 2.3. Embryos were then permeabilised in 0.1% Triton X-100 in PBS (PBT solution) for 1 h at room temperature and incubated overnight in 5% bovine serum albumin (BSA) in PBT blocking solution (after passing through a 0.45 µm filter) at 4°C. They were then incubated overnight with primary antibody diluted at the appropriate concentration (shown below) in 100 µl of fresh blocking solution at 4°C. For multiplex immunofluorescence experiments, primary antibodies raised in different species were combined in the same solution. Subsequently, embryos were washed 3 times for 1 h in blocking solution and then incubated with secondary antibody diluted at the appropriate concentration (shown below) in 100 µl of fresh blocking solution for 2 h at room temperature. For multiplex immunofluorescence experiments, secondary antibodies against different species were combined in the same solution. The secondary antibody solution also contained appropriately diluted DAPI (1:5,000) and phalloidin-568 (1:100) or phalloidin-647 (1:100) when needed. Embryos were then washed once in blocking solution and twice in PBT solution for 1 h (per wash) at room temperature. All incubation and washing steps were performed with gentle agitation. Immunostained embryos were stored at 4 °C in PBS with 0.1% sodium azide to prevent fungal and bacterial growth.

In preparation for imaging, immunostained embryos were mounted in a 4% agarose-coated dish filled PBS, using surgical suture needles (Ethicon, W2881). Mounting was performed by passing a curved needle first through the upper trunk of the embryo and then through the agarose at the angle that achieved the desired orientation for the embryo. Where a cross sectional view of the tissue was required, embryos were immobilised flat on their side by passing a needle through the upper trunk and agarose, and then manually cut transversely at the appropriate axial level with a razor blade. For the pictures shown in Figure 4.2E-F, where imaging of deeper tissues was required, embryos were imaged in 4% agarose-coated dishes filled with ScaleCUBIC-1 clearing solution (instead of PBS), made up of urea (25 wt% final concentration), Quadrol (25 wt% final concentration), Triton X-100 (15 wt% final concentration) and

dH2O (Susaki et al., 2015). Embryos mounted in agarose-coated dishes were imaged on a Zeiss LSM880 confocal microscope with a 10x/NA0.5 W-Plan Apochromat dipping objective (WD 3.7 mm), 20x/NA1.0 Plan Apochromat dipping objective (WD 2.4 mm) or 10x/NA0.3 EC Plan-Neofluar DIC dry objective (WD 5.2mm).

Table 2.6. Primary antibodies and stains.

Target	Host	Dilution	Supplier (Catalogue #)
Cleaved Caspase 3	Rabbit	1:100	Cell Signalling (9661)
E-cadherin	Rabbit	1:100	Cell Signalling (3195)
Fibronectin	Goat	1:50	Santa Cruz (sc-6952)
GFP	Chicken	1:100	Abcam (ab13970)
Integrin β1 (ligand-bound)	Rat	1:50	BD Pharmigen (553715)
Non-muscle Myosin HCII-B	Rabbit	1:100	BioLegend (909901)
Phospho-Histone H3	Rabbit	1:100	Merck Millipore (ab310177)
Phospho-Histone H3	Mouse	1:100	Cell Signalling (9706)
Sox2	Rabbit	1:100	Abcam (ab92494)
Sox2	Mouse	1:100	Abcam (ab79351)
Sox3	Rabbit	1:100	Abcam (ab183606)
Talin	Goat	1:100	Santa Cruz (sc-7534)
DAPI	-	1:5,000	Severn Biotech (30-45-01)
Phalloidin-568	-	1:100	ThermoFisher (A12380)
Phalloidin-647	-	1:100	ThermoFisher (A22287)

Table 2.7. Secondary antibodies.

Target	Host	Conjugate	Dilution	Supplier (catalogue #)
Chicken	Goat	Alexa Fluor 488	1:200	ThermoFisher (A-11039)
Goat	Donkey	Alexa Fluor 568	1:200	ThermoFisher (A-11057)
Mouse	Donkey	Alexa Fluor 405	1:200	ThermoFisher (A48257)
Mouse	Donkey	Alexa Fluor 488	1:200	ThermoFisher (A-21202)
Mouse	Goat	Alexa Fluor 488	1:200	ThermoFisher (A-11029)
Mouse	Goat	Alexa Fluor 568	1:200	ThermoFisher (A-11019)
Mouse	Goat	Alexa Fluor 647	1:200	ThermoFisher (A-21236)
Rabbit	Donkey	Alexa Fluor 405	1:200	ThermoFisher (A48258)
Rabbit	Goat	Alexa Fluor 488	1:200	ThermoFisher (A-11070)
Rabbit	Goat	Alexa Fluor 568	1:200	ThermoFisher (A-11011)
Rabbit	Donkey	Alexa Fluor 647	1:200	ThermoFisher (A-31573)
Rabbit	Goat	Alexa Fluor 647	1:200	ThermoFisher (A-21244)
Rat	Goat	Alexa Fluor 488	1:200	ThermoFisher (A-11006)

2.9 Image analysis

Images were cropped, rotated, max-projected, adjusted and analysed using the Fiji software (Schindelin et al., 2012). Adjustments consisted exclusively of brightness and contrast corrections, and these were applied equally across the images. Details of the various analyses performed are provided below.

2.9.1 Morphometric analyses

Measurements were performed on scale-calibrated images. Analyses of external embryo morphology (Figures 3.8-3.13, 4.1 and 5.3) included somite number, crown-rump length, body length (as well as separate trunk and tail length), PNP length and

width. Body length was measured by drawing along the dorsal midline of the embryo from the caudal end of the forebrain to the caudal extremity of the body axis using Fiji's Freehand line tool. For separate tail and trunk measurements, the caudal end of the hindlimb bud was considered as the border between the trunk and tail. Internal tissue measurements (Figure 4.3) included the length and width of the last fully formed somite pair, and width of neural tube walls at the same antero-posterior level. These dimensions were measured at the dorso-ventral midline of these tissues, and were averaged for the left and right somites and neural tube walls, respectively. Cell shape analyses (Figures 3.22-3.24) assessed cell length, width, area and orientation in the dorsal midline of the surface ectoderm. For this analysis, embryos were immunostained for ZO-1 and cells in the dorsal midline (area indicated in figures) were manually segmented based on max-projected images using the Polygon Selection tool. Cell area was then directly calculated based on cell border outlines, while cell length, width and orientation (angle to antero-posterior axis of the embryo) were calculated based on the Fit Ellipse function.

2.9.2 Immunofluorescence intensity analyses

Quantification of fibronectin staining at the dorsal midline of the surface ectoderm-neuroepithelium (SE-NE) boundary (Figure 3.15) was performed on cross sections immediately anterior to the PNP fusion site by drawing a 30 µm-long line (with sufficient thickness to encompass the entire BM) across the SE-NE BM midline and measuring mean grey values in Fiji. These values were normalised to bilaterally averaged fluorescence intensity of the neuroepithelium-paraxial mesoderm (NE-MES) BM, calculated by similarly measuring mean grey values along 30 µm-long lines at the dorsalmost part of these BMs. Quantification of integrin β1 staining at the fusion site (Figure 3.19) was performed on max-projected images by measuring mean grey values within a 30 µm x 20 µm rectangular selection of the recently fused dorsal midline. This was normalised to the fluorescence intensity in a laterally adjacent region of SE, calculated by measuring mean grey values within a 30 µm x 20 µm rectangular selection 50 µm lateral to the dorsal midline.

2.9.3 Cell division and cell death analyses

These analyses were based on whole-mount immunostaining for the mitosis marker phospho-histone H3 (pHH3) and the apoptosis marker cleaved caspase 3 (CCasp3). The frequencies of mitosis and apoptosis were then primarily determined by manually counting pHH3-positive cells and CCasp3-positive loci and normalising those counts to the surface area of the region examined (measured with the Polygon Selection tool). For Figure 3.20, where these analyses focused on the surface ectoderm overlying the neural tube, counting of pHH3-positive cells and CCasp3-positive loci was performed on an optically resliced cross-sectional view of the entire recently fused region to easily distinguish between staining in the surface ectoderm and underlying neuroepithelium. In Figures 4.4 and 5.4, mitosis rates were determined by counting pHH3-positive cells in 3 random optical coronal sections (per embryo) of the areas indicated in the figure and normalising to tissue area. Normalised values from the 3 sections were averaged for each embryo. Finally, in Figure 4.4, the pattern of CCasp3 staining did not allow counting of individual foci, so the extent of apoptosis was instead quantified by measuring fluorescence intensity (mean grey values) across max-projected images of the tail region and subtracting background intensity.

2.9.4 Fate choice analyses

To determine the relative frequency with which NMPs colonised the neural tube versus the paraxial mesoderm, and how it is affected by loss of Sox2 (Figure 5.5), EYFP-positive and EYFP-negative cells were manually counted in 3 random optical coronal sections (of the regions indicated in the figure) per embryo. Cell segmentation was facilitated by phalloidin and DAPI staining. The fractions of EYFP-positive neural and mesodermal cells (as proportions of total neural and mesoderm cells) were respectively averaged across the 3 sections and a Neural/Mesodermal fraction ratio was calculated for each embryo (thus revealing the balance between

the two fates and allowing comparison of these ratios between mutant and control embryos).

2.10 Statistical analysis

Statistical analysis and graphing were performed in GraphPad Prism 8 software. The normality of the data was assessed by D'Agostino-Pearson test. Where significant deviations from normality were detected, the data was analysed using non-parametric tests. For all conditional gene deletions, the observed frequency of the various genotypes was compared to the expected Mendelian ratios by Chi-square test. The incidence of NTDs and tail defects between genotypes was compared using Fisher's exact test. Comparison of morphological measurements (e.g., somite number, body length) between mutants, heterozygotes and controls at E12.5 was performed by one-way ANOVA with post-hoc Dunnett's test. Comparison of morphological measurements (e.g., somite number, body length, PNP dimensions) between mutants and controls at E9.5 and E10.5 was performed by unpaired, two-tailed Student's t-test. For *Grhl3*^{Cre}*; Fn1*$^{fl/fl}$ mutants and controls, PNP dimensions over somite number were also analysed using linear regression. qRT-PCR data was statistically analysed by unpaired, two-tailed Student's t-test with Holm-Sidak multiple testing correction. Finally, comparisons of all immunofluorescence-based parameters (including fibronectin and integrin β1 staining intensity, mitosis and apoptosis rates, cell shape, NMP cell fate and internal tissue measurements) were performed by Mann-Whitney test (non-parametric equivalent to unpaired Student's t-test). The statistical tests used in each experiment are also described in the corresponding figure legend and P-values are shown in the figures. P-values below 0.05 were considered statistically significant.

2.11 Other Software

Schematics were created with BioRender.com and figures were assembled using Microsoft PowerPoint.

3. The role of fibronectin in neural tube closure

3.1 Introduction

3.1.1 Integrin β1 facilitates spinal neural tube fusion

Studies genetically targeting ECM ligands and integrin receptors have provided ample evidence for the importance of cell-matrix interactions in the successful development of the embryo throughout the stage of neurulation (De Arcangelis et al., 1999; Girós et al., 2011; Takahashi et al., 2007; Yang et al., 1993). Prompted by this research, our lab decided to investigate the potential role of ECM more specifically in the process of neural tube closure. In order to counteract the considerable functional redundancy that exists between ECM components and integrin receptors, this previous study focused on the integrin β1 subunit which is capable of associating with 12 different α subunits and thus mediates adhesion to all major ligand groups (Molè et al., 2020). Furthermore, the early embryonic lethality known to result from global integrin β1 ablation necessitated the use of a conditional Cre/loxP-based approach (Fässler & Meyer, 1995; Stephens et al., 1995).

Initial in situ hybridisation and immunofluorescence analyses in wild type embryos revealed that integrin β1 is significantly upregulated and activated at the site of dorsal neural fold fusion, implying that it might have an important function there. Therefore, two strategies were used to separately target the two tissues making up the dorsal neural folds: a Cre (recombinase) under the control of the *Grhl3* promoter targeting the surface ectoderm (as well as a few neuroepithelial cells), and a Cre under the control of the Pax3 promoter targeting the dorsal neuroepithelium (as well as a few surface ectoderm cells). The *Grhl3*^{Cre}-mediated deletion completely abolished integrin β1 expression at the fusion site and gave rise to spinal NTDs in 78% of mutants (56% spina bifida, 22% tail flexion defect). The Pax3^{Cre}-mediated approach, on the other hand, left the focal integrin upregulation unaffected and led to spinal NTDs in only 23% of mutants (9% spina bifida, 24% tail flexion defect).

These results therefore demonstrated that integrin β1 function is indeed essential for spinal neural tube closure and it is mainly mediated by cells of the surface ectoderm (most likely at the fusion site). In order to then determine the mechanism through which loss of integrin results in NTDs, a series of downstream processes and pathways were assessed in integrin β1 mutants (Molè et al., 2021). Actomyosin assembly, cell proliferation and survival were shown to be unaffected. There were, however, significant differences in the biomechanical and cell shape properties of the surface ectoderm across the dorsal midline. These included a failure of cells at the fusion site to remodel their junctions and form semi-rosettes, which are thought to be important for zippering propagation (Zhou et al., 2020). It was thus concluded that integrin β1 is required for neural tube closure because of the mechanical cell-ECM linkage it provides; allowing contralateral cells at the fusion site to establish a common adhesion to the underlying matrix, become juxtaposed and facilitate zippering propagation.

3.1.2 The case for fibronectin as the main integrin target during fusion

An important next step is to identify the specific ECM ligand(s) bound by integrins during this process. In that regard, a number of observations from previous expression analyses of ECM ligands and integrin subunits collectively suggested fibronectin as the most likely integrin partner (Figure 3.1) (Molè, 2017; Molè et al., 2021). For example, RNA sequencing of the caudal region from E9.5 WT embryos indicated that while the main collagen and laminin subunits are present, *Fn1* is the most highly expressed matrisome gene (Figure 3.1A). An analogous RNA sequencing analysis of integrin subunits allowed inference of available alpha-beta subunit combinations and their respective ligand specificities (Figure 3.1B, C). This revealed the presence of fibronectin (α5β1, αvβ5) and laminin receptors (α3β1, α6β1), but no collagen receptors in this region. Furthermore, immunostaining showed that fibronectin localises at the basement membrane between the dorsal neuroepithelium and overlying surface ectoderm (Figure 3.1E, arrows), while laminin is largely absent from the dorsal midline (Figure 3.1F, arrows). This is a critical

distinction since the dorsal midline is the area where integrin β1 is most highly expressed and activated (Figure 3.1D, arrow), and where cellular defects are observed when integrin β1 is deleted. Fibronectin is therefore well-positioned to interact with integrin β1 in this functionally important region, while laminin is not. Lastly, is situ hybridisation demonstrated that the fusion site upregulation observed for integrin β1 is also mirrored by the fibronectin-specific α5 subunit, but not the laminin-specific α3 and α6 subunits.

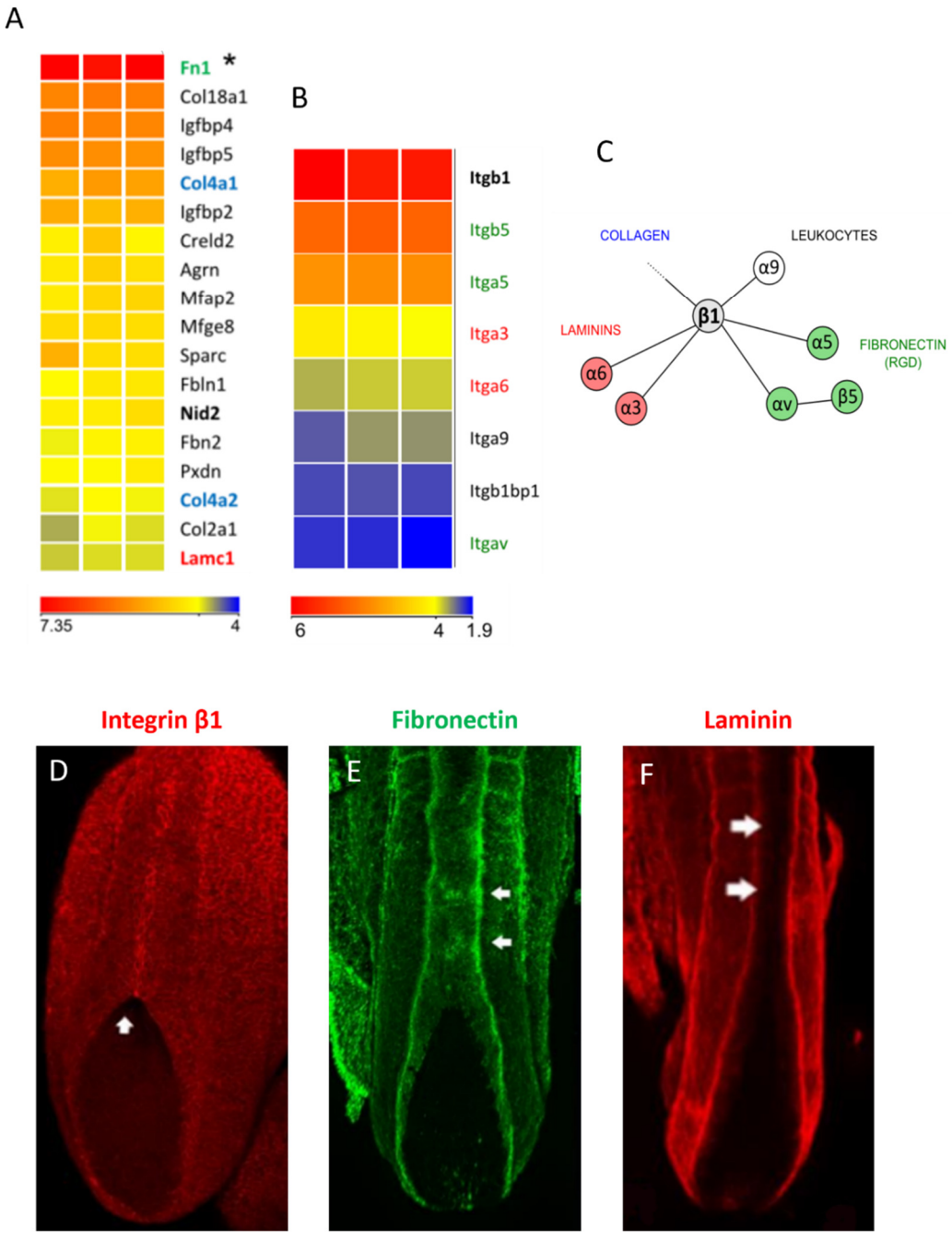

Figure 3.1. Previous expression analyses of ECM ligands and integrin subunits during spinal neural tube closure. (A) RNA sequencing analysis of the caudal region from E9.5 WT embryos for core matrisome reveals *Fn1* is the most highly expressed matrisome gene. The main collagen (*Col4a1*, Col4a2*)* and laminin (*Lamc1*) subunits are also highly expressed. (B) Analogous RNA sequencing analysis of the caudal region for integrin genes reveals subunit availability. (C) Integrin β1 can associate with α5 or αv to bind fibronectin (green), and α3 or α6 to bind laminin (red). No collagen-binding subunits are expressed. (D-F) Maximum intensity projections of the caudal region of E9.5 WT embryos immunostained for integrin β1 (D), fibronectin (E) and laminin (F). Unlike laminin, fibronectin localises at the dorsal midline (white arrows) where interaction with integrin β1 is most likely to occur. Adapted from (Molè, 2017).

Altogether, these previous observational findings collectively provided a strong case for the involvement of fibronectin in the process of neural fold fusion. Prompted by this research, the current project therefore sought to directly evaluate this potential role of fibronectin, and to further delineate the developmental mechanisms underlying the requirement for cell-ECM adhesion in spinal neurulation and axial elongation as a whole. To that end, this study adopted a complementary approach (to the previous integrin β1 cKO), by genetically ablating fibronectin and assessing its impact on embryonic development. Earlier studies have been unable to determine fibronectin's role in the formation of lower spinal segments due to the axial truncation and early embryonic lethality resulting from its complete removal (George et al., 1993; Georges-Labouesse et al., 1996). These severe defects presumably arise due to the many important roles of this key ECM ligand across the embryo (including the developing cardiovascular system). The present study has therefore opted for a conditional approach in order to precisely target the deletion to the stages and tissues of interest, and hence differentiate between fibronectin's various functions.

Nevertheless, even a conditional approach is complicated by the counterintuitive pattern of fibronectin expression and localisation observed in this context. Previous

situ hybridisation experiments have revealed that, in the caudal part of the embryo, *Fn1* is mainly expressed from the paraxial mesoderm flanking the neuroepithelium (Figure 3.2A) (Molè, 2017). Interestingly, a small locus of expression has also been observed at the site of neural fold fusion (Figure 3.2A-vi, black arrow). This could originate from the surface ectoderm or neuroepithelium, and is highly reminiscent of the focal integrin β1 upregulation that is also observed in that area. Conversely, immunostaining analyses have shown that fibronectin protein localises at the mesoderm-neuroepithelium, mesoderm-surface ectoderm and neuroepithelium-surface ectoderm interfaces (Figure 3.2C, D). Fibronectin presence in the first two of these BMs is in accordance with the observed *Fn1* transcription in the adjacent mesoderm. The presence of fibronectin between neuroepithelium and surface ectoderm, on the other hand, is highly surprising given that both of these tissues are largely negative for *Fn1* mRNA. This latter fibronectin layer could in theory derive from the focal fibronectin upregulation observed at the fusion site, but this seems very unlikely given the minuscule size of this transcription locus. An alternative, although not mutually exclusive explanation, is that fibronectin is remotely produced by a different tissue, such as the paraxial mesoderm. It could then passively diffuse or be actively transported towards the dorsal midline of the embryo where it is assembled into a network by neural and/or surface ectoderm cells. Indeed, fibronectin has been known to often polymerise away from the tissues where it was originally secreted (Almeida et al., 2016). It is also worth noting that the intriguing fibronectin enrichment observed dorsally is particularly marked over the recently fused spinal neural tube (and gradually dissipates rostrally), thus further supporting the hypothesised role of fibronectin in the process of neural fold fusion.

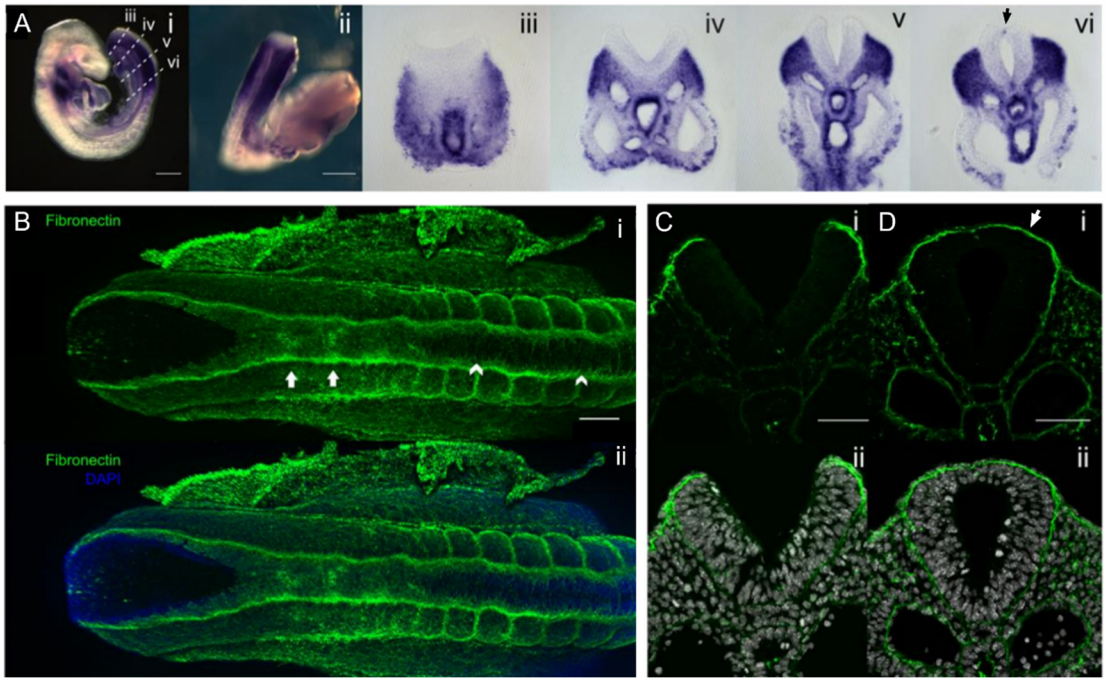

Figure 3.2. Previous expression analyses of fibronectin during spinal neural tube closure. (A) In situ hybridisation for Fn1 in E9.5 WT embryos, shown in whole-mount (A-i, ii) and cross sections (A-iii, iv, v, vi). Fn1 is mainly transcribed by the paraxial mesoderm, but significant upregulation is also detectable at the fusion site (A-vi, black arrow). (B-D) Fibronectin immunostaining in E9.5 WT embryos, shown in whole-mount (B) and cross sections (C, D). Fibronectin forms a dense BM over the recently fused neural tube (B-i, D-i, white arrows) and dissipates further rostrally (B-i, white arrowheads). Adapted from (Molè, 2017).

3.1.3 Fibronectin deletion strategy

Based on the aforementioned integrin β1 ablation and fibronectin expression studies, it was hypothesised that the fibronectin BM between the surface ectoderm and neuroepithelium is involved in the process of neural fold fusion. Furthermore, genetic ablation studies of fibronectin and associated integrin subunits strongly suggest the existence of additional roles for fibronectin in the formation of the neural tube, somites and notochord and thus axial elongation altogether. However, the

origin of fibronectin found in the various BMs surrounding the neural tube remains unknown.

In order to clarify fibronectin's expression and trafficking dynamics, and to determine which aspects of its localisation are actually important for spinal neurulation, a three-pronged strategy was designed to ablate fibronectin in a variety of relevant tissues. For this purpose, *Fn1*$^{fl/fl}$ mice were crossed with three different Cre driver lines, selected on the basis of previous lineage tracing data. Firstly, the previously mentioned constitutive *Grhl3*^{Cre} was selected to delete fibronectin from the surface ectoderm (Camerer et al., 2010). This Cre is known to reliably target the surface ectoderm from E8.5, while also recombining a fraction of neural, mesodermal and hindgut cells at later stages (De Castro et al. 2018a; Gustavsson et al. 2007; Molè et al. 2020). *Grhl3*^{Cre} would therefore effectively target the small fibronectin expression locus at the neural fold fusion site, if that originates from cells of the surface ectoderm.

Secondly, a tamoxifen-inducible *T*^{CreERT2} was chosen to ablate the main source of fibronectin in the paraxial mesoderm (Anderson et al., 2013). As T is already expressed during gastrulation, the inducible version of this Cre allows recombination of the great majority of paraxial mesoderm cells (and a smaller proportion of neural cells) in posterior segments of the embryo, while circumventing the axial truncation that would have likely resulted from the constitutive version of this Cre.

The third conditional approach employed consisted of a constitutive *Cdx2*^{Cre} (Hinoi et al., 2007). While very little published data was available on the recombination pattern of this Cre in early development, it was thought to target the entire caudal region of the embryo from E8.5. Although the relative spatial specificity conferred by the first two lines (*Grhl3*^{Cre} and *T*^{CreERT2}) could be valuable in dissecting the differential contributions of various tissues, it could also prove disadvantageous if remotely produced fibronectin turns out to diffuse through the tissues and compensates for the lack of expression in distant regions. The *Cdx2*^{Cre} was therefore expected to mitigate this possibility with a more widespread deletion - including the fusion site expression locus, irrespectively of its origin.

3.2 Results

3.2.1 Lineage tracing of selected Cre lines

While the recombination domains of *Grhl3*^{Cre} and *T*^{CreERT2} are relatively well-characterised, this information is still mostly lacking for *Cdx2*^{Cre}. Furthermore, previous lineage tracing studies performed for the three Cre drivers have used different reporter lines, tamoxifen administration protocols and visualisation techniques, and have focused on disparate embryonic stages and regions. As a result, it was deemed necessary to accurately assess the efficiency and specificity of each Cre in the context of spinal neurulation using a standardised protocol and thus facilitate direct comparison between the different fibronectin ablation domains and corresponding phenotypes. For this assessment, each Cre driver was crossed with the *Rosa26*$^{mTmG/mTmG}$ reporter line (Muzumdar et al., 2007). Consequently, all resulting embryos harbour an mT/mG allele ubiquitously expressing the membrane-targeted red fluorescent protein tdTomato (mT). In addition, half of the resulting embryos inherit a Cre allele which is expressed in a specific time and place depending on the endogenous driver gene. Upon Cre-mediated recombination, the mT/mG locus stops expressing tdTomato and instead starts expressing the membrane-targeted green fluorescent protein EGFP (mG). The lineage of cells expressing the gene of interest (and the Cre under its control) are therefore visualised in green, while remaining unrecombined tissues are visualised in red.

In the constitutive *Grhl3*^{Cre} and *Cdx2*^{Cre} lines, the Cre recombinase is directly targeted to the cell nucleus where it carries out its function. The inducible *T*^{CreERT2} line, on the other hand, expresses a modified Cre protein that is fused with the ligand-binding domain of the oestrogen receptor (Anderson et al., 2013; Feil et al., 2009; Hayashi & McMahon, 2002). CreERT2 is initially localised in the cytoplasm (and is hence inactive), and only translocates to the nucleus upon binding to tamoxifen. Due to the inducible nature of CreERT2, the resulting recombination domain in the embryo is highly dependent on the timing and dosage of tamoxifen administration. Pharmacological studies utilising CreERT2 and various reporter lines, for example,

have demonstrated an approximate 12-hour delay between intraperitoneal tamoxifen injection and the onset of recombination (Dymecki & Kim, 2007; Nakamura et al., 2006). This represents the time required for tamoxifen to be absorbed into the maternal circulation, metabolised into its active 4-OH-tamoxifen form in the liver, and delivered to embryonic cells. Furthermore, the total time lag between tamoxifen injection and complete activation of reporter genes has been estimated to 24h, which additionally accounts for the need of such genes to be adequately transcribed and translated (Hayashi & McMahon, 2002; Muzumdar et al., 2007). Finally, tamoxifen also represents the limiting factor in the recombination cascade, and therefore CreERT2 is induced in a dose-dependent manner. Higher doses of tamoxifen translate to increased recombination efficiency but must be carefully balanced against the higher risk of concomitant embryotoxicity (Dymecki & Kim, 2007; Hayashi & McMahon, 2002).

In this study, $T^{CreERT2}$ was activated by injecting pregnant females with 1 mg of tamoxifen per 20 g body weight at E7.5. In the $T^{CreERT2}$ line, progressively later induction time points are associated with recombination of successively smaller posterior segments in the embryo (Anderson et al., 2013). Therefore, tamoxifen administration at E7.5 (coupled with a 12 h delay in recombination) was chosen to target the T-expressing lineage at a stage where gastrulation is complete and NMPs have just begun forming the neural and mesodermal tissues of the posterior trunk. This time point therefore maximises the extent of AP axis recombined by the $T^{CreERT2}$, and corresponds to the onset $Grhl3^{Cre}$ and $Cdx2^{Cre}$ activation; thus eliminating a potential source of bias between the three deletion approaches. Lastly, previous studies from our group and others have shown that a dose of 1 mg tamoxifen per 20 g body weight is capable of maximising recombination efficiency while preventing any significant side effects (Danielian et al., 1998; Mugele, 2018).

In order to assess the spatial domains targeted by the three deletion approaches in the context of spinal neurulation, each Cre driver line was crossed with the $Rosa26^{mTmG/mTmG}$ reporter line and embryos were collected at E9.5. Cre-positive embryos were then first examined using a fluorescent stereoscope to evaluate the extent of recombination across the entire AP axis of the embryo. Next, embryos were

analysed using confocal microscopy and 3D reconstruction to obtain a more detailed view of the caudal region. This included whole-mount imaging to assess the overall pattern of recombination in areas of interest (e.g., recently fused dorsal midline of the neural tube), as well as imaging of cross sections at the levels of the closed and open neural tube to accurately determine the extent to which each tissue is affected throughout the DV axis.

Grhl3^{Cre} initially appeared to target the surface ectoderm throughout the AP axis of the embryo (Figure 3.3A). However, confocal microscopy revealed that while recombination of the surface ectoderm is complete in the trunk, it is only partial in the head (Figure 3.3B). In addition to complete recombination of the surface ectoderm, cross section of the PNP region demonstrated much less yet significant recombination in the hindgut, as well as a few EGFP-positive cells in the neuroepithelium and paraxial mesoderm (Figure 3.3D).

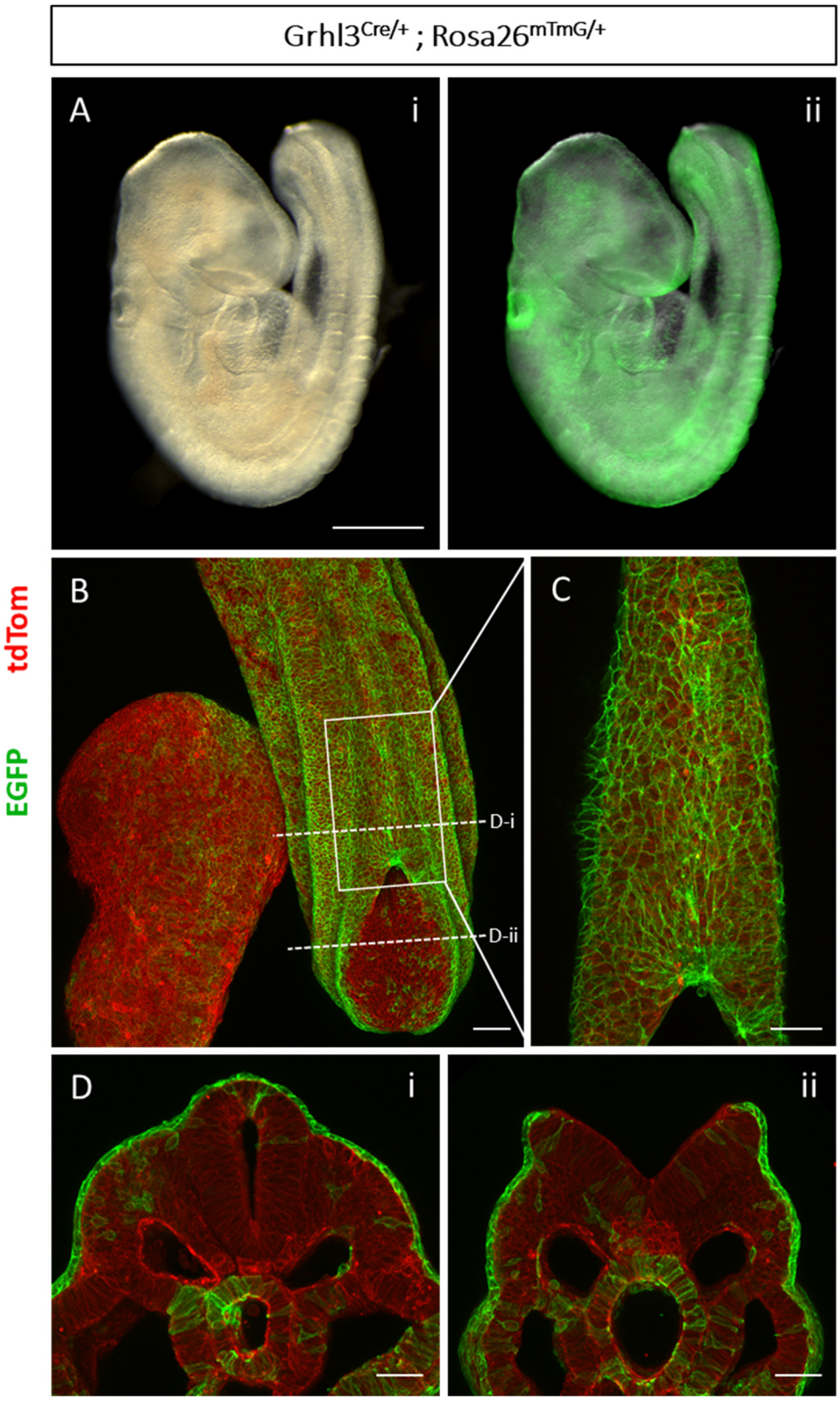

Figure 3.3. *Grhl3*^{Cre} lineage tracing using the mT/mG reporter with embryo collection at E9.5. (A) Brightfield (A-i) and widefield fluorescence (A-ii) images show that *Grhl3*^{Cre} recombines the surface ectoderm throughout most of the embryo (n = 4). (B) Maximum intensity composite projection of the caudal (right) and cranial (left)

regions (n = 4). *Grhl3*^{Cre} strongly targets surface ectoderm in the caudal, but not the cranial region. (C) Higher magnification of recently closed dorsal neural tube region indicated by box in B. The surface ectoderm overlying the neural tube and fusion site is completely recombined. (D) Cross sections through the regions indicated by the dashed lines in B (n = 3). In addition, to the surface ectoderm, *Grhl3*^{Cre} recombines a small fraction of the hindgut and paraxial mesoderm at both the levels of the closed neural tube (D-i) and PNP (D-ii). Scale bars: 500 µm in A; 100 µm in B; 50 µm in C and D.

In accordance with previous reports, *T*^{CreERT2}, which was activated at E7.5, appeared to target the entire trunk of the embryo posterior to the 6th somite (Figure 2A). *T*^{CreERT2} affected most axial and paraxial tissues but recombination was mosaic, as expected based on its tamoxifen-inducible character (Figure 3.4B-D). Recombination rates were highest in the paraxial mesoderm, and more moderate in the neural tube and hindgut, while the surface ectoderm was completely unaffected (Figure 3.4D, arrow). Interestingly, the neural tube appeared more strongly recombined in the region of closed neural tube (Figure 3.4D-i) compared to the PNP region (Figure 3.4D-ii). The opposite trend was detected for the notochord which was largely recombined in the PNP region (Figure 3.4D-ii), but mostly unaffected at the level of the closed neural tube (Figure 3.4D-i). This was surprising, given the status of T as a notochord marker, thus highlighting potential differences in regulation of the CreERT2 compared to the endogenous T gene.

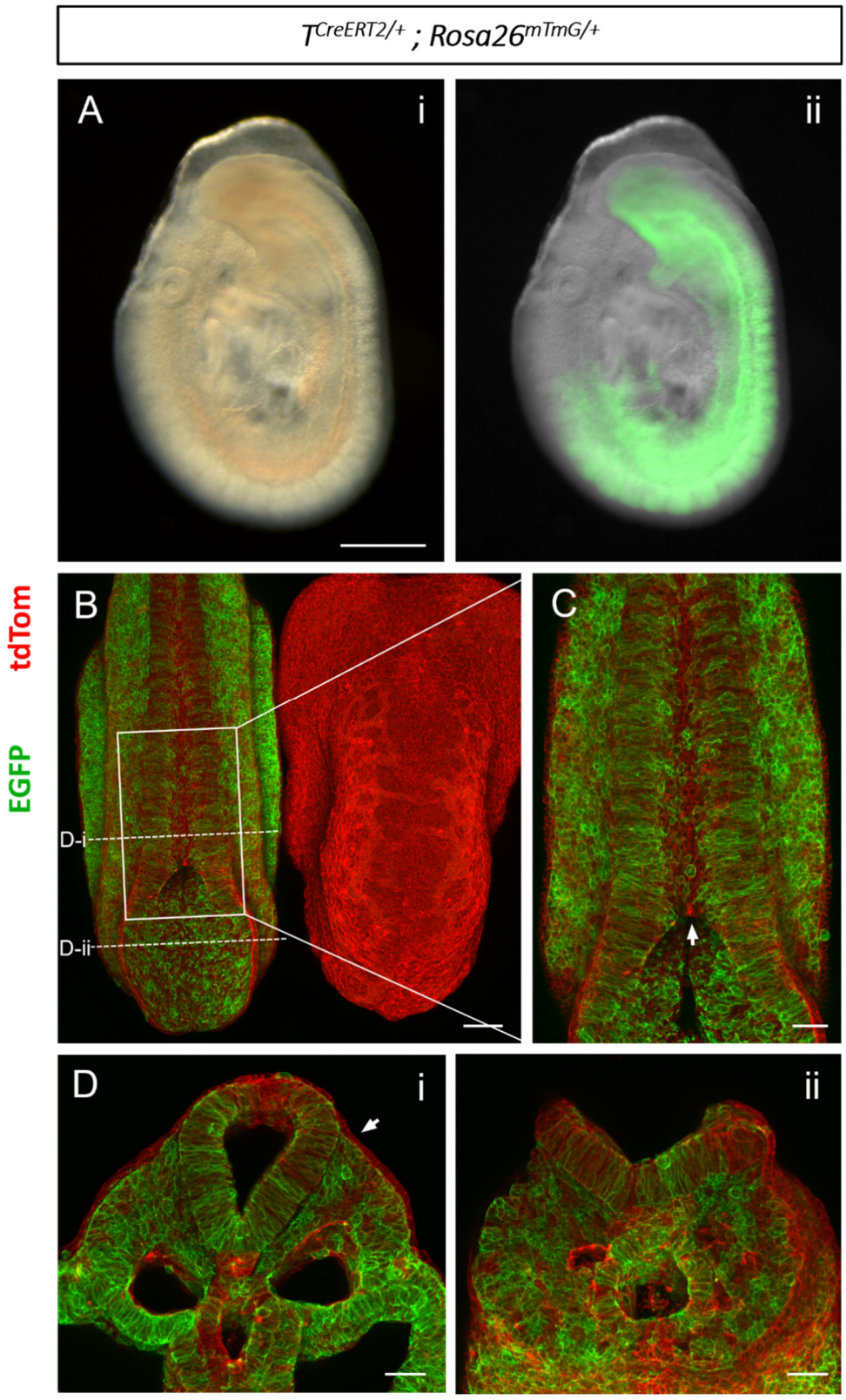

Figure 3.4. *T*^{CreERT2} lineage tracing using the mT/mG reporter with tamoxifen induction at E7.5 and embryo collection at E9.5. (A) Brightfield (A-i) and widefield fluorescence (A-ii) images show that *T*^{CreERT2} recombines most of the posterior body of the embryo (n = 4). (B) Maximum intensity composite projection of the caudal

(left) and cranial (right) regions (n = 4). *T*^{CreERT2} recombines the majority of the paraxial mesoderm and a moderate fraction of the neuroepithelium. (C) Higher magnification of recently closed dorsal neural tube region indicated by box in B. The fusion site is EGFP-negative (arrow). (D) Cross sections through the regions indicated by the dashed lines in B (n = 4). The paraxial mesoderm and hindgut are equally targeted at both axial levels examined, and the surface ectoderm is EGFP-negative throughout (Di, arrow). The neuroepithelium is more strongly recombined in the region of closed neural tube (D-i) compared to the PNP (D-iI), while the converse is true for the notochord. Scale bars: 500 µm in A; 100 µm in B; 50 µm in C and D.

As expected, *Cdx2*^{Cre} also targeted the posterior region of the embryo. However, it selectively recombined the neural tube from the level of the 4th - 8th somite to the level of the 16th somite and only caudal to that did it extend to surrounding tissues (Figure 3.5A-B). *Cdx2*^{Cre} demonstrated more clearly defined borders between targeted and unaffected tissues, compared to the widespread mosaicism of *T*^{CreERT2}. In the caudal region, for example, both neuroepithelium and paraxial mesoderm were completely recombined, while the notochord, aortic walls and mesonephric ducts remained unrecombined (Figure 3.5D). Nevertheless, even with this Cre, mosaicism was evident for both paraxial mesoderm, hindgut and coelomic epithelium in a "transition zone" (from fully unrecombined to fully recombined) between somites 18 and 22 (Figure 3.5B).

Furthermore, even though most of the surface ectoderm was recombined in the caudal region, a significant number of cells from this tissue were still tdTomato-positive (Figure 3.5C, arrows). This included both unrecombined EGFP-negative cells (Figure 3.5C, arrow), as well as recently recombined tdTomato/EGFP double-positive cells (where tdTomato was no longer expressed, but not yet fully degraded either) (Figure 3.5C, arrowhead). This finding indicated that activation of *Cdx2*^{Cre} in the surface ectoderm might not spatiotemporally coincide with its activation in the paraxial mesoderm. This could be a functionally significant property since the surface

ectoderm represents a potentially critical tissue for cell-ECM interactions in the context of neural tube closure.

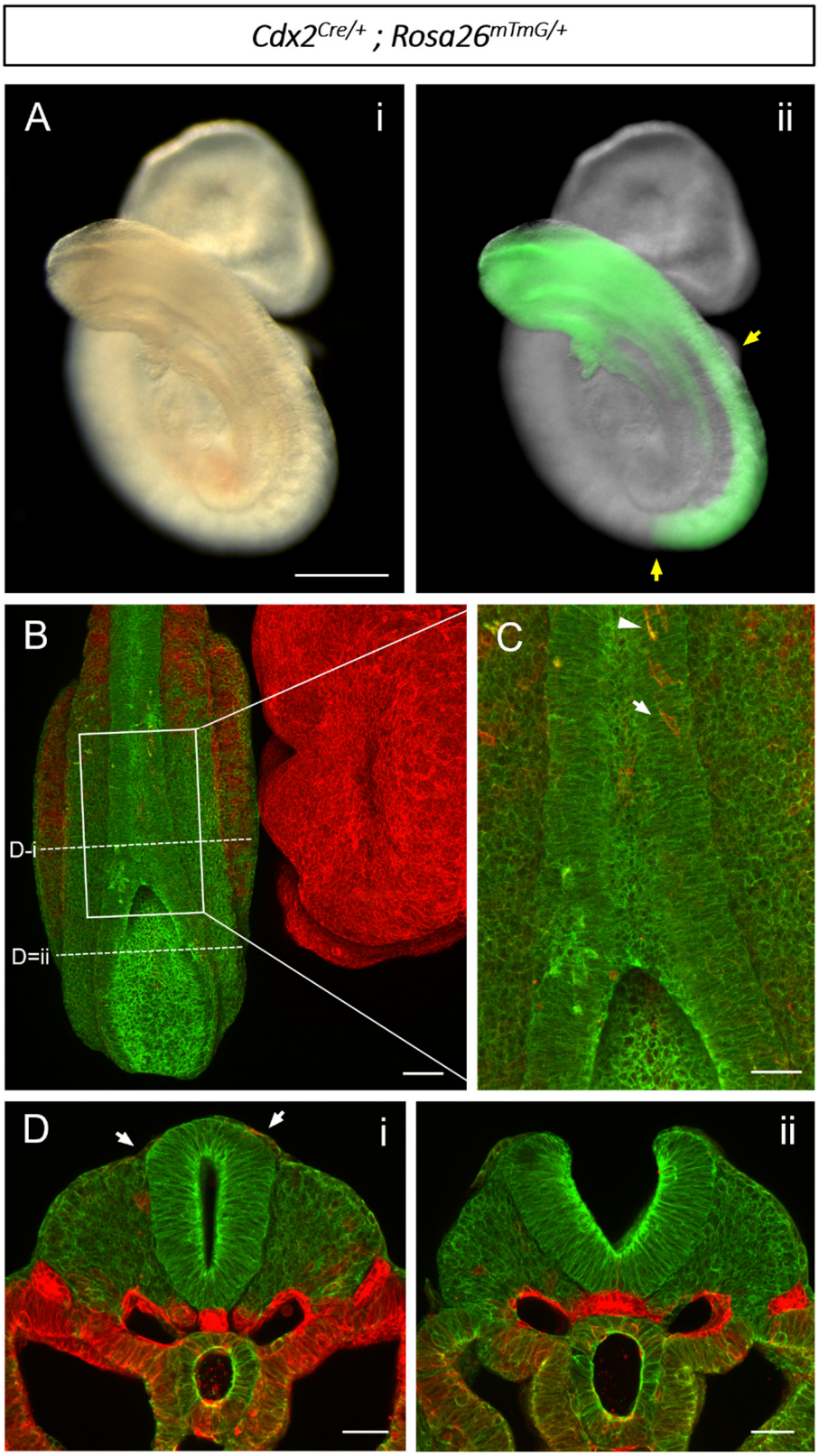

Figure 3.5. *Cdx2*^{Cre} lineage tracing using the mT/mG reporter with embryo collection at E9.5. (A) Brightfield (A-i) and widefield fluorescence (A-ii) images show that *Cdx2*^{Cre} specifically recombines the neural tube from the level of the 4th - 8th somite to the level of the 16th somite (yellow arrows), but then also expands to surrounding tissues posteriorly (n = 4). (B) Maximum intensity composite projection of the caudal (left) and cranial (right) regions (n = 3). The paraxial mesoderm is recombined posteriorly, but not anteriorly, while the neuroepithelium is strongly recombined throughout. The cranial region is totally unrecombined. (C) Higher magnification of recently closed dorsal neural tube region indicated by box in B. Some surface ectoderm cells are still tdTomato-positive (white arrow and arrowhead). (D) Cross sections through the regions indicated by the dashed lines in B (n = 3). The neuroepithelium and vast majority of the PSM posterior to somite 21 are EGFP-positive. The notochord, aortic walls and mesonephric ducts are EGFP-negative, while the hindgut and coelomic epithelium are increasingly EGFP-positive in more posterior regions (D-ii). tdTomato-positive surface ectoderm cells are evident over the closed neural tube (D-I, white arrows). Scale bars: 500 µm in A; 100 µm in B; 50 µm in C and D.

To more fully ascertain the spatiotemporal dynamics of *Cdx2*^{Cre} activation in the surface ectoderm, this analysis was then extended to embryos at earlier somite stages. Imaging slightly younger E9.25 embryos (where *Cdx2*^{Cre} had just been turned on in the caudal-most part of the paraxial mesoderm) revealed a much greater number of tdTomato-positive surface ectoderm cells around the fusion site and PNP (Figure 3.6B), as well as in more anterior regions examined (Figure 3.6C). Interestingly, cross sections confirmed the existence of recombined surface ectoderm cells overlying unrecombined paraxial mesoderm at the level of the recently closed neural tube (Figure 3.6D-iii, arrow), as well as unrecombined surface ectoderm cells overlying the recombined paraxial mesoderm at the level of the PNP (Figure 3.6E-iii, arrow). These data thus illustrate that recombination of the surface ectoderm begins prior to that of the paraxial mesoderm, and yet remains partial at more posterior axial levels where the paraxial mesoderm is fully recombined.

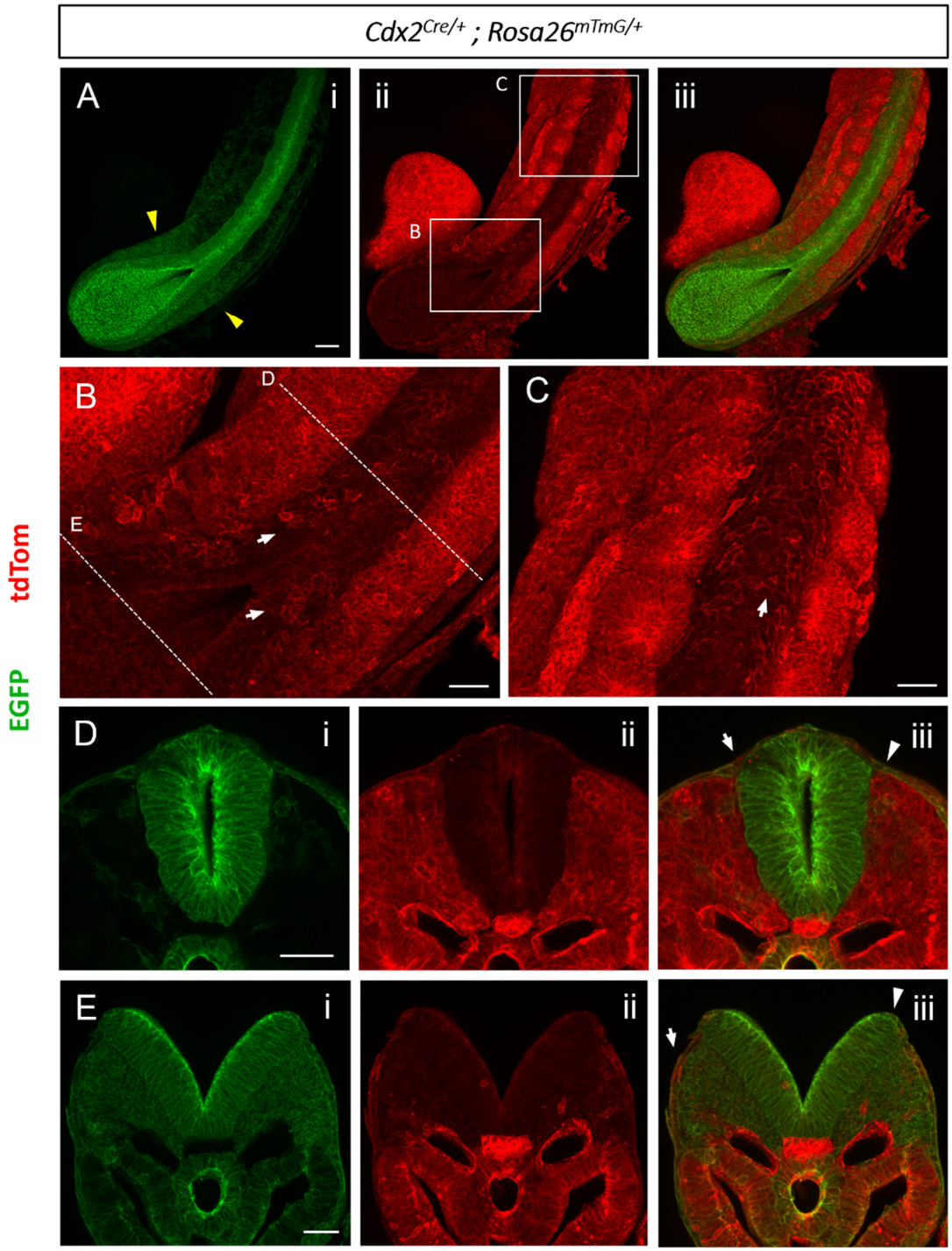

Figure 3.6. *Cdx2*^{Cre} lineage tracing using the mT/mG reporter with embryo collection at E9.25. (A) Maximum intensity projections of the caudal region in EGFP (i) and tdTomato (ii) channels, and composite (iii) (n = 3). Paraxial mesoderm is only recombined in the caudal-most part of the embryo (yellow arrowheads), while somites and most of the PSM remain unrecombined. (B, C) Higher magnification

views of regions indicated by boxes in B-ii. A large proportion of the surface ectoderm remains tdTomato-positive around the fusion site (B, white arrows) and closed neural tube further anteriorly (C, white arrows). (D and E) Cross sections through the regions indicated by the dashed lines in B, in EGFP (i) and tdTomato (ii) channels, and composite (iii) (n = 3). Sections reveal EGFP-positive (white arrowheads) and EGFP-negative (white arrows) cells at both the levels of the closed neural tube (D) and PNP (E). Scale bars: 100 μm in A; 50 μm in B-E.

Lastly, to identify the anterior threshold where surface ectoderm recombination is initiated, lineage tracing for this Cre driver was repeated with embryo collection at E8.5. Indeed, at this stage recombination was almost exclusively confined to the neuroepithelium, with extremely few EGFP-positive surface ectoderm cells detected caudally (Figure 3.7A). Activation of *Cdx2*^{Cre} in the surface ectoderm therefore appears to be a much more protracted process (compared to that in the paraxial mesoderm), resulting in a mosaic "transition zone" spanning the entire region between somites 7 and 22, approximately. An equivalent analysis of *Grhl3*^{Cre}-mediated recombination, on the other hand, confirmed that this driver targets the entire surface ectoderm from the earliest stages of PNP closure (Figure 3.7B). This finding is highly significant in relation to the different phenotypes of embryos in which the *Fn1* gene was conditionally inactivated by either *Cdx2*^{Cre} or *Grhl3*^{Cre} – see Section 3.2.2 below.

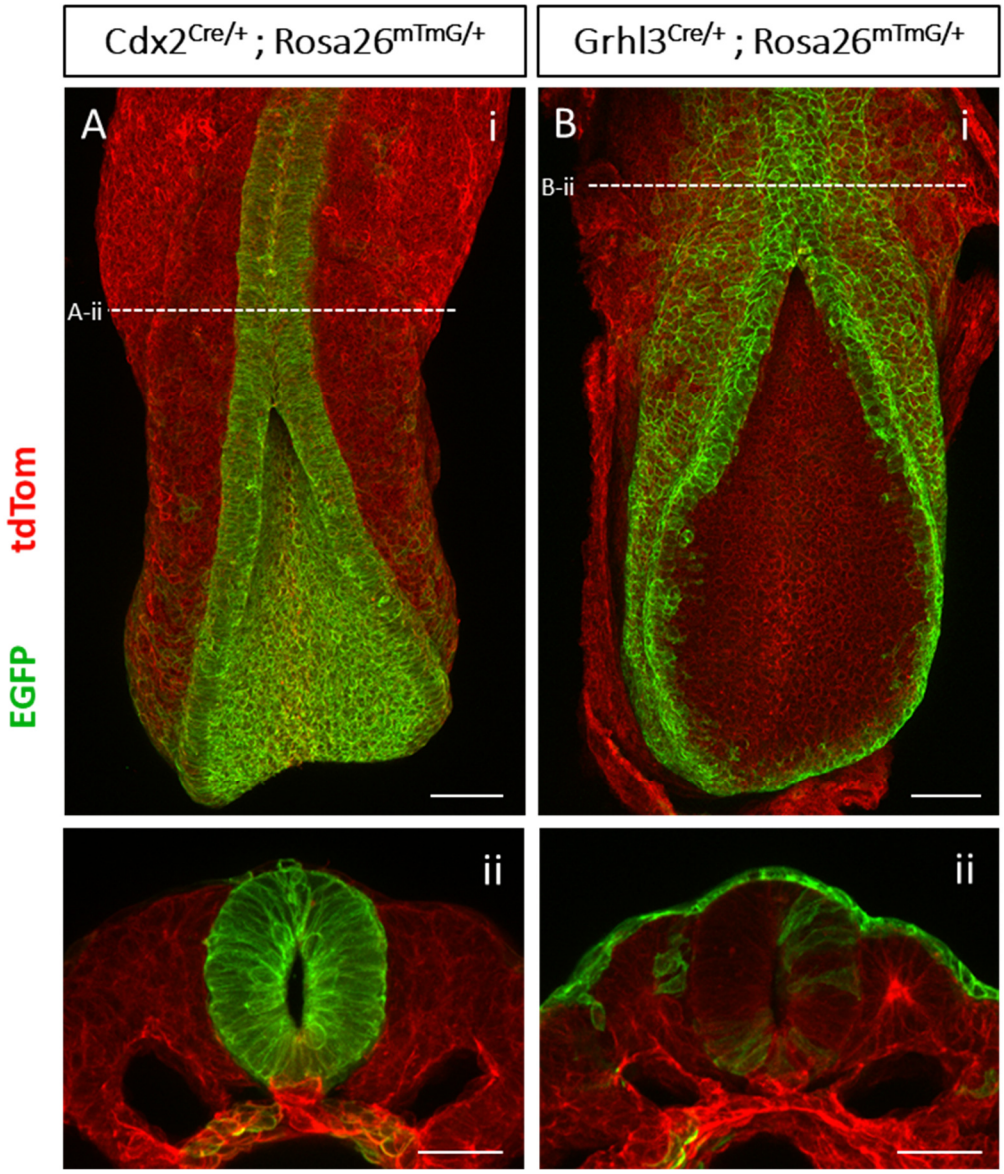

Figure 3.7. *Cdx2*^{Cre} and *Grhl3*^{Cre} lineage tracing using the mT/mG reporter with embryo collection at E8.5. (A-i) Maximum intensity composite projection of the caudal region of *Cdx2*$^{Cre/+}$; *Rosa26*$^{mTmG/+}$ embryo showing complete recombination of the neuroepithelium (n = 3). (A-ii) Cross section through the region indicated by the dashed line in A-i (n = 3). In addition to the neuroepithelium, very few EGFP-positive cells were also detected in the surface ectoderm and gut endoderm, (indicating that the spatiotemporal dynamics of recombination are likely shared in these two tissues). (B-i) Maximum intensity composite projection of the caudal region of *Grhl3*$^{Cre/+}$; *Rosa26*$^{mTmG/+}$ embryo showing complete recombination of the surface ectoderm (n = 3). (A-ii) Cross section through the region indicated by the dashed line in A-i (n = 3). (B-ii) Cross section through the region indicated by the dashed line in B-

i (n = 3). In addition to the surface ectoderm, a few EGFP-positive cells were also detected in the neuroepithelium, paraxial mesoderm and gut endoderm. Scale bars: 100 µm in A-i and B-i; 50 µm in A-ii and B-ii.

On the whole, comparison of these lineage tracing results with previous fibronectin in situ hybridisation analyses yields the following updated predictions for the current fibronectin deletion approaches: 1) *Grhl3*^{Cre} will ablate the small fibronectin expression locus at the fusion site throughout the AP extent of spinal neural tube closure, if that originates from the surface ectoderm. 2) *T*^{CreERT2} will ablate the majority of fibronectin expression from the paraxial mesoderm in the entire region posterior to somite 5. 3) *Cdx2*^{Cre} will ablate the small fibronectin expression locus at the fusion site throughout the process of spinal closure, if that originates from the neuroepithelium. In addition, *Cdx2*^{Cre} will ablate fibronectin expression entirely (from the fusion site and paraxial mesoderm) in the region posterior to somite 22.

3.2.2 Late-stage morphological characterisation following fibronectin ablations

To start investigating the role of fibronectin expressed from these various embryonic regions in posterior development, mice homozygous for the floxed allele of the *Fn1* gene (*Fn1*$^{fl/fl}$) were crossed with mice carrying a Cre driven by the *Grhl3*, T or *Cdx2* promoters, respectively. The resulting double heterozygotes (*Grhl3*$^{Cre/+}$*; Fn1*$^{fl/+}$*,* *T*$^{CreERT2/+}$*; Fn1*$^{fl/+}$ and *Cdx2*$^{Cre/+}$*; Fn1*$^{fl/+}$*)* were in turn independently crossed with *Fn1*$^{fl/fl}$ mice to produce litters containing Cre-positive homozygous and heterozygous mutants, and Cre-negative controls for each of the three deletion approaches. To determine whether loss of fibronectin expression in the targeted tissues affects any aspect of posterior development, such as neural tube closure and axial elongation, embryos were collected and morphologically characterised at E12.5, when these processes are essentially completed. Embryos were examined for NTDs in order to determine the impact of each deletion on neural tube closure, while measurements

of somite number, crown-rump length and body length (measured as the dorsal midline distance from the forebrain to the tail tip) were used to evaluate the impact on axial elongation and overall developmental progression. These analyses also included embryos conditionally heterozygous for *Fn1* expression (*Grhl3*$^{Cre/+}$*; Fn1*$^{fl/+}$ and *Cdx2*$^{Cre/+}$*; Fn1*$^{fl/+}$) to assess whether heterozygous loss of *Grhl3* or *Cdx2* (due to the Cre knock-in which produces a null allele in each case) might interact with heterozygous loss of fibronectin. *T*^{Cre}*; Fn1*$^{fl/+}$ embryos were also examined, in parallel, even though the *T*^{Cre} driver is a transgene insertion, not a knock-in, and so does not produce a null allele (Anderson et al., 2013). The frequency of each genotype was determined and compared to normal Mendelian ratios to exclude the possibility of early embryonic lethality or transmission ratio distortion (e.g., of mutant alleles).

Despite targeting the predominantly *Fn1*-negative surface ectoderm (Figure 3.2), the *Grhl3*^{Cre}-mediated deletion of fibronectin was enough to cause NTDs in 29% (n = 6/21) of *Grhl3*$^{Cre/+}$*; Fn1*$^{fl/fl}$ mutant embryos (Figure 3.8A). Most of these cases (n = 5/6) consisted of an open spina bifida at the lower lumbar and sacral levels accompanied by a tail flexion defect, where the curvature of the tail was reversed from ventral to dorsal (Figure 3.8B-E). In addition, one of the mutants exhibited a tail flexion defect alone with a closed neural tube. This type of tail flexion defect has been previously observed in various mouse models of spinal NTDs and results from a relatively mild delay in neural tube closure, as opposed to the severe delay that gives rise to spina bifida (Copp, 1985; Molè et al., 2020). The remaining 71% (n = 15/21) of *Grhl3*^{Cre}*; Fn1*$^{fl/fl}$ embryos showed no detectable spinal abnormalities. Furthermore, as expected based on the specificity of the *Grhl3*^{Cre}, none of the mutant embryos demonstrated early lethality, or any other defects, or differences in somite number, body length or crown-rump length (Figure 3.8F-H). These results therefore demonstrate that *Fn1* expression in the surface ectoderm is important for spinal neural tube closure, albeit with a phenotype in only 29% of embryos, whereas it is not required for axial elongation or overall embryonic development.

A

	Total	Normal	Affected	Spina bifida & Tail flexion defect	Tail flexion defect
***Grhl3*$^{Cre/+}$; *Fn1*$^{fl/fl}$ (Mutant)**	21	15	6	5	1
Grhl3$^{Cre/+}$; *Fn1*$^{fl/+}$ (Het)	35	35	0	0	0
Grhl3$^{+/+}$; *Fn1*$^{fl/fl}$ (Control)	34	34	0	0	0
Grhl3$^{+/+}$; *Fn1*$^{fl/+}$ (Control)	23	23	0	0	0
Total	113	107	6	5	1

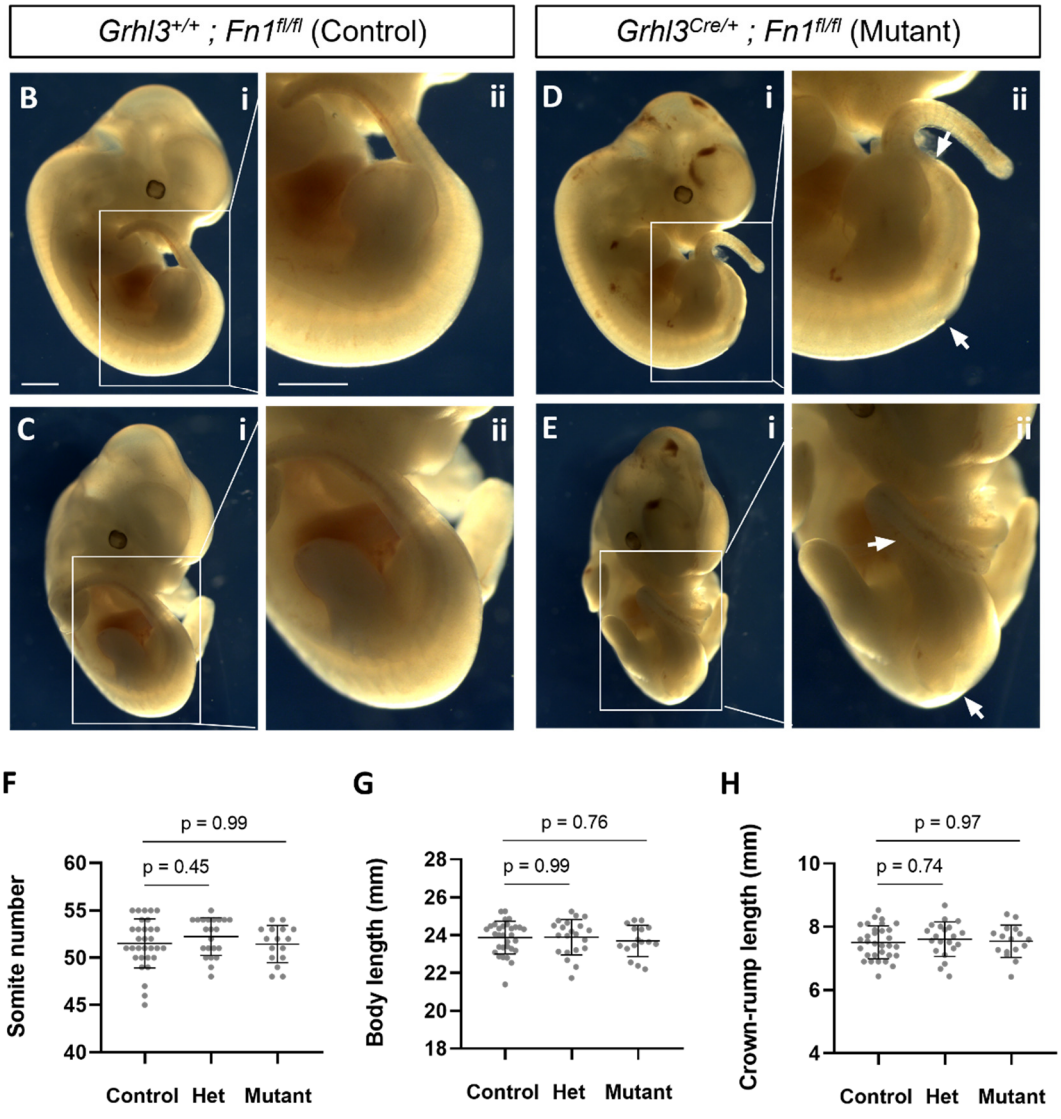

Figure 3.8. Morphological characterisation of E12.5 embryos following *Grhl3*^{Cre}-mediated deletion of the fibronectin gene. (A) Summary table. The frequency of the four genotypes conforms to the expected 1:1:1:1 Mendelian ratio (Chi-square test; p = 0.13; embryos: n total = 113). The 2 control genotypes (*Grhl3*$^{+/+}$; *Fn1*$^{fl/fl}$ and *Grhl3*$^{+/+}$; *Fn1*$^{fl/+}$) were pooled for all subsequent analyses. 6 out of 21 mutant embryos are affected by spinal NTDs (Fisher's exact test; p = 0.0007; embryos: mutants vs

controls). 5 of these cases show open spina bifida combined with a tail flexion defect, while one case only shows the tail flexion defect. No NTDs were observed in the heterozygote and control groups. (B) Brightfield images show the open spina bifida (arrows in D-ii and E-ii demarcate the AP borders of the lesion) and dorsally flexed tail of a mutant embryo (D-E) compared to the closed neural tube and ventrally curved tail of a control embryo (B-C). (F-H) Measurements confirmed that there were no statistically significant differences in somite number (F), body length (G) or crown-rump length (H) between the different genotypes (one-way ANOVA; post-hoc Dunnett's test; p values in figure; embryos: controls n = 31, heterozygotes n = 22, mutants n = 16). Data shown as mean values ± Standard deviation (SD). Scale bars: 1 mm.

Even though it was expected to largely abolish fibronectin expression in the posterior half of the embryo, the $T^{CreERT2}$-mediated deletion did not affect the morphology of the embryos in any detectable way at E12.5. $T^{CreERT2}; Fn1^{fl/fl}$ embryos showed no NTDs or other defects (Figure 3.9A-E) and no differences in somite number, crown-rump length or body length when compared to control embryos (Figure 3.9F-G). While these results might be explained by the mosaicism characterising this deletion strategy, they still stand in stark contrast to the severe axial truncation previously observed in global fibronectin KOs (George et al., 1993; Georges-Labouesse et al., 1996).

A

	Total	Normal	Affected	Spina bifida & Tail flexion defect	Tail flexion defect
$T^{CreERT2/+}$; $Fn1^{fl/fl}$ (Mutant)	20	20	0	0	0
$T^{CreERT2/+}$; $Fn1^{fl/+}$ (Het)	26	26	0	0	0
$T^{+/+}$; $Fn1^{fl/fl}$ (Control)	16	16	0	0	0
$T^{+/+}$; $Fn1^{fl/+}$ (Control)	19	19	0	0	0
Total	81	81	0	0	0

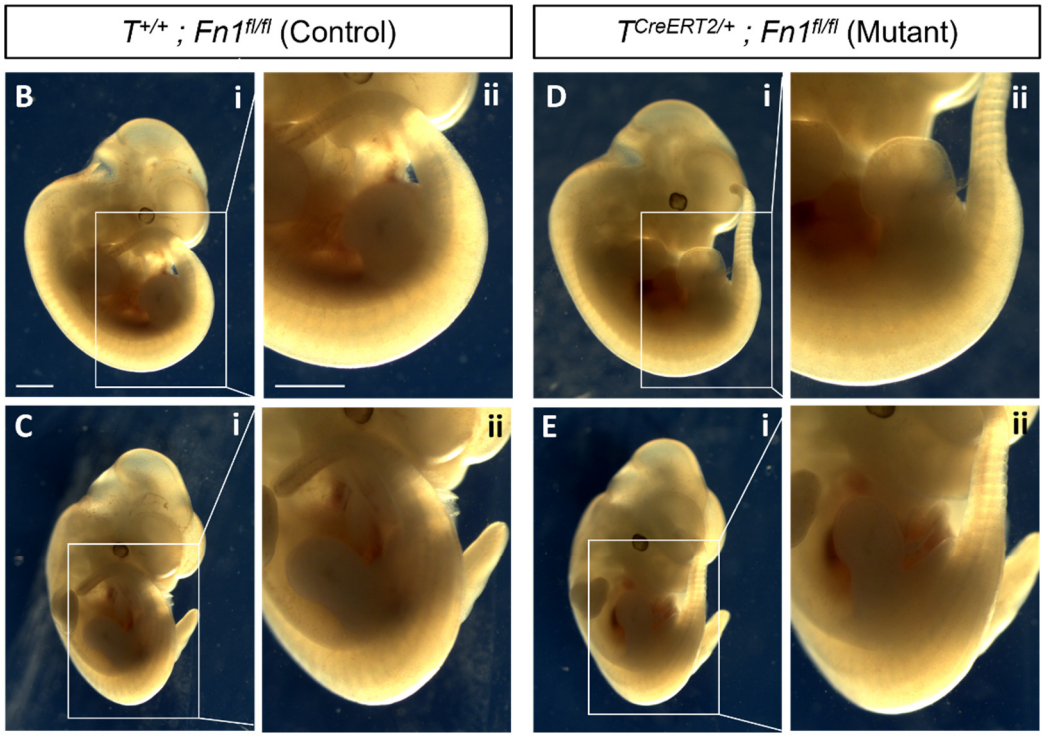

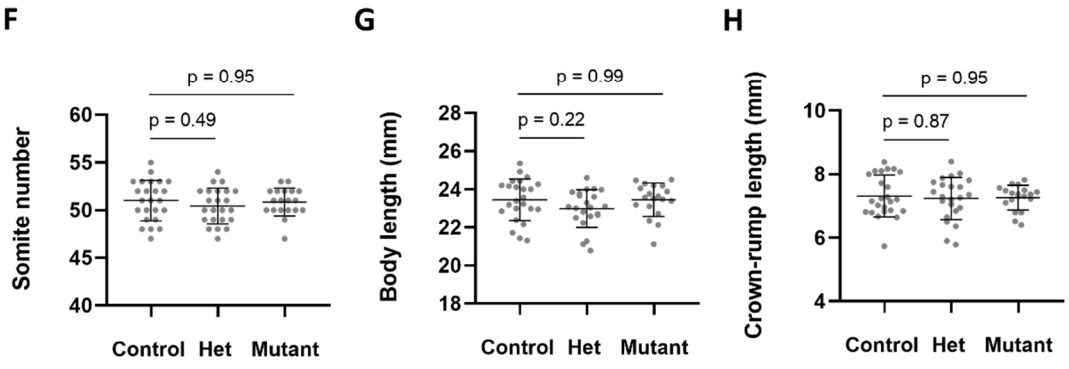

Figure 3.9. Morphological characterisation of E12.5 embryos following $T^{CreERT2}$-mediated deletion of the fibronectin gene with tamoxifen induction at E7.5. (A) Summary table. The frequency of the four genotypes conforms to the expected 1:1:1:1 Mendelian ratio (Chi-square test; p = 0.46; embryos: n total = 81). The 2 control genotypes ($T^{+/+}$; $Fn1^{fl/fl}$ and $T^{+/+}$; $Fn1^{fl/+}$) were pooled for all subsequent

analyses. No NTDs were observed in any of the genotypes. (B) Brightfield images show that mutant embryos (D-E) are indistinguishable from controls (B-C). (F-G) Measurements confirmed that there were no statistically significant differences in somite number (F), body length (G) or crown-rump length (H) between the different genotypes (one-way ANOVA; post-hoc Dunnett's test; p values in figure; embryos: controls n = 24, heterozygotes n = 23, mutants n = 19). Data shown as mean values ± SD. Scale bars: 1 mm.

Among the three conditional approaches *Cdx2*^{Cre} had the most extensive recombination domain in the caudal region, largely encompassing those of both *Grhl3*^{Cre} and *T*^{CreERT2}. It was thus expected to at least give rise to the pattern NTDs observed in the *Grhl3*^{Cre}*; Fn1*$^{fl/fl}$ mutants. Strikingly, however, *Cdx2*^{Cre}*; Fn1*$^{fl/fl}$ embryos showed no cases of spina bifida (Figure 3.10A). Instead, 47% (n = 8/17) of these mutants exhibited a different type of tail defect, where the tail was sharply folded at one or more points along its length (Figure 3.10B-E). This defect therefore appeared distinct from the spina bifida-associated tail flexion defect observed in *Grhl3*^{Cre}*; Fn1*$^{fl/fl}$ mutants. Moreover, it was positioned much further caudally, hence suggesting that it was unrelated to the process of primary neurulation. Mutant embryos showed no differences in somite number or crown-rump length (Figure 3.10F, H), but they did show a significant reduction in body length (Figure 3.10G). As the trunk region of these mutants seemed normal, it was hypothesised that the reduction in length was caused by a defect in tail elongation. Indeed, when separate measurements of the two body regions were taken, Cdx2^{Cre}*; Fn1*$^{fl/fl}$ mutants exhibited a significant reduction of 17% in tail length (Figure 3.10J), but no difference in trunk length (Figure 3.10I).

A

	Total	Normal	Affected	Spina bifida & Tail flexion defect	Tail flexion defect
***Cdx2^{Cre} ; Fn1$^{fl/fl}$* (Mutant)**	17	9	8	0	8
Cdx2^{Cre} ; Fn1$^{fl/+}$ (Het)	20	20	0	0	0
Cdx2$^{+/+}$; Fn1$^{fl/fl}$ (Control)	18	18	0	0	0
Cdx2$^{+/+}$; Fn1$^{fl/+}$ (Control)	13	13	0	0	0
Total	68	60	8	0	8

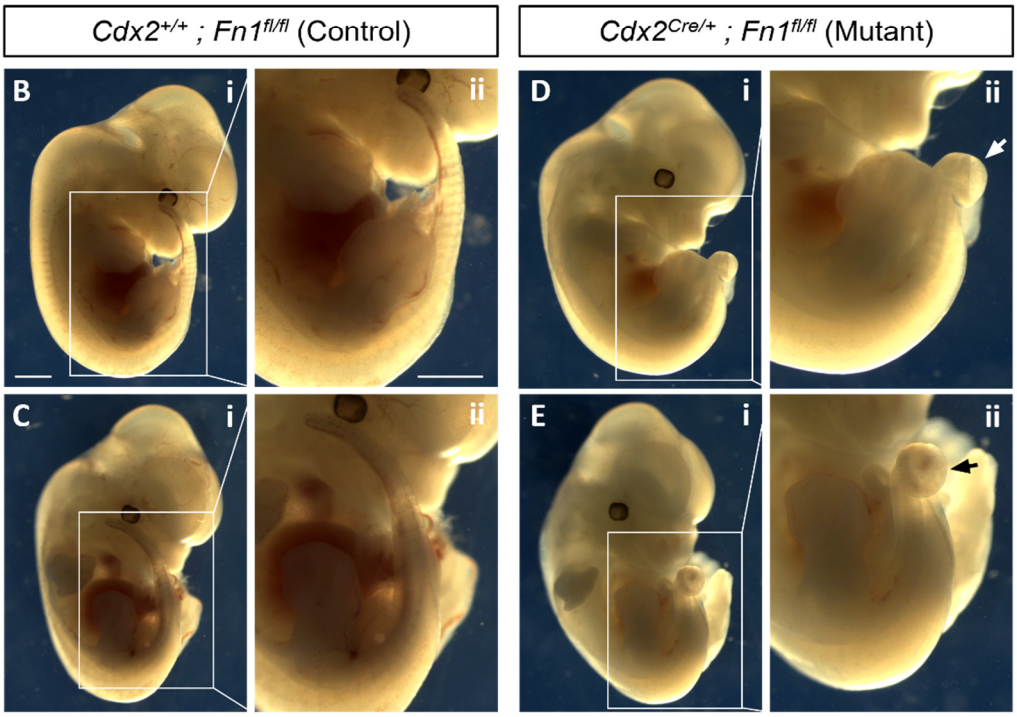

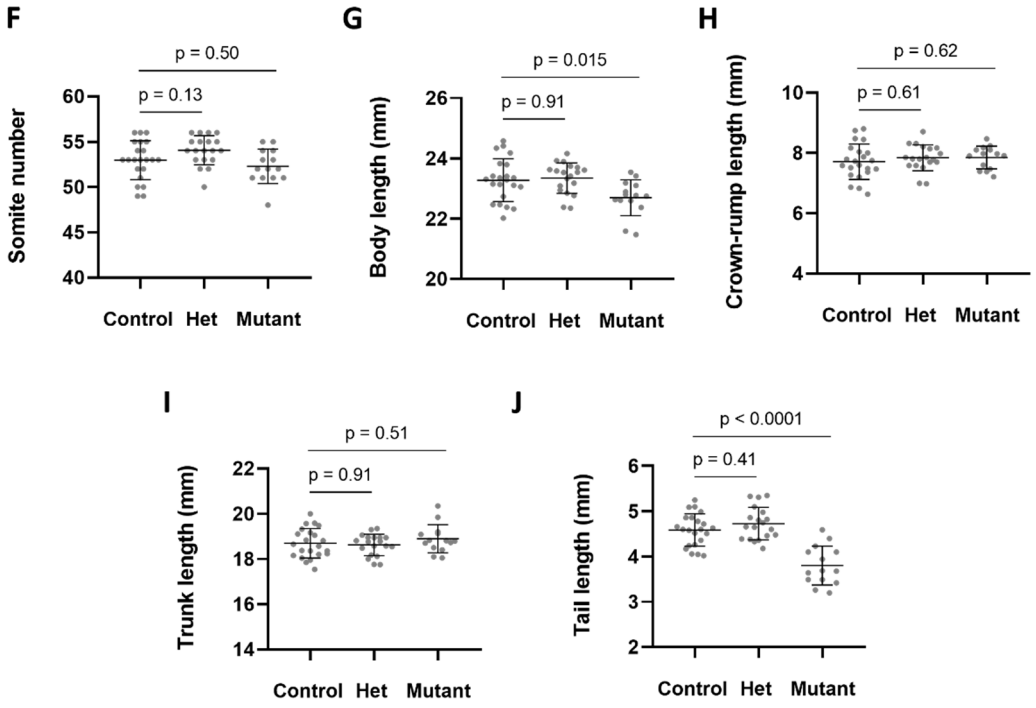

Figure 3.10. Morphological characterisation of E12.5 embryos following *Cdx2*^{Cre}-mediated deletion of the fibronectin gene. (A) Summary table. The frequency of the four genotypes conforms to the expected 1:1:1:1 Mendelian ratio (Chi-square test; p = 0.68; embryos: n total = 68). The 2 control genotypes (*Cdx2*$^{+/+}$; *Fn1*$^{fl/fl}$ and *Cdx2*$^{+/+}$; *Fn1*$^{fl/+}$) were pooled for all subsequent analyses. 8 out of 17 mutant embryos are affected by a tail flexion defect (Fisher's exact test; p < 0.0001; embryos: mutants vs controls). No cases of tail flexion defects were observed in the heterozygote and control groups. No cases of spina bifida were observed in any of the genotypes. (B) Brightfield images show the shortened and abnormally folded tail (arrows in D-ii and E-ii) of a mutant embryo (D-E) compared to the relatively straight tail of a control embryo (B-C). (F-J) Measurements confirmed that there were no differences in somite number (F) or crown-rump length (H) between the different genotypes, but mutant embryos showed a significant reduction in body length (G) (compared to controls) which was shown to fully derive from a reduction tail length (J) rather than trunk length (I) (one-way ANOVA; post-hoc Dunnett's test; p values in figure; embryos: controls n = 22, heterozygotes n = 19, mutants n = 14). Data shown as mean values ± SD. Scale bars: 1 mm.

Overall, these results provide evidence for two distinct previously unrecognised roles of fibronectin in posterior development. Fibronectin expressed by the surface ectoderm is important for the process of spinal neural tube closure, while fibronectin expressed in the caudal-most part of the embryo (likely by the paraxial mesoderm) is required for symmetric elongation of the tail. Nevertheless, all of the phenotypes observed here appear remarkably mild compared to the severe axial defects seen in previous KOs of fibronectin and associated integrin subunits (George et al., 1993; Georges-Labouesse et al., 1996; Goh et al., 1997; Yang et al., 1993). That might be explained by the fact that despite their extensive recombination domains, the three conditional approaches did not affect any of the cardiovascular or extraembryonic structures that are essential for the survival of the embryo. In accordance, the various fibronectin mutants generated here showed normal developmental progression and no early embryonic lethality (Figures 3.6A, 3.7A and 3.8A). Finally, none of the double

heterozygous embryos (*Grhl3^{Cre}; Fn1$^{fl/+}$, T^{CreERT2}; Fn1$^{fl/+}$* and *Cdx2^{Cre}; Fn1$^{fl/+}$*) showed any differences compared to controls, thus suggesting that the observed defects are indeed due to the loss of fibronectin expression, rather than heterozygosity for the endogenous driver genes.

3.2.3 Early-stage morphological characterisation following fibronectin ablations

To understand when and how these developmental defects arise, the same set of genetic crosses was then repeated with embryo collection at E9.5. At this stage, spinal neural tube closure and axial elongation are well underway and fibronectin expression in posterior tissues has been recently ablated by the Cre drivers. Once again, somite number and body length were used to assess axial elongation, whereas PNP dimensions were measured to track the progress of PNP closure. PNP length was defined as the AP distance from the fusion site to the caudal end of the neural plate, while PNP width was defined as the maximum mediolateral (ML) distance between the neural folds.

As expected, *Grhl3^{Cre}; Fn1$^{fl/fl}$* mutant embryos displayed significant increases in both the length (Figure 3.11E) and width (Figure 3.11F) of the PNP, but no differences in somite number (Figure 3.11C) or overall body length (Figure 3.11D) when compared to littermate controls. To further explore the timing of these abnormalities, a linear regression analysis of PNP dimensions against somite number was also performed. As all litters were collected at the same time point, there was very limited variability in terms of somite stages, thus making the dataset somewhat unsuited to this type of analysis. Nevertheless, the results were still informative. The regression lines of mutants, for both length (Figure 3.11G) and width (Figure 3.11H), differed significantly from those of controls in terms of intercept but not in terms of slope. Interestingly, however, the divergence in PNP dimensions seemed higher at early somite stages and was gradually ameliorated as development proceeded (due to the steeper slope of mutant regression lines). It therefore appears that *Grhl3^{Cre}; Fn1$^{fl/fl}$* mutants experience a generalised delay in PNP closure, which they attempt to

correct through an increased rate of closure at later stages. Based on the partial penetrance of spina bifida observed at E12.5, it seems that 71% of mutants succeed in bridging the gap, while the rest fail and go on to develop spina bifida.

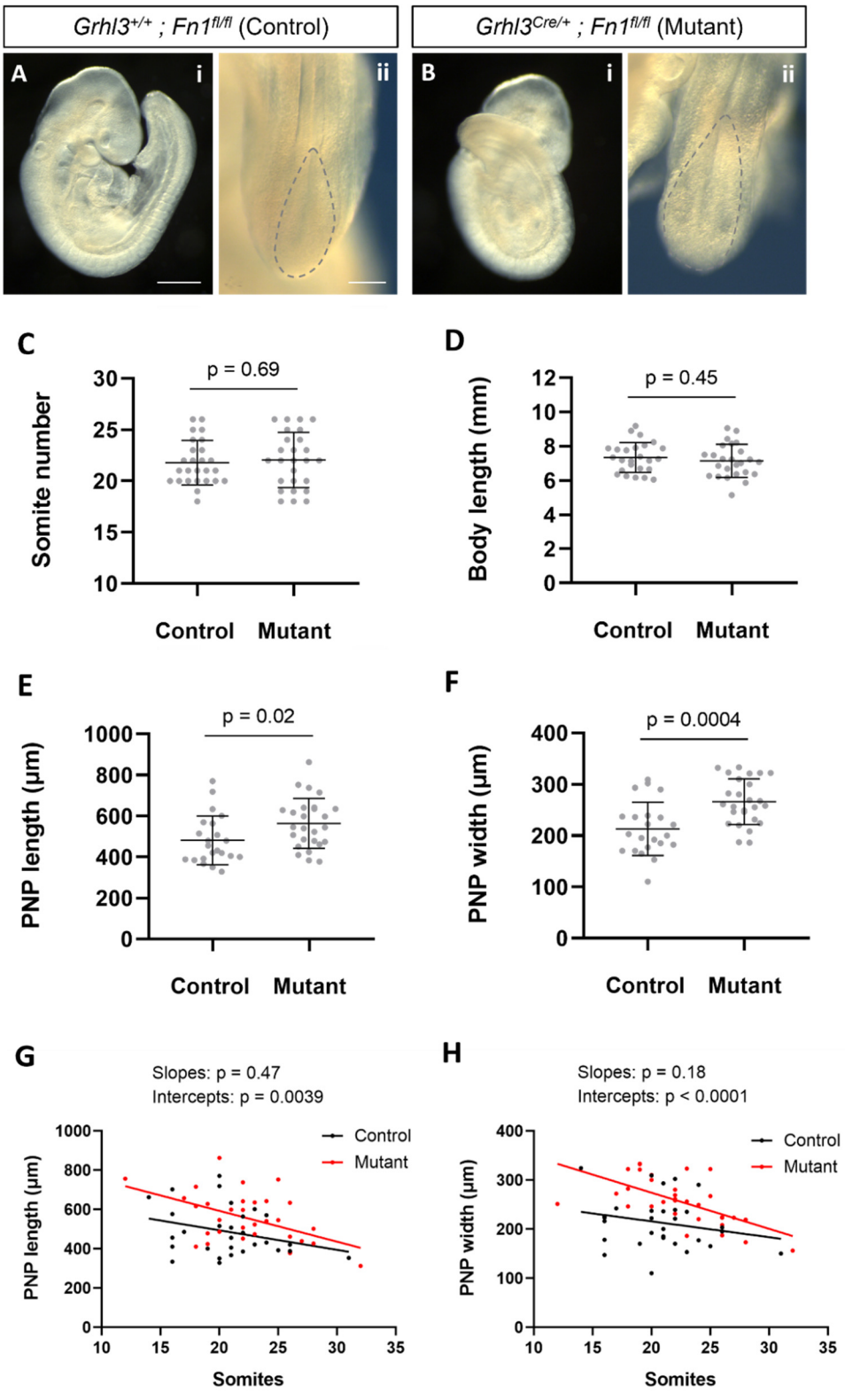

Figure 3.11. Morphological characterisation of E9.5 embryos following *Grhl3*^{Cre}-mediated deletion of the fibronectin gene. (A-B) Brightfield images show that mutant embryos display normal overall morphology (A-i, B-i), but a larger PNP (A-ii, B-ii). (C-F) Measurements confirmed that there were no differences in somite number (C) or body length (H), but mutant embryos showed a significant increase in PNP length (E) and width (F) when compared to controls (unpaired, two-tailed Student's t-test; p values in figure; embryos: controls n = 26, mutants n = 22). Data shown as mean values ± SD. (G-H) Linear regression analyses of PNP length (G) and width (H) at different somite stages in control (n = 30; length, r2 = 0.09; width, r2 = 0.05) and mutant embryos (n = 32; length, r2 = 0.24; width, r2 = 0.38). For both length and width, the regression lines of mutants differ significantly compared to controls in term of intercept, but not in terms of slope (p values in figure). However, note increased divergence of (Control vs Mutant) regression lines at early somite stages and relatively steeper slopes of mutant regression lines. Scale bars: 500 µm in A-i and B-i; 200 µm in A-ii and B-ii.

In accordance with the E12.5 results, *T*^{CreERT2}*; Fn1*$^{fl/+}$ mutants at E9.5 exhibited no differences in any of the morphological measures (Figure 3.12). Similarly, *Cdx2*^{Cre}*; Fn1*$^{fl/fl}$ mutants were identical to their littermate controls at E9.5, showing no defects in PNP closure or axial elongation and no abnormal folding along their AP axis at this stage (Figure 3.13). These results therefore confirm that the tail defect observed in many of these mutants at E12.5 is indeed unrelated to PNP closure and arises at a later stage of development.

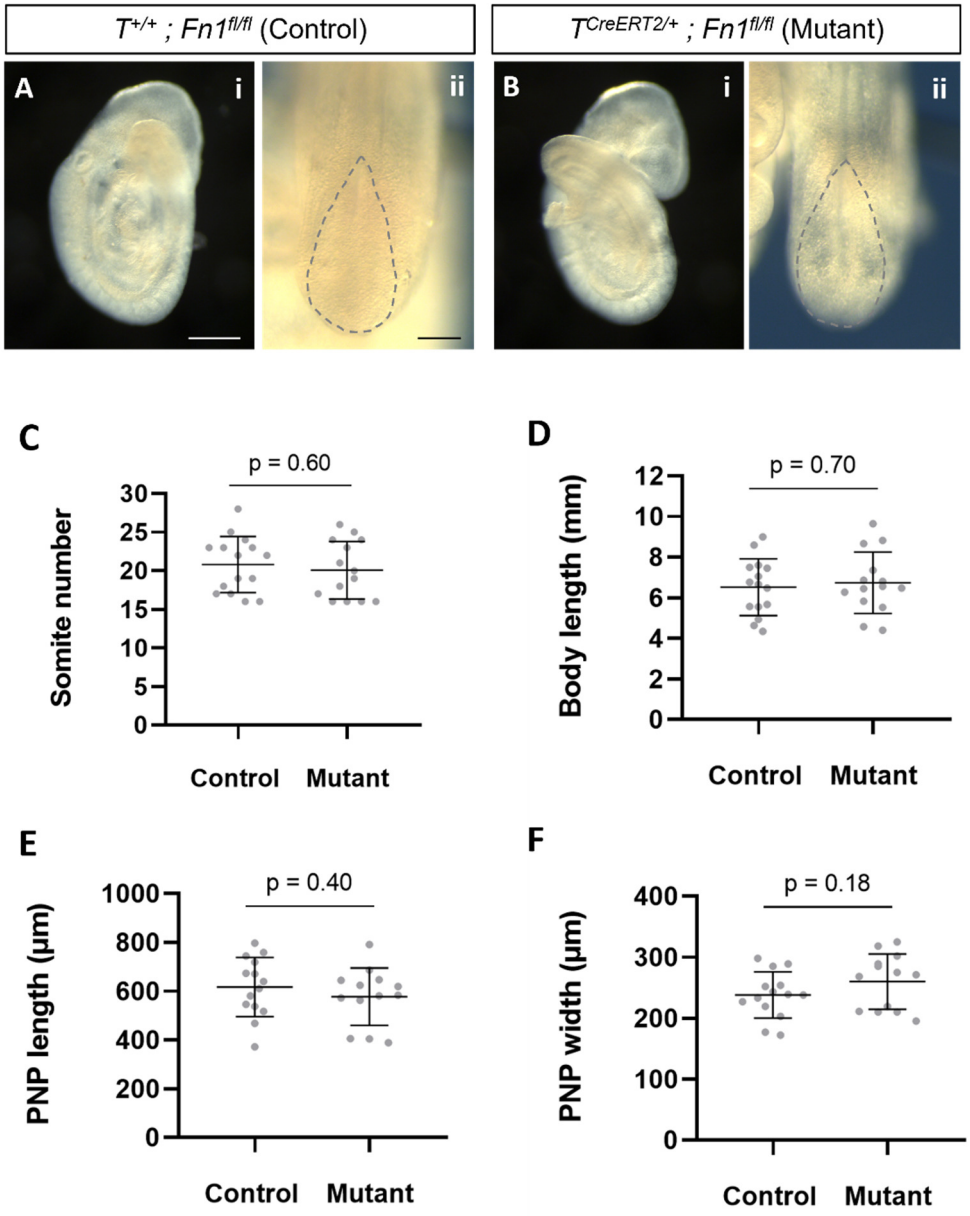

Figure 3.12. Morphological characterisation of E9.5 embryos following $T^{CreERT2}$-mediated deletion of the fibronectin gene with tamoxifen induction at E7.5. (A-B) Brightfield images show that mutant embryos display normal overall morphology and PNP. (C-F) Measurements confirmed that there were no differences in somite number (C), body length (H), PNP length (E) or width (F) when compared to controls (unpaired, two-tailed Student's t-test; p values in figure; embryos: controls n = 15, mutants n = 14). Data shown as mean values ± SD. Scale bars: 500 µm in A-i and B-i; 200 µm in A-ii and B-ii.

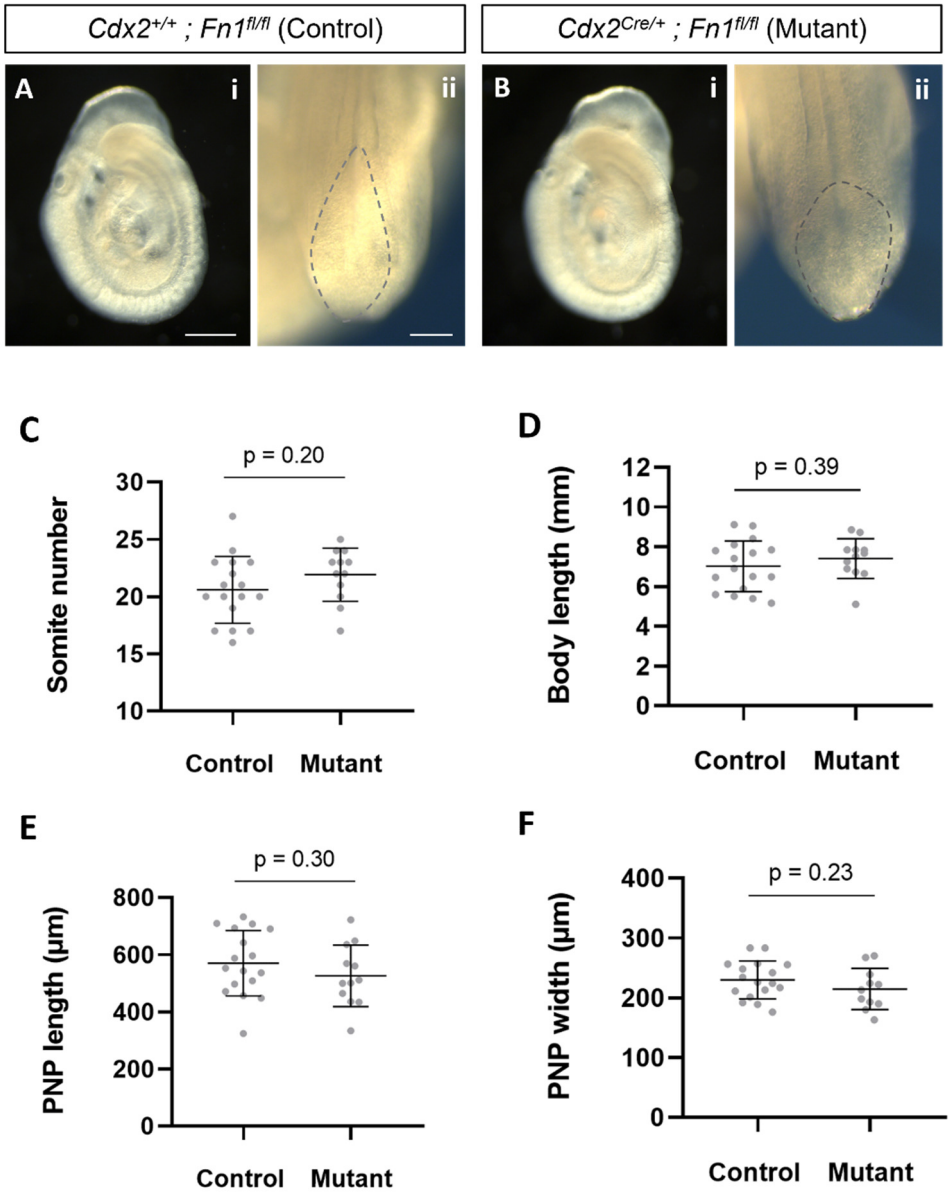

Figure 3. 13. Morphological characterisation of E9.5 embryos following *Cdx2*^{Cre}-mediated deletion of the fibronectin gene. (A-B) Brightfield images show that mutant embryos display normal overall morphology and PNP. (C-F) Measurements confirmed that there were no differences in somite number (C), body length (H), PNP length (E) or width (F) when compared to controls (unpaired, two-tailed Student's t-test; p values in figure; embryos: controls n = 17, mutants n = 12). Data shown as mean values ± SD. Scale bars: 500 µm in A-i and B-i; 200 µm in A-ii and B-ii.

3.2.4 Assessment of fibronectin localisation following fibronectin gene ablations

Next, to determine the origin and functional significance of the different parts of the fibronectin network, the various mutants and controls were immunostained for fibronectin at E9.5 (shortly after the genetic deletion). The impact of each deletion strategy on fibronectin localisation and structure was then evaluated in conjunction with the previously ascertained recombination domain and late-stage mutant phenotype when using each Cre driver. Whole-mount immunofluorescence for fibronectin was followed by confocal microscopy and 3D reconstruction. This allowed large-scale visualisation of fibronectin across the dorsal aspect of the caudal region, as well as a higher resolution imaging of the area surrounding the fusion site. Moreover, cross section images were acquired at the level of the closed neural tube and fusion site to accurately determine the extent to which each BM is affected throughout the DV axis.

The *Grhl3*^{Cre}-mediated approach, targeting the surface ectoderm, appeared to specifically remove fibronectin across the dorsal midline of the recently closed neural tube where it normally forms a dense fibrillar BM (Figure 3.14A, F). This effect was especially marked around the fusion site where the radially oriented fibrils seen in controls were completely absent in the mutants (Figure 3.14B and E vs. G and J). The fibronectin BM at the neuroepithelium-paraxial mesoderm boundary, on the other hand, appeared intact (Figure 3.14E, J, arrowheads).

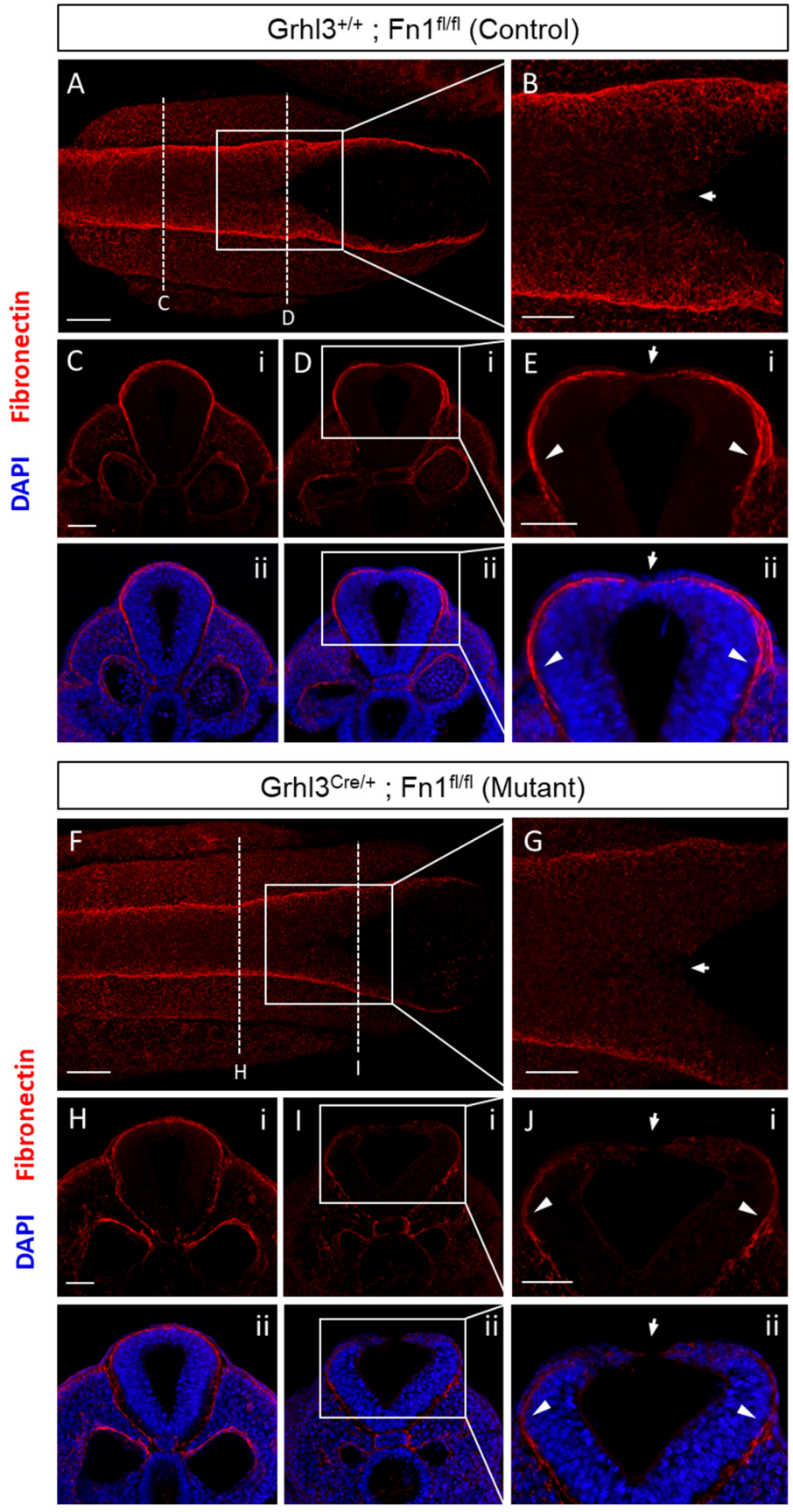

Figure 3.14. Fibronectin immunostaining of E9.5 embryos following *Grhl3*^{Cre}-mediated deletion of the fibronectin gene. (A, F) Maximum intensity projections of

the caudal region of control (A) and mutant (F) embryos (n = 5 per genotype). The *Grhl3*^{Cre}-mediated deletion specifically removes fibronectin from the dorsal interface between neuroepithelium and surface ectoderm. (B, G) Higher magnification of the fusion site indicated by boxes in A and F. (C, D, H, I) Cross sections at the levels of closed neural tube and fusion site indicated by the dashed lines in A and F. (E, J) Higher magnification of the fusion site region indicated by boxes in D and I. The lack fibronectin in mutant embryos is especially pronounced around the fusion site (arrows). Arrowheads indicate the points where surface ectoderm exchanges its contact from the mesoderm to the neuroepithelium. Note that in control embryos fibronectin is more abundant at the interface of the neuroepithelium with the surface ectoderm compared to the interface between the neuroepithelium and paraxial mesoderm, while the converse is true for the mutants. Scale bars: 100 µm in A and F; 50 µm in C-H and G-J.

Whole-mount immunofluorescence and confocal microscopy are often incompatible with accurate quantification of staining signal due to the potential variability in antibody and laser penetration between the compared embryos and tissues. To overcome this problem and confirm that fibronectin was indeed locally reduced by the deletion: fluorescence intensity at the dorsal midline of the surface ectoderm-neuroepithelium (SE-NE) BM (targeted by this deletion strategy) was measured and then normalised to fluorescence intensity at the neuroepithelium-paraxial mesoderm (NE-MES) BM (which is unaffected by this deletion strategy) (Figure 3.15A). Comparison of normalised intensities between mutant and control embryos indeed revealed a significant reduction of at least 40%. These results therefore confirmed that a substantial proportion of the fibronectin localising at the dorsal midline of the recently fused neural tube originates from the surface ectoderm. This localisation pattern presumably corresponds to the small fibronectin transcription locus previously observed at the fusion site (Molè, 2017), hence indicating that fibronectin is focally expressed and assembled there. Furthermore, fibronectin in this region appears to be critical for the process of neural tube closure, since such a highly localised ablation is sufficient to cause NTDs.

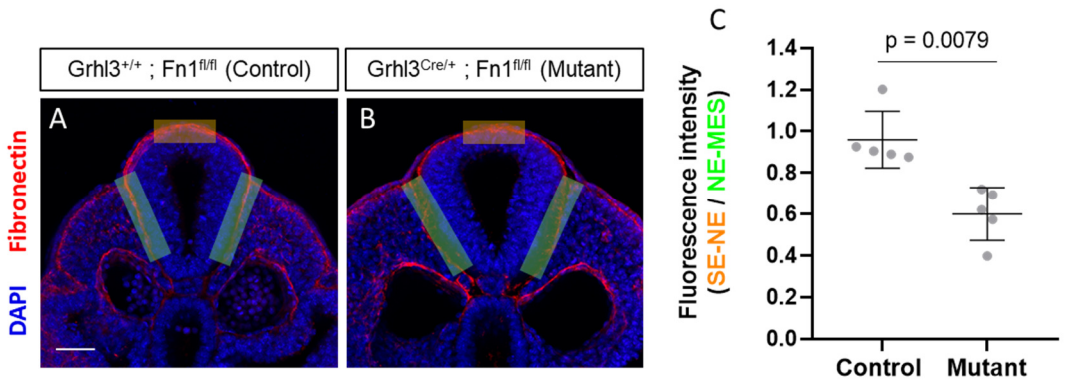

Figure 3.15. Quantification of fibronectin fluorescence intensity in E9.5 embryos following *Grhl3*^{Cre}-mediated deletion of the fibronectin gene. (A, B) Cross sections of immunostained control (A) and mutant (B) embryos at the level of the recently closed neural tube. Fluorescence intensity was measured at the dorsal SE-NE BM (orange) and lateral NE-MES BMs (green). (C) Statistical comparison of SE-NE intensity normalised to (bilaterally averaged) NE-MES intensity between mutants and controls reveals a significant reduction (Mann-Whitney test; p value in figure; embryos: controls n = 5, mutants n = 5). Data shown as mean values ± SD. Scale bar: 50 µm.

Despite its inability to produce any developmental defects, the *T*^{CreERT2}-mediated ablation strategy was surprisingly effective at removing fibronectin from the entire caudal region of the embryo (Figure 3.16A, F). Nevertheless, some fibrils were still consistently present at the dorsal midline, and especially at the fusion site of mutant embryos (Figure 3.16G, arrows). Thus, by targeting the main source of fibronectin expression at the paraxial mesoderm, but leaving the surface ectoderm completely unaffected, *T*^{CreERT2} seemed to have the opposite effect compared with *Grhl3*^{Cre}. Moreover, fibronectin was still detectable to a small extent at the neuroepithelium-paraxial mesoderm boundary and to a larger extent in the notochord sheath (Figure 3.16H-J). Some fibronectin expression was, however, expected to persist in these regions due to the mosaic nature of this deletion.

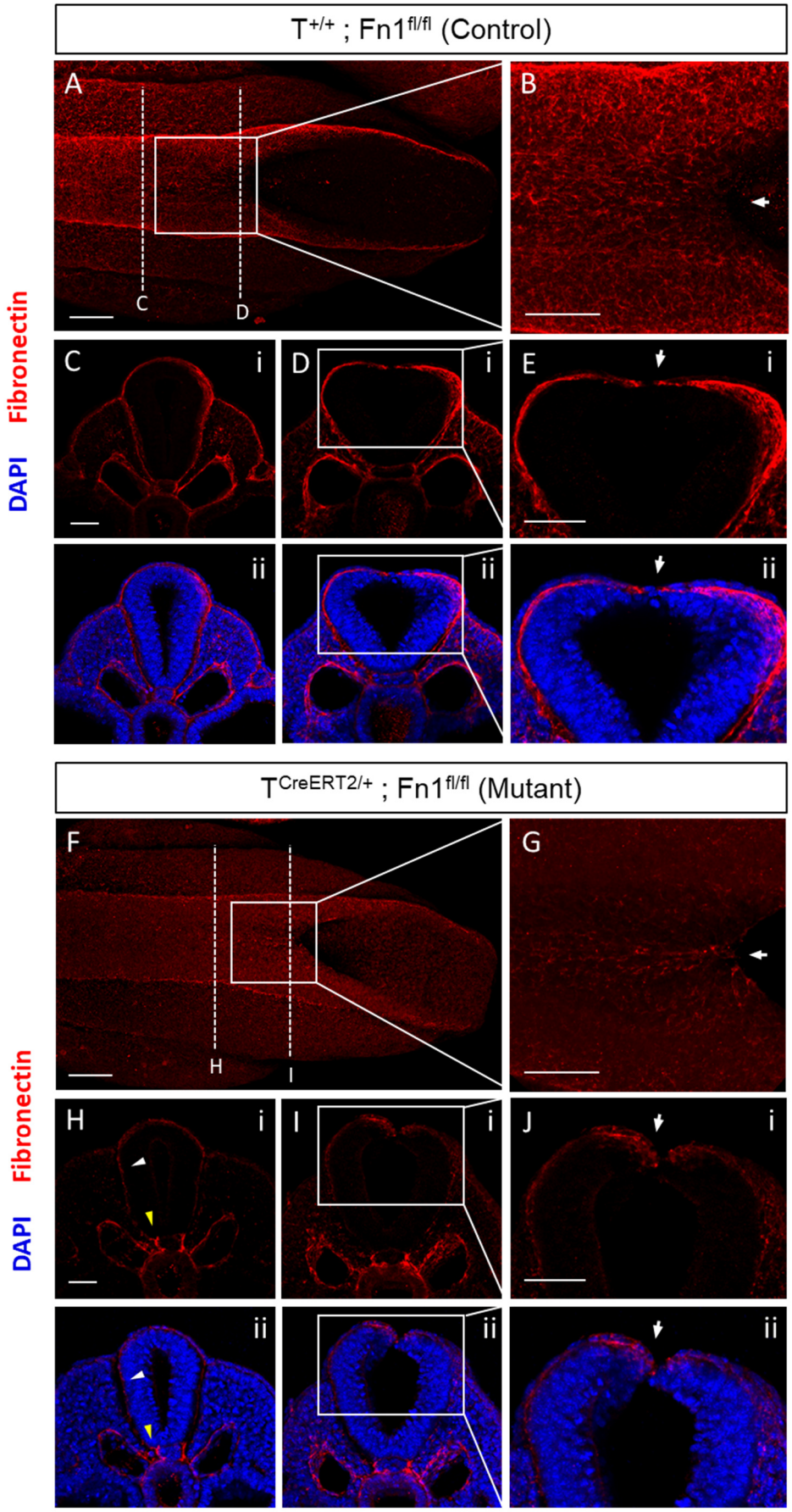
T+/+ ; Fn1fl/fl (Control)
A
B
C
D
C i
D i
E i
ii
ii
ii
Fibronectin
DAPI
TCreERT2/+ ; Fn1fl/fl (Mutant)
F
G
H
I
H i
I i
J i
ii
ii
ii
Fibronectin
DAPI

Figure 3.16. Fibronectin immunostaining of E9.5 embryos following $T^{CreERT2}$-mediated deletion of the fibronectin gene with tamoxifen induction at E7.5. (A, F) Maximum intensity projections of the caudal region of control (A) and mutant (F) embryos (n = 3 per genotype). The $T^{CreERT2}$-mediated deletion dramatically reduces fibronectin throughout the caudal region. (B, G) Higher magnification of the fusion site indicated by boxes in A and F. Arrows indicate the fusion site. Some radially oriented fibrils reproducibly persist around the fusion site of mutant embryos (G). (C, D, H, I) Cross sections at the levels of closed neural tube and fusion site indicated by the dashed lines in A and F. (E, J) Higher magnification of the fusion site region indicated by boxes in D and I. Fibronectin is still present in the neural fold tips (J, arrows), NE-MES BM (H, white arrowheads) and notochordal sheath (H, yellow arrowheads) of mutant embryos. Scale bars: 100 µm in A and F; 50 µm in C-H and G-J.

The *Cdx2*^{Cre}-mediated approach produced an even more dramatic result, with the entire PNP region of mutant embryos appearing devoid of fibronectin at E9.5 (Figure 3.17A, F). However, closer inspection of the fusion site again revealed that fibronectin is still present there, in all 4 of the mutants examined (Figure 3.17G, J). Similar to $T^{CreERT2}$; $Fn1^{fl/fl}$ embryos, the persistence of fibronectin in this small but critical region could explain the lack of NTDs in these mutants. In addition, cross sections revealed the fibronectin-rich notochord sheath was intact in agreement with the lack of recombination in the notochord (Figure 3.17H, yellow arrowhead). Furthermore, cross section images showed that the BM between the neuroepithelium and paraxial mesoderm was effectively devoid of fibronectin in $Cdx2^{Cre}$; $Fn1^{fl/fl}$ embryos (Figure 3.17H, white arrowhead). This contrasted with the persistence of some fibronectin in this BM in the $T^{CreERT2}$; $Fn1^{fl/fl}$ embryos, and could explain the presence of a tail defect in the $Cdx2^{Cre}$; $Fn1^{fl/fl}$ embryos, but not $T^{CreERT2}$; $Fn1^{fl/fl}$ embryos.

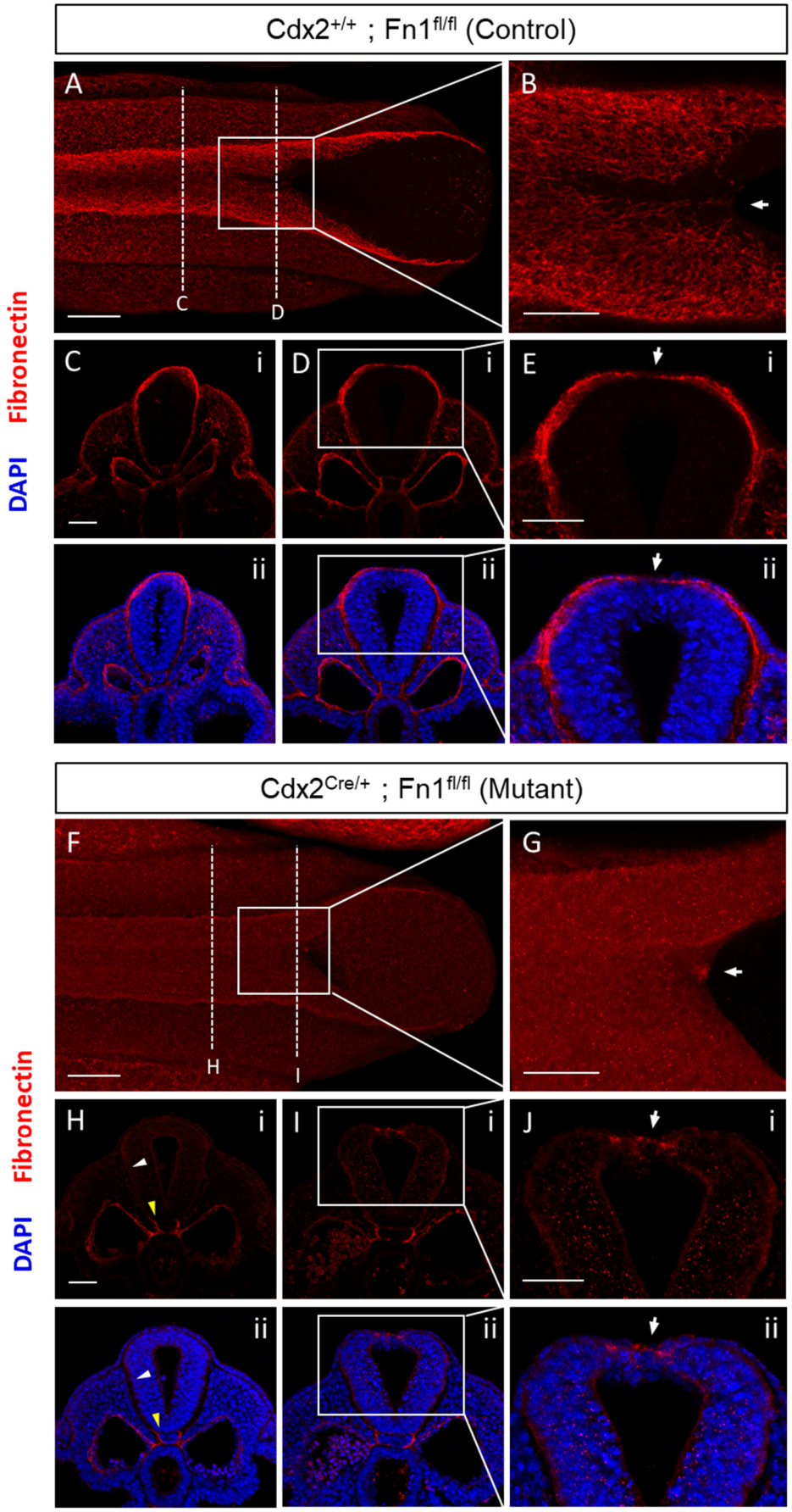
Cdx2+/+ ; Fn1fl/fl (Control)
A
B
C
D
Fibronectin
DAPI
C i
D i
E i
ii
ii
ii
Cdx2Cre/+ ; Fn1fl/fl (Mutant)
F
G
H
I
Fibronectin
DAPI
H i
I i
J i
ii
ii
ii

Figure 3.17. Fibronectin immunostaining of E9.5 embryos following *Cdx2*^{Cre}-mediated deletion of the fibronectin gene. (A, F) Maximum intensity projections of the caudal region of control (A) and mutant (F) embryos (n = 4 per genotype). The *Cdx2*^{Cre}-mediated deletion almost completely removes fibronectin from the caudal region. (B, G) Higher magnification of the fusion site indicated by boxes in A and F. Arrows indicate the fusion site. Fibronectin reproducibly persists exactly at the fusion site of mutant embryos (G, arrow). (C, D, H, I) Cross sections at the levels of closed neural tube and fusion site indicated by the dashed lines in A and F. (E, J) Higher magnification of the fusion site region indicated by boxes in D and I. Fibronectin is still present in the neural fold tips (J, arrows) and notochordal sheath (H, yellow arrowheads) of mutant embryos, but entirely absent from the NE-MES BM (H, white arrowheads). Scale bars: 100 μm in A and F; 50 μm in C-H and G-J.

These data support the hypothesis that fibronectin produced by the surface ectoderm at the fusion site is essential for spinal neural tube closure. However, the initial lineage tracing experiments showed that the spatiotemporal dynamics of surface ectoderm recombination differ substantially between the *Cdx2*^{Cre}- and *Grhl3*^{Cre}-mediated deletions. To determine how these instrumental differences between the two strategies are reflected in terms of their impact on fibronectin localisation, the immunostaining analysis was then extended to slightly younger E9.25 embryos from the two crosses as well. At this stage, the spinal neural folds of *Cdx2*^{Cre}*; Fn1*$^{fl/fl}$ embryos are recombined but the paraxial mesoderm flanking them is not, while the overlying surface ectoderm is only mosaically recombined (Figure 3.6). Accordingly, immunostaining revealed that while fibronectin across the dorsal midline is not as dense in the mutants as in the controls (Figure 3.18A, B), fibrils remain abundant around the fusion site (Figure 3.18C, D). Conversely, the *Grhl3*^{Cre}-mediated deletion effectively removed fibronectin from the fusion site region (Figure 3.18E, F), as expected based on the complete surface ectoderm recombination documented for this Cre from the earliest stages (Figure 3.7B).

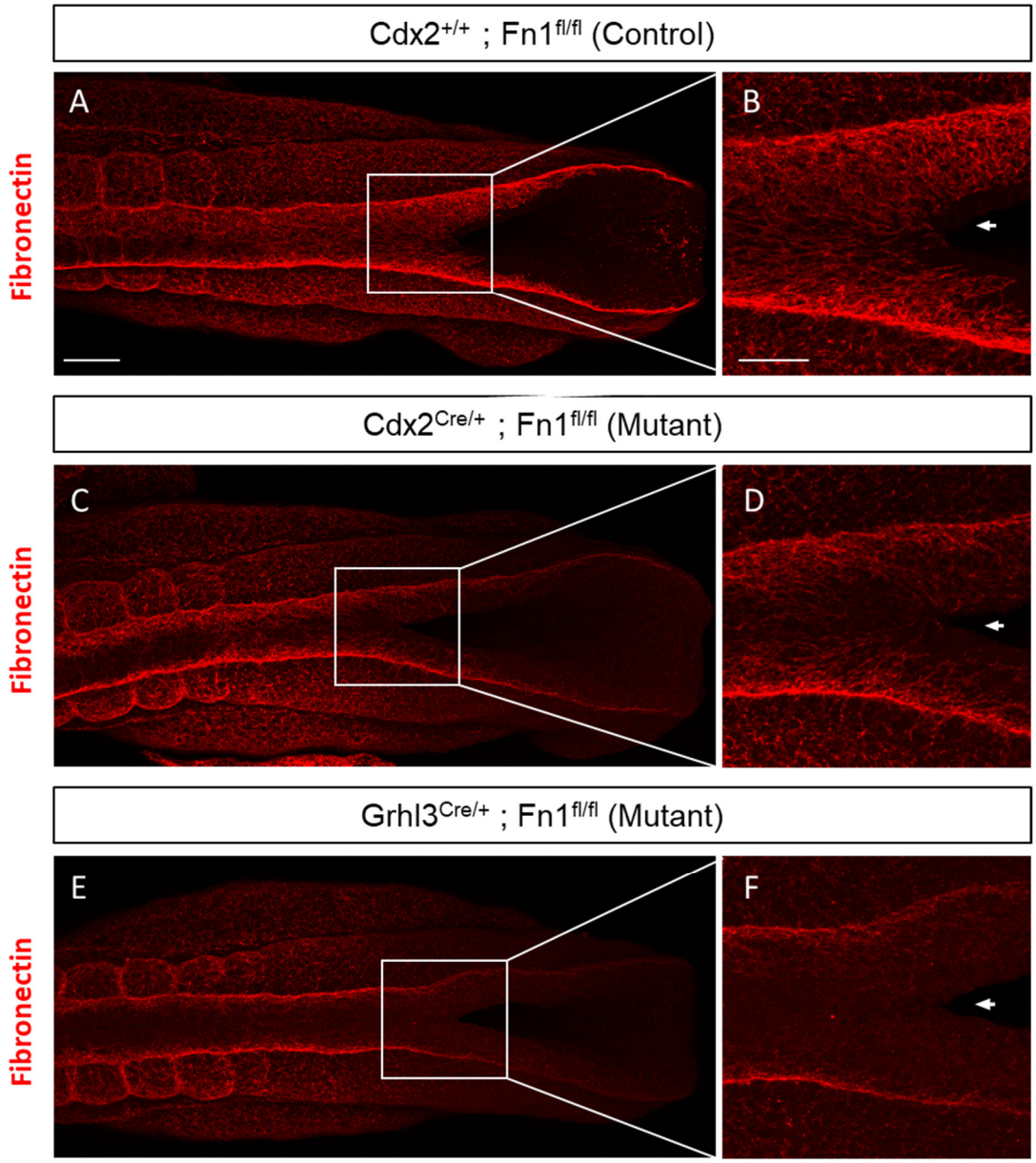

Figure 3.18. Fibronectin immunostaining of E9.25 embryos following *Cdx2*^{Cre}- and *Grhl3*^{Cre}-mediated deletion of the fibronectin gene. (A, C, E) Maximum intensity projections of the caudal region of control (A), *Cdx2*^{Cre}*; Fn1*$^{fl/fl}$ (C) and *Grhl3*^{Cre}*; Fn1*$^{fl/fl}$ *(*E) mutant embryos (n = 3 per genotype). (B, D, F) Higher magnification of the fusion site indicated by boxes in A, C and E. Arrows indicate the fusion site. There is partial removal of fibronectin from the fusion site in *Cdx2*^{Cre}*; Fn1*$^{fl/fl}$ mutants (D), compared to complete removal in *Grhl3*^{Cre}*; Fn1*$^{fl/fl}$ mutants (F). Scale bars: 100 µm in A, C, E; 50 µm in B, D, F.

Comparing the impact of each deletion strategy on fibronectin localisation and posterior development yields a number of important new insights. For example, one of the questions addressed here concerned the origin of the fibronectin BM at the surface ectoderm-neuroepithelium boundary. Juxtaposing *Grhl3*^{Cre}; *Fn1*$^{fl/fl}$ and *T*^{CreERT2}; *Fn1*$^{fl/fl}$ mutants (undergoing genetic ablations mainly in the surface ectoderm and paraxial mesoderm, respectively) illustrated that the fibronectin at the dorsal midline and fusion site is locally secreted by the surface ectoderm, while the remainder of this fibronectin BM is remotely produced by the paraxial mesoderm. Furthermore, morphological characterisation of all three mutant groups revealed that it is only the small locus of fibronectin at the fusion site that is required for the final stages of spinal neural tube closure, while the remainder of the fibronectin network appears redundant for this process. Comparing fibronectin localisation and morphology in *T*^{CreERT2}; *Fn1*$^{fl/fl}$ and *Cdx2*^{Cre}; *Fn1*$^{fl/fl}$ mutants, on the other hand, reveals that the process of axial elongation depends on the presence of fibronectin at the neuroepithelium-paraxial mesoderm interface. This BM most likely originates from the paraxial mesoderm and, interestingly, just a small fraction of the fibronectin there appears to be sufficient to sustain symmetric elongation of the tail (i.e., in *T*^{CreERT2}; *Fn1*$^{fl/fl}$ mutants). The process, however, fails when the BM is completely abolished (i.e., in *Cdx2*^{Cre}; *Fn1*$^{fl/fl}$ mutants).

3.2.5 Loss of fibronectin in the surface ectoderm prevents integrin activation

Having established the requirement of fibronectin expression at the fusion site for successful closure of the spinal neural tube, subsequent experiments (in this chapter) focused on discovering the developmental mechanism through which loss of fibronectin leads to spina bifida. Fibronectin has been shown to influence cell behaviour in a variety of ways by acting as a mechanical scaffold as well as by activating numerous intracellular pathways. The first step in all of these signalling and biomechanical functions is fibronectin binding to the integrin receptor and stabilising it into its active conformation. The integrin β1 subunit forms part of the

primary fibronectin receptor α5β1 and its ablation from the fusion site has been shown to cause highly penetrant spina bifida. As previously described, integrin β1 (along with its partner α5) shows marked upregulation and activation at the fusion site of wild type embryos.

To assess whether this focal integrin β1 activation was affected by any of the conditional fibronectin ablations employed here, control and mutant embryos from each of the three groups were immunostained for the active (ligand-bound) form of integrin β1. High-resolution confocal microscopy of the fusion site revealed that integrin β1 activation was indeed significantly reduced in *Grhl3^{Cre}; Fn1$^{fl/fl}$* mutant embryos (Figure 3.19A-C). Such a loss of integrin activation was in accordance with the selective removal of fibronectin from the fusion site. *T^{CreERT2}; Fn1$^{fl/fl}$ and Cdx2^{Cre}; Fn1$^{fl/fl}$* mutants, on the other hand, were indistinguishable from controls in terms of integrin β1 staining (Figure 3.19D, E). Therefore, the small amount of fibronectin persisting at the fusion site of *T^{CreERT2}; Fn1$^{fl/fl}$* and even *Cdx2^{Cre}; Fn1$^{fl/fl}$* mutants proved sufficient for sustaining normal integrin activation; hence providing an explanation for the lack of NTDs in these embryos.

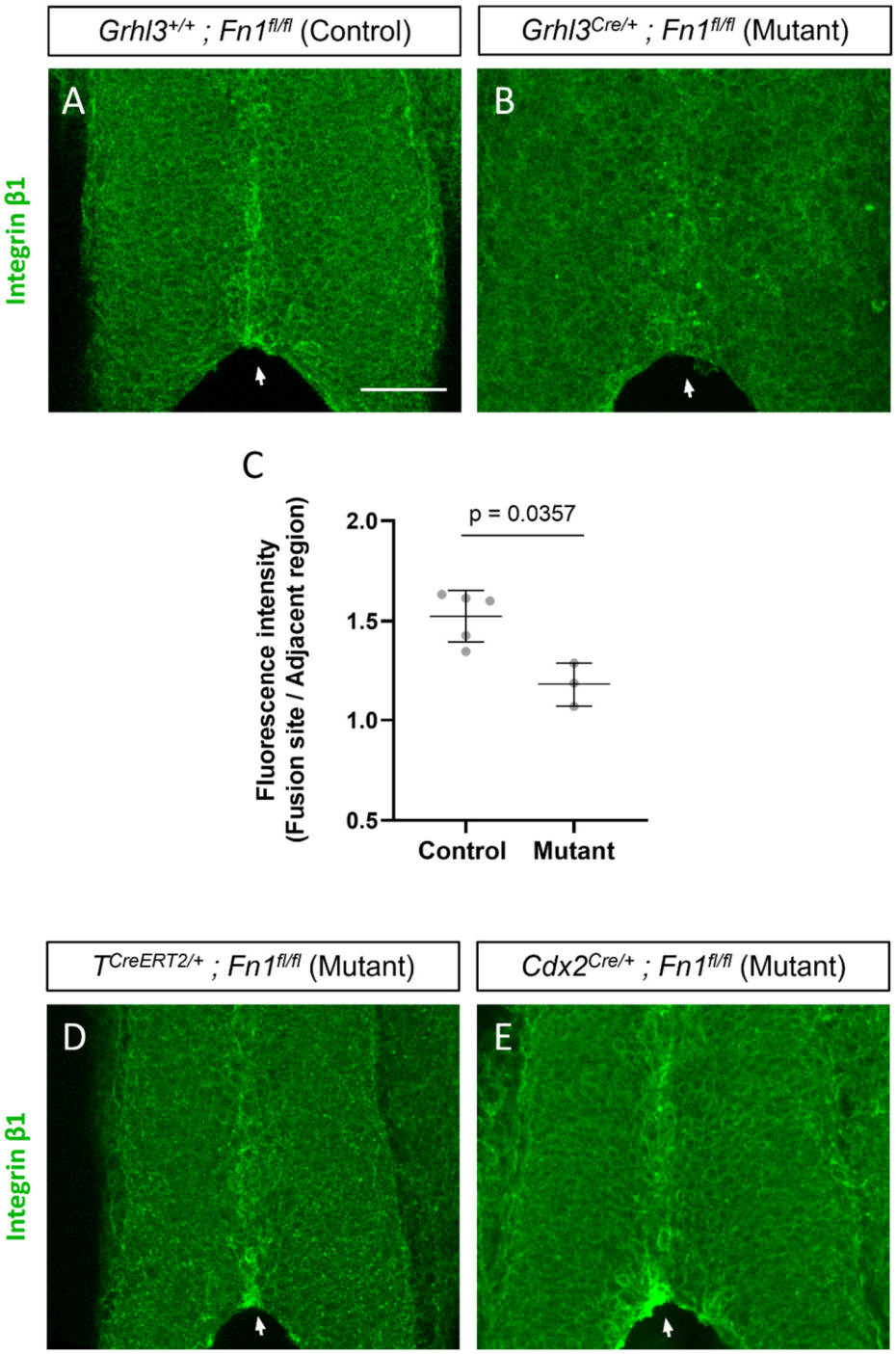

Figure 3.19. Integrin β1 (active) immunostaining of E9.5 embryos following *Grhl3*^{Cre}-, *T*^{CreERT2}- and *Cdx2*^{Cre}-mediated deletion of the fibronectin gene. (A, B, D, E) Maximum intensity projections of the fusion site of control (A), *Grhl3*^{Cre}*; Fn1*$^{fl/fl}$ (B), *T*^{CreERT2}*; Fn1*$^{fl/fl}$ (C) and *Cdx2*^{Cre}*; Fn1*$^{fl/fl}$ (D) mutant embryos (n = 3 per genotype). Arrows indicate the fusion site. Strong integrin activation in the dorsal midline and fusion site is observed in control (A), *T*^{CreERT2}*; Fn1*$^{fl/fl}$ (C) and *Cdx2*^{Cre}*; Fn1*$^{fl/fl}$ (D) embryos but not in *Grhl3*^{Cre}*; Fn1*$^{fl/fl}$ embryos (B). (C) Statistical comparison of integrin β1 intensity at

the fusion site normalised to intensity at an adjacent region lateral to it confirms a significant reduction in *Grhl3*^{Cre}*; Fn1*$^{fl/fl}$ mutants versus controls (Mann-Whitney test; p value in figure; embryos: controls n = 5, mutants n = 3). Data shown as mean values ± SD. Scale bar: 50 µm.

3.2.6 Loss of fibronectin in the surface ectoderm does not affect cell survival or proliferation

Integrin binding and activation by fibronectin is known to initiate a variety of intracellular signalling cascades that ultimately regulate cell survival, proliferation and actomyosin dynamics: processes vital to the formation of the neural tube. For example, loss of adhesion has been shown to result in a type of programmed cell death termed anoikis (Frisch & Francis, 1994; Meredith et al., 1993). Furthermore, cells in the dorsal midline of the neural tube have previously been shown to undergo apoptosis, which might be important for the process of epithelial remodelling (Weil et al., 1997; Yamaguchi et al., 2011). To investigate whether NTDs might be arising from a dysregulation of cell death (in response to fibronectin deletion), *Grhl3*^{Cre}*; Fn1*$^{fl/fl}$ mutants and littermate controls were immunostained for the apoptosis marker cleaved caspase 3 (CCasp3). Confocal microscopy then showed that, in both mutants and controls, apoptosis was mainly concentrated in the dorsal midline (Figure 3.20A, B). Quantification of CCasp3-positive foci within the surface ectoderm revealed a minor non-significant trend for increased cell death in mutant embryos (Figure 3.20C). However, the considerable variability observed in this measure and the small number of cells involved argue against a mechanistic role for this difference in the pathogenesis of NTDs. Immunostaining for the mitotic marker phospho-histone H3 (pHH3) and an analogous quantification detected no differences in the extent or distribution of cell divisions within the surface ectoderm, thereby excluding this process as well (Figure 3.20D-F).

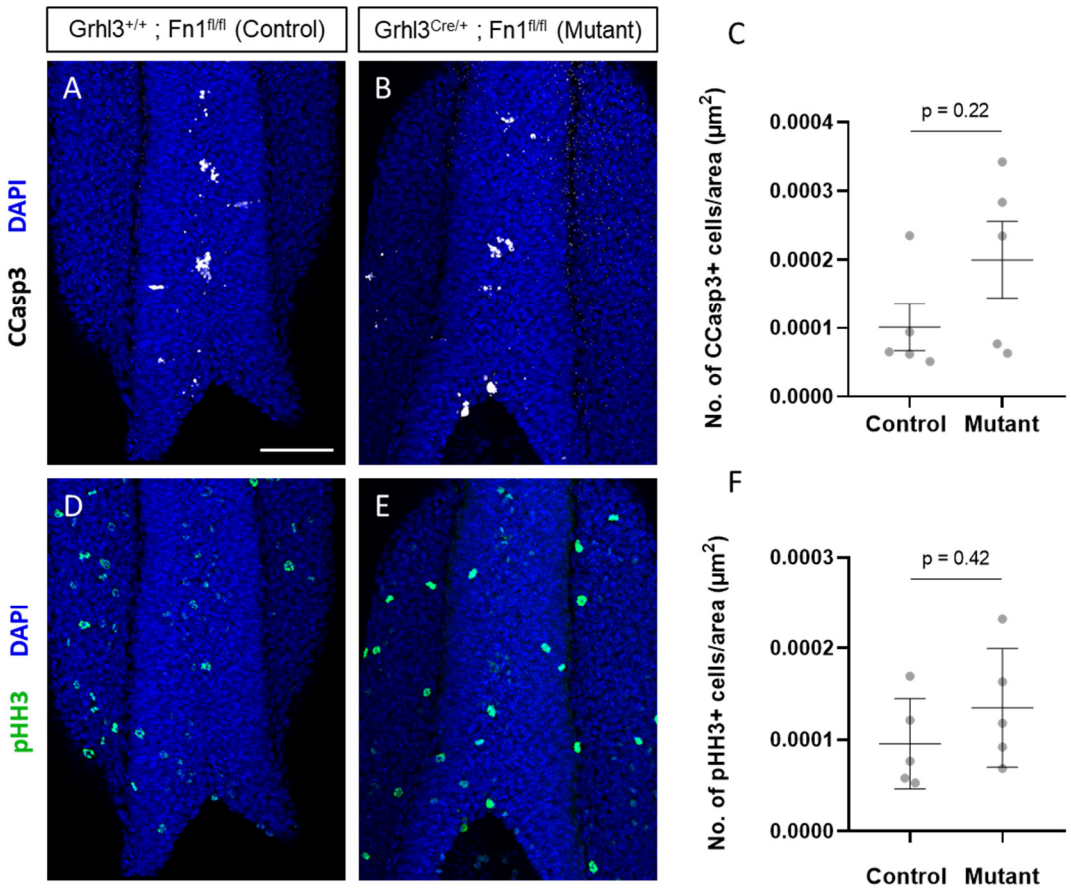

Figure 3.20. CCasp3 and pHH3 immunostaining of E9.5 embryos following *Grhl3*^{Cre}-mediated deletion of the fibronectin gene. (A, B, D, E) Maximum intensity projections of the recently closed neural tube region of control (A, D) and mutant (B, E) embryos show a similar distribution of apoptotic (A, B) and dividing (D, E) cells within the dorsal surface ectoderm (n = 5 per genotype). (C, F) Quantification of CCasp3 and pHH3 signal detected no significant differences in the extent of apoptosis or cell division in this area (Mann-Whitney test; p values in figure; embryos: controls n = 5, mutants n = 5). Data shown as mean values per embryo ± SD. Scale bar: 100 µm.

3.2.7 Loss of fibronectin in the surface ectoderm leads to dysregulation of cell-ECM and cell-cell adhesion at the fusion site

Even more important for embryonic morphogenesis is the ability of integrins to bind to the actin cytoskeleton and regulate actomyosin assembly and contractility. Binding to the fibronectin matrix could therefore serve the need of cells for

mechanical anchorage or stimulate a range of dynamic cell behaviours such as migration, protrusive activity and shape changes. Central to all of these functions is the recruitment of the adaptor protein talin to the intracellular tail of the integrin β1 subunit. Following integrin-ECM binding, talin provides the first link to F-actin, while also recruiting numerous components of the integrin adhesome that strengthen that linkage further and initiate various signalling cascades. To understand how deletion of fibronectin in the surface ectoderm affects these downstream processes and prevents neural fold fusion, *Grhl3*^{Cre}; *Fn1*$^{fl/fl}$ mutants and controls were first immunostained for talin. Talin localises mainly at cell borders and shows a strong enrichment at the fusion site (Figure 3.21A, arrow), overlapping with the locus of integrin β1 activation. While the general appearance of talin in most of the surface ectoderm was unaffected by the fibronectin deletion, the fusion site enrichment was diminished in the mutants (Figure 3.21B, arrow), in accordance with the reduction in integrin β1 activation described previously.

Next, to assess F-actin assembly, these embryos were stained with phalloidin. In control embryos, phalloidin staining reveals the existence of a supra-cellular actin cable running along the neural fold tips and encircling the PNP (Galea et al., 2017), as well as focal enrichment at the fusion site where actin-rich protrusions form (Figure 3.21C). Surprisingly, these landmarks were equally apparent in the mutants, showing that, at least on a large scale, F-actin assembly has been unaffected by the (partial) loss of fibronectin (Figure 3.21D). In addition, immunostaining these embryos for myosin heavy chain (MHC)-IIb confirmed that the contractile machinery is also in place, including enrichment in the dorsal midline of the recently fused neural tube and actin cable (Figure 3.21E, F).

Integrins (mediating cell-ECM adhesion) and cadherins (mediating cell-cell adhesion) share a large proportion of cytoskeletal and signalling effectors and the two systems engage in significant crosstalk (Burute & Thery, 2012; McMillen & Holley, 2015; Tseng et al., 2012; Weber et al., 2011). This crosstalk can be characterised by either positive or negative feedback loops in a context-dependent manner and is essential for regulating the balance between inter- and intracellular tensions. To assess whether the *Grh3*^{Cre}-mediated fibronectin deletion somehow influenced the assembly of

adherens junctions in the surface ectoderm, mutant and control embryos were immunostained for E-cadherin. In control embryos, E-cadherin was confined to the cell borders throughout the surface ectoderm, and showed a clear enrichment in the dorsal midline and fusion site (Figure 3.21G). Interestingly, while the overall pattern of E-cadherin localisation was similar in the mutants, cell border staining around the fusion site appeared weaker and more diffuse compared to the controls (Figure 3.21H).

In summary, the ablation of fibronectin at the dorsal midline has resulted in the loss of integrin activation and talin recruitment in the *Grhl3*^{Cre}; *Fn1*$^{fl/fl}$ mutants, and in turn a dysregulation of cell-cell junctions at the fusion site region. On the other hand, actomyosin assembly and cell proliferation and survival appear unaffected by the fibronectin ablation.

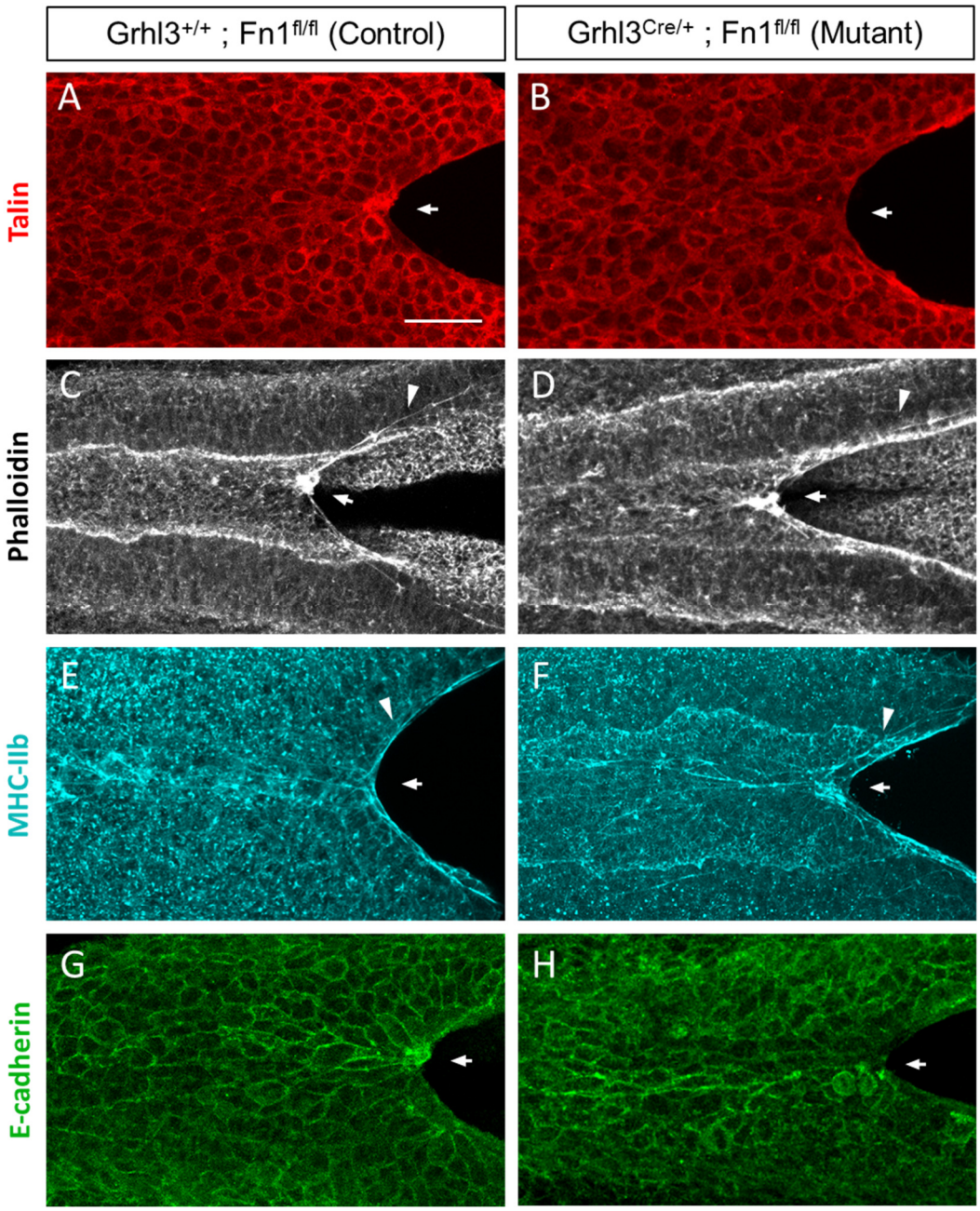

Figure 3.21. Immunostaining of E9.5 embryos for cytoskeletal and adhesion markers following *Grhl3*^{Cre}-mediated deletion of the fibronectin gene. (A-H) Maximum intensity projections of the recently closed neural tube of control (A, C, E, G) and mutant (B, D, F, H) embryos (n = 3 per genotype). Arrows indicate the fusion site. (A, B) The fusion site of mutants lacks the strong talin enrichment observed in controls. (C-F) The overall structure of the cytoskeleton, revealed by phalloidin staining and MHC-IIb immunostaining, is unaffected by the deletion. The actomyosin cable running across the neural fold tips is readily visible in both mutants and controls (arrowheads). (G, H) The overall distribution of E-cadherin is unaffected by the

deletion, but mutants show weaker and more diffuse cell border staining around the fusion site (H, arrow). Scale bar: 50 µm.

3.2.8 Cell shape analyses following fibronectin ablations

Subtle changes in the regulation of actomyosin and cell junction dynamics – that may not be necessarily evident with immunohistochemistry - could gradually alter the biomechanical properties of the surface ectoderm and result in more easily detectable differences in cell shape. Previous morphometric analyses have demonstrated that surface ectoderm cells overlying the dorsal midline of the recently fused neural tube become significantly elongated along the AP axis (Nikolopoulou et al., 2019). Furthermore, as surface ectoderm cells come into contact with the fusion site during the process of zippering, they tend to narrow their posterior junctions, adopt a wedge shape and thus form a semi-rosette around the fusion site (Zhou et al., 2020). Importantly, both cell elongation along the midline and semi-rosette formation were shown to be integrin β1-dependent and are considered important for the propagation of neural fold zippering (Molè et al., 2020).

To ascertain whether fibronectin ablation has hindered neural fold zippering by disrupting these cellular behaviours, *Grhl3*^{Cre}; *Fn1*$^{fl/fl}$ mutants and controls were immunostained for the tight junction protein ZO-1, allowing cell segmentation of surface ectoderm midline cells (Figure 3.22A, B) followed by a series of morphometric analyses (Figure 3.22C-F). These revealed that midline cells in mutant embryos had a significantly increased apical surface area. Furthermore, in silico conversion of cell outlines into ellipses (and measurement of the major and minor axes) showed that the larger surface area of mutant cells was entirely due to an increase in width, while their length and orientation along the AP axis remained unchanged. Moreover, the fusion site of mutant and control embryos was imaged in high resolution to assess the formation of the previously described semi-rosettes (Figure 3.22G, H). Control embryos indeed displayed a clear semi-rosette configuration consisting of 6-7 wedge-shaped cells in contact with the fusion site (Figure 3.22I). The structures,

however, appeared largely disrupted in the mutants where only 4-5 cells were in contact with the fusion site. These cells displayed a much more rectangular shape as well as blurred borders, akin to those observed with the E-cadherin immunostaining. Therefore, deletion of fibronectin in the surface ectoderm appeared to perturb the ability of midline cells to effectively control their shape and remodel their junctions, as was the case for the characterised integrin β1 deletion (Molè et al., 2020).

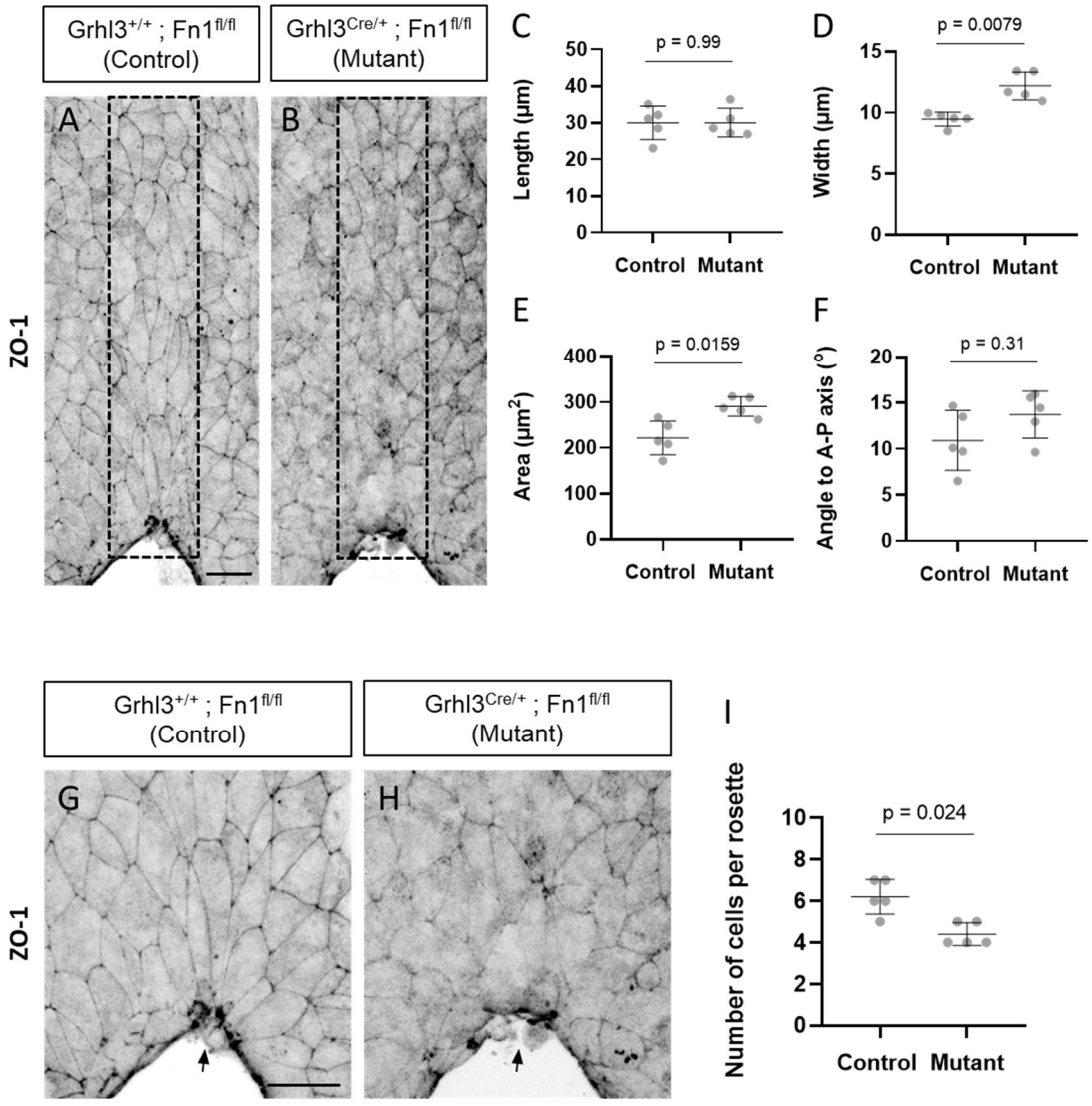

Figure 3.22. Surface ectoderm cell shape analysis in E9.5 embryos immunostained for ZO-1 following *Grhl3*^{Cre}-mediated deletion of the fibronectin gene. (A, B) Maximum intensity projections of the recently closed dorsal neural tube of control (A) and mutant (B) embryos (n = 5 per genotype). (C-F) Morphometric analyses of dorsal

midline surface ectoderm cells (indicated by the dashed box in A and B). The deletion has caused a significant increase in cell width (D) and apical surface area (E), while cell length (C) and orientation (F) are unaffected (Mann-Whitney test; p values in figure; embryos: controls n = 5, mutants n = 5). (G, H) Maximum intensity projections of the fusion site of control (G) and mutant (H) embryos (n = 5 per genotype). In control embryos, cells around the fusion site adopt a wedge shape and form semi-rosettes, while in mutants they often maintain a more rectangular shape and fail to form semi-rosettes. In addition, ZO-1 staining at cell borders is weaker in the mutants than in the controls. (I) Quantification of cells in contact with the fusion site (G, H, arrows) confirms a significant reduction in the mutants (Mann-Whitney test; p values in figure; embryos: controls n = 5, mutants n = 5). Data shown as mean values ± SD. Scale bar: 25 μm.

To determine whether these changes are instrumental to the pathogenesis of spinal NTDs, or merely a side effect of the fibronectin ablation, and to better understand how they relate to fibronectin localisation, these analyses were then repeated with $T^{CreERT2}$; $Fn1^{fl/fl}$ mutants and $Cdx2^{Cre}$; $Fn1^{fl/fl}$ mutants (which display extensive loss of fibronectin, yet no NTDs). When compared to littermate controls, $T^{CreERT2}$; $Fn1^{fl/fl}$ mutants showed no differences in surface ectoderm cell shape, surface area or orientation across the midline and no defects in their ability to assemble semi-rosettes at the fusion site (Figure 3.23). It therefore became apparent that the limited amount of fibronectin secreted by the unrecombined surface ectoderm across the dorsal midline is sufficient to prevent cell shape and junctional dysregulation.

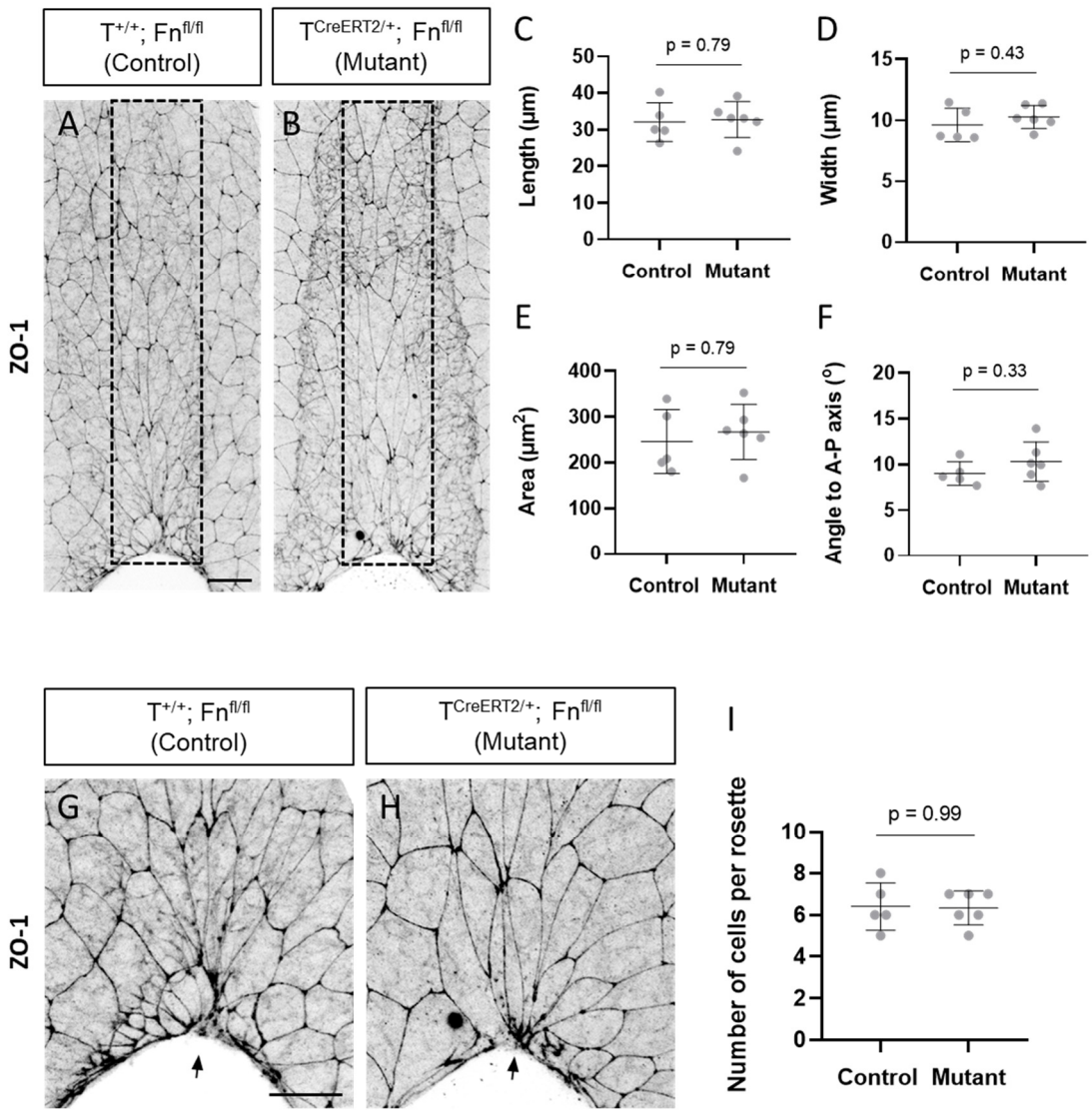

Figure 3.23. Surface ectoderm cell shape analysis in E9.5 embryos immunostained for ZO-1 following *T*^{CreERT2}-mediated deletion of the fibronectin gene with tamoxifen induction at E7.5. (A, B) Maximum intensity projections of the recently closed dorsal neural tube of control (A) and mutant (B) embryos (n = 5 per genotype). (C-F) Morphometric analyses of dorsal midline surface ectoderm cells (indicated by the dashed box in A and B). All measured aspects of cell shape are unaffected by the deletion (Mann-Whitney test; p values in figure; embryos: controls n = 5, mutants n = 6). (G, H) Maximum intensity projections of the fusion site of control (G) and mutant (H) embryos (n = 5 per genotype). Mutant embryos exhibit normal semi-rosette formation. (I) Quantification of cells in contact with the fusion site (G, H, arrows) show no significant difference between mutants and controls (Mann-Whitney test; p

values in figure; embryos: controls n = 5, mutants n = 6). Data shown as mean values ± SD. Scale bar: 25 μm.

Cdx2^{Cre}; *Fn1*$^{fl/fl}$ mutants, on the other hand, exhibited a milder version of the same cell shape abnormalities found in the *Grhl3*^{Cre}; *Fn1*$^{fl/fl}$ mutants. In this case, midline surface ectoderm cells had normal length and orientation (Figure 3.24C, F), but showed a nearly significant increase in width, leading to a trend for increased apical surface area (Figure 3.24D, E). Nevertheless, *Cdx2*^{Cre}; *Fn1*$^{fl/fl}$ embryos showed no significant differences in the number of cells participating in fusion site semi-rosettes (Figure 3.24I). It therefore became clear that the small amount of fibronectin persisting at the fusion site of these mutants was capable of sustaining not only integrin β1 activation, but also the formation of cellular semi-rosettes around it. Conversely, the complete loss of fibronectin from the rest of the dorsal region hindered the narrowing of midline surface ectoderm cells, but this abnormality seemed to be compatible with successful spinal neural tube closure. Together these analyses showed that fusion site semi-rosette formation is the critical mechanism that relies on integrin-fibronectin binding and is necessary for successful spinal neural tube closure.

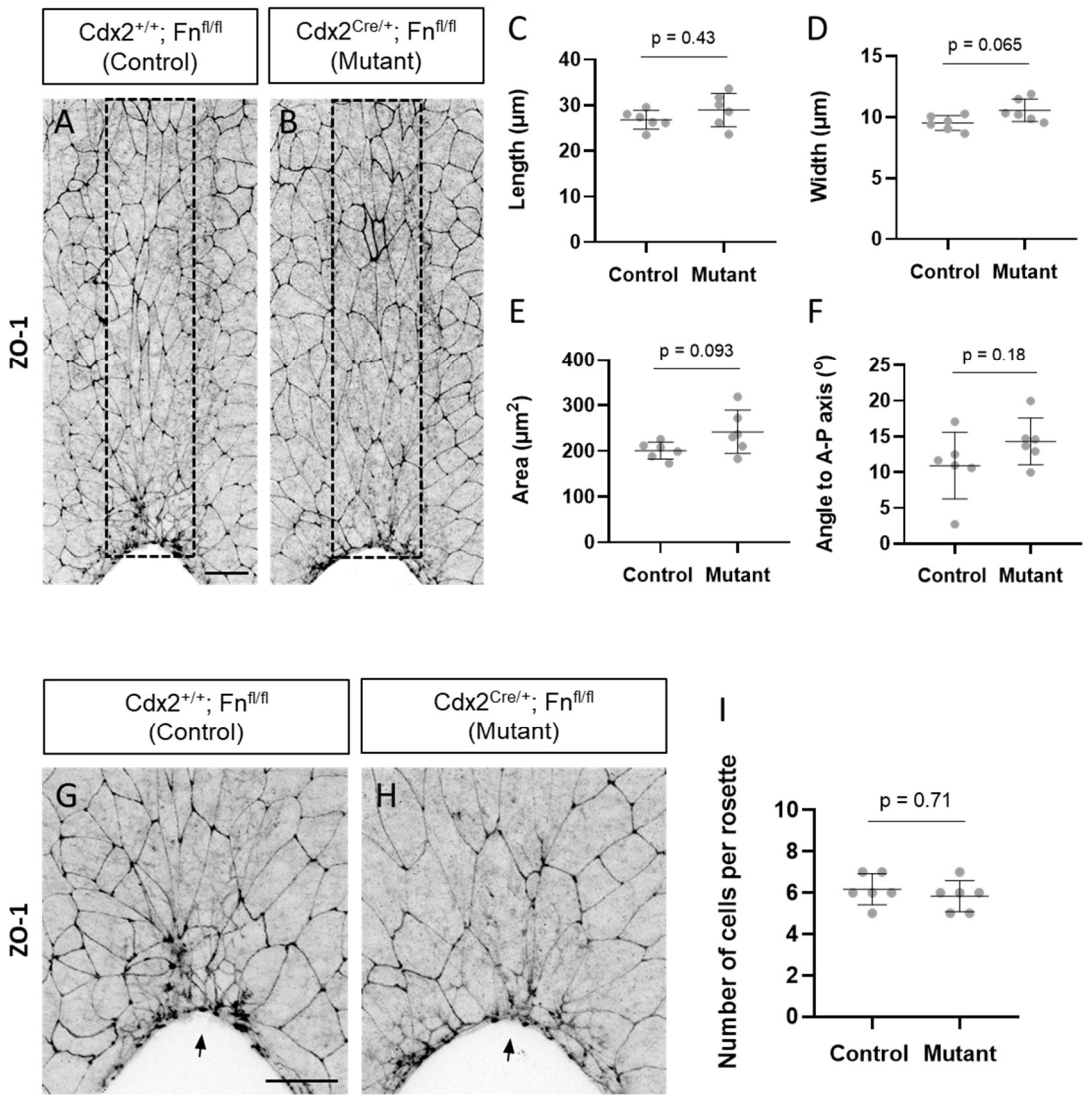

Figure 3.24. Surface ectoderm cell shape analysis in E9.5 embryos immunostained for ZO-1 following *Cdx2*^{Cre}-mediated deletion of the fibronectin gene. (A, B) Maximum intensity projections of the recently closed dorsal neural tube of control (A) and mutant (B) embryos (n = 6 per genotype). (C-F) Morphometric analyses of dorsal midline surface ectoderm cells (indicated by the dashed box in A and B). The deletion has caused nearly significant increases in cell width (D) and (to a lesser extent) apical surface area (E), while cell length (C) and orientation (F) appear unaffected (Mann-Whitney test; p values in figure; embryos: controls n = 6, mutants n = 6). (G, H) Maximum intensity projections of the fusion site of control (G) and mutant (H) embryos (n = 6 per genotype). Mutant embryos exhibit normal semi-rosette formation. (I) Quantification of cells in contact with the fusion site (G, H, arrows) show no significant difference between mutants and controls (Mann-Whitney test; p

values in figure; embryos: controls n = 6, mutants n = 6). Data shown as mean values ± SD. Scale bar: 25 µm.

3.3 Discussion

Fibronectin has long been recognised as an essential ECM component for axial elongation, especially in the formation of mesodermal derivatives (George et al., 1993; Georges-Labouesse et al., 1996). However, more recent evidence from our lab also implicated fibronectin in the process of spinal neural tube closure (Molè et al., 2020). Previous studies have been hampered by the premature axial truncation of fibronectin (and related integrin) mutant embryos, fibronectin's involvement in multiple interconnected developmental processes, and its complex expression and localisation profile. The current study sought to clarify the origin and functional significance of the various parts of the fibronectin network for posterior development by employing three separate conditional deletion strategies to remove fibronectin from different tissues. The recombination domains of the three chosen Cre drivers were precisely mapped through lineage tracing with the mTmG reporter, and each set of mutant embryos was characterised in terms of morphology, fibronectin localisation, and related cellular processes. The conditional deletions used here targeted posterior tissues while sparing cardiovascular and extraembryonic structures (crucial for overall developmental progression) and were thus able to reveal two distinct previously unrecognised roles of fibronectin in caudal morphogenesis. Firstly, spinal neural tube fusion was shown to depend on fibronectin locally expressed at the fusion site by the surface ectoderm. This focal expression was ablated in the NTD-affected *Grhl3*^{Cre}; *Fn1*$^{fl/fl}$ mutant embryos but persisted in the NTD-unaffected *T*^{CreERT2}; *Fn1*$^{fl/fl}$ and *Cdx2*^{Cre}; *Fn1*$^{fl/fl}$ mutants. Secondly, symmetric elongation of the tail was shown to require at least a small amount of fibronectin at the NE-MES interface. This fibronectin BM was partially present in the *T*^{CreERT2}; *Fn1*$^{fl/fl}$ mutants, which appeared normal, but completely absent in the *Cdx2*^{Cre}; *Fn1*$^{fl/fl}$ mutants which exhibited shortened and malformed tails.

The current chapter focused on the role of fibronectin in neural tube closure. In this regard, the comparison of *Grhl3*^{Cre}; *Fn1*$^{fl/fl}$ and *Cdx2*^{Cre}; *Fn1*$^{fl/fl}$ mutant embryos was particularly instructive. As *Cdx2*^{Cre} was initially shown to recombine the surface ectoderm (along with the neuroepithelium and paraxial mesoderm) at E9.5, the

Cdx2^{Cre}-mediated deletion of fibronectin was expected to give rise to spina bifida, similar to the *Grhl3*^{Cre}-mediated deletion (targeting the surface ectoderm). Surprisingly, *Cdx2*^{Cre}; *Fn1*$^{fl/fl}$ mutants were found to be completely normal in terms of neural tube closure. Extended characterisation of these two Cre drivers and their respective mutants produced two explanations for this discrepancy. Firstly, immunofluorescence analyses revealed that while the caudal region of *Cdx2*^{Cre}; *Fn1*$^{fl/fl}$ embryos is mostly devoid of fibronectin, small amounts of the protein can still be reproducibly found at the fusion site of the PNP of these embryos. In addition, that is the exact region where the *Grhl3*^{Cre}-mediated ablation of fibronectin was most effective. These findings, therefore, suggest that a small amount of fibronectin in this critical region is sufficient to facilitate the process of neural fold fusion and prevents spina bifida in the *Cdx2*^{Cre}; *Fn1*$^{fl/fl}$ mutants. This hypothesis is also supported by the normal integrin β1 activation and semi-rosette formation at the fusion site of *Cdx2*^{Cre}; *Fn1*$^{fl/fl}$ mutants (contrary to *Grhl3*^{Cre}; *Fn1*$^{fl/fl}$ mutants).

The alternative explanation relates to differences in the timing with which the two Cre drivers target the surface ectoderm. Lineage tracing and immunofluorescence analyses in younger embryos (E8.5-E9.25) showed that *Grhl3*^{Cre} fully recombines the surface ectoderm and removes fibronectin from the fusion site already from the early stages of PNP closure. *Cdx2*^{Cre}-mediated recombination of the surface ectoderm, on the other hand, was found to be a much more spatially and temporally protracted process. Accordingly, fibronectin was somewhat reduced but still present at the fusion site of E9.25 *Cdx2*^{Cre}; *Fn1*$^{fl/fl}$ embryos. Combined with the presence of NTDs in *Grhl3*^{Cre}; *Fn1*$^{fl/fl}$ but not in *Cdx2*^{Cre}; *Fn1*$^{fl/fl}$ embryos, these findings could hence be taken as evidence that fibronectin is only important for the early stages (and more anterior segments) of PNP closure. In other words, the critical temporal and spatial window for fibronectin's function in spinal neural tube fusion precedes *Cdx2*^{Cre}-mediated recombination of the surface ectoderm but follows (the earlier) *Grhl3*^{Cre}-mediated recombination of the surface ectoderm. In agreement, a linear regression analysis of PNP dimensions against somite number in *Grhl3*^{Cre}*; Fn1*$^{fl/fl}$ mutants and controls revealed that the delay in closure appears at early somite stages in these mutants. Finally, the two explanations presented here are not mutually exclusive

since the increasing capacity of *Cdx2*^{Cre} to ablate fibronectin expression in the surface ectoderm at later stages might coincide with a decreasing dependence of the zippering process on fibronectin.

Having identified the specific part of the fibronectin network that is required for neural tube closure, the second half of the current chapter sought to determine the mechanism through which fibronectin exerts its role. In this regard, fibronectin was shown to facilitate the focal integrin β1 activation at the fusion site which has previously been shown to be essential for zippering (Molè et al., 2020). Furthermore, cellular processes regulated by integrins, including apoptosis, proliferation and cytoskeletal assembly, were shown to be unaffected by the fibronectin gene deletion. Instead, fibronectin's importance in this context appeared to derive from its role as a structural substrate for integrin-mediated mechanical anchorage. The surface ectoderm cells of *Grhl3*^{Cre}*; Fn1*$^{fl/fl}$ mutants exhibited impaired talin and E-cadherin recruitment to cell borders and an inability to narrow their ML junctions along the dorsal midline and to form semi-rosettes at the fusion site. Interestingly, analogous cell shape analyses of (the NTD-unaffected) *Cdx2*^{Cre}; *Fn1*$^{fl/fl}$ mutants also detected cell widening across the dorsal midline but no semi-rosette defects, thus emphasizing the latter as the most critical cell shape property for neural tube closure.

Overall, the phenotype of *Grhl3*^{Cre}; *Fn1*$^{fl/fl}$ mutants (lacking fibronectin expression in the surface ectoderm) is extremely similar to that of the previously characterised *Grhl3*^{Cre}; *Itgb1*$^{fl/fl}$ mutants (lacking integrin β1 expression in the surface ectoderm) (Molè et al., 2020). These two genetic deletions therefore jointly support a model whereby surface ectoderm cells locally secrete and bind fibronectin at the fusion site. This integrin-fibronectin interaction provides mechanical cell-ECM anchorage and facilitates zippering propagation by allowing contralateral surface ectoderm cells to dynamically remodel their junctions and become juxtaposed in a semi-rosette configuration. The integrin and fibronectin mutants do, however, differ with regard to the penetrance of their spinal NTDs; estimated to 78% and 29%, respectively. This divergence might be explained by differences in the capacity of the two deletions to ablate integrin β1-fibronectin interactions in the surface ectoderm. *Grhl3*^{Cre}; *Itgb1*$^{fl/fl}$ mutants, for example, lack integrin β1 (and hence integrin β1-fibronectin binding)

throughout the surface ectoderm. *Grhl3*^{Cre}; *Fn1*$^{fl/fl}$ mutants, on the other hand, display a significant reduction of fibronectin at the dorsal midline, but substantial amounts of fibronectin (likely originating from the paraxial mesoderm) still remain in their dorsal BM. Therefore, integrin β1-fibronectin interactions are only partially ablated. Alternatively, the relatively lower NTD penetrance in *Grhl3*^{Cre}; *Fn1*$^{fl/fl}$ mutants could be due to compensation by a different ECM ligand. Deletion of the integrin β1 subunit prevents assembly of fibronectin- (α5β1 and αvβ1) as well as laminin-interacting receptors (α6β1 and α3β1). Moreover, previous expression analyses showed that laminin (despite being relatively downregulated in the dorsal midline) surrounds the entire surface ectoderm in the caudal embryo. Integrin-laminin interactions – which have been ablated in *Grhl3*^{Cre}; Itgb1$^{fl/fl}$ but not *Grhl3*^{Cre}; *Fn1*$^{fl/fl}$ mutants - might therefore also facilitate spinal neural tube closure by acting in the dorsal midline or more lateral regions. In agreement, laminin-α3/α6 compound mutant embryos have previously been shown to develop craniorachischisis (although this result was not replicable in our lab) (De Arcangelis et al., 1999).

Another instructive difference between the fibronectin and integrin β1 surface ectoderm cKO models relates to the state of the dorsal fibronectin BM (between the surface ectoderm and neuroepithelium). This was shown to be partly lost in *Grhl3*^{Cre}; *Fn1*$^{fl/fl}$ embryos but entirely unaffected in *Grhl3*^{Cre}; *Itgb1*$^{fl/fl}$ embryos (Molè et al., 2020). The latter finding was surprising given that fibronectin assembly is primarily dependent on the α5β1 integrin receptor (which had been ablated in the surface ectoderm). Furthermore, this disparity receives added importance from the findings of the current study indicating that the spinal NTDs arising after integrin β1 ablation were (at least partly) due to loss of integrin-fibronectin interactions at the dorsal midline. So, what accounts for the normal appearance of the fibronectin network in *Grhl3*^{Cre}; *Itgb1*$^{fl/fl}$ mutants? One explanation is that fibronectin was assembled through interactions with alternative integrin receptors in the surface ectoderm, such as αvβ5 which was shown to be expressed in the region (Molè, 2017). However, previous in vitro studies have shown that αv integrin-mediated assembly of fibronectin produces shorter and thicker fibrils and a sparser network overall (Wennerberg et al., 1996). As no such differences were detected in Grhl3^{Cre}; Itgb1$^{fl/fl}$

mutants, this is unlikely to be the compensating mechanism in this case. A more likely explanation is that the fibronectin BM was assembled through interaction with α5β1 receptors from the underlying neuroepithelium which was mostly unaffected by the *Grhl3*^{Cre}-mediated deletion of integrin β1. Interestingly, the highly penetrant NTDs in *Grhl3*^{Cre}; Itgb1$^{fl/fl}$ mutants indicate that, despite ensuring normal fibronectin assembly, neither αvβ5 receptors in the surface ectoderm nor α5β1 receptors in the neuroepithelium were able to compensate for the α5β1-mediated binding of fibronectin by the surface ectoderm that facilitates neural tube fusion. These findings therefore highlight the importance of the surface ectoderm as well as the unique properties of the α5β1 receptor in this process. Indeed, α5β1 receptors are known to have superior adhesion, actin binding and mechanotransduction dynamics compared to αv-containing receptors (Danen et al., 2002; Schiller et al., 2013; Strohmeyer et al., 2017; Wennerberg et al., 1996).

4. The role of fibronectin in axial elongation

4.1 Introduction

4.1.1 Different parts of the fibronectin network facilitate different aspects of posterior development

As the three conditional approaches employed here and many previous KO studies have illustrated, integrin-fibronectin interactions are an essential feature of multiple aspects of embryonic development. While the previous chapter focused on *Grhl3*^{Cre}; *Fn1*$^{fl/fl}$ mutant embryos to elucidate fibronectin's involvement in spinal neural tube fusion, the current chapter performs a more in-depth examination of the *Cdx2*^{Cre}; *Fn1*$^{fl/fl}$ mutant embryos to better understand the role of fibronectin in axial elongation. Comparison of *Cdx2*^{Cre}; *Fn1*$^{fl/fl}$ and *Grhl3*^{Cre}; *Fn1*$^{fl/fl}$ mutant phenotypes indicated that fibronectin facilitates these two processes through separate mechanisms. *Grhl3*^{Cre}; *Fn1*$^{fl/fl}$ mutants show a delay in PNP closure that is evident from E9.5 and eventually results in lumbar or sacral spina bifida in 24% of mutant embryos, while body length remains unaffected at all stages. *Cdx2*^{Cre}; *Fn1*$^{fl/fl}$ mutants, on the other hand, demonstrate normal PNP closure and body length at E9.5, but go on to develop a shortened and kinked tail at E12.5. The two defects are therefore both spatially and temporally separated, as well as qualitatively distinct.

Furthermore, comparison of fibronectin localisation in the affected *Cdx2*^{Cre}; *Fn1*$^{fl/fl}$ and phenotypically normal *T*^{CreERT2}; *Fn1*$^{fl/fl}$ mutants revealed some initial clues about the parts of the fibronectin network that might be most important in the process of tail formation. The *Cdx2*^{Cre}- and *T*^{CreERT2}-mediated strategies target similar tissues, most notably paraxial mesoderm which is the main source of fibronectin. While *Cdx2*^{Cre} recombines the entire paraxial mesoderm, however, *T*^{CreERT2}-mediated recombination is widespread but still mosaic. As shown by fibronectin immunostaining, cells escaping recombination in the *T*^{CreERT2}; *Fn1*$^{fl/fl}$ mutants are capable of secreting enough fibronectin to form a thin BM between the neural tube and paraxial mesoderm. The presence of fibronectin at this interface represents the

main difference between $T^{CreERT2}$; $Fn1^{fl/fl}$ and $Cdx2^{Cre}$; $Fn1^{fl/fl}$ embryos and hence likely accounts for the phenotypic differences observed later in development. However, the mechanism through which loss of this BM disrupts axial elongation remains unknown.

4.1.2 Insights from previous studies and outstanding questions

Identifying the causal mechanism is complicated by the fact that successful axial elongation requires the coordination of multiple interconnected cellular processes happening in parallel, all of which are potentially influenced by cell-ECM adhesion. These include the proliferation and survival of tailbud progenitors, their specification and migration into their target axial and paraxial regions as well as the morphogenetic processes giving the neural tube, somites and notochord their final shape. Previous studies in mice have mainly employed global KOs of fibronectin, its RGD motif or related integrin receptors. These genetic ablations affect multiple embryonic systems from the earliest stages of development and are therefore characterised by a variety of defects (many of which are secondary to others) and early lethality that precludes effective dissection of the primary pathogenic causes. Nevertheless, all of these previous models share a number of phenotypic features and hence point toward some potentially key mechanisms.

All such genetic ablations, for example, result in an arrest of AP axis formation, a deformed neural tube, and mesodermal defects of variable severity. The latter range from a complete lack of notochord and somites - when all integrin-fibronectin interactions are prevented (George et al., 1993; Georges-Labouesse et al., 1996) - to notochord fragmentation, selective loss of posterior somites, left-right asymmetries, and reduced size and epithelialisation defects in the some of the somites that do form – when only α5β1-fibronectin interactions are targeted (Girós et al., 2011; Goh et al., 1997; Takahashi et al., 2007; Yang et al., 1999). Most importantly, studies from both the severe and mild ends of the phenotypic spectrum confirm that mesodermal markers, such as Mox-1, Notch-1, T (Brachyury) and Shh are expressed in the correct

regions of mutant embryos, thus indicating that the initial specification and migration of axial progenitors is unaffected, and the defects rather stem from a failure of subsequent morphogenetic processes (Georges-Labouesse et al., 1996; Goh et al., 1997). Furthermore, previous studies produced highly disparate results with regard to the rates of apoptosis, claiming to have found increased apoptosis only in the neural tube (George et al., 1993), posterior paraxial mesoderm (Takahashi et al., 2007) or neural crest and ventral endoderm (Goh et al., 1997), respectively, or throughout the embryo but only at late stages (Girós et al., 2011). In contrast, all these studies agreed on the lack of any differences in the rates of cell proliferation between fibronectin/integrin mutants and controls (Girós et al., 2011; Goh et al., 1997; Guo et al., 2020; Takahashi et al., 2007).

Finally, zebrafish studies utilising mutations or morpholino-based knock-downs (KDs) of fibronectin and associated integrins have echoed many of these findings including axial truncation (Dray et al., 2013), neural tube deformities (Araya et al., 2016) and left-right paraxial mesoderm asymmetries (Guillon et al., 2020), without significant changes in the proliferation, survival, specification and migration of axial progenitors (Dray et al., 2013). In addition, they have drawn attention to the role of fibronectin in somite boundary maintenance, somite epithelialisation (Koshida et al., 2005) and especially the mechanical coupling of neighbouring tissues during collective elongation movements (Araya et al., 2016; Dray et al., 2013; Guillon et al., 2020).

Collectively, previous studies have highlighted fibronectin's importance for the morphogenetic processes that shape the neural tube and somites, but not the processes that supply the cells for these structures. However, many questions remain. For example, what is the relationship between the neural and mesodermal defects observed? Furthermore, the premature axial truncation and lethality of (even the mildest of) previous mutants have only allowed assessment of developmental defects up to the level of the 13th somite pair. Therefore, fibronectin's role in the formation of the posterior embryo remains unexplored.

4.2 Results

4.2.1 Cdx2^{Cre}; Fn1$^{fl/fl}$ embryos display a shortened tail from E10.5

To better understand how loss of fibronectin expression in caudal tissues gives rise to axial elongation defects, *Cdx2^{Cre}; Fn1$^{fl/+}$* and *Fn1$^{fl/fl}$* mice were crossed and embryos were collected at E10.5. While previous fibronectin immunostaining revealed that the *Cdx2^{Cre}*-mediated ablation effectively removes fibronectin from the caudal region of the embryo at E9.5, *Cdx2^{Cre}; Fn1$^{fl/fl}$* embryos were otherwise indistinguishable from controls at that stage. It was therefore hypothesised that the E10.5 time point would allow sufficient time for the deletion to impact the dynamics of axial elongation, while minimising the confounding of measurements by secondary effects (potentially present at later stages). Moreover, as the observed elongation defect appears to specifically affect the tail region, E10.5 represents a suitable stage where the PNP is fully closed, and tail formation has recently begun.

An initial morphological characterisation of E10.5 *Cdx2^{Cre}; Fn1$^{fl/fl}$* embryos showed no obvious abnormalities and no significant differences in crown-rump length or body length when compared to littermate controls (Figure 4.1A-D). Nevertheless, taking separate measurements of the trunk and tail in these embryos, as previously, revealed a highly significant reduction in tail length, but no differences in trunk length (Figure 4.1E, F). Interestingly, while the length difference was much smaller compared to that detected at E12.5 in absolute terms (0.33 mm at E10.5 vs 0.79 mm at E12.5), it was highly comparable in relative terms between the two stages (20% at E10.5 vs. 17% at E12.5) showing that impact of the fibronectin deletion on the rate of elongation remains constant throughout the process of tail formation. Furthermore, at this stage none of the mutant embryos displayed the sharp axial bends observed at E12.5.

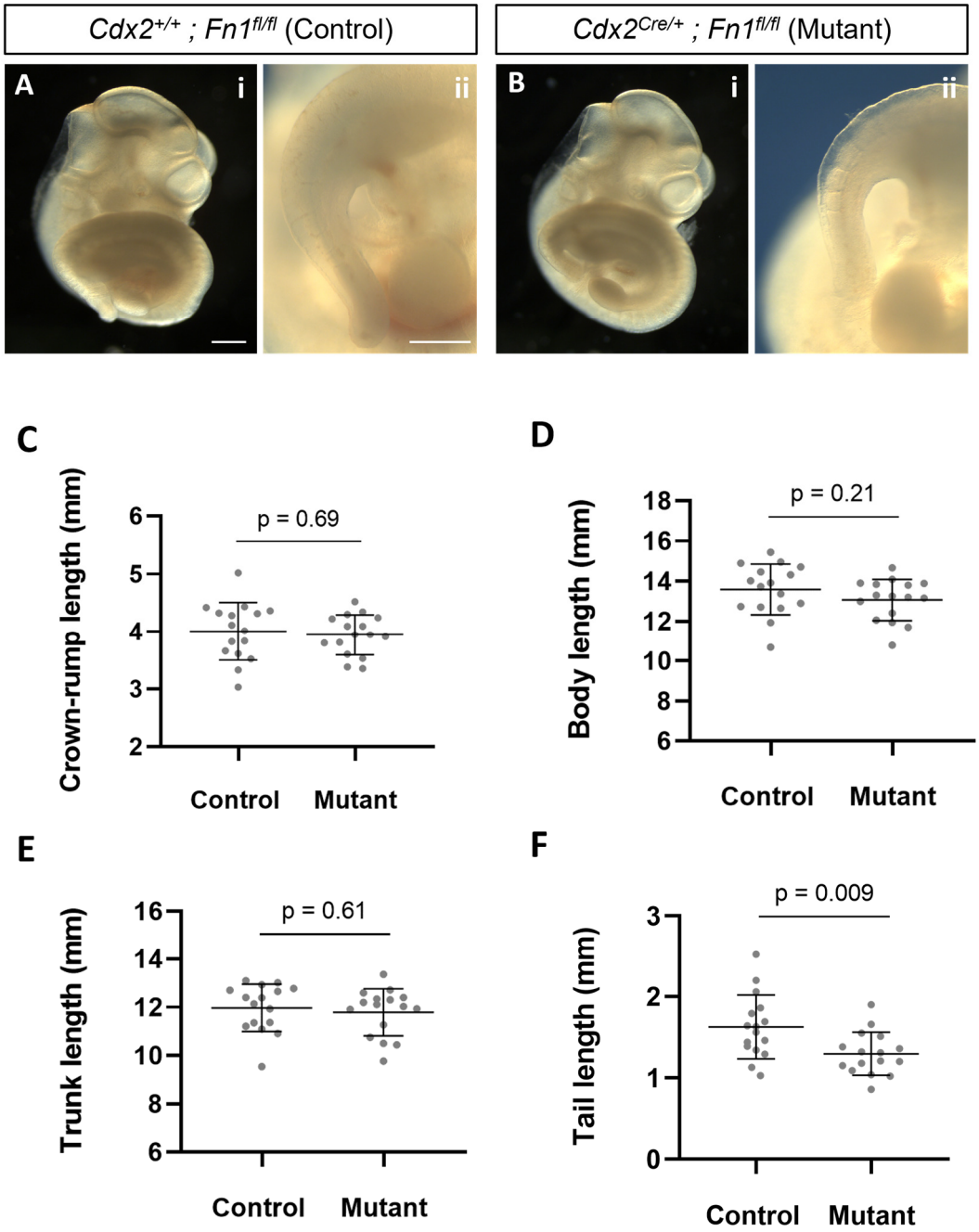

Figure 4.1. Morphological characterisation of E10.5 embryos following *Cdx2*^{Cre}-mediated deletion of the fibronectin gene. (A, B) Brightfield images show a normal overall morphology (A, B), but a shorter tail in the mutant embryo (B-ii) compared to the control (A-ii). Morphometric analyses show no significant differences in crown-rump length (C), body length (D) or trunk length (E), but a significantly reduced tail length (F) (unpaired, two-tailed Student's t-test; p values in figure; embryos: controls n = 16, mutants n = 16). Data shown as mean values ± SD. Scale bars: 500 µm.

4.2.2 Fibronectin is almost completely absent from the tail of Cdx2^{Cre}; Fn1$^{fl/fl}$ embryos

Previous lineage tracing and immunostaining experiments, performed at E9.5, showed that *Cdx2*^{Cre} effectively recombines the neural tube and paraxial mesoderm, and removes fibronectin from all the major axial BMs in the caudal embryo, with the exception of the notochord sheath (deriving from unrecombined notochordal tissue). Based on these findings and previous *Fn1* is situ hybridisation studies, the tail region was expected to remain mostly devoid of fibronectin at E10.5. Nevertheless, to confirm that this is the case and that no de novo expression or recruitment of soluble fibronectin from distant tissues has occurred, *Cdx2*^{Cre}*; Fn1*$^{fl/fl}$ embryos and controls were once again immunostained for fibronectin. Whole-mount confocal microscopy and 3D reconstruction of the tail region demonstrated that in control embryos fibronectin covers the entire surface of the paraxial mesoderm and is particularly concentrated at the somite borders and the interface of the neural tube with the paraxial mesoderm (Figure 4.2A, C). Conversely, in the mutants fibronectin appeared to be completely absent from those regions, and the only visible staining was in the centre of the neural tube (Figure 4.2B, D). However, the location and pattern of this signal (dots and aggregates instead of fibrils) indicated that it represents non-specific antibody trapping in the lumen. Next, to visualise deeper tissues, embryos were cleared (details in Section 2.8) and optical coronal sections were acquired throughout the DV axis of the tailbud. Sections at the level of the neural tube confirmed that in *Cdx2*^{Cre}*; Fn1*$^{fl/fl}$ embryos the interface of the neural tube with the paraxial mesoderm is completely devoid of fibronectin, and that the only signal indeed originates from antibody trapped in the lumen (Figure 4.2F). Furthermore, deeper sections revealed that the notochord sheath was still intact in the mutants, as in earlier stages (Figure 4.2H).

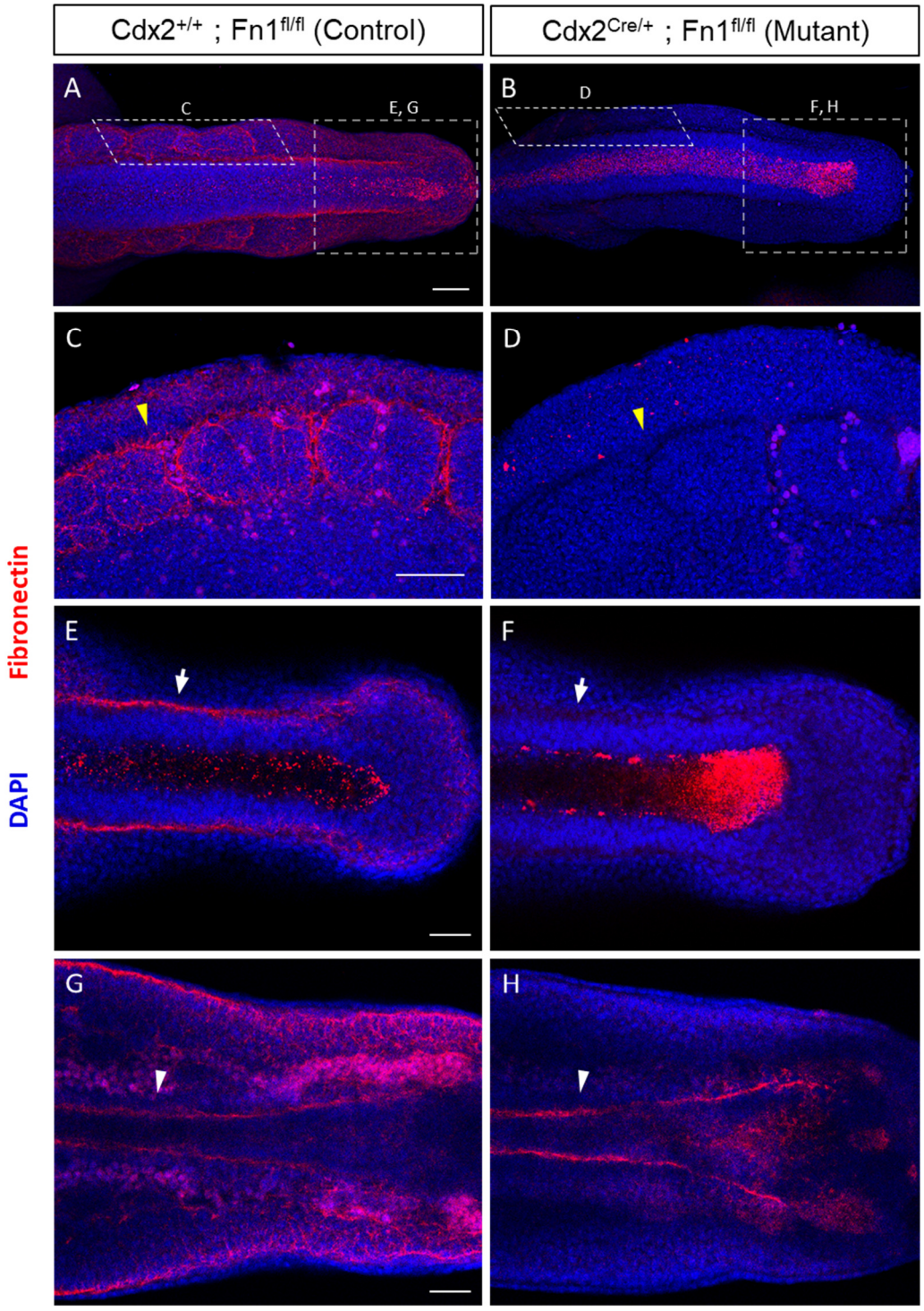

Figure 4.2. Fibronectin immunostaining of E10.5 embryos following *Cdx2*^{Cre}-mediated deletion of the fibronectin gene. (A, B) Maximum intensity projections of the dorsal tail region in control (A) and mutant (B) embryos (n = 3 per genotype). The *Cdx2*^{Cre}-mediated deletion effectively removes fibronectin throughout the surface of the tail. (C, D) Maximum intensity projections of the lateral side of the last 3 somites, indicated by the dashed boxes in A and B (n = 3 per genotype). Fibronectin is

especially concentrated around the somites of control embryos (G, yellow arrowhead), but completely absent from the somites of mutant embryos (H, yellow arrowhead). (E-H) Optical coronal sections of the tailbud region, indicated by the dashed semi-transparent boxes in A and B, at the level of the neural tube (E, F) and notochord (G, H). In mutant embryos, fibronectin can be found around the notochord (H, white arrowhead), but not between the paraxial mesoderm and neural tube (F, arrow). Non-specific staining can be seen in the neural tube lumen of both mutants and controls (E, F). Scale bars: 100 µm in A-D; 50 µm in E-H.

4.2.3 $Cdx2^{Cre}$; $Fn1^{fl/fl}$ embryos display normal somites but deformed neural tube

Previous ablations of integrin-Fn interactions have reproducibly resulted in a kinked neural tube and variably malformed or completely lacking somites (George et al., 1993; Georges-Labouesse et al., 1996; Girós et al., 2011; Goh et al., 1997; Takahashi et al., 2007). Analogous defects might also account for the tail shortening and axial bends observed in *Cdx2^{Cre}; Fn1$^{fl/fl}$* embryos by E12.5. Interestingly, unlike most previously generated mutants, *Cdx2^{Cre}; Fn1$^{fl/fl}$* embryos showed no differences in somite number compared to controls, even towards the end of axial elongation at E12.5 (Figure 3.10F). Their somites, however, could in theory have reduced size, morphological abnormalities or asymmetries that ultimately translate into shortening and deviation of the entire tail axis. To assess the structural integrity and dimensions of neural and mesoderm tissues, *Cdx2^{Cre}; Fn1$^{fl/fl}$* and controls were stained with DAPI and Phalloidin and the tail was imaged using whole-mount confocal microscopy.

Optical coronal cross sections through DV midline showed that in control embryos the neural tube walls were straight, parallel to each other and in continuous contact with the paraxial mesoderm laterally (Figure 4.3A). In the mutants, however, the neural tube walls detached from the paraxial mesoderm, undulated independently and in extreme cases folded upon themselves (Figure 4.3B, arrow). This pattern was

variably pronounced along the AP axis and from one mutant embryo to another, but absent from control embryos. A similarly kinked neural tube has been observed in all the previous fibronectin (and related integrin) KOs. As the observed impact of these KOs had been far greater on mesodermal rather than neural tissues, authors of previous studies suspected that such neural tube deformations might result due to lack of support by the somites. Interestingly, however, *Cdx2*^{Cre}*; Fn1*$^{fl/fl}$ embryos displayed this pattern in the caudal-most regions where the neural tube was flanked by presomitic mesoderm (Figure 4.3A); thus, demonstrating that the neural tube deformation is not secondary to mesodermal defects (as it precedes somitogenesis). Instead, neural tube undulation appears to directly result from the loss of fibronectin at the interface of the neural tube with the paraxial mesoderm that normally couples the movements of these adjacent tissues. Loss of inter-tissue adhesion in *Cdx2*^{Cre}*; Fn1*$^{fl/fl}$ mutants has therefore caused the neural tube to elongate independently. Interestingly, these findings also suggest that the neural tube has a higher elongation rate than the paraxial mesoderm and therefore acts as a driving force in axial elongation.

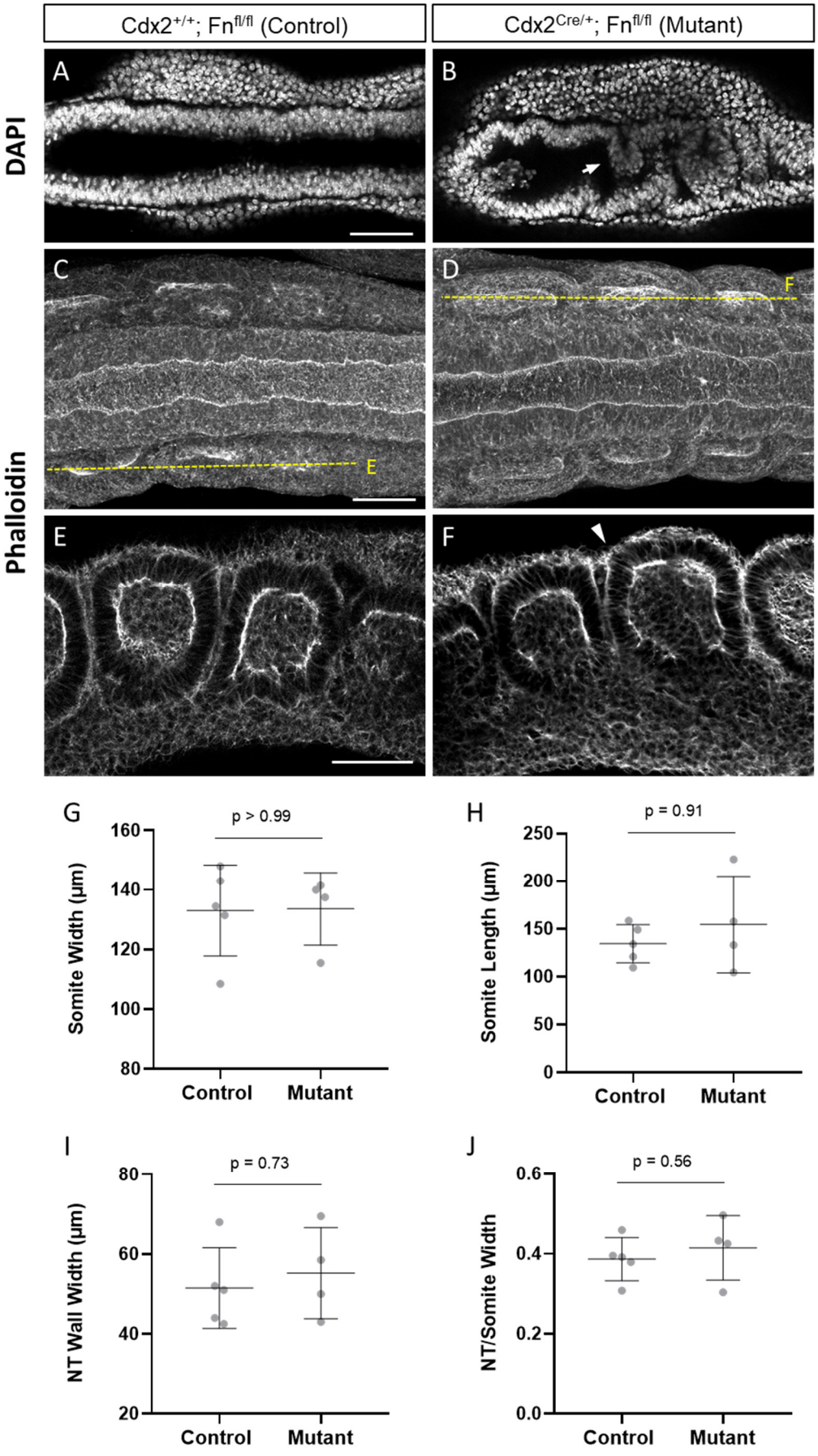
Cdx2+/+; Fnfl/fl (Control)
Cdx2Cre/+; Fnfl/fl (Mutant)
DAPI
Phalloidin
A
B
C
D
E
F
E
F
G
p > 0.99
Somite Width (µm)
160
140
120
100
80
Control
Mutant
H
p = 0.91
Somite Length (µm)
250
200
150
100
50
0
Control
Mutant
I
p = 0.73
NT Wall Width (µm)
80
60
40
20
Control
Mutant
J
p = 0.56
NT/Somite Width
0.6
0.4
0.2
0.0
Control
Mutant

Figure 4.3. Assessment of internal tissue structure in E10.5 embryos stained with DAPI and phalloidin following *Cdx2*^{Cre}-mediated deletion of the fibronectin gene. (A, B) Optical coronal cross sections taken through the DV midline of the tail neural tube in controls (A) and mutants (B) stained with DAPI (n = 5 per genotype). The neural tube walls run straight and parallel to each other, and in contact with the presomitic mesoderm in control embryos (A), but undulate independently in mutant embryos (B, arrow). (C, D) Maximum intensity projections of the dorsal side of the tail in control (C) and mutant (D) embryos stained with phalloidin (n = 5 per genotype). (E, F) Optical sagittal sections through the last somites indicated by the dashed yellow lines in C and D (n = 5 per genotype). *Cdx2*^{Cre}*; Fn1*$^{fl/fl}$ embryos have normal posterior somites consisting of a columnar epithelium surrounding an oval-shaped central cavity (D, arrowhead). (G-J) Morphometric analyses detected no differences in somite width (G), somite length (H), neural tube wall width (I) or neural tube-to-somite width (J) between mutants and controls (Mann-Whitney test; p values in figure; embryos: controls n = 5, mutants n = 4). Data shown as mean values ± SD. Scale bar: 100 µm.

While *Cdx2*^{Cre}*; Fn1*$^{fl/fl}$ mutants already exhibited a reduction in tail length at E10.5, they did not yet show the overt axial bends seen at E12.5. However, it would be easy to imagine how internal neural tube bends (detected at E10.5) could gradually transform into overt bends of the entire tail axis (found at E12.5) as development proceeds. Furthermore, if symmetric neural tube elongation creates the forces that drive axial elongation as a whole, neural tube deformation could additionally account for the shortening of the tail (by absorbing the forces that would normally mediate posterior displacements of the tailbud). Alternatively, the length reduction could originate from subtle mesodermal defects affecting somite structure. To test for the latter possibility, somite size and morphology was assessed through phalloidin staining (Figure 4.3C-F). Surprisingly, *Cdx2*^{Cre}*; Fn1*$^{fl/fl}$ mutants exhibited perfectly formed somites with a columnar epithelium surrounding an oval-shaped central cavity (Figure 4.3D, arrowhead). Individual somites were also clearly delimited showing that, contrary to some previous reports, neither epithelialisation nor

boundary maintenance was affected by the loss of fibronectin. In addition, quantification of the length and width of the last fully formed somite pair in mutants and controls indicated that somite dimensions were also unaffected by the deletion. Similarly, no differences were detected in the width of the neural tube walls or the relative width of neural and mesoderm tissues at that axial level (Figure 4.3G-J). These results hence indicated that the initial generation and shaping of these tissues proceed normally in the absence of fibronectin.

4.2.3 Cdx2^{Cre}; Fn1$^{fl/fl}$ embryos display normal cell proliferation and survival

The previous structural analyses identified the folding of the neural tube walls as the only major abnormality of *Cdx2^{Cre}; Fn1$^{fl/fl}$* mutants. Following loss of fibronectin, the neural tube might therefore become deformed as a result of intrinsic AP-oriented extension forces in the absence of lateral adhesion (to the paraxial mesoderm), which would normally maintain its integrity and symmetry. Alternatively, loss of adhesion to fibronectin could impact neural tube integrity by inducing excessive rates of apoptosis or restricting cell proliferation. Dysregulation of proliferation and apoptosis could also cause neural tube undulation by gradually creating subtle imbalances between the amount of neural and mesodermal tissue (not detected by previous morphometric analyses) or directly reduce tail length by affecting progenitor maintenance and tissue volume.

First, to assess whether proliferation was affected by the fibronectin deletion, *Cdx2^{Cre}; Fn1$^{fl/fl}$* mutants were immunostained for the mitosis marker pHH3 and the tail was imaged using confocal microscopy as previously. 3D reconstruction of the tail region demonstrated a comparable distribution of mitotic cells between mutants and controls (Figure 4.4A, B). In addition, optical coronal sections through the neural tube and presomitic mesoderm revealed that mitotic cells were evenly spread between the two tissues (Figure 4.4C, D). Moreover, quantification of the number of pHH3-positive cells in the posterior neural tube and adjacent presomitic mesoderm of mutants and controls showed no significant differences in the absolute frequencies

of mitosis in neither of these tissues, nor the relative frequencies between them (Figure 4.4I-K).

Subsequently, the extent of apoptosis in these tissues was evaluated through ccasp3 immunostaining. CCasp3-positive foci were limited in the region of the tail and almost exclusively restricted to the neural tube lumen in both mutants and controls (Figure 4.4E-H). While the pattern of CCasp3 staining (ranging from minuscule dots of non-specific signal to large aggregates of dying cells) prevented the counting of individual cells in this case, the overall extent of staining appeared very similar between mutants and controls and a quantification of fluorescence intensity throughout the tail revealed no differences (Figure 4.4K). Taken together, therefore, these results demonstrate that both the length reduction and axial bends observed in *Cdx2*^{Cre}*; Fn1*$^{fl/fl}$ mutants are likely to be due to loss of inter-tissue adhesion between the neural tube and paraxial mesoderm, which leads to the independent undulation of the neural tube.

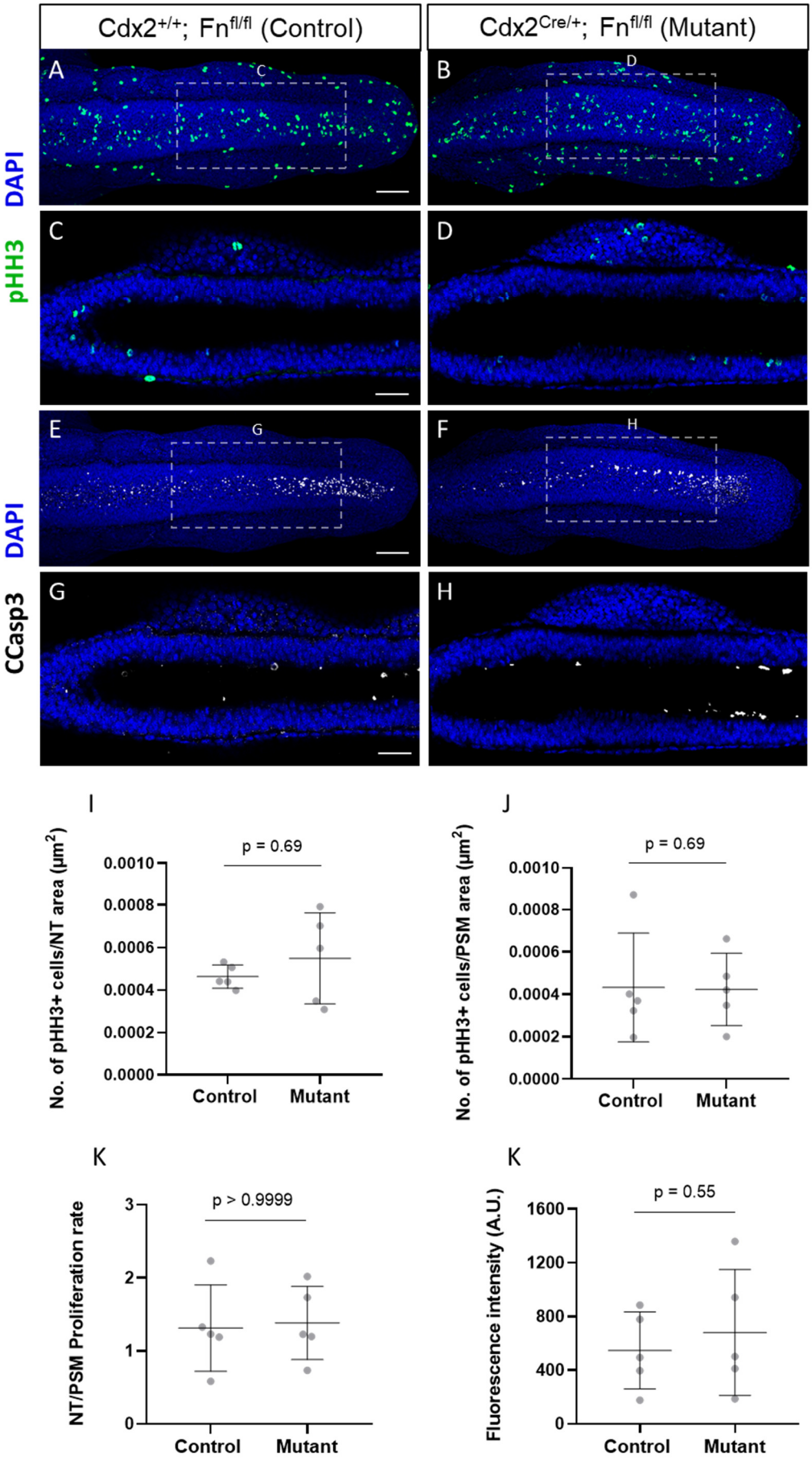
Cdx2+/+; Fnfl/fl (Control)
Cdx2Cre/+; Fnfl/fl (Mutant)
DAPI
pHH3
DAPI
CCasp3
A
B
C
D
E
F
G
H
I
No. of pHH3+ cells/NT area (μm2)
p = 0.69
0.0010
0.0008
0.0006
0.0004
0.0002
0.0000
Control
Mutant
J
No. of pHH3+ cells/PSM area (μm2)
p = 0.69
Control
Mutant
K
NT/PSM Proliferation rate
p > 0.9999
3
2
1
0
Control
Mutant
K
Fluorescence intensity (A.U.)
p = 0.55
1600
1200
800
400
0
Control
Mutant

Figure 4.4. pHH3 and CCasp3 immunostaining of E10.5 embryos following *Cdx2*^{Cre}-mediated deletion of the fibronectin gene. (A, B) Maximum intensity projections of the dorsal tail region in pHH3-stained control (A) and mutant (B) embryos (n = 5 per genotype). (C, D) Optical coronal sections of the posterior tail region, indicated by the dashed semi-transparent boxes in A and B, through the neural tube (bottom) and presomitic mesoderm (top). Cell divisions are evenly distributed throughout the neural tube and presomitic mesoderm of the tail in control embryos (A, C), and appear unaffected in the mutants (B, D). (E, F) Maximum intensity projections of the dorsal tail region in CCasp3-stained control (C) and mutant (F) embryos (n = 5 per genotype). (G, H) Optical coronal sections of the posterior tail region, indicated by the dashed semi-transparent boxes in E and F, through the neural tube (bottom) and presomitic mesoderm (top). Cell death is almost exclusively restricted to the apical neuroepithelium and appears similarly distributed between control (E, G) and mutant (F, H) embryos. (I-J) Quantification of pHH3 signal detected no differences in the number of dividing cells within the neural tube (NT; I) or presomitic mesoderm (PSM; J), or their relative balance (NT/PSM; K), between mutants and controls (Mann-Whitney test; p values in figure; embryos: controls n = 5, mutants n = 5). (K) Quantification of CCasp3 signal (mean fluorescence intensity minus background intensity) in the entire tail region detected no differences between mutants and controls (Mann-Whitney test; p values in figure; embryos: controls n = 5, mutants n = 5). Data shown as mean values ± SD. Scale bars: 100 µm in A, B, E and F; 50 µm in C, D, G and H.

4.3 Discussion

The various fibronectin deletion strategies employed in Chapter 3 revealed a novel role of fibronectin in symmetric elongation of the tail. Comparison of fibronectin localisation in the *Cdx2*^{Cre}; *Fn1*$^{fl/fl}$ mutants, which exhibited shortened and malformed tails, and the phenotypically normal *T*^{CreERT2}; *Fn1*$^{fl/fl}$ mutants indicated that this process depended on the presence of fibronectin at the NE-MES interface. As fibronectin has been previously implicated in numerous cellular processes associated with axial elongation, the current chapter sought to clarify how loss of this BM led to the observed tail defect.

Previous investigations into the role of fibronectin in development have mainly utilised global deletion of fibronectin, its RGD motif or related integrins in mice (George et al., 1993; Georges-Labouesse et al., 1996; Girós et al., 2011; Goh et al., 1997; Takahashi et al., 2007; Yang et al., 1999). The resulting phenotypes vary in severity and have been characterised by early lethality, cardiovascular defects, axial truncation, complete or partial loss of notochord and somites, and an undulating neural tube. Interestingly, these studies revealed that the initial proliferation, migration and specification of neural and mesodermal progenitors are unaffected by the loss of integrin-fibronectin interactions, thus highlighting the importance of subsequent morphogenic processes in the pathogenesis of these defects (Dray et al., 2013; George et al., 1993; Georges-Labouesse et al., 1996; Girós et al., 2011; Goh et al., 1997; Guo et al., 2020; Takahashi et al., 2007). However, due to their global nature, previous genetic ablations have been unable to clarify the relationships between the various abnormalities observed (e.g., neural and mesodermal) or to pinpoint the exact mechanisms involved in each. Furthermore, even the mildest of these mutants never progress beyond the 15-somite stage. As a result, fibronectin's role in the formation of more posterior tissues was hitherto unexplored.

The current fibronectin deletion strategy was more temporally and spatially specific than previous approaches and was therefore capable of elucidating some of these questions. Previous studies had widely reported no differences in the frequency of cell divisions after integrin/fibronectin ablations (Girós et al., 2011; Goh et al., 1997;

Guo et al., 2020; Takahashi et al., 2007). In accordance, *Cdx2*^{Cre}; *Fn1*$^{fl/fl}$ mutant embryos in the present study showed no differences in cell proliferation compared to controls. Conversely, there have been contradictory reports regarding the impact of such genetic ablations on the rate of apoptosis within the different axial tissues. The current study detected no differences in the extent of cell death in neural or mesodermal tissues following fibronectin deletion, even though impairment in tail elongation had already started to become apparent. These results therefore show that the defect observed here does not stem from deficiencies in cell survival, and suggest that the increased rates of cell death reported by some previous studies are unlikely to be causal in the observed phenotypes, but rather a secondary effect of prolonged loss of cell-ECM adhesion or nutrient deficits (caused by the concomitant cardiovascular and placental defects) (George et al., 1993; Girós et al., 2011; Goh et al., 1997; Takahashi et al., 2007).

More importantly, structural analyses of axial tissues in *Cdx2*^{Cre}; *Fn1*$^{fl/fl}$ embryos revealed that loss of fibronectin caused the neural tube to detach from the paraxial mesoderm and undulate independently (without however affecting the thickness of the neuroepithelium). This bent appearance of the neural tube was remarkably similar to that observed in previous fibronectin and integrin mutants (George et al., 1993; Girós et al., 2011; Goh et al., 1997; Takahashi et al., 2007; Yang et al., 1993). Interestingly, in previous models, such neural tube abnormalities appeared secondary to the much more severe losses or malformations of surrounding mesodermal tissues that were observed. In contrast, the present study found that somite number, size and morphology were unaffected in *Cdx2*^{Cre}*; Fn1*$^{fl/fl}$ mutants. In fact, neural tube undulation was most prominent in the caudal-most regions where somitogenesis had not yet occurred. These data therefore demonstrate that such neural tube deformities can arise independently of mesodermal defects. Furthermore, undulation of the neural tube can fully account for the elongation defect observed here by absorbing the forces that would normally mediate posterior displacement of the tailbud, while also producing the overt bends of the entire tail axis at later stages. Interestingly, the undulation was most pronounced at the latest stages and caudal-most segments of tail elongation. This bias could relate to the

smaller diameter of the neural tube and entire embryonic axis at those segments which could in turn result in loss of tissue stiffness and mechanical support from surrounding tissues, respectively. Lastly, in terms of the underlying mechanism, the current evidence suggests that fibronectin's role in tail elongation does not relate to the initial generation of neural or mesodermal tissues. Instead, fibronectin appears to maintain the structural integrity and linear elongation of the neural tube by ensuring its continuous attachment to the paraxial mesoderm. This mechanism is considered further in Section 6.1.2 of the General Discussion chapter.

Previous integrin/fibronectin ablation models have been mainly characterised by mesodermal defects. The most severe phenotypes were observed in response to fibronectin or RGD deletions which led to a complete lack of notochord and somites (Benito-Jardón et al., 2020; George et al., 1993; Georges-Labouesse et al., 1996). When only α5β1-fibronectin interactions were targeted, on the other hand, the resulting mutant embryos exhibited a fragmented notochord, normal or mildly affected (in terms of size or epithelisation) anterior somites, and a complete lack of posterior somites (after somite pair 15) (Girós et al., 2011; Takahashi et al., 2007; Yang et al., 1999). These studies therefore demonstrated the critical role of fibronectin in the formation of mesodermal derivatives, as well as the ability of αv-integrin-mediated binding to compensate (to some extent) for the action of α5 integrin in the anterior embryo, but not in the posterior. While the present study shows that neural tube and axial elongation defects can arise independently of mesodermal abnormalities, it is still surprising and noteworthy that mesodermal development, and especially somitogenesis, appeared to be entirely unaffected by the near-total loss of fibronectin in the posterior part of the embryo. In addition, the length reduction exhibited by *Cdx2*^{Cre}; *Fn1*$^{fl/fl}$ mutants was significant, yet dramatically milder than the complete cessation of axis formation observed in previous models.

There are a number of possible (and potentially overlapping) explanations for the relatively low impact of the current fibronectin gene deletion. Firstly, previous models utilised global gene deletions that perturbed the development of the embryonic heart, vasculature and extraembryonic membranes (George et al., 1993,

1997; Georges-Labouesse et al., 1996; Girós et al., 2011; Takahashi et al., 2007). The severe mesodermal and axial elongation defects observed could hence be secondary to circulatory deficits. Nevertheless, such deficits would be expected to primarily exert their impact by hindering cell survival and proliferation; which was not generally observed in previous models (at the time of assessment) despite the already existing mesodermal abnormalities. Therefore, while cardiovascular defects are likely responsible for the generalised developmental delay and eventual lethality of previous mutants, they are unlikely to fully account for the remainder of the phenotype. Rather fibronectin appears to be directly required for the morphogenetic mechanisms that give rise to the somites and notochord.

The important role of integrin-fibronectin interactions in notochordal development was also recently highlighted through a study by Guo et al. that conditionally deleted integrin β1 in the notochord of mouse embryos from E8 (Guo et al., 2020). This genetic ablation led to discontinuities, displacement and defective convergent extension of the notochord, as well as failure to assemble a fibronectin (but not laminin) notochordal sheath. *Cdx2*^{Cre}; *Fn1*$^{fl/fl}$ mutant embryos did not exhibit any of these abnormalities which is clearly explained by the lack of notochord recombination by *Cdx2*^{Cre}. In particular, the evidence presented here indicates that the fibronectin sheath surrounding the notochord is expressed by the notochord and that it is sufficient to maintain normal notochordal development despite loss of fibronectin in most neighbouring tissues. Interestingly, normal development of the notochord might have in turn ameliorated the impact of the *Cdx2*^{Cre}-mediated fibronectin deletion on somitogenesis and axial elongation as a whole. In support of this hypothesis, the aforementioned notochord-specific integrin β1 ablation led to shortening of the notochord and entire tail, thus indicating that the notochord is partly responsible for mechanically mediating axial elongation. Furthermore, the notochord is known to secrete Shh signals which are essential for neural tube and somite patterning (Chamberlain et al., 2008; Echelard et al., 1993). Therefore, some of the more severe defects observed in previous fibronectin/integrin mutants might have been due to loss of the mechanical and signalling functions of the notochord.

Unlike most of the previous fibronectin/integrin ablation models, the current fibronectin deletion was restricted to the posterior part of the embryo. Therefore, the lack of somitic defects in *Cdx2*^{Cre}; *Fn1*$^{fl/fl}$ mutants could also be explained by the differential dependence of somitogenesis on fibronectin along the AP axis. For example, fibronectin might not be mechanistically involved at all in the formation of posterior somites, or perhaps it is involved but alternative ECM ligands can compensate for its absence (in posterior but not in anterior somites). Lastly, an interesting finding from previous ablation studies is that embryos lacking integrin α5-fibronectin binding never form more than 15 somite pairs (Girós et al., 2011). Intriguingly, the stage at which axial elongation arrests in these mutants coincides with embryo turning and internalisation of the node and surrounding regions into the CNH. In combination with the results of the present study (showing normal formation of posterior somites in the absence of fibronectin), this finding could therefore indicate that fibronectin is not required for posterior somitogenesis per se, but rather the large-scale morphogenetic transition on which posterior somitogenesis depends on. In support of this idea, both the position and shape of the node have been shown to be regulated by integrin-fibronectin binding (Pulina et al., 2011).

5. The role of Sox2 in neuromesodermal progenitors and neural specification

5.1 Introduction

The anterior and posterior parts of the embryo follow very different modes of germ layer formation. The three germ layers that give rise to the head and upper trunk emerge from the epiblast during the relatively brief morphogenetic process of gastrulation. The lower trunk and tail, on the other hand, follow a protracted programme of caudally directed elongation underpinned by the continuous incorporation of progenitors from the tailbud region. Among these progenitors are the NMPs which give rise to both the neural tube and somites of the lower body. The dual potency of NMPs, which persists long after the end of gastrulation, challenged the traditional germ layer model and consequently these cells have been the focus of intensive research.

Homotopic transplantation and DiO tracing studies located NMPs in the anterior CLE during the first stages of neurulation, and then in the CNH from E9 onwards (Cambray & Wilson, 2002, 2007; Mugele, 2018; Mugele et al., 2018). Interestingly, these NMP-harbouring regions were shown to contain cells that are double-positive for the mesodermal marker T and the neural progenitor marker Sox2 (Olivera-Martinez et al., 2012; Wymeersch et al., 2016). Due to the accordance of this expression pattern with the position and dual potency of NMPs, and due to the lack of any unique NMP markers, NMPs have since then often been defined on the basis of T/Sox2 co-expression (Garriock et al., 2015; Gouti et al., 2014, 2017; Koch et al., 2017). Nevertheless, T/Sox2 double-positive cells and NMPs represent subsets of the total cell populations in CLE and CNH, and may therefore not necessarily overlap.

A better experimental approach to conclusively address the question of whether NMPs express these markers is genetic lineage tracing. For instance, studies utilising T^{Cre} lines have demonstrated that the lineage of T-expressing cells gives rise to both the neural tube and somites of the posterior embryo, thus confirming the expression

of T in NMPs (Anderson et al., 2013; Mugele, 2018; Mugele et al., 2018; Perantoni et al., 2005). However, until recently no analogous experiment had been performed for Sox2, thus rendering the assumption of Sox2 expression in NMPs merely conjectural. To decisively resolve the question, our lab recently performed a series of lineage tracing experiments using an inducible $Sox2^{CreERT2}$ line in combination with the mT/mG reporter (Mugele, 2018; Mugele et al., 2018). These experiments incorporated a variety of tamoxifen induction protocols with regard to timing, ranging from E6.5 to E8.5. Strikingly, when CreERT2 was activated from E8 onwards, Sox2-expressing cells gave rise to exclusively neural tissues (i.e., neural tube and neural crest). This finding therefore demonstrated that, contrary to previous assumptions, Sox2 is only expressed in cells that have already committed to the neural fate (not NMPs). With earlier tamoxifen induction (E6.5 or E7.5), on the other hand, the descendants of Sox2-expressing cells colonised both neural and mesodermal tissues, reflecting the widespread expression of Sox2 in the epiblast during gastrulation (Mugele, 2018; Mugele et al., 2018; Wood & Episkopou, 1999).

Previous studies have stipulated that Sox2 is not only expressed in NMPs, but also regulates their fate choice (Koch et al., 2017). To investigate that potential role of Sox2 in NMPs and/or neural progenitors, our lab previously performed $T^{CreERT2/+}$; $Sox2^{fl/+}$ x $Sox2^{fl/fl}$ matings (with tamoxifen induction at E7.5 or E8.5) to delete Sox2 in T-expressing cells (of which NMPs are a subset) (Mugele, 2018; Mugele et al., 2018). Assessment at E9.5 and E10.5 showed that *Sox2*-deficient embryos had normal overall morphology and axial elongation. Furthermore, immunostainings for mesodermal (Dll1 and Pax1) and neural markers (Pax3, Pax6 and Nkx6.1) confirmed that the formation of the somites and neural tube was indeed unaffected. Surprisingly, these findings hence indicated the redundancy of Sox2, not only for NMP function, but also for the initial stages of neural specification.

Overall, the evidence from these recent lineage tracing and cKO studies from our lab appears to contradict previous assumptions about the role of Sox2 in NMPs, as well as a central regulator of neural identity (Cavallaro et al., 2008; Graham et al., 2003). To validate and extend these results, and explain the apparent contradictions, this chapter's experiments sought to assess: 1) the existence of T/Sox2 co-expressing cells

in putative NMP regions, 2) the ability of the previously used *Sox2*^{CreERT2} driver to recombine all *Sox2*-expressing cells, 3) the effect of the TCreERT2-mediated Sox2 deletion on NMP fate choice and 4) potential genetic or cellular mechanisms compensating for Sox2 after its deletion.

5.2 Results

5.2.1 Sox2 mRNA is negligible in the CNH of WT embryos

The assumption that NMPs co-express *T* and *Sox2* originated from immunostaining studies showing T/Sox2 double-positive cells in the CLE and CNH: regions known to harbour NMPs. While the existence of T/Sox2 double-positive cells has been conclusively demonstrated on the protein level, however, no study has so far appropriately tested for T/Sox2 co-expression on the level of RNA in these regions. In this regard, *Sox2* is known to be expressed throughout the epiblast and to be characterised by very high protein stability of over 48 hours (Avilion et al., 2003; Ji et al., 2018). The previously observed immunoreactivity could thus derive from residual rather than newly expressed Sox2.

To conclusively resolve the question of *T/Sox2* co-expression in NMPs, this investigation began by performing RNAscope – a highly sensitive multiplex fluorescence in situ hybridisation method (Wang et al., 2012) – for *T* and *Sox2* on mid-sagittal and cross sections of E9.5 wild type embryos (Figure 5.1). This analysis focused on the CNH region, where NMPs are known to reside (Figure 5.1D, F), as well as the open PNP region anteriorly to it (Figure 5.1C) and the tailbud posteriorly (Figure 5.1E). *T* was found to be strongly expressed throughout posterior tissues at the levels of the tailbud and CNH, and gradually became restricted to the notochord further anteriorly. Surprisingly, low-level expression of *T* was still detectable in the neuroepithelium of the PNP. *Sox2*, on the other hand, demonstrated strong expression in most of the neuroepithelium, but hardly any staining in the caudal-most areas. Only minuscule traces of *Sox2* staining were detected in the CNH region. However, as not all cells within the CNH are NMPs, it remains unknown whether the few *T/Sox2* double-positive cells observed here are NMPs or not. Instead, the main region of *T/Sox2* co-expression observed here was the neuroepithelium of the PNP, thus supporting the lab's previous finding that Sox2 lineage-traced cells are neural, and demonstrating the unsuitability of *T/Sox2* co-expression as an identifying feature of NMPs.

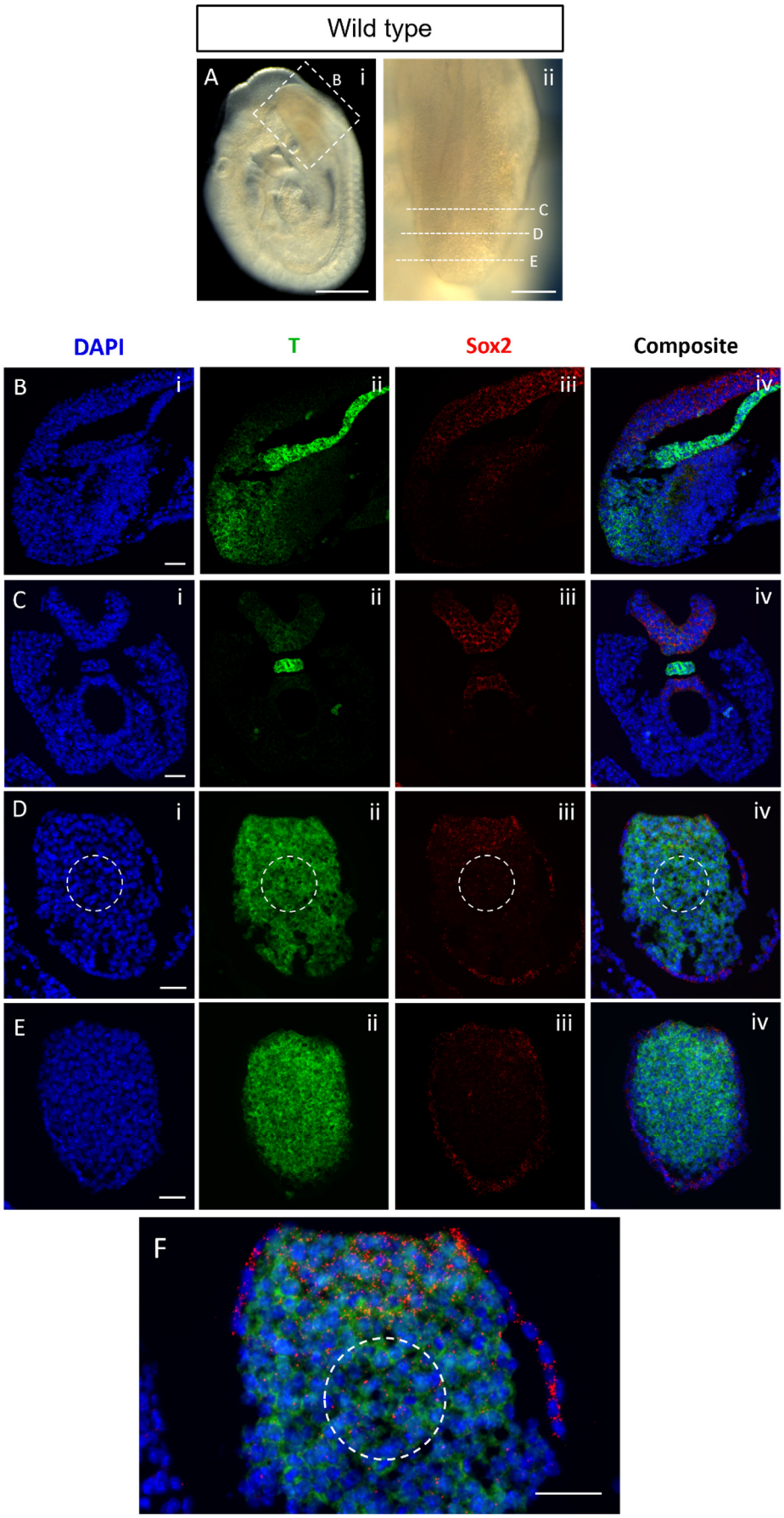
Wild type
A
B
i
ii
C
D
E
DAPI
T
Sox2
Composite
B
C
D
E
iii
iv
F

Figure 5.1. Multiplex fluorescent RNAscope for *T* and *Sox2* in paraffin sections of E9.5 WT embryos. (A) Brightfield images indicate the sectioned areas. (B) Mid-sagittal section through the PNP region, indicated by dashed semi-transparent box in A-i (n = 3). (C-F) Cross sections through the mid-PNP (C), CNH (D) and tailbud (E) regions indicated by dashed lines in A-ii (n = 3). (F) Higher magnification of D-iv. Dashed circles in D and F indicate the CNH. The CNH region shows strong transcription of *T*, but only negligible levels of *Sox2* mRNA. Scale bars: 500 µm in A-i, 200 µm in A-ii and 50 µm in B-F.

5.2.2 Validation of *Sox2^{CreERT2}* and previous lineage tracing results

A more appropriate experiment to determine whether *Sox2* is expressed in NMPs is the previously described genetic lineage tracing performed by our lab (Mugele, 2018; Mugele et al., 2018). This revealed that from E8 the descendants of *Sox2*-expressing cells give rise to neural tube and neural crest, but not paraxial mesoderm, thus suggesting that *Sox2* is only expressed in neural progenitors (not NMPs). However, the credibility of these results hinges on how faithfully *Sox2^{CreERT2}* reports all *Sox2*-expressing cells and their descendants. The Cre driver used in these experiments was constructed by introducing the CreERT2 coding sequence upstream of the *Sox2* exons, thus bringing the recombinase under the control of the *Sox2* regulatory regions (Andoniadou et al., 2013). The pattern of CreERT2 expression would therefore be expected to fully mimic that of *Sox2*. Of relevance here is also the tamoxifen-inducible nature of CreERT2, which allows precise control over the timing of the deletion, but at the same time makes the recombinase less efficient than its non-inducible counterparts (Jahn et al., 2018). This latter aspect would be unlikely to pose an issue if tamoxifen is readily available (which was achieved through large doses and repeated injections in the original experiments) and the *CreERT2* is expressed at high levels. However, potentially low levels of *Sox2* expression in NMPs could have resulted in concomitantly low levels of *CreERT2* that are insufficient to effectively trace all NMPs.

To address this caveat, it is therefore important to confirm that *CreERT2* is amply expressed throughout the *Sox2* expression domain (especially in putative NMP regions), during the stage of tamoxifen induction chosen in the original lineage tracing experiment (i.e., E8.5). For this purpose, duplex RNAscope for *Sox2* and *CreERT2* was performed on cross sections of E8.5 $Sox2^{CreERT2/+}$ embryos at the level of the rostral CLE and neighbouring regions (Figure 5.2). Sox2 displayed strong expression at the level of the node (Figure 5.2B), moderate expression at the level of the anterior CLE (Figure 5.2C), and almost no expression in the tailbud region (Figure 5.2D). CreERT2 closely mimicked this staining throughout all of the regions examined, including the anterior CLE (Figure 5.2C-iv). The results confirmed that *CreERT2* is indeed effectively expressed throughout the *Sox2*-positive domain in the CLE, hence validating the $Sox2^{CreERT2}$ driver and prior lineage tracing conclusions.

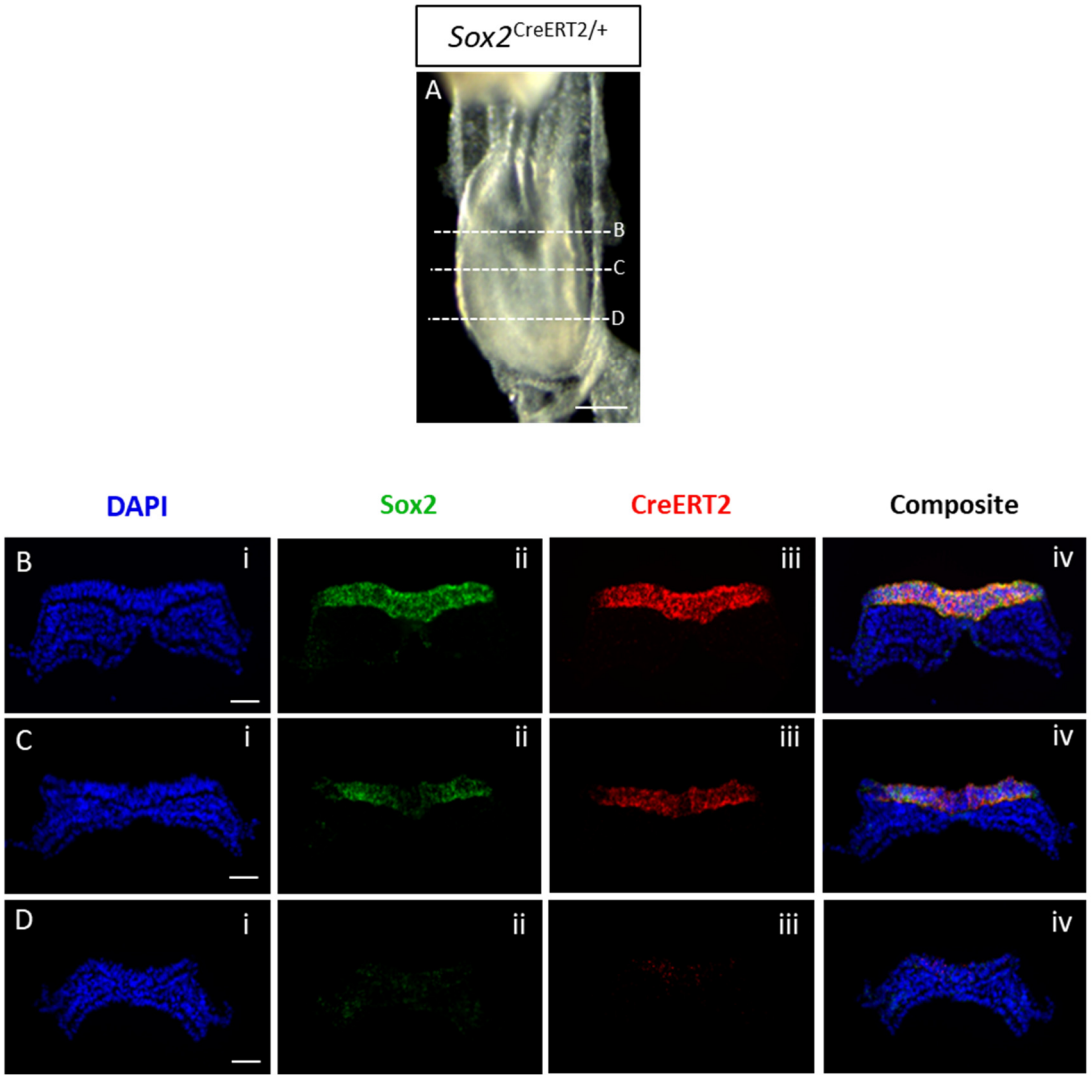

Figure 5.2. Multiplex fluorescent RNAscope for *Sox2* and *CreERT2* in paraffin sections of E8.5 *Sox2*^{CreERT2} embryos. (A) Brightfield image (rostral to top) indicates levels of sectioning. (B-D) Cross sections through the levels of the node (B), anterior CLE (C) and tailbud (D) regions indicated by dashed lines in A (n = 3). *Sox2* and *Cre*ERT2 show entirely overlapping expression domains throughout all of the regions examined, including the anterior CLE (C-iv). Scale bars: 200 µm in A and 50 µm in B-D.

5.2.3 *Sox2* is dispensable for posterior body formation up to E12.5

In a previous functional study, our lab deleted *Sox2* in NMPs by performing *T*$^{CreERT2/+}$*; Sox2*$^{fl/+}$ *x Sox2*$^{fl/fl}$ matings, followed by tamoxifen activation at E7.5 or E8.5 (Mugele, 2018; Mugele et al., 2018). The resulting E9.5 mutant embryos displayed normal mesoderm formation, in accordance with the lack of *Sox2* expression in NMPs (demonstrated by the previous lineage tracing and in situ hybridisation experiments). Moreover, assessment of mutant embryos at E10.5 showed that neural tube formation was equally unaffected, which was very surprising given the well-established role of Sox2 as a key regulator of neural progenitor maintenance (Bylund et al., 2003; Gómez-López et al., 2011; Graham et al., 2003), and thus deserving of further investigation. Furthermore, as noted previously, Sox2 protein exhibits a remarkable stability of over 48 hours. Thus, it is conceivable that low levels of residual Sox2 (produced before tamoxifen-induced deletion of the gene) sustained normal development up to E10.5. In that case, defects would be expected to arise later in development when Sox2 has been entirely degraded.

To clarify and extend these previous findings, the *Sox2* knock-out experiment was repeated here with tamoxifen injections at E7.5, E8.5 and E9.5 (for consistency with the previously used protocol), followed by collection and morphological characterisation of embryos at E12.5. None of the *T*$^{CreERT2/+}$*; Sox2*$^{fl/fl}$ mutant embryos showed any signs of spina bifida, but 5 out of 11 mutants displayed a mild tail flexion defect where the curvature of the tail was reversed from ventral to dorsal (Figure 5.3C). This defect was identical to that found in cases of delayed spinal neural tube closure (Copp, 1985; Molè et al., 2020). The observed phenotype could therefore

stem from the latency in the activation of alternative mechanisms that compensate for the (lost) function of Sox2 in neural tube formation. Furthermore, Sox2 appeared to be redundant for overall developmental progression and axial elongation, as $T^{CreERT2/+}$; $Sox2^{fl/fl}$ embryos showed no significant differences in somite number, crown-rump length, body length or tail length when compared to littermate controls (Figure 5.3D-G).

A

	Total	Normal	Affected	Spina bifida	Tail flexion defect
$T^{CreERT2/+}$; $Sox2^{fl/fl}$ **(Mutant)**	11	6	5	0	5
$T^{CreERT2/+}$; $Sox2^{fl/+}$ (Het)	9	9	0	0	0
$T^{+/+}$; $Sox2^{fl/+}$ (Control)	10	10	0	0	0
$T^{+/+}$; $Sox2^{fl/fl}$ (Control)	11	11	0	0	0
Total	41	41	5	0	5

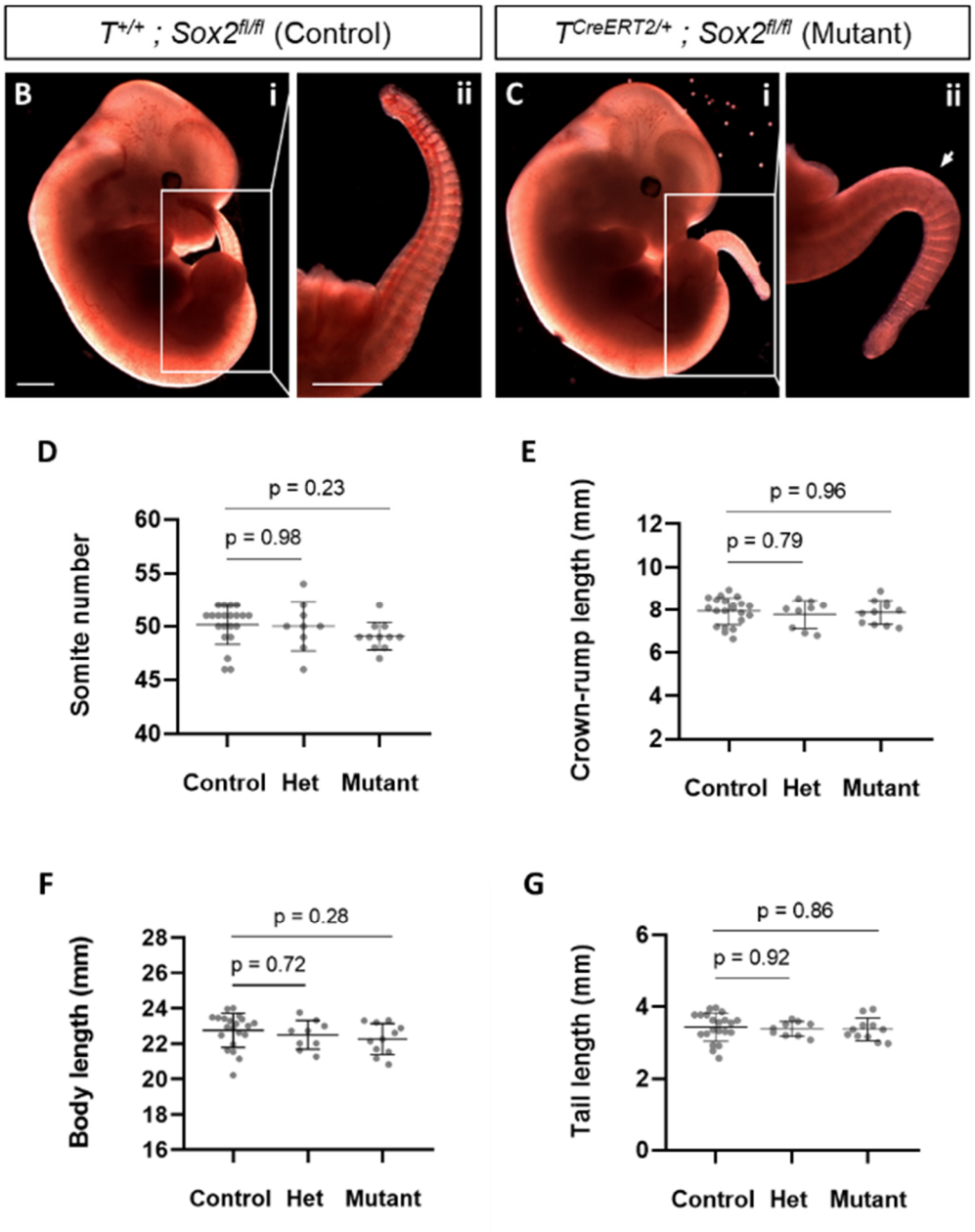

Figure 5.3. Morphological characterisation of E12.5 embryos following $T^{CreERT2}$-mediated deletion of *Sox2* with tamoxifen administration at E7.5, E8.5 and E9.5. (A) Summary table. The frequency of the four genotypes conforms to the expected

Mendelian ratios (Chi-square test; p = 0.97; embryos: n total = 41). The 2 control genotypes (*T*$^{+/+}$*; Sox2*$^{fl/fl}$ and *T*$^{+/+}$*; Sox2*$^{fl/+}$) were pooled for all subsequent analyses. 5 out of 11 mutant embryos are affected by a tail flexion defect (Fisher's exact test; p = 0.0023; embryos: mutants vs controls). Mutant embryos did not display any cases of spina bifida. No defects of any kind were observed in the heterozygote and control groups. (B) Brightfield images show the dorsally flexed tail of a mutant embryo (C-ii, arrow) compared to the ventrally flexed tail of a control embryo (B). (D-G) Measurements showed that there were no statistically significant differences in somite number (D), crown-rump length (E), body length (F) or tail length (G) between the different genotypes (one-way ANOVA; post-hoc Dunnett's test; p values in figure; embryos: controls n = 21, heterozygotes n = 9, mutants n = 11). Data shown as mean values ± SD. Scale bars: 1 mm.

5.2.4 Cell proliferation in the neural plate is unaffected by loss of Sox2

The newly documented redundancy of Sox2 function for posterior neurulation prompted the question of which cellular or genetic mechanisms might be compensating in its absence. One hypothesis is that Sox2 is required for specification of NMP-derived neural progenitors. In that case, *T*^{CreERT2}-mediated deletion of *Sox2* would bias NMP fate choice toward the mesodermal direction and NMP colonization of the neural tube would be impaired. In this scenario, the neural tube would need to be formed from a different pool of T-negative progenitors. In this regard, it has been previously found that 60% of cells in the caudal neural tube are NMP-derived (Chalamalasetty et al., 2014). The rest of the neural tube presumably stems from neural plate progenitors specified at the end of gastrulation. If these cells were to compensate for the loss of the NMP neural lineage, they would have to drastically increase their proliferation rates. To test this hypothesis, *T*$^{CreERT2/+}$*; Sox2*$^{fl/+}$ *x Sox2*$^{fl/fl}$ matings were performed with tamoxifen induction at E7.5. The resulting embryos were then collected at E8.5 and immunostained for Sox2 - to confirm that it is effectively removed by the deletion - and the mitosis marker pHH3 - to assess the impact of the deletion on cell proliferation within the neuroepithelium. Contrary to

the above prediction, however, whole-mount confocal microscopy and quantification demonstrated that, despite a dramatic reduction of Sox2 protein (Figure 5.4B), the number and distribution of cell divisions in the neuroepithelium of the PNP were unaffected (Figure 5.4D, E).

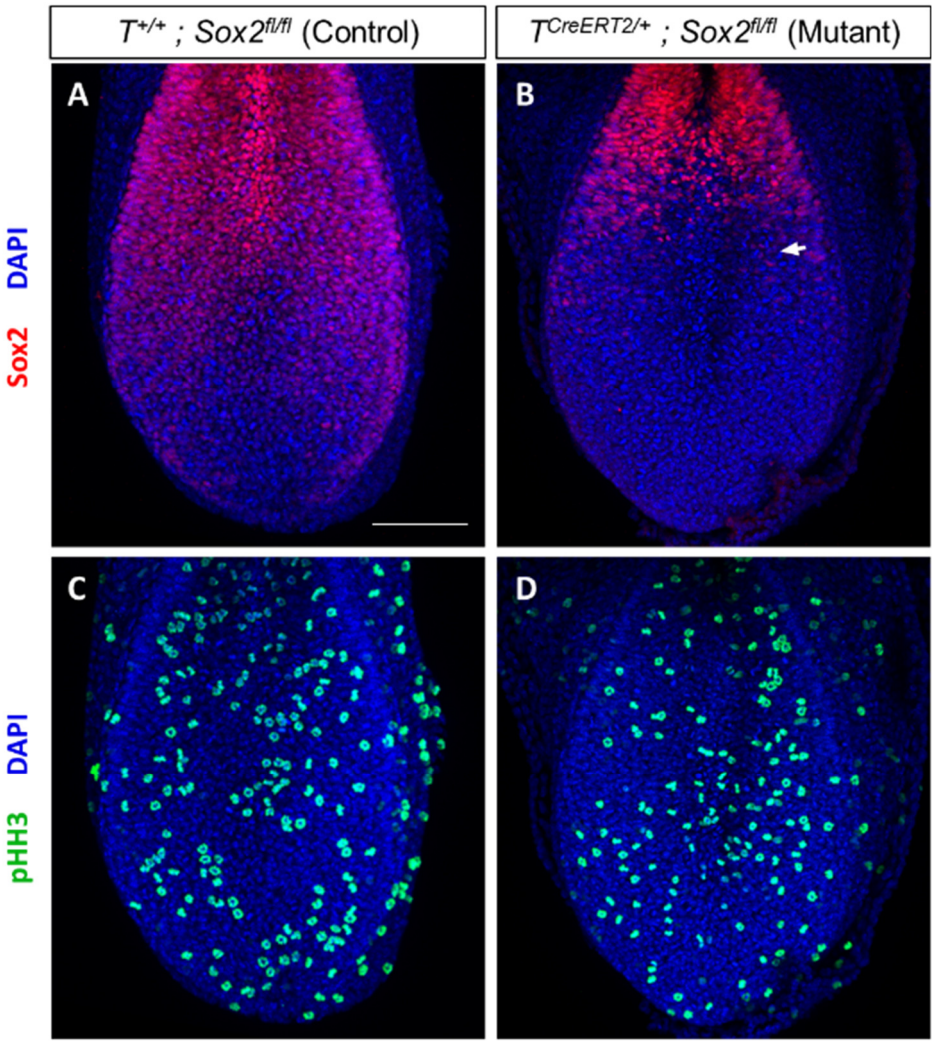

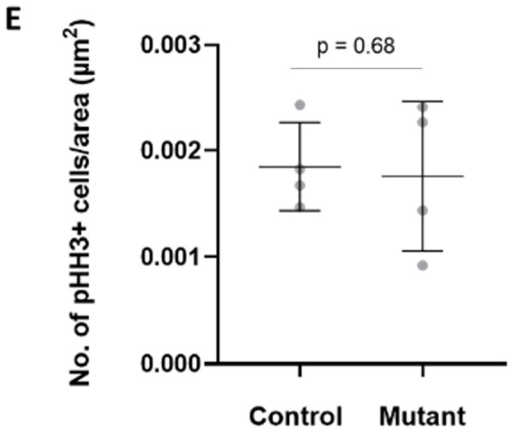

Figure 5.4. Sox2 and pHH3 immunostaining of E8.5 embryos following $T^{CreERT2}$-mediated deletion of Sox2 with tamoxifen administration at E7.5. (A, B) Maximum intensity projections of the PNP in Sox2- immunostained control (A) and mutant (B) embryos (n = 4 per genotype). The deletion was effective in removing Sox2 from the caudal neuroepithelium (B, arrow). (C, D) Maximum intensity projections of the PNP in Sox2-stained control (A) and mutant (B) embryos (n = 4 per genotype). Cell divisions are similarly distributed in the neuroepithelium of mutant and control embryos. (E) Quantification of pHH3 signal detected no differences in the number of dividing cells within the neuroepithelium of the PNP between mutants and controls (Mann-Whitney test; p value in figure; embryos: controls n = 4, mutants n = 4). Data shown as mean values ± SD. Scale bar: 100 µm.

5.2.5 NMP fate choice is unaffected by loss of Sox2

Next, to directly evaluate the impact of *Sox2* deletion on NMP fate choice, the *TCreERT2*-mediated deletion of Sox2 was combined with genetic lineage tracing utilising the $Rosa26^{EYFP/EYFP}$ reporter. For this purpose, $T^{CreERT2/+}$; $Sox2^{fl/+}$ and $Rosa26^{EYFP/EYFP}$ mice were crossed to breed $T^{CreERT2/+}$; $Sox2^{fl/+}$; $Rosa26^{EYFP/+}$ mice. $T^{CreERT2/+}$; $Sox2^{fl/+}$; $Rosa26^{EYFP/+}$ and $T^{CreERT2/+}$; $Sox2^{fl/+}$ were then crossed to generate $T^{CreERT2/+}$; $Sox2^{+/+}$; $Rosa26^{EYFP/+}$ (*Sox2* wild type), and $T^{CreERT2/CreERT2}$; $Sox2^{fl/fl}$; $Rosa26^{EYFP/+}$ (*Sox2* mutant) embryos, thus allowing the comparative lineage tracing of normal as well as Sox2-deficient NMPs. Notably, homozygosity for the $T^{CreERT2}$ was deemed important in this case, due to the need for recombination of three floxed alleles. In that regard, $T^{CreERT2/CreERT2}$ animals have previously been shown to be healthy and fertile (Anderson et al., 2013). Tamoxifen was administered at E7.5 and E8.5, and embryos were collected at E9.5.

In accordance with previous findings, an initial morphological examination revealed no differences between mutant and control embryos at this stage (Figure 5.5 A-i, B-i). Furthermore, imaging the embryos using a fluorescence stereoscope showed that the extent of axial colonisation by the *T*-expressing lineage was similarly unaffected, approximately reaching the level of the 6th somite in both mutants and controls

(Figure 5.5 A-ii, B-ii). Subsequently, embryos were immunostained for Sox2 to evaluate the effectiveness of the deletion, and for GFP to enhance the signal of the EYFP reporter. Confocal microscopy and 3D reconstruction of the PNP region then revealed that (in accordance with the RNAscope results) Sox2 was strongly expressed in the neural tube of wild type embryos (Figure 5.5C). In $T^{CreERT2/CreERT2}$; $Sox2^{fl/fl}$; $Rosa26^{EYFP/+}$ mutant embryos, on the other hand, Sox2 was wholly absent (Figure 5.5D). Despite the loss of Sox2, however, the EYFP-labelled NMPs widely colonised the neural tube (along with the paraxial mesoderm) of mutant embryos, similar to controls (Figure 5.5E, F).

In order to more precisely assess the impact of *Sox2* deletion on NMP fate choice, the proportion of EYFP-positive cells within the caudal neural tube and paraxial mesoderm was then quantified in optical coronal sections of mutant and control embryos. $T^{CreERT2/CreERT2}$; $Sox2^{fl/fl}$; $Rosa26^{EYFP/+}$ embryos demonstrated a higher overall degree of recombination in both the paraxial mesoderm and neural tube, compared with $T^{CreERT2/+}$; $Sox2^{+/+}$; $Rosa26^{EYFP/+}$ embryos, owing to the presence of a second copy of *CreERT2* (Figure 5.5G, H). However, comparison of the recombined Neural/Mesodermal Fraction Ratio between *Sox2* mutants and controls revealed that the frequency with which NMPs choose the neural versus mesodermal fate was unaltered by the loss of *Sox2* (Figure 5.5I). Overall, these experiments thus demonstrated that *Sox2* is indeed dispensable for neural specification of NMPs.

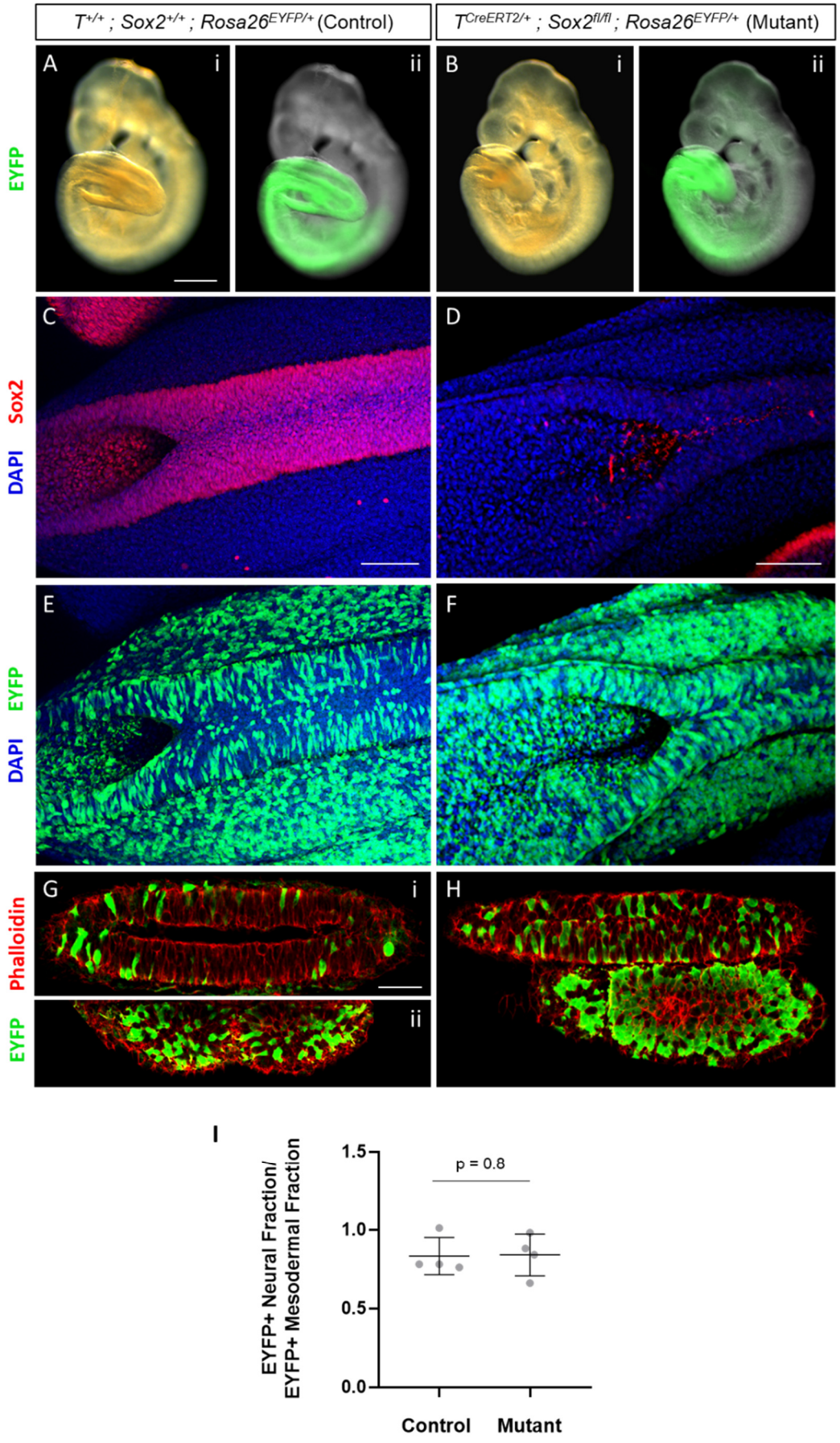
T+/+ ; Sox2+/+ ; Rosa26EYFP/+ (Control)
TCreERT2/+ ; Sox2fl/fl ; Rosa26EYFP/+ (Mutant)
A
i
ii
B
i
ii
EYFP
C
D
Sox2
DAPI
E
F
EYFP
DAPI
G
i
H
Phalloidin
EYFP
ii
I
EYFP+ Neural Fraction/
EYFP+ Mesodermal Fraction
1.5
1.0
0.5
0.0
p = 0.8
Control
Mutant

Figure 5.5. $T^{CreERT2}$-mediated deletion of Sox2 and lineage tracing using the Rosa26^{EYFP} reporter with tamoxifen administration at E7.5 and E8.5, followed by embryo collection at E9.5. (A, B) Brightfield (A-i, B-i) and widefield fluorescence (A-ii, B-ii) images show that loss of Sox2 does not affect overall embryo morphology or the extent of axial colonisation by the T-expressing lineage (n = 4 per genotype). C, D) Maximum intensity projections of the PNP and recently fused neural tube region in Sox2-immunostained control (C) and mutant (D) embryos (n = 3 per genotype). Sox2 is thoroughly removed from the neuroepithelium of mutant embryos. (E, F) Maximum intensity projections of the PNP and recently fused neural tube region in GFP-immunostained control (E) and mutant (F) embryos (n = 4 per genotype). EYFP-positive cells are widespread in the paraxial mesoderm and (to a lesser extent) the neural tube of both mutant and control embryos. (G, H) Optical coronal sections through the recently closed neural tube (top) and paraxial mesoderm (bottom) in control (G) and mutant (H) embryos (n = 4 per genotype). Phalloidin staining was performed to facilitate cell segmentation. Mutant embryos show a larger fraction of EYFP-positive cells in both neural and mesodermal tissue due to having a second copy of CreERT2. (I) Quantification EYFP-positive fraction in neural and mesoderm tissue of control and mutant embryos and statistical comparison of Neural/Mesodermal EYFP-positive Fraction ratio between mutants and controls shows that the dynamics of NMP fate choice remain unchanged by loss of Sox2 (Mann-Whitney test; p value in figure; embryos: controls n = 4, mutants n = 4). Data shown as mean values ± SD. Scale bars: 500 µm in A and B; 100 µm in C-F; 50 µm in G and H.

5.2.6 Sox3 is likely compensating for the loss of Sox2

While previous literature has identified Sox2 as a key regulator of neural potency (Bylund et al., 2003; Graham et al., 2003), the aforementioned results indicate that neural specification in the caudal embryo is unaffected by loss of *Sox2*. This apparent contradiction might be explained by the existence of alternative transcription factors that compensate for the function of *Sox2* when it is deleted. In this regard, the closely related SoxB1 transcription factors *Sox1* and *Sox3* display substantial sequence

homology, implying potential functional redundancy (Collignon et al., 1996; Wood & Episkopou, 1999). Previous studies have shown that *Sox3* is expressed in the caudal neuroepithelium, while *Sox1* is not (Mugele, 2018; Mugele et al., 2018; Takemoto et al., 2011; Wood & Episkopou, 1999). *Sox3* thus represents the most likely candidate for compensation in the absence of *Sox2*.

To explore this possibility, $T^{CreERT2/+}$; $Sox2^{fl/+}$ x $Sox2^{fl/fl}$ matings were once again performed with tamoxifen administration at E7.5 and E8.5, followed by embryo collection at E9.5. Embryos were then immunostained for Sox3. Confocal microscopy and 3D reconstruction of caudal region showed strong Sox3 staining throughout the neuroepithelium of both mutant and control embryos, thus demonstrating that the spatial pattern of Sox3 expression was unaffected by the loss of Sox2 (Figure 5.4A, B). Next, to quantitively assess for possible *Sox3* upregulation in response to *Sox2* deletion, the $T^{CreERT2}$-mediated deletion of *Sox2* was repeated as previously and embryos were collected at E9.5 and E12.5. The caudal-most region was then dissected from mutants and controls at both stages, RNA was extracted and used to perform a qRT-PCR for *Sox2* and *Sox3*. While *Sox2* mRNA was dramatically reduced, however, there was no significant change in the levels of *Sox3* between mutants and controls at either developmental stage (Figure 5.4C). These results therefore indicated that *Sox3* is not upregulated in response to *Sox2* deletion, even after allowing sufficient time for the degradation of any residual Sox2 protein (i.e., at E12.5).

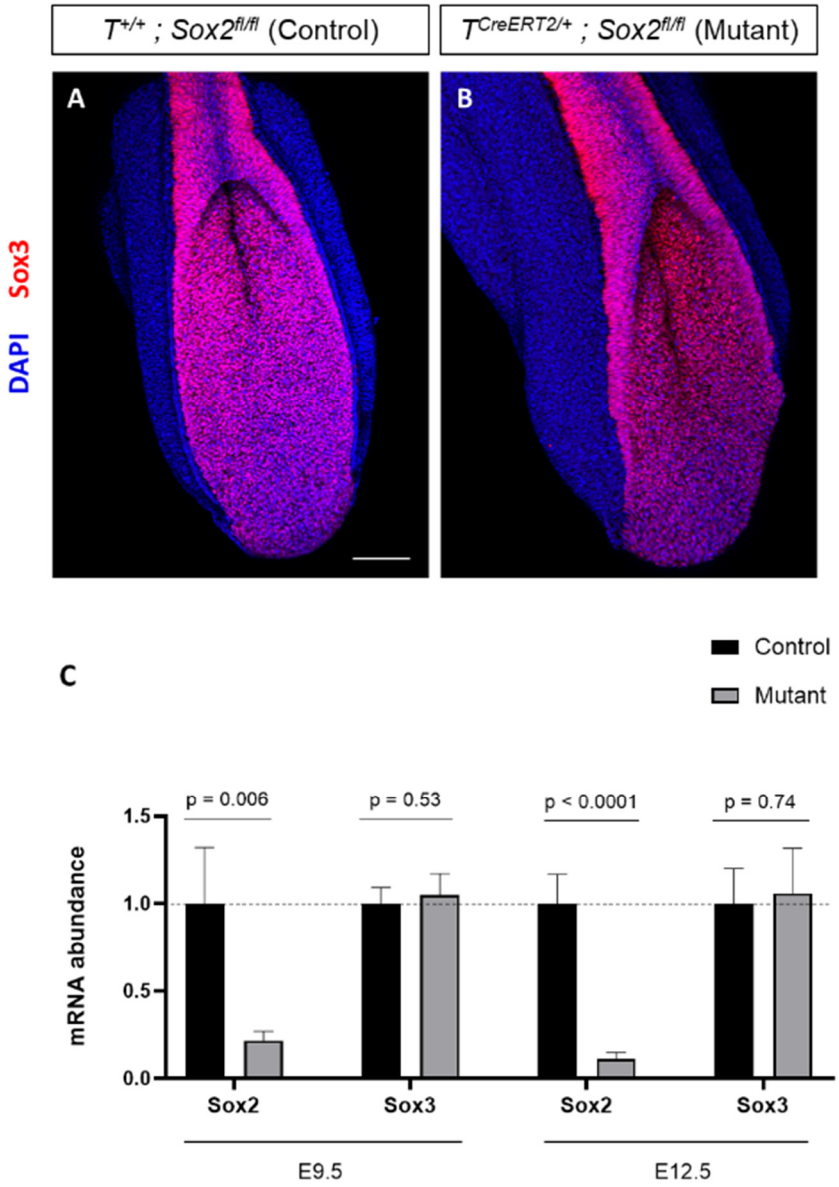

Figure 5.6. Assessment for Sox3 upregulation in E9.5 and E12.5 embryos following $T^{CreERT2}$-mediated deletion of *Sox2* with tamoxifen administration at E7.5, E8.5 (and E9.5). (A, B) Maximum intensity projections of the PNP and recently fused neural tube in Sox3-immuno stained control (A) and mutant (B) embryos at E9.5 (n = 3 per genotype). The expression domain of Sox3 is identical between mutants and controls. (B) qRT-PCR analysis of the caudal-most region shows a dramatic reduction of *Sox2* expression, but no significant differences in *Sox3* between $T^{CreERT2/+}$; $Sox2^{fl/fl}$ mutant embryos and *CreERT2*-negative littermate controls at E9.5 or E12.5 (Unpaired, two-tailed student's t-tests with Holm-Sidak multiple testing correction; p values in figure; embryos: controls n = 4, mutants n = 4, for each stage). Data shown as mean values (normalised to control group) ± SD. Scale bar: 100 µm.

5.3 Discussion

Recent findings from our lab indicated that, contrary to the previously held view, *Sox2* is not expressed in NMPs, based on lineage tracing, and is not required for neural tube formation, based on gene deletion in the T expression domain (Mugele, 2018; Mugele et al., 2018). The current chapter sought to strengthen these observations, resolve the apparent contradictions and extend these findings by assessing for *Sox2* expression in NMPs and investigating the potential role of *Sox2* in NMP function and lineage choice. The idea that NMPs co-express *T* and *Sox2* originated from the discovery of overlapping *T* and *Sox2* expression domains in putative NMP regions of embryos from a variety of species (Martin & Kimelman, 2012; Olivera-Martinez et al., 2012; Wymeersch et al., 2016). Previous studies conclusively demonstrated the existence of T/Sox2 double-positive cells on the protein level. However, due to the long half-life of Sox2 protein, immunoreactivity does not constitute a reliable readout of real-time gene expression (Avilion et al., 2003; Ji et al., 2018).

Conversely, previous in situ hybridisation studies have been inadequately designed to detect co-expression of the two factors and have produced contradictory findings. Studies that reported the existence of *T/Sox2* co-expressing cells, for example, did so based on separately stained embryos (Martin & Kimelman, 2012; Olivera-Martinez et al., 2012) or double stained images of insufficient clarity (Wymeersch et al., 2016). When in situ hybridisation for *T* and *Sox2* was previously repeated in our lab, *T/Sox2* co-expression was detected at the level of the anterior CLE at E8.5, but not at the CNH at E9.5 (where Sox2 was found to be completely absent) (Mugele, 2018; Mugele et al., 2018). Nevertheless, this latter study also used colorimetric whole-mount in situ hybridisation on separate embryos, which is ill-suited for the assessment of co-localisation and might also lack the sensitivity to detect low levels of *Sox2* expression.

To mitigate these limitations and conclusively address the question of *T*/*Sox2* co-expression in the CNH, the in situ hybridisation experiment was repeated here, utilising the multiplex fluorescent version of the RNAscope technique which is known to have much greater sensitivity and specificity than the previously used methods.

This demonstrated that *Sox2* is indeed present in some cells within the CNH, albeit at very low levels compared to the neuroepithelium. As NMPs are entirely contained within the CNH at this stage, demonstrating complete absence of *Sox2* transcription within the CNH would have constituted strong evidence for the lack of *Sox2* expression in NMPs. Since some *Sox2*-positive cells were in fact detected, however, the question remained (at that point) unresolved. That was because it was unknown whether those *Sox2*-positive cells were NMPs, committed neural progenitors or some other cell type. The distinction between NMPs (individual cells that produce both neural and mesodermal derivatives) and neuromesodermally competent (NMC) regions (that contain NMPs together with a variety of other cell types of diverse developmental potentials) was recently highlighted by Binagui-Casas et al., and is one that has often been neglected in the NMP literature (Binagui-Casas et al., 2021). The current in situ hybridisation experiment demonstrated that *Sox2*-positive cells also represent a minority of the total cell population in the CNH, in agreement with previous single-cell RNA-sequencing and immunofluorescence studies (Koch et al., 2017; Wymeersch et al., 2016).

Unlike static expression studies, genetic lineage tracing reveals the eventual fate of the target cell population, and is thus much better suited to answering the question of potential Sox2 expression in NMPs. In this regard, previous experiments in our lab demonstrated that *Sox2*-expressing cells give rise to neural but not mesodermal tissues after E8 (Mugele, 2018; Mugele et al., 2018). This result would therefore constitute solid evidence that *Sox2* is expressed in committed neural progenitors but not NMPs. However, the validity of this conclusion had been initially questioned by concerns regarding the ability of the employed *Sox2*^{CreERT2} driver to recombine all *Sox2*-expressing cells. Interestingly, *Sox2* expression in the caudal region has been shown to derive from a different enhancer (N1) than Sox2 expression in the epiblast and anterior neural plate (N2) (Kondoh et al., 2016; Takemoto et al., 2011). The first concern therefore related to whether *CreERT2* expression is driven by the N1 enhancer at all. If it is, a second concern related to expression of sufficient amounts of CreERT2, given its inducible nature and the potentially low levels of Sox2 expression in NMP-harbouring regions.

To address these concerns, RNAscope was once again employed to assess whether Sox2 and CreERT2 coincide in the regions of interest. Despite assuming the eventual translation of *CreERT2* RNA into the functional Cre recombinase protein, RNAscope was deemed more appropriate than an immunohistochemical study in this case, as it would provide a real-time snapshot of gene expression in each cell. An equivalent immunohistochemical study, on the other hand, would have been temporally confounded by the higher stability of the target proteins (compared to the respective RNA molecules), and the relative lag between tamoxifen absorption and reporter gene expression, which differs from cell to cell. Indeed, this experiment shows *CreERT2* is strongly expressed throughout the *Sox2* expression domain in the rostral CLE and all regions examined, thus validating the previous lineage tracing experiment and the conclusion that Sox2 is only expressed downstream of neural commitment of NMPs. Furthermore, this finding indicates that the few *Sox2*-expressing cells - identified within the CNH in previous RNAscope experiment and previous studies (Wymeersch et al., 2016) – likely represent recently committed neural progenitors about to migrate out of the CNH and into the extending neuroepithelium. In accordance, the original *Sox2* lineage tracing experiment found extremely few GFP-positive cells in the tailbud, suggesting that neural progenitors migrate into the neural tube shortly after their commitment (Mugele, 2018; Mugele et al., 2018).

To assess the role of Sox2 in the NMP-mediated process of axial elongation, previous experiments from our lab deleted *Sox2* from the *T*-expressing lineage (Mugele, 2018; Mugele et al., 2018). However, morphological examination and staining for a range of tissue-specific markers revealed that formation of mesodermal and, surprisingly, even neural tissues was entirely unaffected by the deletion up until E10.5. Sox2 protein has a documented stability of over 48 hours and therefore it is conceivable that residual Sox2 protein (produced before the deletion of the gene) could have sustained normal development up to that stage. To test this possibility, the deletion was repeated here, and embryos were morphologically characterised at E12.5 (when Sox2 should have been entirely degraded). Mutant embryos display no abnormalities, other than a mild tail flexion defect which is identical to that found in cases of delayed spinal neural tube closure (Copp, 1985; Molè et al., 2020). This

finding therefore indicates that Sox2 is indeed dispensable for neural tube closure and axial elongation, but that the potential lag in the activation compensating mechanisms (after Sox2 ablation) could delay neural tube closure. In accordance, laser ablations of the NMP-harbouring rostral CLE, followed by 24 h embryo culture, were previously shown to transiently affect neural tube formation and lead to a significantly larger PNP (Mugele, 2018; Mugele et al., 2018). Both experiments therefore suggest that a delay in the generation of neural tissue can translate into a delay in PNP closure, but compensating mechanisms eventually ensure normal development.

Nevertheless, the fact that neural tube formation is unaffected by loss of Sox2 remains highly surprising. Sox2 is known to be important for neural induction (Thomson et al., 2011; Wang et al., 2012; Zhao et al., 2004), as well as the maintenance of the undifferentiated state of neural progenitors (Bylund et al., 2003; Graham et al., 2003). Furthermore, Sox2 has been reported to antagonise T in NMPs, thus maintaining their bipotent state and regulating their face choice (Koch et al., 2017; Sambasivan & Steventon, 2021). If such an antagonism existed, removal of either T or Sox2 would be predicted to shift the balance of NMP commitment toward the neural or mesodermal fate, respectively. This hypothesis has been partly supported by studies showing that deletion of T, or upstream mesodermal drivers Fgfr1 and Wnt3a, results in axial truncation and ectopic neural tubes at the expense of paraxial mesoderm (Ciruna et al., 1997; Yamaguchi et al., 1999; Yoshikawa et al., 1997). In addition, genetic lineage tracing revealed that *T*-expressing cells lacking Wnt3a or β-catenin are biased toward the neural fate (Garriock et al., 2015). To test the opposite side of this prediction and determine whether Sox2 has a role in NMP fate choice and neural commitment, a complementary experiment was performed here by lineage tracing Sox2-deficient and wild type NMPs. Strikingly, comparison of the neural/mesodermal balance of the NMP progeny in mutants and controls revealed that face choice dynamics had been unaffected by the loss of Sox2. This lack of a complementary phenotype to the T inactivation (i.e., excess mesoderm at the expense of neuroepithelium) argues against T/Sox2 antagonism in NMPs, and instead places Sox2 downstream of T and neural commitment in accordance with the

conclusions of the now validated Sox2 lineage tracing results (Mugele, 2018; Mugele et al., 2018).

NMP fate choice was previously thought to be governed by T/Sox2 antagonism based on a transcriptomic study (Koch et al., 2017). However, a closer examination of the study for the purposes of the current thesis reveals that the two pieces of evidence presented there do not necessarily warrant such a conclusion. The first of these originated from an RNA-sequencing analysis of (fluorescently labelled and FACS-sorted T-positive/Sox2-negative, T-positive/Sox2-positive and T-negative/Sox2-positive) cells isolated from NMP-harbouring regions combined with a chromatin immunoprecipitation study for T and Sox2 binding sites in NMPs derived in vitro from embryonic stem cells. This analysis revealed that 71.7% of the 1,402 genes that are differentially expressed between the 3 groups of isolated cells (sorted based on T and Sox2 expression) are associated with T and/or Sox2 binding. This was taken as evidence for the control of NMP lineage choice by T and Sox2. However, the proportion of differentially expressed genes bound by T and/or Sox2 did not appear significantly different from the total proportion of genes (13,674) that was bound by T and/or Sox2 (across the entire genome). In other words, differentially expressed genes were not more likely to be bound by T and/or Sox2 compared to non-differentially expressed genes in NMPs. The second piece of evidence provided in support of T/Sox2 antagonism derived from an RNA-sequencing analysis of cells, isolated from the tail bud of E8.5 mouse embryos, which expressed an inactivated form of T. Caudal cells lacking T function were shown to have upregulated Sox2 and other genes associated with the neural lineage. Based on this, the authors concluded T/Sox2 antagonism without performing the complementary experiment of assessing for upregulation of mesodermal markers after Sox2 inactivation. Therefore, the study concluded the existence of T/Sox2 antagonism (mutual inhibition) when only one-sided inhibition (of Sox2 by T) was actually shown.

Lastly, the current results, jointly with previous work from our lab, demonstrated that loss of Sox2 affects neither colonisation of the neural tube by NMPs nor the expression of the appropriate neural markers. Therefore, the potential function of Sox2 in neural specification appears to be redundant. The compensation is most

likely mediated by the closely related SoxB1 transcription factor Sox3 which exhibits a largely overlapping expression domain and substantial sequence similarity; especially in the DNA binding regions (Collignon et al., 1996; Miyagi et al., 2009; Wood & Episkopou, 1999). In this regard, *Sox2* and *Sox3* have been shown to have overlapping roles in neural progenitors and share a large proportion of their gene targets (Bergsland et al., 2011). Furthermore, a previous study that deleted *Sox2* specifically in the developing brain observed that (despite ventricular defects and perinatal lethality) neural stem cells retained their multipotency and capacity for self-renewal (Miyagi et al., 2009). Interestingly, the study also detected upregulation of Sox3 which was likely responsible for preserving these properties in neural cells. To assess whether an analogous upregulation has compensated for the lost Sox2 function in the current study, *Sox2* mutants were analysed using immunofluorescence and qRT-PCR for Sox3. While no changes were found in the spatial pattern or the levels of Sox3 expression, these experiments revealed that Sox3 is already strongly expressed throughout the neuroepithelium and thus likely in a position to compensate for Sox2, even in the absence of upregulation.

6. General discussion

6.1 The role of fibronectin in neural tube closure and axial elongation

6.1.1 Fibronectin mediates epithelial fusion

The first part of this project employed a variety of conditional gene deletion strategies to investigate fibronectin's role in the early development of the spinal segments of the mouse embryo. These experiments demonstrated that fibronectin at the dorsal midline is important for neural fold fusion, while fibronectin between the neuroepithelium and paraxial mesoderm facilitates symmetric elongation of the tail. The former of these two functions is underpinned by highly localised secretion and (integrin β1-mediated) binding of fibronectin by surface ectoderm cells at the PNP fusion site. This integrin-fibronectin interaction was shown to be critical in allowing surface ectoderm cells to remodel their junctions and become juxtaposed into semi-rosettes which in turn facilitate zippering propagation (Figure 6.1). The current findings therefore suggest a model whereby fibronectin mediates the first contact between the opposing neural fold tips. Initial binding to a common strand of fibronectin then allows contralateral surface ectoderm cells to remodel their shape and come into proximity to form novel cell-cell junctions. Indeed, formation of adherens junctions requires opposing cell surfaces to be within only 30 nm of each other, while fibronectin fibrils can reach micrometres in length (Perez & Nelson, 2004; Theocharis et al., 2016). This model is also supported by the disorganised E-cadherin and ZO-1 localisation at cell borders surrounding the fusion site of *Grhl3*^{Cre}*; Fn1*$^{fl/fl}$ mutants, thus illustrating that maturation of cell-cell adhesions in the area depends on effective cell-ECM adhesion.

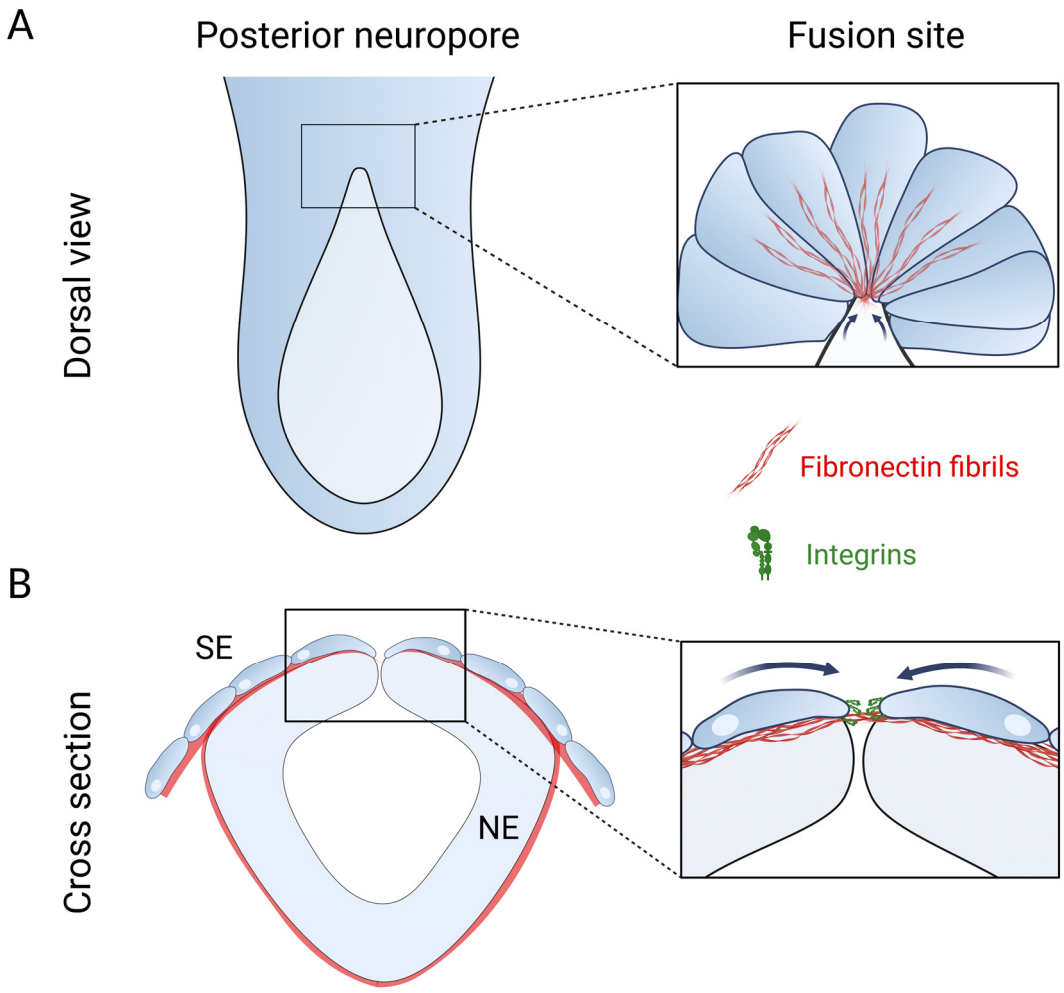

Figure 6.1. Model of fibronectin-mediated neural fold zippering. (A) Schematic dorsal view of the PNP and higher magnification of the fusion site. Radially oriented fibronectin fibrils around the fusion site allow SE cells (dark blue) to contract their proximal junctions (indicated by arrows) and form semi-rosettes that facilitate zippering propagation. (B) Cross section view of neural fold apposition and higher magnification of the fusion site. Integrin-mediated anchorage to a shared fibronectin matrix allows contralateral SE cells at neural fold tips to converge towards the midline (indicated by arrows) and come into proximity to form novel cell-cell adhesions.

Interestingly, while fibronectin's role in neural tube fusion was hitherto unrecognised, this is not the first time that fibronectin has been implicated in the process of epithelial closure. Epithelial closure is very common during embryonic

development, as well as wound healing, and usually involves two opposing epithelia that converge towards each other to seal a gap and eventually become continuous. A close parallel can be found in mouse eyelid closure where eyelid epithelia first appear at E11.5 and then extend and eventually fuse (temporarily) over the cornea by E16. This process was shown to involve cell intercalation (perpendicular to the axis of closure) at the eyelid front which creates a region of active shear and tows the rest of the epithelium towards the midline of the cornea (Heller et al., 2014). Strikingly, both fibronectin and integrin α5 were found to be enriched in eyelid front cells and knock-down of either component led to a failure of eyelid closure. The reduced rate of closure observed was associated with decreased cell movement and elongation thus preventing effective intercalation at the eyelid front.

Such cell-ECM interactions seem to be equally important in the process of wound closure. For example, fibronectin has been found to appear in the surface of wounds of both foetal and adult mice within 1 h post-wounding (Whitby & Ferguson, 1991). To elucidate the role of fibronectin in the process of wound closure, a previous study performed microsurgically-induced wounds on a 3D soft tissue model coupled with live imaging and addition of various cytoskeletal and cell adhesion inhibitors (Sakar et al., 2016). These experiments revealed that stromal wound closure includes two mechanistically different stages: a first stage of whole tissue deformation mediated by cell contractility, and a second stage of tangential migration of fibroblasts at the wound edge. Interestingly, blocking antibodies against fibronectin-binding integrins (α5β1 and αvβ3) were able to specifically inhibit the second stage of closure, thus demonstrating the dependence of this process on fibronectin. Furthermore, fibroblasts at the wound edge were shown to deposit, tow and remodel fibronectin fibrils which were then used as a substrate for migration into the gap area. Finally, while no cell intercalation was observed, this process was highly comparable to eyelid closure since the migration of fibroblasts at the wound edge had a towing effect on cells further back.

These examples illustrate that the secretion and assembly of fibronectin matrix at the boundaries of epithelia is a common characteristic of epithelial fusion across biological contexts. Adhesion to such provisional fibronectin matrices then allows

cells at the epithelial front to migrate and remodel their shape and junctions. Furthermore, as the examples of eyelid closure and wound healing demonstrate, such dynamic processes at the epithelial front can have long-range effects for the rest of the epithelium. As such, integrin-fibronectin interactions at the PNP zippering point might be essential not only for zippering, by mediating a constant flux of new surface ectoderm cells into the semi-rosette, but also for aiding the overall convergence of the neural folds towards the midline. This notion is supported by the finding that *Grhl3*^{Cre}*; Fn1*$^{fl/fl}$ mutants show significant increases in PNP width as well as length.

6.1.2 Fibronectin maintains inter-tissue adhesion

The second role of fibronectin revealed in the present study was that of ensuring the efficacy and symmetry of tail elongation by mechanically coupling the neural tube and paraxial mesoderm. *Cdx2*^{Cre}; *Fn1*$^{fl/fl}$ embryos often exhibited a neural tube that detached from the paraxial mesoderm and undulated independently at E10.5, and consequently a shortened and bent tail at E12.5. Structural and immunofluorescence analyses showing normal formation of all tissues surrounding the neural tube in these mutants indicated that the observed defects were entirely due to loss of inter-tissue adhesion between the neural tube and paraxial mesoderm. Interestingly, this evidence also suggested that the neural tube has a higher elongation rate than the paraxial mesoderm and therefore acts as a driving force in axial elongation. The fibronectin matrix at the NE-MES boundary therefore appears to facilitate axial elongation by mediating force propagation between the two tissues along both the AP and ML axes (Figure 6.2). The paraxial mesoderm resists medially directed forces from the neural tube walls thus maintaining their structural integrity and symmetric caudally directed elongation. The neural tube in turn (due to its higher elongation rate) exerts a caudally directed force on the paraxial mesoderm thus actively assisting its elongation.

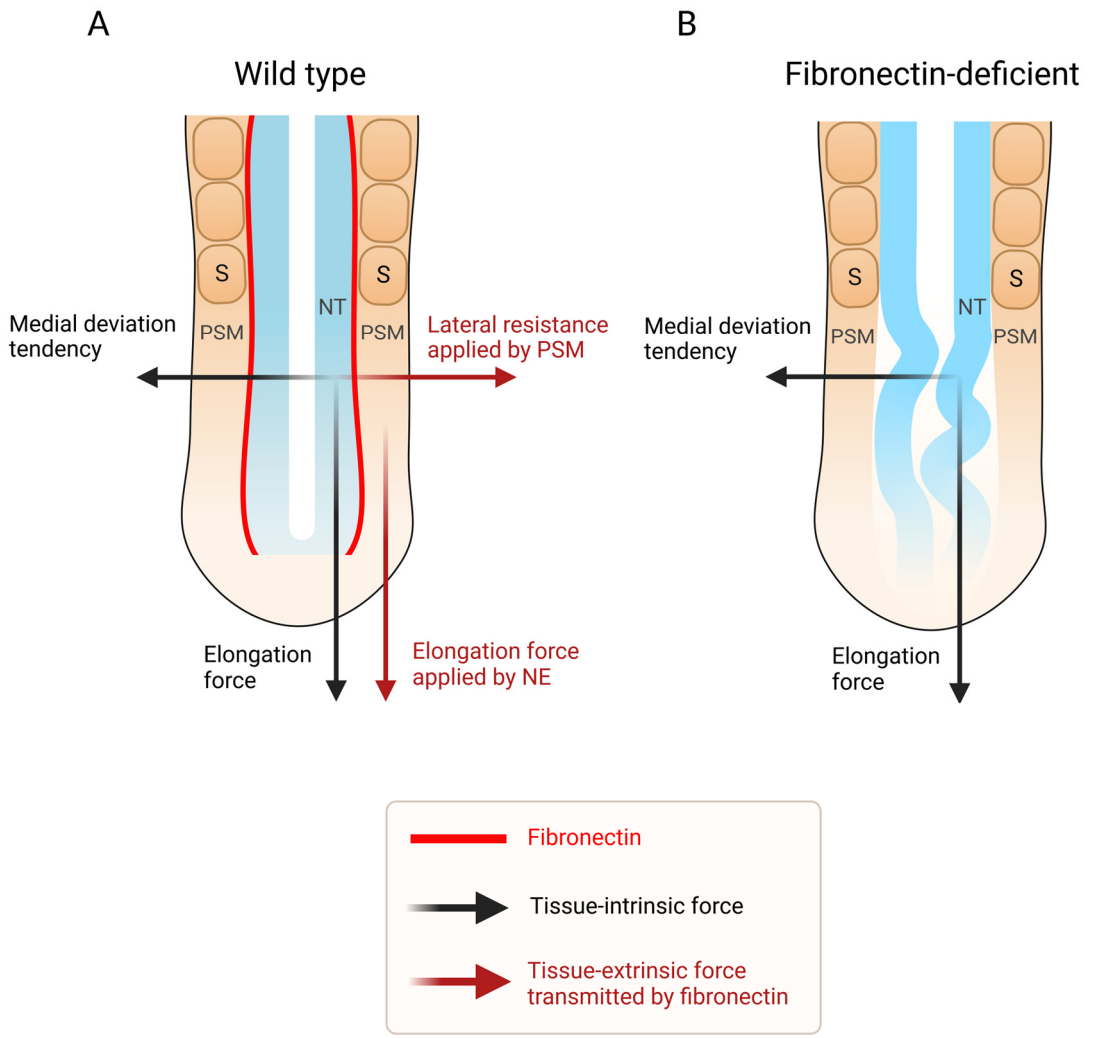

Figure 6.2. Biomechanical interactions of the neural tube and paraxial mesoderm during tail elongation. Schematic view of the elongating tail summarising the forces (represented by arrows) deduced by the current study. (A, B) Each neural tube (NT) wall exhibits two forces that are intrinsically generated by the neuroepithelium: a caudally directed elongation force and a tendency to deviate medially (black arrows). (A) Under normal conditions, the fibronectin matrix (red) mechanically couples each NT wall with the adjacent column of presomitic mesoderm (PSM). As a result, fibronectin transmits some of the neuroepithelium's caudal elongation force to the PSM, while also allowing the lateral columns of PSM to resist the medial deviation tendencies of the NT walls (brown arrows). The latter maintains a net force of zero along the medio-lateral axis of the NT walls, thus ensuring linear caudally directed elongation. (B) Loss of fibronectin uncouples the NT walls from the PSM and causes

them to deviate mediolaterally and elongate independently in an undulating fashion. Additional abbreviations: S, somite.

While the proposed role of fibronectin in mechanically coupling these tissues during axial elongation had not been previously demonstrated in the mouse, it is strongly supported by various studies in zebrafish. The BM between the neural tube and paraxial mesoderm in zebrafish is made up of laminin and fibronectin and morpholino-mediated double KD of these proteins has been shown to give rise to severe neural tube malformations (Araya et al., 2016). Furthermore, live imaging and cell tracking revealed that while medial convergence of neural and mesodermal cells is tightly coupled in control embryos, ECM depletion makes the paraxial mesoderm detach from the neuroepithelium and lag behind in terms of convergence. Similarly, a more recent live imaging study showed that zebrafish embryos lacking either fibronectin or its receptor subunit integrin α5, show enhanced convergence of the neural tube towards the midline but significant left-right asymmetries in PSM area (Guillon et al., 2020). In accordance with the present study, this evidence therefore demonstrates that fibronectin-mediated inter-tissue adhesion between the neural tube and paraxial mesoderm opposes medial convergence of the neural tube and ensures bilaterally symmetric morphogenesis.

Another interesting set of findings comes from a study by Dray et al. that utilised a combined knock-down of the fibronectin receptor subunits integrin α5 and αv (Dray et al., 2013). Treated embryos exhibited a dramatic loss of fibronectin assembly and significantly reduced axial length. Notably, the specification and migration of neural and mesodermal progenitors were shown to be unaffected. Instead, the elongation defect seemed to arise due to loss of inter-tissue adhesion. Unlike control embryos where the notochord and paraxial mesoderm were closely aligned, treated embryos exhibited large gaps between these tissues, and the notochord undulated independently with an appearance highly reminiscent of the neural tube in the *Cdx2*^{Cre}*; Fn*$^{fl/fl}$ mutants. While the authors focused on the notochord, the neural tube of integrin-deficient embryos also showed a degree of abnormal undulation and

detachment from the paraxial mesoderm. These data could therefore indicate that while inter-tissue adhesion is equally important for axial elongation in the two species, the main tissue that generates the elongation forces could differ (i.e., the neural tube in the mouse vs. the notochord in the zebrafish). The potentially greater contribution of the notochord to axial elongation in zebrafish might also relate to its much larger relative size (as a proportion of the entire axis) in zebrafish compared to mice (Stemple, 2005).

This role of the neural tube and notochord as mechanical drivers of axial elongation has also been demonstrated in avian embryos. In this regard, transgenic quail embryos ubiquitously expressing nuclear-localized cherry fluorescent protein allowed tracking of the AP movements of different tissues, thus revealing that the neural tube and the notochord elongate faster than the paraxial mesoderm (Huss et al., 2015). These findings were also confirmed by a more recent study that replaced various tissues in the elongating posterior body of the chick embryo with soft gels and tracked gel deformation to determine the forces applied by neighbouring tissues, while also simulating some of these forces with magnetically controlled pins (Xiong et al., 2020). This experimental setup showed that the elongation of the neural tube and notochord is not only responsible for the posterior displacement of the tailbud, but also for stimulating cell flow and elongation in the PSM through inter-tissue mechanical coupling. Overall, these studies are therefore increasingly highlighting the distinct morphogenetic behaviours of neighbouring tissues, the importance of inter-tissue adhesion and accordingly the need for future studies to treat axial elongation as a multi-tissue problem.

6.1.3 Open questions

In addition to identifying two distinct roles of fibronectin - in spinal neural tube fusion and inter-tissue adhesion during axial elongation - the current project has highlighted a number of open questions and corresponding directions for future studies into these developmental processes. The experiments in Chapter 3, for example,

demonstrated the importance of highly localised secretion and (integrin β1-mediated) binding of fibronectin at the PNP fusion site for the process of neural fold zippering. Such integrin-fibronectin interactions are in turn enabled through the focal expression of fibronectin and the related integrin subunits (α5 and β1) by a few surface ectoderm cells precisely at the fusion site. As the cells that constitute the fusion site constantly change, this raises the question of how this distinct transcriptional signature is regulated. For instance, is the fate of these cells predetermined or can local (chemical or mechanical) factors induce integrin and fibronectin expression in any surface ectoderm cells that assume a position at the fusion site? As these cells would be extremely difficult to isolate, new spatial transcriptomic methods hold great promise for mapping potentially distinct cell populations in the area, while highly localised laser or optogenetic ablations of fusion site cells could help characterise functional plasticity in the area (Eng et al., 2019; Junker et al., 2014; Liu et al., 2019; Rodriques et al., 2019).

The findings presented in Chapter 4 supported a model whereby fibronectin-mediated inter-tissue adhesion transmits posteriorly directed elongation forces from the neural tube to the paraxial mesoderm, while allowing the paraxial mesoderm to stabilise neural tube elongation by resisting medial bending. However, it is now important to test these predictions and fully map the flow of forces between the various axial tissues. Such experiments would hugely benefit from novel techniques that can directly quantify the biophysical properties of tissues in vivo, such as atomic force microscopy, Brillouin microscopy and magnetically controlled ferrofluid droplets (Barriga et al., 2018; Mongera et al., 2019; Raghunathan et al., 2017; Serwane et al., 2017).

One of the main impediments to the present study, and any study of cell-ECM adhesion, is the heterogeneity of functionally overlapping integrin receptors and matrix ligands, as well as the ability of such ligands to diffuse away from their original source. It is therefore likely that these factors are largely responsible for the mild nature of the phenotypes resulting from the current fibronectin gene deletions. For example, despite their otherwise extensive phenotypic and mechanistic similarities, *Grhl3*^{Cre}; *Fn1*$^{fl/fl}$ mutants exhibited spina bifida at a much lower penetrance (29%)

than the previously characterised Grhl3^{Cre}; Itgb1$^{fl/fl}$ mutants (78%). It is currently unknown whether the milder phenotype of *Grhl3*^{Cre}; *Fn1*$^{fl/fl}$ embryos is due to compensating interactions of the surface ectoderm with fibronectin originating from the paraxial mesoderm or with a different ECM ligand such as laminin (both such interactions are ablated in *Grhl3*^{Cre}*; Itgb1*$^{fl/fl}$ embryos). However, this question could theoretically be resolved through deletion of integrin α5 in the surface ectoderm (specifically ablating integrin-fibronectin interactions), a spatially broader deletion of fibronectin (encompassing the paraxial mesoderm) or compound deletion of both fibronectin and laminin.

Similarly, the tail elongation defect found in *Cdx2*^{Cre}*; Fn*$^{fl/fl}$ mutants was surprisingly mild compared to the axial truncation characterising previous fibronectin KO models. This could be attributed to the potentially critical function of the notochord and its fibronectin sheath, which has evaded the *Cdx2*^{Cre}-mediated ablation, or to compensation by alternative ECM ligands. These alternative hypotheses could therefore be tested through a spatially broader deletion of fibronectin (encompassing the notochord), and *Cdx2*^{Cre}-mediated deletion of integrin β1 (abolishing most cell-ECM interactions), respectively. Moreover, such genetic ablation studies could be complemented and informed by transcriptomic, in situ hybridisation and immunohistochemical analyses of ECM ligands and integrin subunits that would further refine our understanding of the expression domains of these proteins throughout the developing embryo.

6.1.4 Clinical relevance

The genetic causes of NTDs and congenital spine disorders remain largely unknown. Therefore, answering the questions described above will not only elucidate the developmental mechanisms in mice, but also pinpoint relevant pathogenic pathways for such conditions in humans (and hence potential targets for intervention). The open neural tube lesion observed in *Grhl3*^{Cre}; *Fn1*$^{fl/fl}$ mutant embryos closely corresponds to the condition of open spina bifida (myelomeningocele) in humans.

Interestingly, while most of the previous genetic research in spina bifida patients has focused on the folate and PCP pathways, recent studies are increasingly implicating ECM-related genes. A recent whole-exome sequencing study of 51 NTD-affected families, for example, used a candidate gene approach and detected a loss-of-function variant in ITGB1 (the human integrin β1 encoding gene) (Lemay et al., 2018). This variant was predicted to cause a premature stop codon, thus eliminating more than half of the cytoplasmic domain of the integrin β1 subunit and by extension much of its capacity to transduce signals and connect to the cytoskeleton. Consequently, heterozygosity for this variant will have presumably resulted in a 50% loss of integrin β1 function in the affected patient. Another study examined 506 myelomeningocele-affected subjects for ultra-rare deleterious variants (URDVs) in 302 candidate genes that had been previously associated with NTDs in humans or animal models (Au et al., 2021). Strikingly, nearly 15% of the subjects were found to carry URDVs in ECM-related candidate genes, including ITGB1, LAMC1 (encoding laminin subunit γ1), ITGA3 and ITGA6 (encoding the laminin-binding integrin α3 and α6 subunits).

Evidently, due to the rarity, genetic heterogeneity and oligogenic nature of NTDs (Copp & Greene, 2010), a large proportion of previous studies opted for candidate gene-based approaches that overlooked *Fn1* and genes coding for fibronectin-binding integrin subunits. Following the current demonstration of the important role of integrin-fibronectin interactions in neural fold fusion, it will therefore be interesting to see whether inclusion of these genes in future study protocols will find such interactions to be relevant in humans as well. Indeed, a recent whole-genome sequencing study attempted to tackle some of the aforementioned obstacles in an unbiased manner by comparing 149 ancestry-matched spina bifida case-control pairs for enrichment in likely gene disrupting (LGD) variants using machine learning (Aguiar-Pulido et al., 2021). Among the genes that showed significant enrichment for LGD variants were LAMC2 (encoding laminin subunit γ2), COL18A1 (encoding collagen Type XII Alpha 1 Chain) and most notably ITGA8 (encoding the fibronectin-binding integrin a8 subunit). Overall, while the exact ECM ligands and integrin subunits involved remain uncertain, the existing evidence already makes a strong case for the role of cell-ECM adhesion in the pathogenesis of spina bifida, thus

suggesting that ECM-assisted zippering of the neural folds could represent a conserved mechanism in humans.

Conversely, the abnormal axial curvature and length reduction observed in *Cdx2^{Cre}; Fn$^{fl/fl}$* (and previously characterised integrin/fibronectin) mutants resemble the human conditions of scoliosis and short stature, respectively. In this regard, recent exome-sequencing studies identified a variety of de novo *Fn1* mutations in individuals affected by a rare subtype of spondylometaphyseal dysplasia, characterised by severe scoliosis, developmental coxa vara, short stature and irregularly shaped metaphyses (Costantini et al., 2019; Lee et al., 2017). Furthermore, introduction of these disease-associated missense variants into a recombinant form of fibronectin revealed that the mutations prevented secretion of fibronectin which was instead abnormally retained in the endoplasmic reticulum and Golgi apparatus. However, the mechanism through which failure of fibronectin secretion leads to spondylometaphyseal dysplasia remains unknown. While some aspects of the phenotype (e.g., developmental coxa vara, irregularly shaped metaphyses) likely derive from fibronectin's role in bone and cartilage development (Singh & Schwarzbauer, 2014), it would be interesting to investigate whether scoliosis and short stature might relate to fibronectin's earlier function in inter-tissue adhesion during axial elongation.

6.2 The role of Sox2 in neuromesodermal progenitors and neural specification

6.2.1 Overview of findings

The current thesis has contributed to our understanding of the role of Sox2 (or lack thereof) in neuromesodermal and neural progenitors in several ways. Firstly, in situ hybridisation experiments validated the previously used *Sox2^{CreERT2}* line and the associated lineage tracing results, thereby conclusively demonstrating that *Sox2* is not expressed in NMPs, but only downstream of neural commitment (Mugele, 2018;

Mugele et al., 2018). This finding in turn indicated that the Sox2-expressing cells identified in the CNH represent recently committed neural progenitors about to migrate into the neuroepithelium. Secondly, lineage tracing of Sox2-deficient NMPs revealed that loss of *Sox2* does not affect the dynamics of NMP fate choice and further reinforced the idea that Sox2 is expressed downstream of neural commitment. Thirdly, the late-stage morphological characterisation of *Sox2* mutants presented here, in combination with previous expression studies of neural and mesodermal markers, showed that Sox2 is dispensable for neural tube formation, as well as axial elongation as a whole (Mugele, 2018; Mugele et al., 2018). Lastly, immunohistochemical and qRT-PCR analyses of *Sox2* mutants found that the closely related transcription factor Sox3 is not upregulated but is expressed in the correct regions and might therefore be able to compensate for any lost Sox2 function.

6.2.2 Impact on previous and future research

To date, research on NMPs has often focused on T/Sox2 double-positive cells. The results presented here indicate that these studies analysed neural rather than neuromesodermal progenitors, and therefore dictate a revised analysis and interpretation of their data. For example, it would be predicted that the Sox2-positive cells captured by transcriptomic studies of NMC regions would also express other neural, but not mesodermal markers (Gouti et al., 2017; Koch et al., 2017). Moreover, the newly ascertained position of Sox2 in the chronology of NMP lineage choice necessitates a different strategy for how future experiments are designed. This is especially pertinent for studies that try to overcome obstacles relating to the study of human NMPs in vivo (e.g., limited and heterogeneous cell population, ethical issues relating to human embryos) by generating NMP-like cells in vitro. Such studies start with human or mouse pluripotent stem cells and attempt to recreate the signalling environment of the endogenous NMP niche by stimulating the Wnt and Fgf signalling pathways until the cells co-express T and Sox2 (de Lemos et al., 2022; Gouti et al., 2014; Tsakiridis & Wilson, 2015; Turner et al., 2014; Verrier et al., 2018). The resulting cell populations have been shown to be capable of producing both neural

and mesodermal cells in vitro and of colonising both the neural tube and paraxial mesoderm after transplantation into mouse or chick embryos.

Interestingly, however, no study has so far demonstrated the successful generation of bipotent T/Sox2 co-expressing single cells that produce both neural and mesodermal derivatives (Wymeersch et al., 2021). Furthermore, in accordance with the findings of the present study, the T/Sox2 double-positive state has proven extremely unstable and such colonies often show an overwhelming bias towards the neural fate (Tsakiridis & Wilson, 2015; Wymeersch et al., 2021). In addition, Sox2 expression in such NMP-like cells is typically assessed based on immunoreactivity which could derive from residual Sox2 protein from stem cells. In this regard, a comparative analysis of transcriptomic data from micro-dissected mouse NMP-containing populations and in vitro derived mouse and human NMP-like cells did not find *Sox2* among the commonly enriched genes (Verrier et al., 2018). Lastly, when extrapolating findings from in vitro studies, it is important to keep in mind the important (and especially relevant in the case of NMPs) distinction between cell fate and potency (Binagui-Casas et al., 2021). It might be possible, for example, for Sox2-expressing cells to give rise to mesodermal derivatives after being functionally challenged through grafting or modification of signalling pathways, when they do not exhibit such propensities in unperturbed conditions. In this respect, heterotopically grafting axial progenitors or genetically modifying the signalling molecules they are exposed to in vivo has been shown to substantially alter their fate, thus illustrating the strong developmental plasticity of these progenitors (Martin & Kimelman, 2012; Wymeersch et al., 2016).

6.2.3 Open questions

The findings presented here also highlight a number of open questions and directions for future research in NMPs and the role of SoxB1 transcription factors in the neural lineage. Firstly, this study has emphasized the need to search for alternative markers of NMPs beyond T/Sox2 co-expression. In this regard, a recent report identified

Epha1 as a promising cell surface marker for the NMC cell population (de Lemos et al., 2022). While Epha1 does not appear to be entirely specific to NMPs, it likely represents an improvement compared to the use of T or T/Sox2 expression for NMP identification. Furthermore, it remains unknown whether NMPs have a distinct molecular signature from other cells within the NMC region and, if so, which of these factors actually determine their behaviour as NMPs; and what proportion of the total NMC cell population NMPs comprise (Binagui-Casas et al., 2021). New quantitative and spatial transcriptomic methods are likely to be invaluable tools in generating a precise spatiotemporal map of gene expression profiles in the NMC region in vivo, and hence answering these questions (Choi et al., 2018; Eng et al., 2019; Junker et al., 2014; Rodriques et al., 2019).

Secondly, the current study attempted to assess the role of Sox2 in neural tube formation. However, these analyses were likely hampered by the overlapping expression patterns and functional redundancy between Sox2 and Sox3. Therefore, the optimal future strategy to determine whether Sox3 compensated for the lack of Sox2 and decisively ascertain the role of SoxB1 transcription factors in neural tube formation would utilise a conditional double knock-out of both Sox2 and Sox3.

Lastly, while experiments performed here focus on the first steps of neural development, it is likely that loss of Sox2 would have various adverse effects on neuronal differentiation and mature function at later stages. This prediction is supported by the observation that Sox2 and Sox3 bind silenced genes in neural cells to prime them for subsequent binding by other transcription factors (e.g., Sox11) in differentiating neurons (Bergsland et al., 2011). In accordance, Sox2 hypomorphic mutant neurospheres have previously demonstrated arborization defects and an inability to differentiate into mature MAP2-positive neurons (Cavallaro et al., 2008). Furthermore, Sox2 has been shown to function in Schwann cell clustering during nerve regeneration. The current model therefore provides opportunities for the study of the role of Sox2 in posterior neural differentiation and mature function. Moreover, as Sox3 has been documented to compensate for Sox2 later in development as well, such studies might also benefit from the *Sox2/Sox3* double knock-out proposed above (Miyagi et al., 2008; Taranova et al., 2006).

6.2.4 Clinical relevance

Resolving the key questions described above will undoubtedly also provide insights with clinical relevance. As NMPs give rise to neural and mesodermal tissues along most of the AP axis, they are likely to be at the root of a spectrum of congenital human malformations of the lower body, ranging from NTDs to axial truncations (e.g., caudal regression syndrome, CRS) (Copp et al., 2015; Warner et al., 2020). While this hypothesis has not been directly investigated yet, it is strongly supported by the genes and pathways that have been implicated in both human and animal studies of these developmental defects. Genetic association studies, for example, have identified mutations in *TBXT* (corresponding to *T* in mice) – a gene with an integral role in NMP maintenance and differentiation – in patients and families affected by spina bifida (Agopian et al., 2013; Carter et al., 2011; Jensen et al., 2004), sacral agenesis (Postma et al., 2014) and vertebral malformations (Ghebranious et al., 2008). These conditions are highly comparable to the axial truncation and skeletal defects observed in mouse *T* mutants (Herrmann et al., 1990; Pennimpede et al., 2012). The other major component implicated in these conditions is RA which is normally secreted by the caudal somites and antagonises Wnt signalling and T to promote the neural specification of NMPs (Gouti et al., 2017; Shum et al., 1999). In this regard, mouse embryos subjected to excess RA (or its mimetic etretinate), through maternal administration or null mutation of the RA-catabolizing enzyme Cyp26a1, exhibit axial truncation accompanied by spina bifida or a large caudal mass of neural tissue (Abu-Abed et al., 2001; Liu et al., 2003; Padmanabhan, 1998); similar to that observed in *T* mutants (Schmidt et al., 1997). Interestingly, CYP26A1 polymorphisms associated with impaired RA catabolism have been also implicated in CRS patients (De Marco et al., 2006; Lee et al., 2007; Warner et al., 2020). Therefore, as illustrated by these examples, an improved understanding of the cellular and molecular mechanisms that govern NMP function and axial elongation will be instrumental in the development of preventative interventions for conditions such as spina bifida and CRS, which, to this date, remain only partially treatable.

7. Bibliography

Abdul-Aziz, N. M., Turmaine, M., Greene, N. D. E., & Copp, A. J. (2009). EphrinA-EphA receptor interactions in mouse spinal neurulation: Implications for neural fold fusion. *The International Journal of Developmental Biology*, *53*(4), 559–568. https://doi.org/10.1387/ijdb.082777na

Abu-Abed, S., Dollé, P., Metzger, D., Beckett, B., Chambon, P., & Petkovich, M. (2001). The retinoic acid-metabolizing enzyme, CYP26A1, is essential for normal hindbrain patterning, vertebral identity, and development of posterior structures. *Genes & Development*, *15*(2), 226–240. https://doi.org/10.1101/gad.855001

Adikusuma, F., Pederick, D., McAninch, D., Hughes, J., & Thomas, P. (2017). Functional Equivalence of the SOX2 and SOX3 Transcription Factors in the Developing Mouse Brain and Testes. *Genetics*, *206*(3), 1495–1503. https://doi.org/10.1534/genetics.117.202549

Agopian, A. j., Bhalla, A. D., Boerwinkle, E., Finnell, R. H., Grove, M. L., Hixson, J. E., Shimmin, L. C., Sewda, A., Stuart, C., Zhong, Y., Zhu, H., & Mitchell, L. E. (2013). Exon sequencing of PAX3 and T (brachyury) in cases with spina bifida. *Birth Defects Research Part A: Clinical and Molecular Teratology*, *97*(9), 597–601. https://doi.org/10.1002/bdra.23163

Aguiar-Pulido, V., Wolujewicz, P., Martinez-Fundichely, A., Elhaik, E., Thareja, G., Abdel Aleem, A., Chalhoub, N., Cuykendall, T., Al-Zamer, J., Lei, Y., El-Bashir, H., Musser, J. M., Al-Kaabi, A., Shaw, G. M., Khurana, E., Suhre, K., Mason, C. E., Elemento, O., Finnell, R. H., & Ross, M. E. (2021). Systems biology analysis of human genomes points to key pathways conferring spina bifida risk. *Proceedings of the National Academy of Sciences*, *118*(51), e2106844118. https://doi.org/10.1073/pnas.2106844118

Alberts, B. (2015). *Molecular biology of the cell* (Sixth edition). Garland Science, Taylor and Francis Group.

Almeida, P. G. de, Pinheiro, G. G., Nunes, A. M., Gonçalves, A. B., & Thorsteinsdóttir, S. (2016). Fibronectin assembly during early embryo development: A versatile communication system between cells and tissues. *Developmental Dynamics*, *245*(4), 520–535. https://doi.org/10.1002/dvdy.24391

Alvarez, I. S., & Schoenwolf, G. C. (1992). Expansion of surface epithelium provides the major extrinsic force for bending of the neural plate. *The Journal of Experimental Zoology*, *261*(3), 340–348. https://doi.org/10.1002/jez.1402610313

Anderson, M. J., Naiche, L. A., Wilson, C. P., Elder, C., Swing, D. A., & Lewandoski, M. (2013). TCreERT2, a Transgenic Mouse Line for Temporal Control of Cre-Mediated

Recombination in Lineages Emerging from the Primitive Streak or Tail Bud. *PLOS ONE*, *8*(4), e62479. https://doi.org/10.1371/journal.pone.0062479

Andoniadou, C. L., Matsushima, D., Mousavy Gharavy, S. N., Signore, M., Mackintosh, A. I., Schaeffer, M., Gaston-Massuet, C., Mollard, P., Jacques, T. S., Le Tissier, P., Dattani, M. T., Pevny, L. H., & Martinez-Barbera, J. P. (2013). Sox2+ Stem/Progenitor Cells in the Adult Mouse Pituitary Support Organ Homeostasis and Have Tumor-Inducing Potential. *Cell Stem Cell*, *13*(4), 433–445. https://doi.org/10.1016/j.stem.2013.07.004

Araya, C., Ward, L. C., Girdler, G. C., & Miranda, M. (2016). Coordinating cell and tissue behavior during zebrafish neural tube morphogenesis. *Developmental Dynamics*, *245*(3), 197–208. https://doi.org/10.1002/dvdy.24304

Au, K. S., Hebert, L., Hillman, P., Baker, C., Brown, M. R., Kim, D.-K., Soldano, K., Garrett, M., Ashley-Koch, A., Lee, S., Gleeson, J., Hixson, J. E., Morrison, A. C., & Northrup, H. (2021). Human myelomeningocele risk and ultra-rare deleterious variants in genes associated with cilium, WNT-signaling, ECM, cytoskeleton and cell migration. *Scientific Reports*, *11*(1), Article 1. https://doi.org/10.1038/s41598-021-83058-7

Auden, A., Caddy, J., Wilanowski, T., Ting, S. B., Cunningham, J. M., & Jane, S. M. (2006). Spatial and temporal expression of the Grainyhead-like transcription factor family during murine development. *Gene Expression Patterns*, *6*(8), 964–970. https://doi.org/10.1016/j.modgep.2006.03.011

Avilion, A. A., Nicolis, S. K., Pevny, L. H., Perez, L., Vivian, N., & Lovell-Badge, R. (2003). Multipotent cell lineages in early mouse development depend on SOX2 function. *Genes & Development*, *17*(1), 126–140. https://doi.org/10.1101/gad.224503

Bader, B. L., Rayburn, H., Crowley, D., & Hynes, R. O. (1998). Extensive Vasculogenesis, Angiogenesis, and Organogenesis Precede Lethality in Mice Lacking All αv Integrins. *Cell*, *95*(4), 507–519. https://doi.org/10.1016/S0092-8674(00)81618-9

Balmer, S., Nowotschin, S., & Hadjantonakis, A.-K. (2016). Notochord morphogenesis in mice: Current understanding & open questions. *Developmental Dynamics*, *245*(5), 547–557. https://doi.org/10.1002/dvdy.24392

Bardot, E. S., & Hadjantonakis, A.-K. (2020). Mouse gastrulation: Coordination of tissue patterning, specification and diversification of cell fate. *Mechanisms of Development*, *163*, 103617. https://doi.org/10.1016/j.mod.2020.103617

Barriga, E. H., Franze, K., Charras, G., & Mayor, R. (2018). Tissue stiffening coordinates morphogenesis by triggering collective cell migration in vivo. *Nature*, *554*(7693), Article 7693. https://doi.org/10.1038/nature25742

Barrios, A., Poole, R. J., Durbin, L., Brennan, C., Holder, N., & Wilson, S. W. (2003). Eph/Ephrin Signaling Regulates the Mesenchymal-to-Epithelial Transition of the Paraxial

Mesoderm during Somite Morphogenesis. *Current Biology*, *13*(18), 1571–1582. https://doi.org/10.1016/j.cub.2003.08.030

Bénazéraf, B. (2019). Dynamics and mechanisms of posterior axis elongation in the vertebrate embryo. *Cellular and Molecular Life Sciences*, *76*(1), 89–98. https://doi.org/10.1007/s00018-018-2927-4

Bénazéraf, B., Beaupeux, M., Tchernookov, M., Wallingford, A., Salisbury, T., Shirtz, A., Shirtz, A., Huss, D., Pourquié, O., François, P., & Lansford, R. (2017). Multi-scale quantification of tissue behavior during amniote embryo axis elongation. *Development*, *144*(23), 4462–4472. https://doi.org/10.1242/dev.150557

Bénazéraf, B., Francois, P., Baker, R. E., Denans, N., Little, C. D., & Pourquié, O. (2010). A random cell motility gradient downstream of FGF controls elongation of an amniote embryo. *Nature*, *466*(7303), 248–252. https://doi.org/10.1038/nature09151

Bénazéraf, B., & Pourquié, O. (2013). Formation and Segmentation of the Vertebrate Body Axis. *Annual Review of Cell and Developmental Biology*, *29*(1), 1–26. https://doi.org/10.1146/annurev-cellbio-101011-155703

Bengtsson, T., Aszodi, A., Nicolae, C., Hunziker, E. B., Lundgren-Akerlund, E., & Fässler, R. (2005). Loss of alpha10beta1 integrin expression leads to moderate dysfunction of growth plate chondrocytes. *Journal of Cell Science*, *118*(Pt 5), 929–936. https://doi.org/10.1242/jcs.01678

Benito-Jardón, M., Strohmeyer, N., Ortega-Sanchís, S., Bharadwaj, M., Moser, M., Müller, D. J., Fässler, R., & Costell, M. (2020). Av-Class integrin binding to fibronectin is solely mediated by RGD and unaffected by an RGE mutation. *Journal of Cell Biology*, *219*(12). https://doi.org/10.1083/jcb.202004198

Bergsland, M., Ramsköld, D., Zaouter, C., Klum, S., Sandberg, R., & Muhr, J. (2011). Sequentially acting Sox transcription factors in neural lineage development. *Genes & Development*, *25*(23), 2453–2464. https://doi.org/10.1101/gad.176008.111

Bertet, C., Sulak, L., & Lecuit, T. (2004). Myosin-dependent junction remodelling controls planar cell intercalation and axis elongation. *Nature*, *429*(6992), 667–671. https://doi.org/10.1038/nature02590

Binagui-Casas, A., Dias, A., Guillot, C., Metzis, V., & Saunders, D. (2021). Building consensus in neuromesodermal research: Current advances and future biomedical perspectives. *Current Opinion in Cell Biology*, *73*, 133–140. https://doi.org/10.1016/j.ceb.2021.08.003

Bonnerot, C., & Nicolas, J. F. (1993). Clonal analysis in the intact mouse embryo by intragenic homologous recombination. *Comptes Rendus de l'Academie Des Sciences. Serie III, Sciences de La Vie*, *316*(10), 1207–1217.

Brook, F. A., Shum, A. S., Van Straaten, H. W., & Copp, A. J. (1991). Curvature of the caudal region is responsible for failure of neural tube closure in the curly tail (ct) mouse embryo. *Development*, *113*(2), 671–678. https://doi.org/10.1242/dev.113.2.671

Bulusu, V., Prior, N., Snaebjornsson, M. T., Kuehne, A., Sonnen, K. F., Kress, J., Stein, F., Schultz, C., Sauer, U., & Aulehla, A. (2017). Spatiotemporal Analysis of a Glycolytic Activity Gradient Linked to Mouse Embryo Mesoderm Development. *Developmental Cell*, *40*(4), 331-341.e4. https://doi.org/10.1016/j.devcel.2017.01.015

Burute, M., & Thery, M. (2012). Spatial segregation between cell–cell and cell–matrix adhesions. *Current Opinion in Cell Biology*, *24*(5), 628–636. https://doi.org/10.1016/j.ceb.2012.07.003

Butler, M. B., Short, N. E., Maniou, E., Alexandre, P., Greene, N. D. E., Copp, A. J., & Galea, G. L. (2019). Rho kinase-dependent apical constriction counteracts M-phase apical expansion to enable mouse neural tube closure. *Journal of Cell Science*, *132*(13). https://doi.org/10.1242/jcs.230300

Bylund, M., Andersson, E., Novitch, B. G., & Muhr, J. (2003). Vertebrate neurogenesis is counteracted by Sox1–3 activity. *Nature Neuroscience*, *6*(11), Article 11. https://doi.org/10.1038/nn1131

Cambray, N., & Wilson, V. (2002). Axial progenitors with extensive potency are localised to the mouse chordoneural hinge. *Development*, *129*(20), 4855–4866.

Cambray, N., & Wilson, V. (2007). Two distinct sources for a population of maturing axial progenitors. *Development*, *134*(15), 2829–2840. https://doi.org/10.1242/dev.02877

Camerer, E., Barker, A., Duong, D. N., Ganesan, R., Kataoka, H., Cornelissen, I., Darragh, M. R., Hussain, A., Zheng, Y.-W., Srinivasan, Y., Brown, C., Xu, S.-M., Regard, J. B., Lin, C.-Y., Craik, C. S., Kirchhofer, D., & Coughlin, S. R. (2010). Local Protease Signaling Contributes to Neural Tube Closure in the Mouse Embryo. *Developmental Cell*, *18*(1), 25. https://doi.org/10.1016/j.devcel.2009.11.014

Carter, T. C., Pangilinan, F., Troendle, J. F., Molloy, A. M., VanderMeer, J., Mitchell, A., Kirke, P. N., Conley, M. R., Shane, B., Scott, J. M., Brody, L. C., & Mills, J. L. (2011). Evaluation of 64 candidate single nucleotide polymorphisms as risk factors for neural tube defects in a large Irish study population. *American Journal of Medical Genetics Part A*, *155*(1), 14–21. https://doi.org/10.1002/ajmg.a.33755

Cavallaro, M., Mariani, J., Lancini, C., Latorre, E., Caccia, R., Gullo, F., Valotta, M., DeBiasi, S., Spinardi, L., Ronchi, A., Wanke, E., Brunelli, S., Favaro, R., Ottolenghi, S., & Nicolis, S. K. (2008). Impaired generation of mature neurons by neural stem cells from hypomorphic Sox2 mutants. *Development*, *135*(3), 541–557. https://doi.org/10.1242/dev.010801

Cervantes, S., Yamaguchi, T. P., & Hebrok, M. (2009). Wnt5a is essential for intestinal elongation in mice. *Developmental Biology*, *326*(2), 285–294. https://doi.org/10.1016/j.ydbio.2008.11.020

Chalamalasetty, R. B., Garriock, R. J., Dunty, W. C., Kennedy, M. W., Jailwala, P., Si, H., & Yamaguchi, T. P. (2014). Mesogenin 1 is a master regulator of paraxial presomitic mesoderm differentiation. *Development*, *141*(22), 4285–4297. https://doi.org/10.1242/dev.110908

Chamberlain, C. E., Jeong, J., Guo, C., Allen, B. L., & McMahon, A. P. (2008). Notochord-derived Shh concentrates in close association with the apically positioned basal body in neural target cells and forms a dynamic gradient during neural patterning. *Development*, *135*(6), 1097–1106. https://doi.org/10.1242/dev.013086

Chang, L., Azzolin, L., Di Biagio, D., Zanconato, F., Battilana, G., Lucon Xiccato, R., Aragona, M., Giulitti, S., Panciera, T., Gandin, A., Sigismondo, G., Krijgsveld, J., Fassan, M., Brusatin, G., Cordenonsi, M., & Piccolo, S. (2018). The SWI/SNF complex is a mechanoregulated inhibitor of YAP and TAZ. *Nature*, *563*(7730), 265–269. https://doi.org/10.1038/s41586-018-0658-1

Chen, Z. F., & Behringer, R. R. (1995). Twist is required in head mesenchyme for cranial neural tube morphogenesis. *Genes & Development*, *9*(6), 686–699. https://doi.org/10.1101/gad.9.6.686

Chiarugi, P., & Giannoni, E. (2008). Anoikis: A necessary death program for anchorage-dependent cells. *Biochemical Pharmacology*, *76*(11), 1352–1364. https://doi.org/10.1016/j.bcp.2008.07.023

Choi, H. M. T., Schwarzkopf, M., Fornace, M. E., Acharya, A., Artavanis, G., Stegmaier, J., Cunha, A., & Pierce, N. A. (2018). Third-generation in situ hybridization chain reaction: Multiplexed, quantitative, sensitive, versatile, robust. *Development*, *145*(12), dev165753. https://doi.org/10.1242/dev.165753

Ciruna, B. G., Schwartz, L., Harpal, K., Yamaguchi, T. P., & Rossant, J. (1997). Chimeric analysis of fibroblast growth factor receptor-1 (Fgfr1) function: A role for FGFR1 in morphogenetic movement through the primitive streak. *Development*, *124*(14), 2829–2841. https://doi.org/10.1242/dev.124.14.2829

Collignon, J., Sockanathan, S., Hacker, A., Cohen-Tannoudji, M., Norris, D., Rastan, S., Stevanovic, M., Goodfellow, P. N., & Lovell-Badge, R. (1996). A comparison of the properties of Sox-3 with Sry and two related genes, Sox-1 and Sox-2. *Development*, *122*(2), 509–520.

Conlon, F. L., Lyons, K. M., Takaesu, N., Barth, K. S., Kispert, A., Herrmann, B., & Robertson, E. J. (1994). A primary requirement for nodal in the formation and maintenance of the primitive streak in the mouse. *Development (Cambridge, England)*, *120*(7), 1919–1928.

Copp, A. J. (1985). Relationship between timing of posterior neuropore closure and development of spinal neural tube defects in mutant (curly tail) and normal mouse embryos in culture. *Journal of Embryology and Experimental Morphology*, *88*, 39–54.

Copp, A. J., Adzick, N. S., Chitty, L. S., Fletcher, J. M., Holmbeck, G. N., & Shaw, G. M. (2015). Spina bifida. *Nature Reviews Disease Primers*, *1*(1), Article 1. https://doi.org/10.1038/nrdp.2015.7

Copp, A. J., Brook, F. A., & Roberts, H. J. (1988). A cell-type-specific abnormality of cell proliferation in mutant (curly tail) mouse embryos developing spinal neural tube defects. *Development*, *104*(2), 285–295. https://doi.org/10.1242/dev.104.2.285

Copp, A. J., & Greene, N. D. (2010). Genetics and development of neural tube defects. *The Journal of Pathology*, *220*(2), 217–230. https://doi.org/10.1002/path.2643

Copp, A. J., Greene, N. D. E., & Murdoch, J. N. (2003). The genetic basis of mammalian neurulation. *Nature Reviews Genetics*, *4*(10), 784–793. https://doi.org/10.1038/nrg1181

Copp, A. J., Stanier, P., & Greene, N. D. (2013). Neural tube defects: Recent advances, unsolved questions, and controversies. *The Lancet Neurology*, *12*(8), 799–810. https://doi.org/10.1016/S1474-4422(13)70110-8

Corallo, D., Trapani, V., & Bonaldo, P. (2015). The notochord: Structure and functions. *Cellular and Molecular Life Sciences*, *72*(16), 2989–3008. https://doi.org/10.1007/s00018-015-1897-z

Costantini, A., Valta, H., Baratang, N. V., Yap, P., Bertola, D. R., Yamamoto, G. L., Kim, C. A., Chen, J., Wierenga, K. J., Fanning, E. A., Escobar, L., McWalter, K., McLaughlin, H., Willaert, R., Begtrup, A., Alm, J. J., Reinhardt, D. P., Mäkitie, O., & Campeau, P. M. (2019). Novel fibronectin mutations and expansion of the phenotype in spondylometaphyseal dysplasia with “corner fractures”. *Bone*, *121*, 163–171. https://doi.org/10.1016/j.bone.2018.12.020

Czirók, A., Rongish, B. J., & Little, C. D. (2004). Extracellular matrix dynamics during vertebrate axis formation. *Developmental Biology*, *268*(1), 111–122. https://doi.org/10.1016/j.ydbio.2003.09.040

Danen, E. H. J., Sonneveld, P., Brakebusch, C., Fässler, R., & Sonnenberg, A. (2002). The fibronectin-binding integrins α5β1 and αvβ3 differentially modulate RhoA–GTP loading, organization of cell matrix adhesions, and fibronectin fibrillogenesis. *Journal of Cell Biology*, *159*(6), 1071–1086. https://doi.org/10.1083/jcb.200205014

Danielian, P. S., Muccino, D., Rowitch, D. H., Michael, S. K., & McMahon, A. P. (1998). Modification of gene activity in mouse embryos in utero by a tamoxifen-inducible form of Cre recombinase. *Current Biology*, *8*(24), S1–S2. https://doi.org/10.1016/S0960-9822(07)00562-3

Davidson, B. P., Kinder, S. J., Steiner, K., Schoenwolf, G. C., & Tam, P. P. L. (1999). Impact of Node Ablation on the Morphogenesis of the Body Axis and the Lateral Asymmetry of the Mouse Embryo during Early Organogenesis. *Developmental Biology*, *211*(1), 11–26. https://doi.org/10.1006/dbio.1999.9276

De Arcangelis, A., Mark, M., Kreidberg, J., Sorokin, L., & Georges-Labouesse, E. (1999). Synergistic activities of alpha3 and alpha6 integrins are required during apical ectodermal ridge formation and organogenesis in the mouse. *Development*, *126*(17), 3957–3968. https://doi.org/10.1242/dev.126.17.3957

De Castro, S. C. P., Gustavsson, P., Marshall, A. R., Gordon, W. M., Galea, G., Nikolopoulou, E., Savery, D., Rolo, A., Stanier, P., Andersen, B., Copp, A. J., & Greene, N. D. E. (2018b). Overexpression of Grainyhead-like 3 causes spina bifida and interacts genetically with mutant alleles of Grhl2 and Vangl2 in mice. *Human Molecular Genetics*. https://doi.org/10.1093/hmg/ddy313

De Castro, S. C. P., Hirst, C. S., Savery, D., Rolo, A., Lickert, H., Andersen, B., Copp, A. J., & Greene, N. D. E. (2018a). Neural tube closure depends on expression of Grainyhead-like 3 in multiple tissues. *Developmental Biology*, *435*(2), 130–137. https://doi.org/10.1016/j.ydbio.2018.01.016

de Lemos, L., Dias, A., Nóvoa, A., & Mallo, M. (2022). Epha1 is a cell-surface marker for the neuromesodermal competent population. *Development*, *149*(6), dev198812. https://doi.org/10.1242/dev.198812

De Marco, P., Merello, E., Mascelli, S., Raso, A., Santamaria, A., Ottaviano, C., Calevo, M. G., Cama, A., & Capra, V. (2006). Mutational screening of the CYP26A1 gene in patients with caudal regression syndrome. *Birth Defects Research Part A: Clinical and Molecular Teratology*, *76*(2), 86–95. https://doi.org/10.1002/bdra.20225

Del Rio, A., Perez-Jimenez, R., Liu, R., Roca-Cusachs, P., Fernandez, J. M., & Sheetz, M. P. (2009). Stretching single talin rod molecules activates vinculin binding. *Science (New York, N.Y.)*, *323*(5914), 638–641. https://doi.org/10.1126/science.1162912

Diez del Corral, R., & Storey, K. G. (2004). Opposing FGF and retinoid pathways: A signalling switch that controls differentiation and patterning onset in the extending vertebrate body axis. *BioEssays*, *26*(8), 857–869. https://doi.org/10.1002/bies.20080

Dray, N., Lawton, A., Nandi, A., Jülich, D., Emonet, T., & Holley, S. A. (2013). Cell-Fibronectin Interactions Propel Vertebrate Trunk Elongation via Tissue Mechanics. *Current Biology*, *23*(14), 1335–1341. https://doi.org/10.1016/j.cub.2013.05.052

Dubrulle, J., McGrew, M. J., & Pourquié, O. (2001). FGF Signaling Controls Somite Boundary Position and Regulates Segmentation Clock Control of Spatiotemporal Hox Gene Activation. *Cell*, *106*(2), 219–232. https://doi.org/10.1016/S0092-8674(01)00437-8

Dymecki, S. M., & Kim, J. C. (2007). Molecular Neuroanatomy's 'Three Gs': A Primer. *Neuron*, *54*(1), 17–34. https://doi.org/10.1016/j.neuron.2007.03.009

Echelard, Y., Epstein, D. J., St-Jacques, B., Shen, L., Mohler, J., McMahon, J. A., & McMahon, A. P. (1993). Sonic hedgehog, a member of a family of putative signaling molecules, is implicated in the regulation of CNS polarity. *Cell*, *75*(7), 1417–1430. https://doi.org/10.1016/0092-8674(93)90627-3

Ellis, K., Bagwell, J., & Bagnat, M. (2013). Notochord vacuoles are lysosome-related organelles that function in axis and spine morphogenesis. *Journal of Cell Biology*, *200*(5), 667–679. https://doi.org/10.1083/jcb.201212095

Elosegui-Artola, A., Andreu, I., Beedle, A. E. M., Lezamiz, A., Uroz, M., Kosmalska, A. J., Oria, R., Kechagia, J. Z., Rico-Lastres, P., Le Roux, A.-L., Shanahan, C. M., Trepat, X., Navajas, D., Garcia-Manyes, S., & Roca-Cusachs, P. (2017). Force Triggers YAP Nuclear Entry by Regulating Transport across Nuclear Pores. *Cell*, *171*(6), 1397-1410.e14. https://doi.org/10.1016/j.cell.2017.10.008

Eng, C.-H. L., Lawson, M., Zhu, Q., Dries, R., Koulena, N., Takei, Y., Yun, J., Cronin, C., Karp, C., Yuan, G.-C., & Cai, L. (2019). Transcriptome-scale super-resolved imaging in tissues by RNA seqFISH+. *Nature*, *568*(7751), Article 7751. https://doi.org/10.1038/s41586-019-1049-y

Escuin, S., Vernay, B., Savery, D., Gurniak, C. B., Witke, W., Greene, N. D. E., & Copp, A. J. (2015). Rho-kinase-dependent actin turnover and actomyosin disassembly are necessary for mouse spinal neural tube closure. *Journal of Cell Science*, *128*(14), 2468–2481. https://doi.org/10.1242/jcs.164574

Fässler, R., & Meyer, M. (1995). Consequences of lack of beta 1 integrin gene expression in mice. *Genes & Development*, *9*(15), 1896–1908. https://doi.org/10.1101/gad.9.15.1896

Feil, S., Valtcheva, N., & Feil, R. (2009). Inducible Cre Mice. In W. Wurst & R. Kühn (Eds.), *Gene Knockout Protocols: Second Edition* (pp. 343–363). Humana Press. https://doi.org/10.1007/978-1-59745-471-1_18

Franklin, V., Khoo, P. L., Bildsoe, H., Wong, N., Lewis, S., & Tam, P. P. L. (2008). Regionalisation of the endoderm progenitors and morphogenesis of the gut portals of the mouse embryo. *Mechanisms of Development*, *125*(7), 587–600. https://doi.org/10.1016/j.mod.2008.04.001

Frisch, S., & Francis, H. (1994). Disruption of epithelial cell-matrix interactions induces apoptosis. *Journal of Cell Biology*, *124*(4), 619–626. https://doi.org/10.1083/jcb.124.4.619

Füchtbauer, E. M. (1995). Expression of M-twist during postimplantation development of the mouse. *Developmental Dynamics: An Official Publication of the American Association of Anatomists*, *204*(3), 316–322. https://doi.org/10.1002/aja.1002040309

Fukuda, K., Gupta, S., Chen, K., Wu, C., & Qin, J. (2009). The pseudoactive site of ILK is essential for its binding to alpha-Parvin and localization to focal adhesions. *Molecular Cell*, *36*(5), 819–830. https://doi.org/10.1016/j.molcel.2009.11.028

Futaki, S., Nakano, I., Kawasaki, M., Sanzen, N., & Sekiguchi, K. (2019). Molecular profiling of the basement membrane of pluripotent epiblast cells in post-implantation stage mouse embryos. *Regenerative Therapy*, *12*, 55–65. https://doi.org/10.1016/j.reth.2019.04.010

Galea, G. L., Cho, Y.-J., Galea, G., Molè, M. A., Rolo, A., Savery, D., Moulding, D., Culshaw, L. H., Nikolopoulou, E., Greene, N. D. E., & Copp, A. J. (2017). Biomechanical coupling facilitates spinal neural tube closure in mouse embryos. *Proceedings of the National Academy of Sciences*, *114*(26), E5177–E5186. https://doi.org/10.1073/pnas.1700934114

Galea, G. L., Maniou, E., Edwards, T. J., Marshall, A. R., Ampartzidis, I., Greene, N. D. E., & Copp, A. J. (2021). Cell non-autonomy amplifies disruption of neurulation by mosaic Vangl2 deletion in mice. *Nature Communications*, *12*(1), 1159. https://doi.org/10.1038/s41467-021-21372-4

Galea, G. L., Nychyk, O., Mole, M. A., Moulding, D., Savery, D., Nikolopoulou, E., Henderson, D. J., Greene, N. D. E., & Copp, A. J. (2018). Vangl2 disruption alters the biomechanics of late spinal neurulation leading to spina bifida in mouse embryos. *Disease Models & Mechanisms*, *11*(3). https://doi.org/10.1242/dmm.032219

Garriock, R. J., Chalamalasetty, R. B., Kennedy, M. W., Canizales, L. C., Lewandoski, M., & Yamaguchi, T. P. (2015). Lineage tracing of neuromesodermal progenitors reveals novel Wnt-dependent roles in trunk progenitor cell maintenance and differentiation. *Development*, *142*(9), 1628–1638. https://doi.org/10.1242/dev.111922

Geelen, J. A., & Langman, J. (1977). Closure of the neural tube in the cephalic region of the mouse embryo. *The Anatomical Record*, *189*(4), 625–640. https://doi.org/10.1002/ar.1091890407

Geelen, J. A., & Langman, J. (1979). Ultrastructural observations on closure of the neural tube in the mouse. *Anatomy and Embryology*, *156*(1), 73–88. https://doi.org/10.1007/BF00315716

George, E. L., Baldwin, H. S., & Hynes, R. O. (1997). Fibronectins Are Essential for Heart and Blood Vessel Morphogenesis But Are Dispensable for Initial Specification of Precursor Cells. *Blood*, *90*(8), 3073–3081. https://doi.org/10.1182/blood.V90.8.3073

George, E. L., Georges-Labouesse, E. N., Patel-King, R. S., Rayburn, H., & Hynes, R. O. (1993). Defects in mesoderm, neural tube and vascular development in mouse embryos lacking fibronectin. *Development*, *119*(4), 1079–1091.

Georges-Labouesse, E. N., George, E. L., Rayburn, H., & Hynes, R. O. (1996). Mesodermal development in mouse embryos mutant for fibronectin. *Developmental Dynamics*, *207*(2), 145–156. https://doi.org/10.1002/(SICI)1097-0177(199610)207:2<145::AID-AJA3>3.0.CO;2-H

Ghebranious, N., Blank, R. D., Raggio, C. L., Staubli, J., McPherson, E., Ivacic, L., Rasmussen, K., Jacobsen, F. S., Faciszewski, T., Burmester, J. K., Pauli, R. M., Boachie-Adjei, O., Glurich, I., & Giampietro, P. F. (2008). A Missense T(Brachyury) Mutation Contributes to Vertebral Malformations. *Journal of Bone and Mineral Research*, *23*(10), 1576–1583. https://doi.org/10.1359/jbmr.080503

Girós, A., Grgur, K., Gossler, A., & Costell, M. (2011). A5β1 Integrin-Mediated Adhesion to Fibronectin Is Required for Axis Elongation and Somitogenesis in Mice. *PLOS ONE*, *6*(7), e22002. https://doi.org/10.1371/journal.pone.0022002

Goh, K. L., Yang, J. T., & Hynes, R. O. (1997). Mesodermal defects and cranial neural crest apoptosis in alpha5 integrin-null embryos. *Development*, *124*(21), 4309–4319. https://doi.org/10.1242/dev.124.21.4309

Gómez-López, S., Wiskow, O., Favaro, R., Nicolis, S. K., Price, D. J., Pollard, S. M., & Smith, A. (2011). Sox2 and Pax6 maintain the proliferative and developmental potential of gliogenic neural stem cells In vitro. *Glia*, *59*(11), 1588–1599. https://doi.org/10.1002/glia.21201

Goult, B. T., Yan, J., & Schwartz, M. A. (2018). Talin as a mechanosensitive signaling hub. *Journal of Cell Biology*, *217*(11), 3776–3784. https://doi.org/10.1083/jcb.201808061

Gouti, M., Delile, J., Stamataki, D., Wymeersch, F. J., Huang, Y., Kleinjung, J., Wilson, V., & Briscoe, J. (2017). A Gene Regulatory Network Balances Neural and Mesoderm Specification during Vertebrate Trunk Development. *Developmental Cell*, *41*(3), 243-261.e7. https://doi.org/10.1016/j.devcel.2017.04.002

Gouti, M., Tsakiridis, A., Wymeersch, F. J., Huang, Y., Kleinjung, J., Wilson, V., & Briscoe, J. (2014). In Vitro Generation of Neuromesodermal Progenitors Reveals Distinct Roles for Wnt Signalling in the Specification of Spinal Cord and Paraxial Mesoderm Identity. *PLOS Biology*, *12*(8), e1001937. https://doi.org/10.1371/journal.pbio.1001937

Graham, V., Khudyakov, J., Ellis, P., & Pevny, L. (2003). SOX2 Functions to Maintain Neural Progenitor Identity. *Neuron*, *39*(5), 749–765. https://doi.org/10.1016/S0896-6273(03)00497-5

Greene, N. D. E., Gerrelli, D., Van Straaten, H. W. M., & Copp, A. J. (1998). Abnormalities of floor plate, notochord and somite differentiation in the loop-tail (Lp) mouse: A model

of severe neural tube defects. *Mechanisms of Development*, *73*(1), 59–72. https://doi.org/10.1016/S0925-4773(98)00029-X

Greene, N. D. E., Stanier, P., & Copp, A. J. (2009). Genetics of human neural tube defects. *Human Molecular Genetics*, *18*(R2), R113–R129. https://doi.org/10.1093/hmg/ddp347

Guillon, E., Das, D., Jülich, D., Hassan, A.-R., Geller, H., & Holley, S. (2020). Fibronectin is a smart adhesive that both influences and responds to the mechanics of early spinal column development. *ELife*, *9*, e48964. https://doi.org/10.7554/eLife.48964

Guillot, C., Djeffal, Y., Michaut, A., Rabe, B., & Pourquié, O. (2021). Dynamics of primitive streak regression controls the fate of neuromesodermal progenitors in the chicken embryo. *ELife*, *10*, e64819. https://doi.org/10.7554/eLife.64819

Guo, S. S., Au, T. Y. K., Wynn, S., Aszodi, A., Chan, D., Fässler, R., & Cheah, K. S. E. (2020). B1 Integrin regulates convergent extension in mouse notogenesis, ensures notochord integrity and the morphogenesis of vertebrae and intervertebral discs. *Development*, *147*(22). https://doi.org/10.1242/dev.192724

Gustavsson, P., Greene, N. D. E., Lad, D., Pauws, E., de Castro, S. C. P., Stanier, P., & Copp, A. J. (2007). Increased expression of Grainyhead-like-3 rescues spina bifida in a folate-resistant mouse model. *Human Molecular Genetics*, *16*(21), 2640–2646. https://doi.org/10.1093/hmg/ddm221

Halfter, W., Oertle, P., Monnier, C. A., Camenzind, L., Reyes-Lua, M., Hu, H., Candiello, J., Labilloy, A., Balasubramani, M., Henrich, P. B., & Plodinec, M. (2015). New concepts in basement membrane biology. *The FEBS Journal*, *282*(23), 4466–4479. https://doi.org/10.1111/febs.13495

Harburger, D. S., & Calderwood, D. A. (2009). Integrin signalling at a glance. *Journal of Cell Science*, *122*(2), 159–163. https://doi.org/10.1242/jcs.018093

Harland, R. (2000). Neural induction. *Current Opinion in Genetics & Development*, *10*(4), 357–362. https://doi.org/10.1016/S0959-437X(00)00096-4

Hayashi, S., & McMahon, A. P. (2002). Efficient Recombination in Diverse Tissues by a Tamoxifen-Inducible Form of Cre: A Tool for Temporally Regulated Gene Activation/Inactivation in the Mouse. *Developmental Biology*, *244*(2), 305–318. https://doi.org/10.1006/dbio.2002.0597

Heller, E., Kumar, K. V., Grill, S. W., & Fuchs, E. (2014). Forces Generated by Cell Intercalation Tow Epidermal Sheets in Mammalian Tissue Morphogenesis. *Developmental Cell*, *28*(6), 617–632. https://doi.org/10.1016/j.devcel.2014.02.011

Henrique, D., Abranches, E., Verrier, L., & Storey, K. G. (2015). Neuromesodermal progenitors and the making of the spinal cord. *Development*, *142*(17), 2864–2875. https://doi.org/10.1242/dev.119768

Herrmann, B. G., Labeit, S., Poustka, A., King, T. R., & Lehrach, H. (1990). Cloning of the T gene required in mesoderm formation in the mouse. *Nature*, *343*(6259), Article 6259. https://doi.org/10.1038/343617a0

Hinoi, T., Akyol, A., Theisen, B. K., Ferguson, D. O., Greenson, J. K., Williams, B. O., Cho, K. R., & Fearon, E. R. (2007). Mouse Model of Colonic Adenoma-Carcinoma Progression Based on Somatic Apc Inactivation. *Cancer Research*, *67*(20), 9721–9730. https://doi.org/10.1158/0008-5472.CAN-07-2735

Hofmann, M., Schuster-Gossler, K., Watabe-Rudolph, M., Aulehla, A., Herrmann, B. G., & Gossler, A. (2004). WNT signaling, in synergy with T/TBX6, controls Notch signaling by regulating Dll1 expression in the presomitic mesoderm of mouse embryos. *Genes & Development*, *18*(22), 2712–2717. https://doi.org/10.1101/gad.1248604

Holmberg, J., Clarke, D. L., & Frisén, J. (2000). Regulation of repulsion versus adhesion by different splice forms of an Eph receptor. *Nature*, *408*(6809), 203–206. https://doi.org/10.1038/35041577

Huebner, R. J., & Wallingford, J. B. (2018). Coming to Consensus: A Unifying Model Emerges for Convergent Extension. *Developmental Cell*, *46*(4), 389–396. https://doi.org/10.1016/j.devcel.2018.08.003

Humphries, J. D., Byron, A., & Humphries, M. J. (2006). Integrin ligands at a glance. *Journal of Cell Science*, *119*(19), 3901–3903. https://doi.org/10.1242/jcs.03098

Humphries, J. D., Wang, P., Streuli, C., Geiger, B., Humphries, M. J., & Ballestrem, C. (2007). Vinculin controls focal adhesion formation by direct interactions with talin and actin. *Journal of Cell Biology*, *179*(5), 1043–1057. https://doi.org/10.1083/jcb.200703036

Huss, D., Benazeraf, B., Wallingford, A., Filla, M., Yang, J., Fraser, S. E., & Lansford, R. (2015). A transgenic quail model that enables dynamic imaging of amniote embryogenesis. *Development*, *142*(16), 2850–2859. https://doi.org/10.1242/dev.121392

Hynes, R. O. (2004). The emergence of integrins: A personal and historical perspective. *Matrix Biology : Journal of the International Society for Matrix Biology*, *23*(6), 333–340. https://doi.org/10.1016/j.matbio.2004.08.001

Hynes, R. O., & Naba, A. (2012). Overview of the Matrisome—An Inventory of Extracellular Matrix Constituents and Functions. *Cold Spring Harbor Perspectives in Biology*, *4*(1), a004903. https://doi.org/10.1101/cshperspect.a004903

Iwafuchi-Doi, M., Matsuda, K., Murakami, K., Niwa, H., Tesar, P. J., Aruga, J., Matsuo, I., & Kondoh, H. (2012). Transcriptional regulatory networks in epiblast cells and during

anterior neural plate development as modeled in epiblast stem cells. *Development*, *139*(21), 3926–3937. https://doi.org/10.1242/dev.085936

Jahn, H. M., Kasakow, C. V., Helfer, A., Michely, J., Verkhratsky, A., Maurer, H. H., Scheller, A., & Kirchhoff, F. (2018). Refined protocols of tamoxifen injection for inducible DNA recombination in mouse astroglia. *Scientific Reports*, *8*. https://doi.org/10.1038/s41598-018-24085-9

Järveläinen, H., Sainio, A., Koulu, M., Wight, T. N., & Penttinen, R. (2009). Extracellular Matrix Molecules: Potential Targets in Pharmacotherapy. *Pharmacological Reviews*, *61*(2), 198–223. https://doi.org/10.1124/pr.109.001289

Javali, A., Misra, A., Leonavicius, K., Acharyya, D., Vyas, B., & Sambasivan, R. (2017). Co-expression of Tbx6 and Sox2 identifies a novel transient neuromesoderm progenitor cell state. *Development*, *144*(24), 4522–4529. https://doi.org/10.1242/dev.153262

Jensen, L. E., Barbaux, S., Hoess, K., Fraterman, S., Whitehead, A. S., & Mitchell, L. E. (2004). The human T locus and spina bifida risk. *Human Genetics*, *115*(6), 475–482. Scopus. https://doi.org/10.1007/s00439-004-1185-8

Ji, J., Yu, Y., Li, Z.-L., Chen, M.-Y., Deng, R., Huang, X., Wang, G.-F., Zhang, M.-X., Yang, Q., Ravichandran, S., Feng, G.-K., Xu, X.-L., Yang, C.-L., Qiu, M.-Z., Jiao, L., Yang, D., & Zhu, X.-F. (2018). XIAP Limits Autophagic Degradation of Sox2 and Is A Therapeutic Target in Nasopharyngeal Carcinoma Stem Cells. *Theranostics*, *8*(6), 1494–1510. https://doi.org/10.7150/thno.21717

Jülich, D., Mould, A. P., Koper, E., & Holley, S. A. (2009). Control of extracellular matrix assembly along tissue boundaries via Integrin and Eph/Ephrin signaling. *Development (Cambridge, England)*, *136*(17), 2913–2921. https://doi.org/10.1242/dev.038935

Junker, J. P., Noël, E. S., Guryev, V., Peterson, K. A., Shah, G., Huisken, J., McMahon, A. P., Berezikov, E., Bakkers, J., & van Oudenaarden, A. (2014). Genome-wide RNA Tomography in the Zebrafish Embryo. *Cell*, *159*(3), 662–675. https://doi.org/10.1016/j.cell.2014.09.038

Jurand, A. (1974). Some aspects of the development of the notochord in mouse embryos. *Journal of Embryology and Experimental Morphology*, *32*(1), 1–33.

Kadry, Y. A., & Calderwood, D. A. (2020). Chapter 22: Structural and signaling functions of integrins. *Biochimica et Biophysica Acta (BBA) - Biomembranes*, *1862*(5), 183206. https://doi.org/10.1016/j.bbamem.2020.183206

Kechagia, J. Z., Ivaska, J., & Roca-Cusachs, P. (2019). Integrins as biomechanical sensors of the microenvironment. *Nature Reviews Molecular Cell Biology*, *20*(8), Article 8. https://doi.org/10.1038/s41580-019-0134-2

Keller, R., Shih, J., & Domingo, C. (1992). The patterning and functioning of protrusive activity during convergence and extension of the Xenopus organiser. *Development (Cambridge, England). Supplement*, 81–91.

Kim, C., Ye, F., Hu, X., & Ginsberg, M. H. (2012). Talin activates integrins by altering the topology of the β transmembrane domain. *Journal of Cell Biology*, *197*(5), 605–611. https://doi.org/10.1083/jcb.201112141

Kimelman, D. (2016). Chapter Twenty-Nine - Tales of Tails (and Trunks): Forming the Posterior Body in Vertebrate Embryos. In P. M. Wassarman (Ed.), *Current Topics in Developmental Biology* (Vol. 116, pp. 517–536). Academic Press. https://doi.org/10.1016/bs.ctdb.2015.12.008

Kimura, C., Yoshinaga, K., Tian, E., Suzuki, M., Aizawa, S., & Matsuo, I. (2000). Visceral Endoderm Mediates Forebrain Development by Suppressing Posteriorizing Signals. *Developmental Biology*, *225*(2), 304–321. https://doi.org/10.1006/dbio.2000.9835

Kinder, S. J., Tsang, T. E., Quinlan, G. A., Hadjantonakis, A. K., Nagy, A., & Tam, P. P. (1999). The orderly allocation of mesodermal cells to the extraembryonic structures and the anteroposterior axis during gastrulation of the mouse embryo. *Development*, *126*(21), 4691–4701. https://doi.org/10.1242/dev.126.21.4691

Kirby, T. J., & Lammerding, J. (2018). Emerging views of the nucleus as a cellular mechanosensor. *Nature Cell Biology*, *20*(4), 373–381. https://doi.org/10.1038/s41556-018-0038-y

Koch, F., Scholze, M., Wittler, L., Schifferl, D., Sudheer, S., Grote, P., Timmermann, B., Macura, K., & Herrmann, B. G. (2017). Antagonistic Activities of Sox2 and Brachyury Control the Fate Choice of Neuro-Mesodermal Progenitors. *Developmental Cell*, *42*(5), 514-526.e7. https://doi.org/10.1016/j.devcel.2017.07.021

Kölliker, A. von. (1884). *Die embryonalen Keimblätter und die Gewebe. 40*, 179–213.

Kondoh, H., Takada, S., & Takemoto, T. (2016). Axial level-dependent molecular and cellular mechanisms underlying the genesis of the embryonic neural plate. *Development, Growth & Differentiation*, *58*(5), 427–436. https://doi.org/10.1111/dgd.12295

Koshida, S., Kishimoto, Y., Ustumi, H., Shimizu, T., Furutani-Seiki, M., Kondoh, H., & Takada, S. (2005). Integrinα5-Dependent Fibronectin Accumulation for Maintenance of Somite Boundaries in Zebrafish Embryos. *Developmental Cell*, *8*(4), 587–598. https://doi.org/10.1016/j.devcel.2005.03.006

Kwon, G. S., Viotti, M., & Hadjantonakis, A.-K. (2008). The Endoderm of the Mouse Embryo Arises by Dynamic Widespread Intercalation of Embryonic and Extraembryonic Lineages. *Developmental Cell*, *15*(4), 509–520. https://doi.org/10.1016/j.devcel.2008.07.017

Lamandé, S. R., & Bateman, J. F. (2020). Genetic Disorders of the Extracellular Matrix. *The Anatomical Record*, *303*(6), 1527–1542. https://doi.org/10.1002/ar.24086

Lange, A., Wickström, S. A., Jakobson, M., Zent, R., Sainio, K., & Fässler, R. (2009). Integrin-linked kinase is an adaptor with essential functions during mouse development. *Nature*, *461*(7266), 1002–1006. https://doi.org/10.1038/nature08468

Lawson, K. A., Meneses, J. J., & Pedersen, R. A. (1991). Clonal analysis of epiblast fate during germ layer formation in the mouse embryo. *Development*, *113*(3), 891–911.

LeBleu, V. S., MacDonald, B., & Kalluri, R. (2007). Structure and Function of Basement Membranes. *Experimental Biology and Medicine*, *232*(9), 1121–1129. https://doi.org/10.3181/0703-MR-72

Lee, C. S., Fu, H., Baratang, N., Rousseau, J., Kumra, H., Sutton, V. R., Niceta, M., Ciolfi, A., Yamamoto, G., Bertola, D., Marcelis, C. L., Lugtenberg, D., Bartuli, A., Kim, C., Hoover-Fong, J., Sobreira, N., Pauli, R., Bacino, C., Krakow, D., … Campeau, P. M. (2017). Mutations in Fibronectin Cause a Subtype of Spondylometaphyseal Dysplasia with "Corner Fractures". *The American Journal of Human Genetics*, *101*(5), 815–823. https://doi.org/10.1016/j.ajhg.2017.09.019

Lee, S.-J., Perera, L., Coulter, S. J., Mohrenweiser, H. W., Jetten, A., & Goldstein, J. A. (2007). The discovery of new coding alleles of human CYP26A1 which are potentially defective in the metabolism of all-trans retinoic acid and their assessment in a recombinant cDNA expression system. *Pharmacogenetics and Genomics*, *17*(3), 169–180. https://doi.org/10.1097/FPC.0b013e32801152d6

Lemay, P., De Marco, P., Traverso, M., Merello, E., Dionne-Laporte, A., Spiegelman, D., Henrion, É., Diallo, O., Audibert, F., Michaud, J. L., Cama, A., Rouleau, G. A., Kibar, Z., & Capra, V. (2018). Whole exome sequencing identifies novel predisposing genes in neural tube defects. *Molecular Genetics & Genomic Medicine*, *7*(1). https://doi.org/10.1002/mgg3.467

Liu, F., Dai, S., Feng, D., Peng, X., Qin, Z., Kearns, A. C., Huang, W., Chen, Y., Ergün, S., Wang, H., Rappaport, J., Bryda, E. C., Chandrasekhar, A., Aktas, B., Hu, H., Chang, S. L., Gao, B., & Qin, X. (2019). Versatile cell ablation tools and their applications to study loss of cell functions. *Cellular and Molecular Life Sciences : CMLS*, *76*(23), 4725–4743. https://doi.org/10.1007/s00018-019-03243-w

Liu, Y., Sugiyama, F., Yagami, K., & Ohkawa, H. (2003). Sharing of the same embryogenic pathway in anorectal malformations and anterior sacral myelomeningocele formation. *Pediatric Surgery International*, *19*(3), 152–156. https://doi.org/10.1007/s00383-002-0908-y

Maroto, M., Bone, R. A., & Dale, J. K. (2012). Somitogenesis. *Development*, *139*(14), 2453–2456. https://doi.org/10.1242/dev.069310

Martin, B. L., & Kimelman, D. (2012). Canonical Wnt Signaling Dynamically Controls Multiple Stem Cell Fate Decisions during Vertebrate Body Formation. *Developmental Cell*, *22*(1), 223–232. https://doi.org/10.1016/j.devcel.2011.11.001

Martins-Green, M. (1988). Origin of the dorsal surface of the neural tube by progressive delamination of epidermal ectoderm and neuroepithelium: Implications for neurulation and neural tube defects. *Development (Cambridge, England)*, *103*(4), 687–706.

McCann, M. R., Tamplin, O. J., Rossant, J., & Séguin, C. A. (2012). Tracing notochord-derived cells using a Noto-cre mouse: Implications for intervertebral disc development. *Disease Models & Mechanisms*, *5*(1), 73–82. https://doi.org/10.1242/dmm.008128

McMillen, P., & Holley, S. A. (2015). Integration of cell–cell and cell–ECM adhesion in vertebrate morphogenesis. *Current Opinion in Cell Biology*, *36*, 48–53. https://doi.org/10.1016/j.ceb.2015.07.002

McShane, S. G., Molè, M. A., Savery, D., Greene, N. D. E., Tam, P. P. L., & Copp, A. J. (2015). Cellular basis of neuroepithelial bending during mouse spinal neural tube closure. *Developmental Biology*, *404*(2), 113–124. https://doi.org/10.1016/j.ydbio.2015.06.003

Meredith, J. E., Fazeli, B., & Schwartz, M. A. (1993). The extracellular matrix as a cell survival factor. *Molecular Biology of the Cell*, *4*(9), 953–961.

Miner, J. H., Cunningham, J., & Sanes, J. R. (1998). Roles for Laminin in Embryogenesis: Exencephaly, Syndactyly, and Placentopathy in Mice Lacking the Laminin α5 Chain. *The Journal of Cell Biology*, *143*(6), 1713–1723.

Miner, J. H., Li, C., Mudd, J. L., Go, G., & Sutherland, A. E. (2004). Compositional and structural requirements for laminin and basement membranes during mouse embryo implantation and gastrulation. *Development (Cambridge, England)*, *131*(10), 2247–2256. https://doi.org/10.1242/dev.01112

Mitra, S. K., Hanson, D. A., & Schlaepfer, D. D. (2005). Focal adhesion kinase: In command and control of cell motility. *Nature Reviews Molecular Cell Biology*, *6*(1), 56–68. https://doi.org/10.1038/nrm1549

Miyagi, S., Kato, H., & Okuda, A. (2009). Role of SoxB1 transcription factors in development. *Cellular and Molecular Life Sciences*, *66*(23), 3675. https://doi.org/10.1007/s00018-009-0097-0

Miyagi, S., Masui, S., Niwa, H., Saito, T., Shimazaki, T., Okano, H., Nishimoto, M., Muramatsu, M., Iwama, A., & Okuda, A. (2008). Consequence of the loss of Sox2 in the developing brain of the mouse. *FEBS Letters*, *582*(18), 2811–2815. https://doi.org/10.1016/j.febslet.2008.07.011

Molè, M. A. (2017). Cell dynamics and cell-matrix interactions during neural tube closure [Doctoral]. In *Doctoral thesis, UCL (University College London).* UCL. https://discovery.ucl.ac.uk/id/eprint/1549577/

Molè, M. A., Galea, G. L., Rolo, A., Weberling, A., Nychyk, O., De Castro, S. C., Savery, D., Fässler, R., Ybot-González, P., Greene, N. D. E., & Copp, A. J. (2020). Integrin-Mediated Focal Anchorage Drives Epithelial Zippering during Mouse Neural Tube Closure. *Developmental Cell*, *52*(3), 321-334.e6. https://doi.org/10.1016/j.devcel.2020.01.012

Molè, M. A., Weberling, A., Fässler, R., Campbell, A., Fishel, S., & Zernicka-Goetz, M. (2021). Integrin β1 coordinates survival and morphogenesis of the embryonic lineage upon implantation and pluripotency transition. *Cell Reports*, *34*(10). https://doi.org/10.1016/j.celrep.2021.108834

Molotkova, N., Molotkov, A., Sirbu, I. O., & Duester, G. (2005). Requirement of mesodermal retinoic acid generated by Raldh2 for posterior neural transformation. *Mechanisms of Development*, *122*(2), 145–155. https://doi.org/10.1016/j.mod.2004.10.008

Mongera, A., Michaut, A., Guillot, C., Xiong, F., & Pourquié, O. (2019). Mechanics of Anteroposterior Axis Formation in Vertebrates. *Annual Review of Cell and Developmental Biology*, *35*(1), 259–283. https://doi.org/10.1146/annurev-cellbio-100818-125436

Morgan, M. R., Humphries, M. J., & Bass, M. D. (2007). Synergistic control of cell adhesion by integrins and syndecans. *Nature Reviews Molecular Cell Biology*, *8*(12), 957–969. https://doi.org/10.1038/nrm2289

Moury, J. D., & Schoenwolf, G. C. (1995). Cooperative model of epithelial shaping and bending during avian neurulation: Autonomous movements of the neural plate, autonomous movements of the epidermis, and interactions in the neural plate/epidermis transition zone. *Developmental Dynamics*, *204*(3), 323–337. https://doi.org/10.1002/aja.1002040310

Mouw, J. K., Ou, G., & Weaver, V. M. (2014). Extracellular matrix assembly: A multiscale deconstruction. *Nature Reviews Molecular Cell Biology*, *15*(12), Article 12. https://doi.org/10.1038/nrm3902

Mugele, D. (2018). Role of neuro-mesodermal progenitors in neural tube formation [Doctoral]. In *Doctoral thesis, UCL (University College London).* (pp. 1–137). https://discovery.ucl.ac.uk/id/eprint/10057534/

Mugele, D., Moulding, D. A., Savery, D., Molè, M. A., Greene, N. D. E., Martinez-Barbera, J. P., & Copp, A. J. (2018). Genetic approaches in mice demonstrate that neuro-mesodermal progenitors express T/Brachyury but not Sox2. *BioRxiv*, 503854. https://doi.org/10.1101/503854

Muzumdar, M. D., Tasic, B., Miyamichi, K., Li, L., & Luo, L. (2007). A global double-fluorescent Cre reporter mouse. *Genesis*, *45*(9), 593–605. https://doi.org/10.1002/dvg.20335

Nakajima, Y., Morimoto, M., Takahashi, Y., Koseki, H., & Saga, Y. (2006). Identification of Epha4 enhancer required for segmental expression and the regulation by Mesp2. *Development*, *133*(13), 2517–2525. https://doi.org/10.1242/dev.02422

Nakamura, E., Nguyen, M.-T., & Mackem, S. (2006). Kinetics of tamoxifen-regulated Cre activity in mice using a cartilage-specific CreERT to assay temporal activity windows along the proximodistal limb skeleton. *Developmental Dynamics*, *235*(9), 2603–2612. https://doi.org/10.1002/dvdy.20892

Niederreither, K., Subbarayan, V., Dollé, P., & Chambon, P. (1999). Embryonic retinoic acid synthesis is essential for early mouse post-implantation development. *Nature Genetics*, *21*(4), Article 4. https://doi.org/10.1038/7788

Nikolopoulou, E., Galea, G. L., Rolo, A., Greene, N. D. E., & Copp, A. J. (2017). Neural tube closure: Cellular, molecular and biomechanical mechanisms. *Development*, *144*(4), 552–566. https://doi.org/10.1242/dev.145904

Nikolopoulou, E., Hirst, C. S., Galea, G., Venturini, C., Moulding, D., Marshall, A. R., Rolo, A., De Castro, S. C. P., Copp, A. J., & Greene, N. D. E. (2019). Spinal neural tube closure depends on regulation of surface ectoderm identity and biomechanics by Grhl2. *Nature Communications*, *10*(1), Article 1. https://doi.org/10.1038/s41467-019-10164-6

Oginuma, M., Niwa, Y., Chapman, D. L., & Saga, Y. (2008). Mesp2 and Tbx6 cooperatively create periodic patterns coupled with the clock machinery during mouse somitogenesis. *Development*, *135*(15), 2555–2562. https://doi.org/10.1242/dev.019877

Olivera-Martinez, I., Harada, H., Halley, P. A., & Storey, K. G. (2012). Loss of FGF-Dependent Mesoderm Identity and Rise of Endogenous Retinoid Signalling Determine Cessation of Body Axis Elongation. *PLOS Biology*, *10*(10), e1001415. https://doi.org/10.1371/journal.pbio.1001415

Olivier, N., Luengo-Oroz, M. A., Duloquin, L., Faure, E., Savy, T., Veilleux, I., Solinas, X., Débarre, D., Bourgine, P., Santos, A., Peyriéras, N., & Beaurepaire, E. (2010). Cell lineage reconstruction of early zebrafish embryos using label-free nonlinear microscopy. *Science (New York, N.Y.)*, *329*(5994), 967–971. https://doi.org/10.1126/science.1189428

O'Shea, K. S. (1987). Differential deposition of basement membrane components during formation of the caudal neural tube in the mouse embryo. *Development (Cambridge, England)*, *99*(4), 509–519.

O'Shea, K. S., & Liu, L. H. (1987). Basal lamina and extracellular matrix alterations in the caudal neural tube of the delayed Splotch embryo. *Brain Research*, *465*(1–2), 11–20. https://doi.org/10.1016/0165-3806(87)90225-2

Padmanabhan, R. (1998). Retinoic acid-induced caudal regression syndrome in the mouse fetus. *Reproductive Toxicology*, *12*(2), 139–151. https://doi.org/10.1016/S0890-6238(97)00153-6

Pai, Y.-J., Abdullah, N. L., Mohd.-Zin, S. W., Mohammed, R. S., Rolo, A., Greene, N. D. E., Abdul-Aziz, N. M., & Copp, A. J. (2012). Epithelial fusion during neural tube morphogenesis. *Birth Defects Research Part A: Clinical and Molecular Teratology*, *94*(10), 817–823. https://doi.org/10.1002/bdra.23072

Pangilinan, F., Molloy, A. M., Mills, J. L., Troendle, J. F., Parle-McDermott, A., Signore, C., O'Leary, V. B., Chines, P., Seay, J. M., Geiler-Samerotte, K., Mitchell, A., VanderMeer, J. E., Krebs, K. M., Sanchez, A., Cornman-Homonoff, J., Stone, N., Conley, M., Kirke, P. N., Shane, B., … Brody, L. C. (2012). Evaluation of common genetic variants in 82 candidate genes as risk factors for neural tube defects. *BMC Medical Genetics*, *13*(1), 62. https://doi.org/10.1186/1471-2350-13-62

Pawłowski, R., Rajakylä, E. K., Vartiainen, M. K., & Treisman, R. (2010). An actin-regulated importin α/β-dependent extended bipartite NLS directs nuclear import of MRTF-A. *The EMBO Journal*, *29*(20), 3448–3458. https://doi.org/10.1038/emboj.2010.216

Pennimpede, T., Proske, J., König, A., Vidigal, J. A., Morkel, M., Bramsen, J. B., Herrmann, B. G., & Wittler, L. (2012). In vivo knockdown of Brachyury results in skeletal defects and urorectal malformations resembling caudal regression syndrome. *Developmental Biology*, *372*(1), 55–67. https://doi.org/10.1016/j.ydbio.2012.09.003

Perantoni, A. O., Timofeeva, O., Naillat, F., Richman, C., Pajni-Underwood, S., Wilson, C., Vainio, S., Dove, L. F., & Lewandoski, M. (2005). Inactivation of FGF8 in early mesoderm reveals an essential role in kidney development. *Development*, *132*(17), 3859–3871. https://doi.org/10.1242/dev.01945

Perez, T. D., & Nelson, W. J. (2004). Cadherin Adhesion: Mechanisms and Molecular Interactions. *Handbook of Experimental Pharmacology*, *165*, 3–21. https://doi.org/10.1007/978-3-540-68170-0_1

Pla, P., & Monsoro-Burq, A. H. (2018). The neural border: Induction, specification and maturation of the territory that generates neural crest cells. *Developmental Biology*, *444*, S36–S46. https://doi.org/10.1016/j.ydbio.2018.05.018

Popova, S. N., Barczyk, M., Tiger, C.-F., Beertsen, W., Zigrino, P., Aszodi, A., Miosge, N., Forsberg, E., & Gullberg, D. (2007). Alpha11 beta1 integrin-dependent regulation of periodontal ligament function in the erupting mouse incisor. *Molecular and Cellular Biology*, *27*(12), 4306–4316. https://doi.org/10.1128/MCB.00041-07

Pöschl, E., Schlötzer-Schrehardt, U., Brachvogel, B., Saito, K., Ninomiya, Y., & Mayer, U. (2004). Collagen IV is essential for basement membrane stability but dispensable for initiation of its assembly during early development. *Development*, *131*(7), 1619–1628. https://doi.org/10.1242/dev.01037

Postma, A. V., Alders, M., Sylva, M., Bilardo, C. M., Pajkrt, E., Rijn, R. R. van, Schulte-Merker, S., Bulk, S., Stefanovic, S., Ilgun, A., Barnett, P., Mannens, M. M. a. M., Moorman, A. F. M., Oostra, R. J., & Maarle, M. C. van. (2014). Mutations in the T (brachyury) gene cause a novel syndrome consisting of sacral agenesis, abnormal ossification of the vertebral bodies and a persistent notochordal canal. *Journal of Medical Genetics*, *51*(2), 90–97. https://doi.org/10.1136/jmedgenet-2013-102001

Pourquié, O. (2011). Vertebrate Segmentation: From Cyclic Gene Networks to Scoliosis. *Cell*, *145*(5), 650–663. https://doi.org/10.1016/j.cell.2011.05.011

Pourquié, O. (2022). A brief history of the segmentation clock. *Developmental Biology*, *485*, 24–36. https://doi.org/10.1016/j.ydbio.2022.02.011

Pozzi, A., Yurchenco, P. D., & Iozzo, R. V. (2017). The nature and biology of basement membranes. *Matrix Biology*, *57–58*, 1–11. https://doi.org/10.1016/j.matbio.2016.12.009

Pulina, M. V., Hou, S.-Y., Mittal, A., Julich, D., Whittaker, C. A., Holley, S. A., Hynes, R. O., & Astrof, S. (2011). Essential roles of fibronectin in the development of the left–right embryonic body plan. *Developmental Biology*, *354*(2), 208–220. https://doi.org/10.1016/j.ydbio.2011.03.026

Raghunathan, R., Zhang, J., Wu, C., Rippy, J., Singh, M., Larin, K. V., & Scarcelli, G. (2017). Evaluating biomechanical properties of murine embryos using Brillouin microscopy and optical coherence tomography. *Journal of Biomedical Optics*, *22*(8), 086013. https://doi.org/10.1117/1.JBO.22.8.086013

Rajah, A., Boudreau, C. G., Ilie, A., Wee, T.-L., Tang, K., Borisov, A. Z., Orlowski, J., & Brown, C. M. (2019). Paxillin S273 Phosphorylation Regulates Adhesion Dynamics and Cell Migration through a Common Protein Complex with PAK1 and βPIX. *Scientific Reports*, *9*(1), 11430. https://doi.org/10.1038/s41598-019-47722-3

Regev, I., Guevorkian, K., Pourquie, O., & Mahadevan, L. (2017). *Motility-gradient induced elongation of the vertebrate embryo* (p. 187443). https://doi.org/10.1101/187443

Rhinn, M., Dierich, A., Shawlot, W., Behringer, R. R., Le Meur, M., & Ang, S. L. (1998). Sequential roles for Otx2 in visceral endoderm and neuroectoderm for forebrain and midbrain induction and specification. *Development (Cambridge, England)*, *125*(5), 845–856.

Rodriques, S. G., Stickels, R. R., Goeva, A., Martin, C. A., Murray, E., Vanderburg, C. R., Welch, J., Chen, L. M., Chen, F., & Macosko, E. Z. (2019). Slide-seq: A scalable technology for

measuring genome-wide expression at high spatial resolution. *Science*, *363*(6434), 1463–1467. https://doi.org/10.1126/science.aaw1219

Rolo, A., Savery, D., Escuin, S., de Castro, S. C., Armer, H. E., Munro, P. M., Molè, M. A., Greene, N. D., & Copp, A. J. (2016). Regulation of cell protrusions by small GTPases during fusion of the neural folds. *ELife*, *5*, e13273. https://doi.org/10.7554/eLife.13273

Rozario, T., & DeSimone, D. W. (2010). The extracellular matrix in development and morphogenesis: A dynamic view. *Developmental Biology*, *341*(1), 126–140. https://doi.org/10.1016/j.ydbio.2009.10.026

Saga, Y. (2007). Segmental border is defined by the key transcription factor Mesp2, by means of the suppression of notch activity. *Developmental Dynamics*, *236*(6), 1450–1455. https://doi.org/10.1002/dvdy.21143

Sakai, T., Johnson, K. J., Murozono, M., Sakai, K., Magnuson, M. A., Wieloch, T., Cronberg, T., Isshiki, A., Erickson, H. P., & Fässler, R. (2001). Plasma fibronectin supports neuronal survival and reduces brain injury following transient focal cerebral ischemia but is not essential for skin-wound healing and hemostasis. *Nature Medicine*, *7*(3), Article 3. https://doi.org/10.1038/85471

Sakar, M. S., Eyckmans, J., Pieters, R., Eberli, D., Nelson, B. J., & Chen, C. S. (2016). Cellular forces and matrix assembly coordinate fibrous tissue repair. *Nature Communications*, *7*(1), Article 1. https://doi.org/10.1038/ncomms11036

Sambasivan, R., & Steventon, B. (2021). Neuromesodermal Progenitors: A Basis for Robust Axial Patterning in Development and Evolution. *Frontiers in Cell and Developmental Biology*, *8*. https://doi.org/10.3389/fcell.2020.607516

Sander, K., & Faessler, P. E. (2003). Introducing the Spemann-Mangold organizer: Experiments and insights that generated a key concept in developmental biology. *International Journal of Developmental Biology*, *45*(1), Article 1. https://doi.org/10.1387/ijdb.11291840

Sasaki, N., Kiso, M., Kitagawa, M., & Saga, Y. (2011). The repression of Notch signaling occurs via the destabilization of mastermind-like 1 by Mesp2 and is essential for somitogenesis. *Development*, *138*(1), 55–64. https://doi.org/10.1242/dev.055533

Schiller, H. B., Hermann, M.-R., Polleux, J., Vignaud, T., Zanivan, S., Friedel, C. C., Sun, Z., Raducanu, A., Gottschalk, K.-E., Théry, M., Mann, M., & Fässler, R. (2013). β 1—And α v -class integrins cooperate to regulate myosin II during rigidity sensing of fibronectin-based microenvironments. *Nature Cell Biology*, *15*(6), 625–636. https://doi.org/10.1038/ncb2747

Schindelin, J., Arganda-Carreras, I., Frise, E., Kaynig, V., Longair, M., Pietzsch, T., Preibisch, S., Rueden, C., Saalfeld, S., Schmid, B., Tinevez, J.-Y., White, D. J., Hartenstein, V., Eliceiri,

K., Tomancak, P., & Cardona, A. (2012). Fiji—An Open Source platform for biological image analysis. *Nature Methods*, *9*(7). https://doi.org/10.1038/nmeth.2019

Schmidt, C., Wilson, V., Stott, D., & Beddington, R. S. P. (1997). TPromoter Activity in the Absence of Functional T Protein during Axis Formation and Elongation in the Mouse. *Developmental Biology*, *189*(2), 161–173. https://doi.org/10.1006/dbio.1997.8661

Schoenwolf, G. C. (1984). Histological and ultrastructural studies of secondary neurulation in mouse embryos. *The American Journal of Anatomy*, *169*(4), 361–376. https://doi.org/10.1002/aja.1001690402

Schwarzbauer, J. E., & DeSimone, D. W. (2011). Fibronectins, Their Fibrillogenesis, and In Vivo Functions. *Cold Spring Harbor Perspectives in Biology*, *3*(7), a005041. https://doi.org/10.1101/cshperspect.a005041

Serwane, F., Mongera, A., Rowghanian, P., Kealhofer, D. A., Lucio, A. A., Hockenbery, Z. M., & Campàs, O. (2017). In vivo quantification of spatially varying mechanical properties in developing tissues. *Nature Methods*, *14*(2), Article 2. https://doi.org/10.1038/nmeth.4101

Shaham, O., Smith, A. N., Robinson, M. L., Taketo, M. M., Lang, R. A., & Ashery-Padan, R. (2009). Pax6 is essential for lens fiber cell differentiation. *Development*, *136*(15), 2567–2578. https://doi.org/10.1242/dev.032888

Shum, A. S. W., & Copp, A. J. (1996). Regional differences in morphogenesis of the neuroepithelium suggest multiple mechanisms of spinal neurulation in the mouse. *Anatomy and Embryology*, *194*(1), 65–73. https://doi.org/10.1007/BF00196316

Shum, A. S. W., Poon, L. L. M., Tang, W. W. T., Koide, T., Chan, B. W. H., Leung, Y.-C. G., Shiroishi, T., & Copp, A. J. (1999). Retinoic acid induces down-regulation of Wnt-3a, apoptosis and diversion of tail bud cells to a neural fate in the mouse embryo. *Mechanisms of Development*, *84*(1), 17–30. https://doi.org/10.1016/S0925-4773(99)00059-3

Singh, P., Carraher, C., & Schwarzbauer, J. E. (2010). Assembly of fibronectin extracellular matrix. *Annual Review of Cell and Developmental Biology*, *26*, 397–419. https://doi.org/10.1146/annurev-cellbio-100109-104020

Singh, P., & Schwarzbauer, J. E. (2014). Fibronectin matrix assembly is essential for cell condensation during chondrogenesis. *Journal of Cell Science*, *127*(20), 4420–4428. https://doi.org/10.1242/jcs.150276

Smith, J. L., & Schoenwolf, G. C. (1989). Notochordal induction of cell wedging in the chick neural plate and its role in neural tube formation. *Journal of Experimental Zoology*, *250*(1), 49–62. https://doi.org/10.1002/jez.1402500107

Smyth, N., Vatansever, H. S., Murray, P., Meyer, M., Frie, C., Paulsson, M., & Edgar, D. (1999). Absence of Basement Membranes after Targeting the LAMC1 Gene Results in Embryonic Lethality Due to Failure of Endoderm Differentiation. *The Journal of Cell Biology*, *144*(1), 151–160.

Spence, J. R., Lauf, R., & Shroyer, N. F. (2011). Vertebrate Intestinal Endoderm Development. *Developmental Dynamics : An Official Publication of the American Association of Anatomists*, *240*(3), 501–520. https://doi.org/10.1002/dvdy.22540

Srinivas, S., Watanabe, T., Lin, C.-S., William, C. M., Tanabe, Y., Jessell, T. M., & Costantini, F. (2001). Cre reporter strains produced by targeted insertion of EYFP and ECFP into the ROSA26 locus. *BMC Developmental Biology*, *1*, 4. https://doi.org/10.1186/1471-213X-1-4

Stemple, D. L. (2005). Structure and function of the notochord: An essential organ for chordate development. *Development (Cambridge, England)*, *132*(11), 2503–2512. https://doi.org/10.1242/dev.01812

Stephens, L. E., Sutherland, A. E., Klimanskaya, I. V., Andrieux, A., Meneses, J., Pedersen, R. A., & Damsky, C. H. (1995). Deletion of beta 1 integrins in mice results in inner cell mass failure and peri-implantation lethality. *Genes & Development*, *9*(15), 1883–1895. https://doi.org/10.1101/gad.9.15.1883

Stern, C. D. (2005). Neural induction: Old problem, new findings, yet more questions. *Development*, *132*(9), 2007–2021. https://doi.org/10.1242/dev.01794

Sternberg, J., & Kimber, S. J. (1986a). Distribution of fibronectin, laminin and entactin in the environment of migrating neural crest cells in early mouse embryos. *Journal of Embryology and Experimental Morphology*, *91*, 267–282.

Sternberg, J., & Kimber, S. J. (1986b). The relationship between emerging neural crest cells and basement membranes in the trunk of the mouse embryo: A TEM and immunocytochemical study. *Journal of Embryology and Experimental Morphology*, *98*, 251–268.

Steventon, B., Duarte, F., Lagadec, R., Mazan, S., Nicolas, J.-F., & Hirsinger, E. (2016). Species-specific contribution of volumetric growth and tissue convergence to posterior body elongation in vertebrates. *Development*, *143*(10), 1732–1741. https://doi.org/10.1242/dev.126375

Stoetzel, C., Weber, B., Bourgeois, P., Bolcato-Bellemin, A. L., & Perrin-Schmitt, F. (1995). Dorso-ventral and rostro-caudal sequential expression of M-twist in the postimplantation murine embryo. *Mechanisms of Development*, *51*(2–3), 251–263. https://doi.org/10.1016/0925-4773(95)00369-x

Stower, M. J., & Srinivas, S. (2018). The Head's Tale: Anterior-Posterior Axis Formation in the Mouse Embryo. *Current Topics in Developmental Biology*, *128*, 365–390. https://doi.org/10.1016/bs.ctdb.2017.11.003

Strohmeyer, N., Bharadwaj, M., Costell, M., Fässler, R., & Müller, D. J. (2017). Fibronectin-bound α5β1 integrins sense load and signal to reinforce adhesion in less than a second. *Nature Materials*, *16*(12), 1262–1270. https://doi.org/10.1038/nmat5023

Susaki, E. A., Tainaka, K., Perrin, D., Yukinaga, H., Kuno, A., & Ueda, H. R. (2015). Advanced CUBIC protocols for whole-brain and whole-body clearing and imaging. *Nature Protocols*, *10*(11), Article 11. https://doi.org/10.1038/nprot.2015.085

Sutherland, A., Keller, R., & Lesko, A. (2020). Convergent extension in mammalian morphogenesis. *Seminars in Cell & Developmental Biology*, *100*, 199–211. https://doi.org/10.1016/j.semcdb.2019.11.002

Tajik, A., Zhang, Y., Wei, F., Sun, J., Jia, Q., Zhou, W., Singh, R., Khanna, N., Belmont, A. S., & Wang, N. (2016). Transcription upregulation via force-induced direct stretching of chromatin. *Nature Materials*, *15*(12), 1287–1296. https://doi.org/10.1038/nmat4729

Takahashi, S., Leiss, M., Moser, M., Ohashi, T., Kitao, T., Heckmann, D., Pfeifer, A., Kessler, H., Takagi, J., Erickson, H. P., & Fässler, R. (2007). The RGD motif in fibronectin is essential for development but dispensable for fibril assembly. *The Journal of Cell Biology*, *178*(1), 167–178. https://doi.org/10.1083/jcb.200703021

Takemoto, T., Uchikawa, M., Yoshida, M., Bell, D. M., Lovell-Badge, R., Papaioannou, V. E., & Kondoh, H. (2011). Tbx6-dependent Sox2 regulation determines neural vs mesodermal fate in axial stem cells. *Nature*, *470*(7334), 394–398. https://doi.org/10.1038/nature09729

Tam, & Beddington, R. S. (1987). The formation of mesodermal tissues in the mouse embryo during gastrulation and early organogenesis. *Development*, *99*(1), 109–126. https://doi.org/10.1242/dev.99.1.109

Tam, P. P. L., & Behringer, R. R. (1997). Mouse gastrulation: The formation of a mammalian body plan. *Mechanisms of Development*, *68*(1), 3–25. https://doi.org/10.1016/S0925-4773(97)00123-8

Tam, P. P. L., & Loebel, D. A. F. (2007). Gene function in mouse embryogenesis: Get set for gastrulation. *Nature Reviews Genetics*, *8*(5), 368–381. https://doi.org/10.1038/nrg2084

Tam, P. P. L., Williams, E. A., & Chan, W. Y. (1993). Gastrulation in the mouse embryo: Ultrastructural and molecular aspects of germ layer morphogenesis. *Microscopy Research and Technique*, *26*(4), 301–328. https://doi.org/10.1002/jemt.1070260405

Taranova, O. V., Magness, S. T., Fagan, B. M., Wu, Y., Surzenko, N., Hutton, S. R., & Pevny, L. H. (2006). SOX2 is a dose-dependent regulator of retinal neural progenitor competence. *Genes & Development*, *20*(9), 1187–1202. https://doi.org/10.1101/gad.1407906

Theocharis, A. D., Skandalis, S. S., Gialeli, C., & Karamanos, N. K. (2016). Extracellular matrix structure. *Advanced Drug Delivery Reviews*, *97*, 4–27. https://doi.org/10.1016/j.addr.2015.11.001

Thomson, M., Liu, S. J., Zou, L.-N., Smith, Z., Meissner, A., & Ramanathan, S. (2011). Pluripotency Factors in Embryonic Stem Cells Regulate Differentiation into Germ Layers. *Cell*, *145*(6), 875–889. https://doi.org/10.1016/j.cell.2011.05.017

Trapani, V., Bonaldo, P., & Corallo, D. (2017). Role of the ECM in notochord formation, function and disease. *Journal of Cell Science*, *130*(19), 3203–3211. https://doi.org/10.1242/jcs.175950

Tsakiridis, A., & Wilson, V. (2015). *Assessing the bipotency of in vitro-derived neuromesodermal progenitors* (4:100). F1000Research. https://doi.org/10.12688/f1000research.6345.1

Tseng, Q., Duchemin-Pelletier, E., Deshiere, A., Balland, M., Guillou, H., Filhol, O., & Théry, M. (2012). Spatial organization of the extracellular matrix regulates cell–cell junction positioning. *Proceedings of the National Academy of Sciences*, *109*(5), 1506–1511. https://doi.org/10.1073/pnas.1106377109

Turner, D. A., Hayward, P. C., Baillie-Johnson, P., Rué, P., Broome, R., Faunes, F., & Arias, A. M. (2014). Wnt/β-catenin and FGF signalling direct the specification and maintenance of a neuromesodermal axial progenitor in ensembles of mouse embryonic stem cells. *Development*, *141*(22), 4243–4253. https://doi.org/10.1242/dev.112979

Tzouanacou, E., Wegener, A., Wymeersch, F. J., Wilson, V., & Nicolas, J.-F. (2009). Redefining the Progression of Lineage Segregations during Mammalian Embryogenesis by Clonal Analysis. *Developmental Cell*, *17*(3), 365–376. https://doi.org/10.1016/j.devcel.2009.08.002

van Straaten, H. W. M., & Copp, A. J. (2001). Curly tail: A 50-year history of the mouse spina bifida model. *Anatomy and Embryology*, *203*(4), 225–238. https://doi.org/10.1007/s004290100169

Vaynberg, J., Fukuda, K., Lu, F., Bialkowska, K., Chen, Y., Plow, E. F., & Qin, J. (2018). Non-catalytic signaling by pseudokinase ILK for regulating cell adhesion. *Nature Communications*, *9*(1), 4465. https://doi.org/10.1038/s41467-018-06906-7

Verrier, L., Davidson, L., Gierliński, M., Dady, A., & Storey, K. G. (2018). Neural differentiation, selection and transcriptomic profiling of human neuromesodermal progenitor-like

cells in vitro. *Development*, *145*(16), dev166215. https://doi.org/10.1242/dev.166215

Vincent, S. D., Dunn, N. R., Hayashi, S., Norris, D. P., & Robertson, E. J. (2003). Cell fate decisions within the mouse organizer are governed by graded Nodal signals. *Genes & Development*, *17*(13), 1646–1662. https://doi.org/10.1101/gad.1100503

Walker, C., Mojares, E., & del Río Hernández, A. (2018). Role of Extracellular Matrix in Development and Cancer Progression. *International Journal of Molecular Sciences*, *19*(10), 3028. https://doi.org/10.3390/ijms19103028

Wallingford, J. B., Fraser, S. E., & Harland, R. M. (2002). Convergent Extension: The Molecular Control of Polarized Cell Movement during Embryonic Development. *Developmental Cell*, *2*(6), 695–706. https://doi.org/10.1016/S1534-5807(02)00197-1

Walma, D. A. C., & Yamada, K. M. (2020). The extracellular matrix in development. *Development*, *147*(dev175596). https://doi.org/10.1242/dev.175596

Wang, F., Flanagan, J., Su, N., Wang, L.-C., Bui, S., Nielson, A., Wu, X., Vo, H.-T., Ma, X.-J., & Luo, Y. (2012). RNAscope: A Novel in Situ RNA Analysis Platform for Formalin-Fixed, Paraffin-Embedded Tissues. *The Journal of Molecular Diagnostics*, *14*(1), 22–29. https://doi.org/10.1016/j.jmoldx.2011.08.002

Wang, Z., Oron, E., Nelson, B., Razis, S., & Ivanova, N. (2012). Distinct Lineage Specification Roles for NANOG, OCT4, and SOX2 in Human Embryonic Stem Cells. *Cell Stem Cell*, *10*(4), 440–454. https://doi.org/10.1016/j.stem.2012.02.016

Warner, T., Scullen, T. A., Iwanaga, J., Loukas, M., Bui, C. J., Dumont, A. S., & Tubbs, R. S. (2020). Caudal Regression Syndrome—A Review Focusing on Genetic Associations. *World Neurosurgery*, *138*, 461–467. https://doi.org/10.1016/j.wneu.2020.03.057

Watanabe, T., Sato, Y., Saito, D., Tadokoro, R., & Takahashi, Y. (2009). EphrinB2 coordinates the formation of a morphological boundary and cell epithelialization during somite segmentation. *Proceedings of the National Academy of Sciences*, *106*(18), 7467–7472. https://doi.org/10.1073/pnas.0902859106

Weber, G. F., Bjerke, M. A., & DeSimone, D. W. (2011). Integrins and cadherins join forces to form adhesive networks. *Journal of Cell Science*, *124*(8), 1183–1193. https://doi.org/10.1242/jcs.064618

Wegener, K. L., Partridge, A. W., Han, J., Pickford, A. R., Liddington, R. C., Ginsberg, M. H., & Campbell, I. D. (2007). Structural Basis of Integrin Activation by Talin. *Cell*, *128*(1), 171–182. https://doi.org/10.1016/j.cell.2006.10.048

Weil, M., Jacobson, M. D., & Raff, M. C. (1997). Is programmed cell death required for neural tube closure? *Current Biology*, *7*(4), 281–284. https://doi.org/10.1016/S0960-9822(06)00125-4

Wen, J., Chiang, Y. J., Gao, C., Xue, H., Xu, J., Ning, Y., Hodes, R. J., Gao, X., & Chen, Y.-G. (2010). Loss of Dact1 disrupts planar cell polarity signaling by altering dishevelled activity and leads to posterior malformation in mice. *The Journal of Biological Chemistry*, *285*(14), 11023–11030. https://doi.org/10.1074/jbc.M109.085381

Wennerberg, K., Lohikangas, L., Gullberg, D., Pfaff, M., Johansson, S., & Fässler, R. (1996). Beta 1 integrin-dependent and -independent polymerization of fibronectin. *Journal of Cell Biology*, *132*(1), 227–238. https://doi.org/10.1083/jcb.132.1.227

Whitby, D. J., & Ferguson, M. W. (1991). The extracellular matrix of lip wounds in fetal, neonatal and adult mice. *Development*, *112*(2), 651–668. https://doi.org/10.1242/dev.112.2.651

Wilde, J. J., Petersen, J. R., & Niswander, L. (2014). Genetic, Epigenetic, and Environmental Contributions to Neural Tube Closure. *Annual Review of Genetics*, *48*(1), 583–611. https://doi.org/10.1146/annurev-genet-120213-092208

Williams, M., Burdsal, C., Periasamy, A., Lewandoski, M., & Sutherland, A. (2012). Mouse primitive streak forms in situ by initiation of epithelial to mesenchymal transition without migration of a cell population. *Developmental Dynamics*, *241*(2), 270–283. https://doi.org/10.1002/dvdy.23711

Williams, M., Yen, W., Lu, X., & Sutherland, A. (2014). Distinct Apical and Basolateral Mechanisms Drive Planar Cell Polarity-Dependent Convergent Extension of the Mouse Neural Plate. *Developmental Cell*, *29*(1), 34–46. https://doi.org/10.1016/j.devcel.2014.02.007

Winnier, G., Blessing, M., Labosky, P. A., & Hogan, B. L. (1995). Bone morphogenetic protein-4 is required for mesoderm formation and patterning in the mouse. *Genes & Development*, *9*(17), 2105–2116. https://doi.org/10.1101/gad.9.17.2105

Wood, H. B., & Episkopou, V. (1999). Comparative expression of the mouse Sox1, Sox2 and Sox3 genes from pre-gastrulation to early somite stages. *Mechanisms of Development*, *86*(1), 197–201. https://doi.org/10.1016/S0925-4773(99)00116-1

Wymeersch, F. J., Huang, Y., Blin, G., Cambray, N., Wilkie, R., Wong, F. C., & Wilson, V. (2016). Position-dependent plasticity of distinct progenitor types in the primitive streak. *ELife*, *5*, e10042. https://doi.org/10.7554/eLife.10042

Wymeersch, F. J., Skylaki, S., Huang, Y., Watson, J. A., Economou, C., Marek-Johnston, C., Tomlinson, S. R., & Wilson, V. (2019). Transcriptionally dynamic progenitor populations organised around a stable niche drive axial patterning. *Development*, *146*(1), dev168161. https://doi.org/10.1242/dev.168161

Wymeersch, F. J., Wilson, V., & Tsakiridis, A. (2021). Understanding axial progenitor biology in vivo and in vitro. *Development (Cambridge, England)*, *148*(4). https://doi.org/10.1242/dev.180612

Xiong, F., Ma, W., Bénazéraf, B., Mahadevan, L., & Pourquié, O. (2020). Mechanical Coupling Coordinates the Co-elongation of Axial and Paraxial Tissues in Avian Embryos. *Developmental Cell*, *55*(3), 354-366.e5. https://doi.org/10.1016/j.devcel.2020.08.007

Yamaguchi, T., Takada, S., Yoshikawa, Y., Wu, N., & McMahon, A. P. (1999). T (Brachyury) is a direct target of Wnt3a during paraxial mesoderm specification. *Genes & Development*, *13*(24), 3185–3190.

Yamaguchi, Y., Shinotsuka, N., Nonomura, K., Takemoto, K., Kuida, K., Yosida, H., & Miura, M. (2011). Live imaging of apoptosis in a novel transgenic mouse highlights its role in neural tube closure. *Journal of Cell Biology*, *195*(6), 1047–1060. https://doi.org/10.1083/jcb.201104057

Yamanaka, Y., Tamplin, O. J., Beckers, A., Gossler, A., & Rossant, J. (2007). Live Imaging and Genetic Analysis of Mouse Notochord Formation Reveals Regional Morphogenetic Mechanisms. *Developmental Cell*, *13*(6), 884–896. https://doi.org/10.1016/j.devcel.2007.10.016

Yang, J. T., Bader, B. L., Kreidberg, J. A., Ullman-Culleré, M., Trevithick, J. E., & Hynes, R. O. (1999). Overlapping and Independent Functions of Fibronectin Receptor Integrins in Early Mesodermal Development. *Developmental Biology*, *215*(2), 264–277. https://doi.org/10.1006/dbio.1999.9451

Yang, J. T., Rayburn, H., & Hynes, R. O. (1993). Embryonic mesodermal defects in alpha 5 integrin-deficient mice. *Development*, *119*(4), 1093–1105.

Yazlovitskaya, E. M., Tseng, H.-Y., Viquez, O., Tu, T., Mernaugh, G., McKee, K. K., Riggins, K., Quaranta, V., Pathak, A., Carter, B. D., Yurchenco, P., Sonnenberg, A., Böttcher, R. T., Pozzi, A., & Zent, R. (2015). Integrin α3β1 regulates kidney collecting duct development via TRAF6-dependent K63-linked polyubiquitination of Akt. *Molecular Biology of the Cell*, *26*(10), 1857–1874. https://doi.org/10.1091/mbc.E14-07-1203

Ybot-Gonzalez, P., Cogram, P., Gerrelli, D., & Copp, A. J. (2002). Sonic hedgehog and the molecular regulation of mouse neural tube closure. *Development*, *129*(10), 2507–2517.

Ybot-Gonzalez, P., Gaston-Massuet, C., Girdler, G., Klingensmith, J., Arkell, R., Greene, N. D. E., & Copp, A. J. (2007). Neural plate morphogenesis during mouse neurulation is regulated by antagonism of Bmp signalling. *Development*, *134*(17), 3203–3211. https://doi.org/10.1242/dev.008177

Ybot-Gonzalez, P., Savery, D., Gerrelli, D., Signore, M., Mitchell, C. E., Faux, C. H., Greene, N. D. E., & Copp, A. J. (2007). Convergent extension, planar-cell-polarity signalling and initiation of mouse neural tube closure. *Development*, *134*(4), 789–799. https://doi.org/10.1242/dev.000380

Yoshikawa, Y., Fujimori, T., McMahon, A. P., & Takada, S. (1997). Evidence That Absence ofWnt-3aSignaling Promotes Neuralization Instead of Paraxial Mesoderm Development in the Mouse. *Developmental Biology*, *183*(2), 234–242. https://doi.org/10.1006/dbio.1997.8502

Yurchenco, P. D. (2011). Basement Membranes: Cell Scaffoldings and Signaling Platforms. *Cold Spring Harbor Perspectives in Biology*, *3*(2), a004911. https://doi.org/10.1101/cshperspect.a004911

Zaidel-Bar, R., & Geiger, B. (2010). The switchable integrin adhesome. *Journal of Cell Science*, *123*(Pt 9), 1385–1388. https://doi.org/10.1242/jcs.066183

Zaidel-Bar, R., Itzkovitz, S., Ma'ayan, A., Iyengar, R., & Geiger, B. (2007). Functional atlas of the integrin adhesome. *Nature Cell Biology*, *9*(8), 858–867. https://doi.org/10.1038/ncb0807-858

Zamir, E. A., Czirók, A., Cui, C., Little, C. D., & Rongish, B. J. (2006). Mesodermal cell displacements during avian gastrulation are due to both individual cell-autonomous and convective tissue movements. *Proceedings of the National Academy of Sciences*, *103*(52), 19806–19811. https://doi.org/10.1073/pnas.0606100103

Zamir, E. A., Rongish, B. J., & Little, C. D. (2008). The ECM Moves during Primitive Streak Formation—Computation of ECM Versus Cellular Motion. *PLOS Biology*, *6*(10), e247. https://doi.org/10.1371/journal.pbio.0060247

Zhao, S., Nichols, J., Smith, A. G., & Li, M. (2004). SoxB transcription factors specify neuroectodermal lineage choice in ES cells. *Molecular and Cellular Neuroscience*, *27*(3), 332–342. https://doi.org/10.1016/j.mcn.2004.08.002

Zhou, C. J., Ji, Y., Reynolds, K., McMahon, M., Garland, M. A., Zhang, S., Sun, B., Gu, R., Islam, M., Liu, Y., Zhao, T., Hsu, G., & Iwasa, J. (2020). Non-neural surface ectodermal rosette formation and F-actin dynamics drive mammalian neural tube closure. *Biochemical and Biophysical Research Communications*, *526*(3), 647–653. https://doi.org/10.1016/j.bbrc.2020.03.138

Zohn, I. E., & Sarkar, A. A. (2012). Does the cranial mesenchyme contribute to neural fold elevation during neurulation? *Birth Defects Research. Part A, Clinical and Molecular Teratology*, *94*(10), 841–848. https://doi.org/10.1002/bdra.23073

Zollinger, A. J., & Smith, M. L. (2017). Fibronectin, the extracellular glue. *Matrix Biology*, *60–61*, 27–37. https://doi.org/10.1016/j.matbio.2016.07.011

Zorn, A. M., & Wells, J. M. (2007). Molecular basis of vertebrate endoderm development. *International Review of Cytology*, *259*, 49–111. https://doi.org/10.1016/S0074-7696(06)59002-3

Zorn, A. M., & Wells, J. M. (2009). Vertebrate endoderm development and organ formation. *Annual Review of Cell and Developmental Biology*, *25*, 221–251. https://doi.org/10.1146/annurev.cellbio.042308.113344